Title
Synthesis and Characterization of Several Fullerene Polyadducts

Author
Knutson, Nicholas Scott

Publication Date
2017

Peer reviewed|Thesis/dissertation

UNIVERSITY OF CALIFORNIA

Los Angeles

Synthesis and Characterization of Several Fullerene Polyadducts

A dissertation submitted

in partial satisfaction of the requirements for the degree

Doctor of Philosophy in Chemistry

by

Nicholas Scott Knutson

2017

ABSTRACT OF THE DISSERTATION

Synthesis and Characterization of Several Fullerene Polyadducts

by

Nicholas Scott Knutson

Doctor of Philosophy in Chemistry

University of California, Los Angeles, 2017

Professor Yves F. Rubin, Chair

This dissertation describes the synthesis and characterization of several types of fullerene polyadducts including: 6,9,12,15,18-pentakisorgano-1-hydro[60]fullerenes, 6,9,12,15-tetrakisorgano[60]fullerenes, and 1,4-bisbenzyl[60]fullerenes as well as the performance of several in photovoltaic devices. Several of these projects are collaborations with material scientists and some are original research projects.

Chapter 1 describes the synthesis of a variety of pentakisorgano fullerenes containing a potentially labile addend that could be selectively removed to produce a fulvene substructure containing aryl tetrakisfullerene adduct as well as its potential application in photovoltaic devices.

Chapter 2 describes the performance of a series of electron-accepting methoxylated 1,4-bisbenzyl fullerene adducts blended with several electron-donating polymers in photovoltaic devices.

Chapter 3 describes how different regiosiomeric bis-N,N-dimethyl[60]fuller-pyrrolidinium cations can co-assemble in water with micelle-forming cationic semiconducting polymers to create photoinduced electron-transfer cascades, producing long-lived polarons.

The dissertation of Nicholas Scott Knutson is approved.

Kendall N. Houk

Vasilios Manousiouthakis

Yves F. Rubin, Committee Chair

University of California, Los Angeles

2017

Table of Contents

List of Figures

List of Tables

Acknowledgments

To my parents, upon reflection of my life, I realize the amount of time and effort that you both invested in me. You fostered in me an interest in learning and science, and pushed me to do well academically. I am truly lucky to have been raised by you. It is impossible to separate your contributions in my life from any of my achievements.

To my P.I., Dr. Yves Rubin, you took me on as a graduate student during one of the lowest periods of my life. You have always been a kind and patient mentor

I would like to thank my collaborators: Dr. Sarah Tolbert and Dr. Benjamin Schwartz as well as Dr. Jane Strouse and Dr. Greg Khitrov for all of their help and advice throughout my thesis.

Finally, I would like to my thank my initial P.I., Dr. Patrick Harran, for continuously demonstrating through example, the importance of having good interpersonal skills.

Published work:

Chapter 2 is reprinted (adapted) with permission from “Beyond PCBM: Methoxylated 1,4-bisbenzyl[60]fullerene Adducts for Efficient Organic Solar Cells,” Huang, S.; Zhang, G.; Knutson, N. S.; Fontana, M. T.; Huber, R. C.; Ferreira, A. S.; Tolbert, S. H.; Schwartz, B. J.; and Rubin, Y. *J. Mater. Chem. A*, **2016**, *0*, 1–9.

In this work, I was responsible for the synthesis and characterization of some of the 1,4-bisbenzyl[60]fullerene Adducts. I also wrote the corresponding portion of the experimental section and generated all of the ^{1}H NMR and ^{13}C NMR figures.

Chapter 3 is reprinted (adapted) from “POLARON DYNAMICS. Long-Lived Photoinduced Polaron Formation in Conjugated Polyelectrolyte-Fullerene Assemblies.” Huber, R. C.; Ferreira, A. S.; Thompson, R.; Kilbride, D.; Knutson, N. S.; Devi, L. S.; Toso, D. B.; Challa, J. R.; Zhou, Z. H.; Rubin, Y.; Schwartz, B. J.; and Tolbert, S. H. *Science*, **2015**, *348*, 1340–3. Reprinted with permission from AAAS.

In this work, I was responsible for some of the synthesis, separation and characterization of the regioisomers of the charged fullerene derivatives C_{60}-N,N-dimethylpyrrolidinium iodide.

Vita

2008-2009	Teaching Assistant University of Washington
2008-2009	Undergraduate Research Dr. Scott D. Wilbur University of Washington
2009	B.S., Chemistry, ACS certified University of Washington
2009	B.S., Biochemistry University of Washington
2009-2012	Teaching Assistant University of California, Los Angeles Courses: general chemistry lecture, organic chemistry lecture, organic chemistry lab
2012-2016	NMR Assistant University of California, Los Angeles

1. Towards the Synthesis of Four-Feathered Fullerene Shuttlecocks

Introduction

Organocopper additions to C_{60}

6,9,12,15,18-pentaorgano-1-hydro[60]fullerenes, informally referred to as fullerene shuttlecocks (due to their resemblance to badminton shuttlecocks) and abbreviated here as $C_{60}(Org)_5H$ or 5FSC, are the product of the addition of an excess (>15 eq.) of alkyl, alkenyl or aryl organocopper reagents to [60]fullerene (C_{60}).[1,2,3,4,5] Standing in stark contrast to the monoaddition of Grignard or organolithium reagents,[6] this novel class of fullerenes, first discovered by Sawamura et. al., has a five-fold pseudosymmetry resulting from a pentaaddition pattern to [60]fullerene. These pentadducts are usually orange to red solids, and can be obtained in up to 96% yield. The structure of the first member of this class, 6,9,12,15,18-pentaphenyl-1-hydro[60]fullerene ($C_{60}Ph_5H$), was determined by x-ray crystallography. Following this initial discovery, a wide panorama of fullerene shuttlecocks has been synthesized, including, with some modification to the original procedures, alkyl and alkenyl shuttlecocks. It was also discovered that in the presence of pyridine, higher additions up to octa- and deca-additions could be achieved, Figure 1.01.

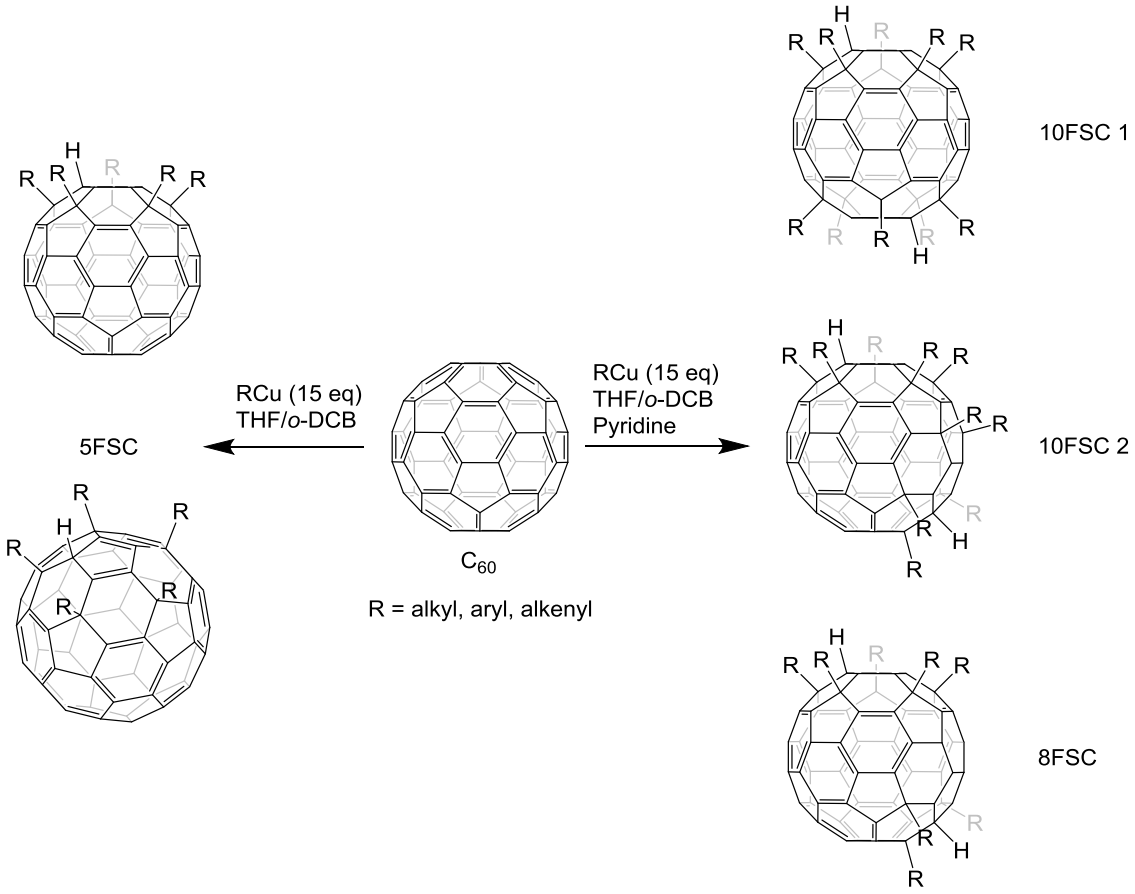

Figure 1.01 Addition of organocopper reagents to C_{60}. Left: pentaaddition pattern (5FSC) shown from two different angles. Right: octa- (8FSC) and decaaddition (10FSC) patterns.

The mechanism of this addition pattern is believed to occur via a stepwise addition/oxidation/radical mechanism, Figure 1.02. High performance liquid chromatography (HPLC) monitoring of the organocopper addition reveals that the addition occurs rapidly once started, as no intermediates are observed; however, a strong argument can be made for this mechanism if one considers that:

1. Two substituents larger than hydrogen, prefer to undergo 1,4- rather than a 1,2-addition

2. Grignard and organolithium reagents, in the absence of an oxidant, produce only the monoaddition product while in the presence of an oxidant (such as O_2) produce the 1,7-bisaddition products.
3. The addition of certain organometallic reagents, in the absence of oxygen otherwise affording the 1,7-bisorgano adduct, produce 1-hydro-6,9,12-trisorgano adducts in a highly selective manner.
4. The addition of organocopper reagents to fullerene 9-organo-1-hydro-1,7-bisaryl-, and 6,9,12-trisadducts gives the corresponding “mixed” fullerene shuttlecocks: $C_{60}X_nY_{(5-n)}H$
5. Other radical reactions with [60]fullerene give analogous tetra-, penta-, and hexaaddition patterns

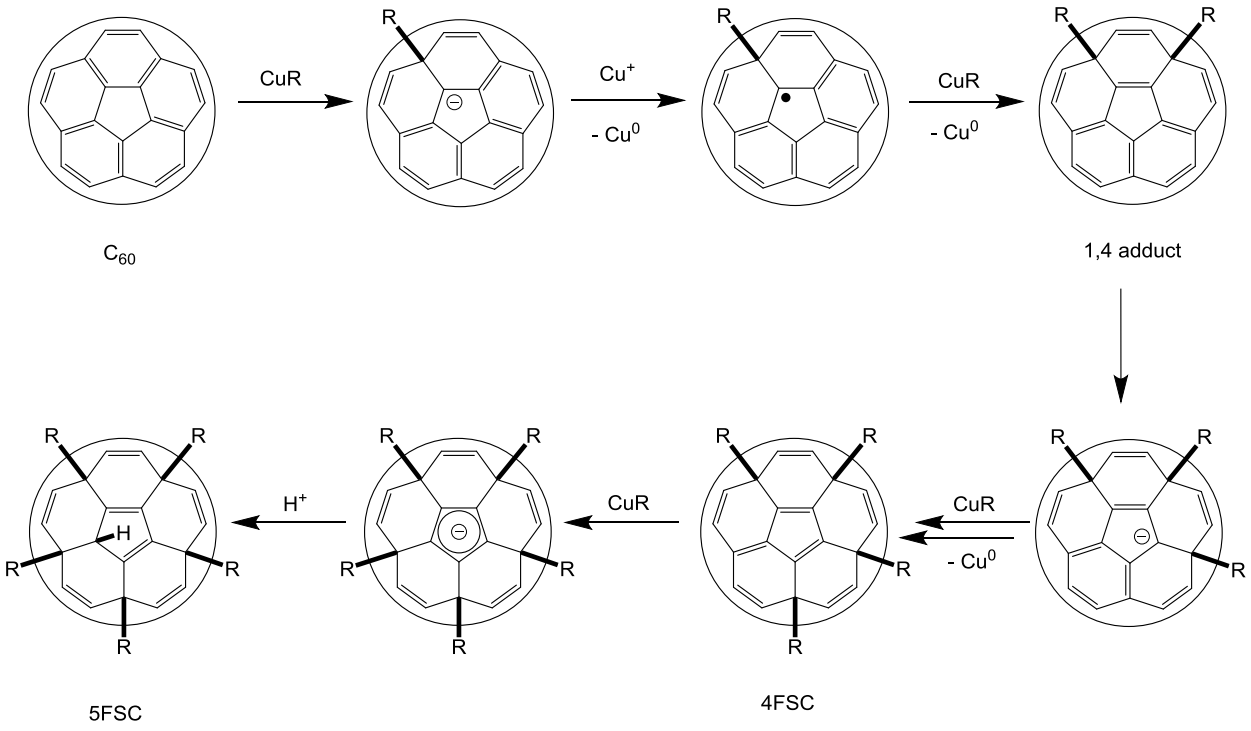

Figure 1.02. Proposed mechanism of organopeantaaddition to C_{60}.

Fullerene Shuttlecock Self-Assembly

The size and shape of the cavity created by the five substituent “feathers” on the fullerene shuttlecocks have been shown to influence their aggregation in the solid state, which can be broadly divided into stacked and non-stacked motifs.[7,8] The stacked motifs occur when the fullerene (ball) of each shuttlecock positions itself into the cavity of a neighboring shuttlecock, which has been described as 1D Nanowires. These columnar stacks can be further subdivided into “straight” and “zig-zag” formations, depending on how each sequential fullerene in the stack orients itself, Figure 1.03. In contrast, non-stacked motifs occur when the fullerene ball of each shuttlecock prefers to orient itself outside the feather-cavity of its neighboring fullerenes, which can produce a dimeric, feathered or feather-in-cavity formation.

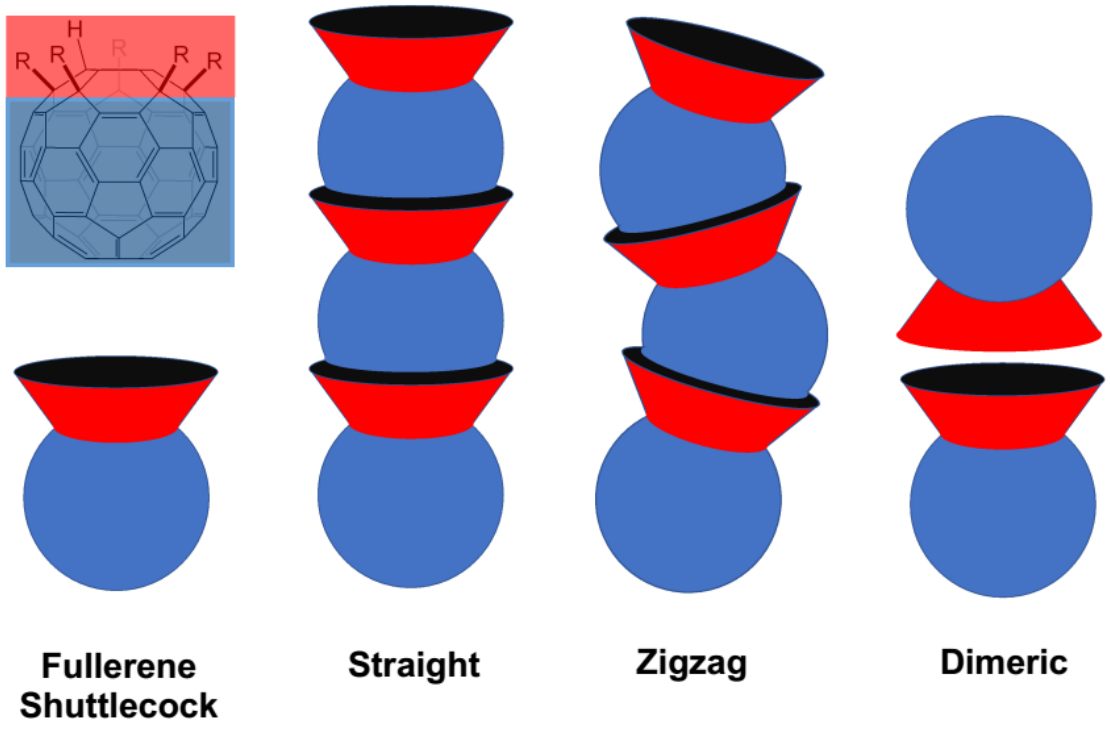

Figure 1.03. Straight, zigzag, and dimeric stacking patterns of 5FSCs.

When the shuttlecock substituents are aryl groups with large, roughly spheroidal para substituents (e.g. tert-butyl), a deep, well-defined cavity is formed which promotes straight-stacking and is usually crystallization-solvent independent. If, however, the cone size is reduced, or wider and less well-defined, the next fullerene in the stack has more degrees of freedom and can either kink to produce the zig-zag-stacking motif or aggregate into one of the non-stacking motifs, and is much more dependent on crystallization and solvent conditions. The dimeric motif appears to be preferred when the feathers are “rod-shaped” and able to intercalate with each other feather-to-feather.

Bulk Heterojunction Organic Solar cells

Organic photovoltaic devices (OPVs), utilizing various fullerene/polymer blends have now, under the right processing conditions, surpassed power conversion efficiencies of 10%.[9] Most of these OPVs are fabricated using a blend cast (BC) method, where the polymer donor and fullerene acceptor are mixed in solution together before being cast into a film, which forms the active layer of these organic solar cells. The fullerene and polymer components of these films must be sufficiently blended together to allow charge transfer while also being phase-separated enough to allow these charges to efficiently transport themselves to their respective electrodes. Hence the morphology of these films heavily dictates their overall power conversion efficiency.

The morphology, in turn, is highly dependent on processing conditions (solvent choice, drying kinetics, additives, etc.) which can be difficult to control and thus leads to high variability/reproducibility in the overall performance of these photovoltaic devices. One strategy to help control the morphology is to use self-assembling components such

as the fullerene shuttlecocks, which have a propensity to stack into predictable orientations based on their “feather” substituents. This idea was explored by the labs of Rubin, Tolbert, and Schwartz, which compared the device efficiency of BHJs made from blends of the polymer P3HT with pentaaryl shuttlecocks substituted at the para position with: Me, Et, i-Pr, and t-Bu groups.[7] It was found that while the V_{oc} of all four devices were similar, the Jsc of the Me, and Et shuttlecocks were dramatically (6x) lower than the i-Pr and t-Bu ones, which it was suggested was due to difference in film morphology. The Me and Ethyl SCs were more crystalline and phase segregated, resulting in a poor fullerene network causing higher charge recombination and trapping and poorer overall device performance. While this work demonstrated that morphology and hence device performance can be controlled by self-assembly, the best performing device (i-Pr) still only gave a paltry PCE of 0.97%, compared to the >2% of similar devices made from P3HT:[60]PCBM or [70]PCBM.

It has been suspected that the reason for this overall poor device performance is poor LUMO overlap of the SCs with each other in their columnar stacks. Calculations of the LUMO density show that there is very little LUMO density inside the aryl cavity of the SCs, Figure 4.[10] Therefore, even though they have a tendency to self-assemble into 1D “nanowires”, an electron in the LUMO of a SC sitting in the cavity of an adjacent shuttlecock is not able to efficiently transfer to the next fullerene in the “wire.”

This poor LUMO density in the SC cavity is likely due to the lack of conjugation between the 5-member ring inside the cavity and the rest of the fullerene cage. If, however, one of the aryl feathers is removed, creating a fulvene moiety with a double bond connecting the inner cavity to the rest of the fullerene pi-system, calculations of the

LUMO density show that these four-feather fullerene shuttlecocks have much better LUMO density inside their feather cavity, Figure 1.04.[10] Based on the LUMO orbital distribution of the four-feathered shuttlecock shown in Figure 4, it was proposed by professor Rubin that four-feather shuttlecocks may have superior electron mobility in PVs to their five-feather counterparts while still taking advantage of a propensity to self-assemble.

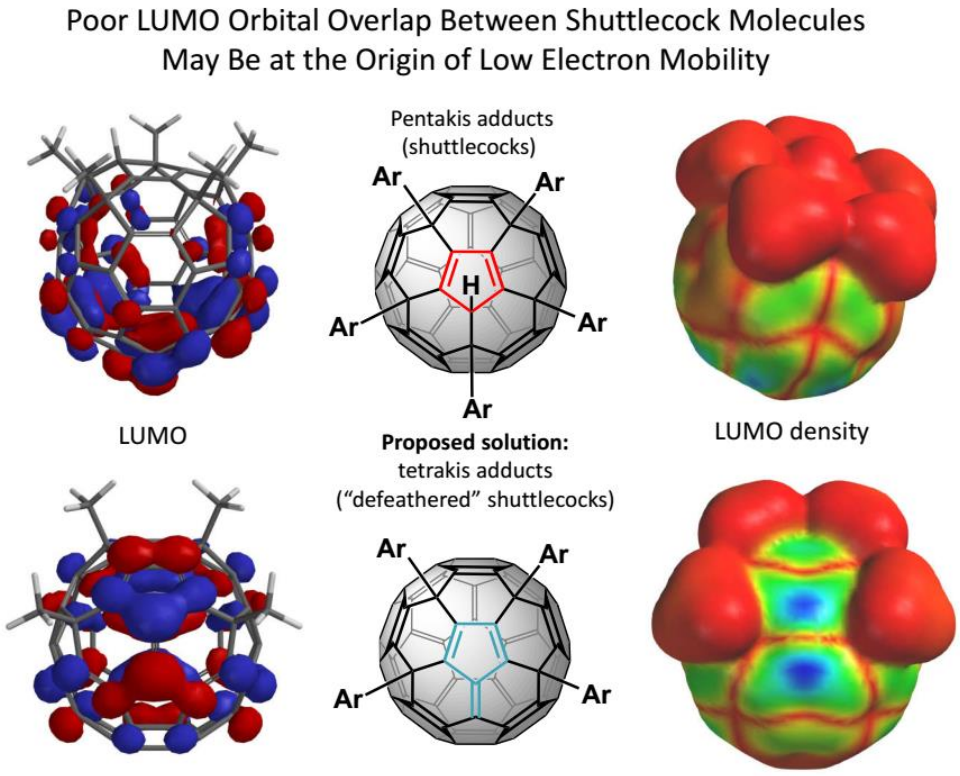

Figure 1.04. Comparison of calculated LUMO and LUMO densities between 4FSC and 5FSC.[10]

Four-feathered Shuttlecocks (4FSC)

While conditions to selectively synthesize the mono-,[11] 1,7-bis-, and 6,9,12-trisaddition[12,13] products with aryl groups on the fullerene cage are known, there are only a few spurious examples of the 6,9,12,15-tetrakisadduct (four-feathered shuttlecock, 4FSC), containing the desired fulvene moiety or its corresponding epoxide in the literature, Figure 5.[14,15,16,17,18] All these reactions suffer from at least one of the following drawbacks:

1. The resulting product of the reaction is unique to that particular addend and produces widely different results when the addend is changed
2. The reaction is not selective and yields a mixture of regioisomers that often require further purification by HPLC
3. The product is unstable, or in the case of some of the epoxides, does reduce to the desired fulvene moiety

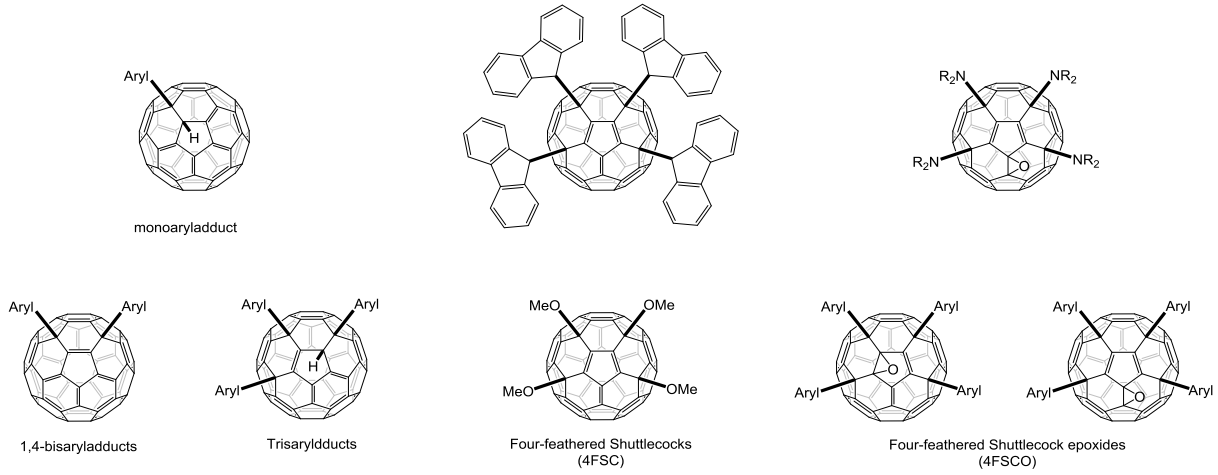

Figure 1.05. Known mono, bis, tris, tetra, and tetra epoxy aryl fullerene adducts.

The first reported four-feathered shuttlecock, the tetrakis(9-fluorenyl) adduct of C_{60}, was synthesized from C_{60} and a 3:2 mixture of potassium fluorenide and fluorene in THF, that was allowed to stir for a prolonged period of time (72 h) under inert atmosphere.[15] The course of the reaction is interesting in that rather than merely stopping after the fourth fluorenyl group addition, it actually first adds five fluorenyl addends, demonstrated by acidically quenching the reaction during the initial 24 h, producing the pentakis(9-fluorenyl) adduct as the major product. It is only after the reaction is allowed to stir for an additional 48 hours that the four-feathered tetrakisadduct becomes the dominant product. It is suggested by the authors that a small amount of oxygen present in (or that seeps into) the reaction is responsible for this particular 'defeathering." The oxygen oxidizes the pentakis anion to its radical, which then causes the fragmentation of a fluorenyl radical, Figure 1.06. This is supported by the fact that when oxygen is exhaustively excluded from the reaction, the tetrakisadduct is not formed. In this example, it is both the steric crowding of the bulky fluorenyl groups as well as their propensity to stabilize a radical that produces the resulting four-feathered shuttlecock.

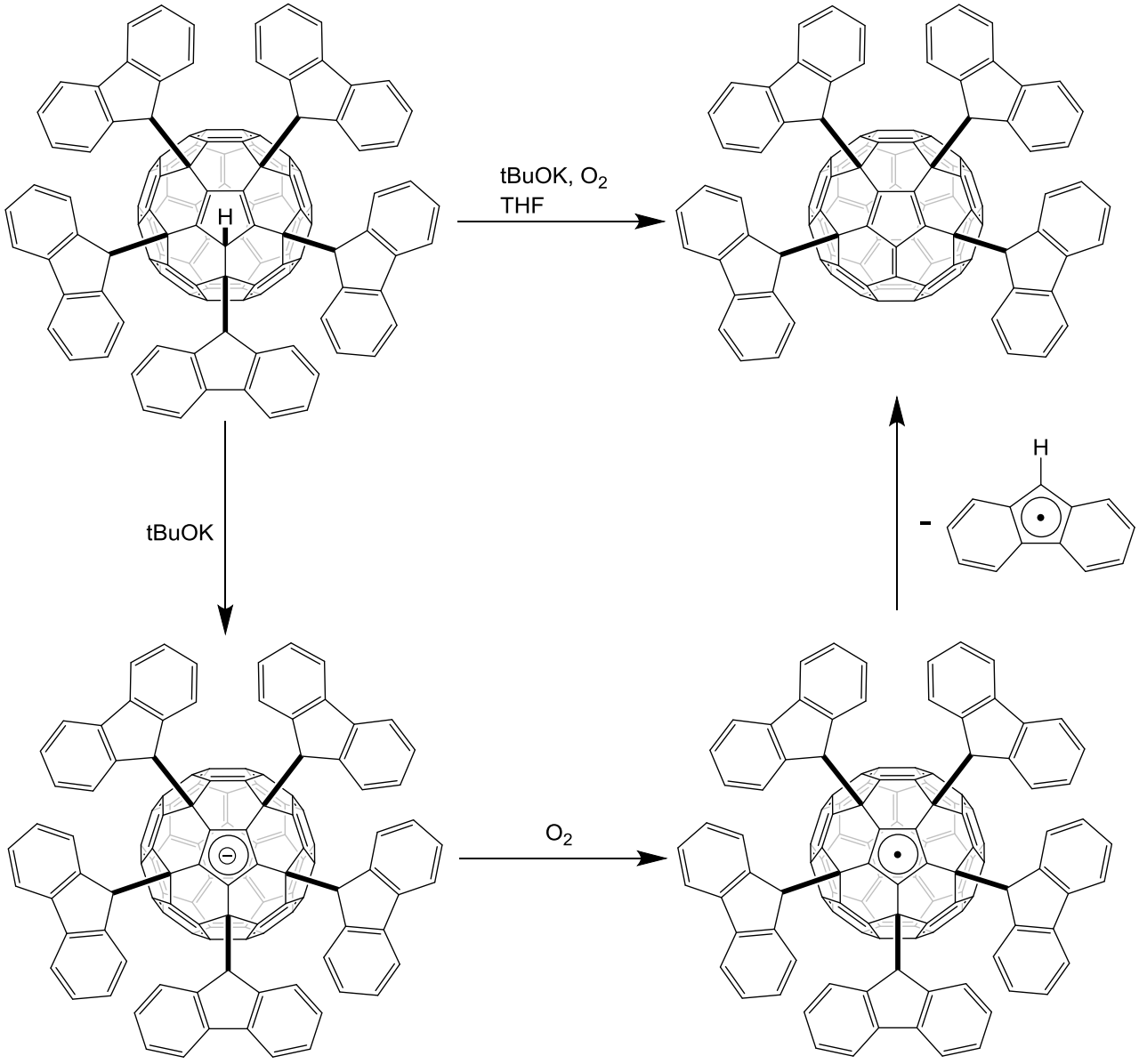

Figure 1.06. Loss of a fluorenyl group (defeathering) from the fluorenyl 5FSC to form the corresponding 4FSC in the presence of oxygen.

After an extensive search of the literature, the only other example of a four-feathered shuttlecock produced as a major product that could be found was the tetrakis(methoxy) adduct.[19] This adduct was synthesized from the reaction of $C_{60}Cl_6$ with MeOH in DMSO/chlorobenzene in air at 85 ˚C. The $C_{60}Cl_6$ starting material shares the same substitution pattern as the protonated five-feathered shuttlecock, Figure 1.07.

Unfortunately, $C_{60}Cl_6$ does not selectively give the desired four-feathered product with other nucleophiles, Figure 1.07.[20,21,22]

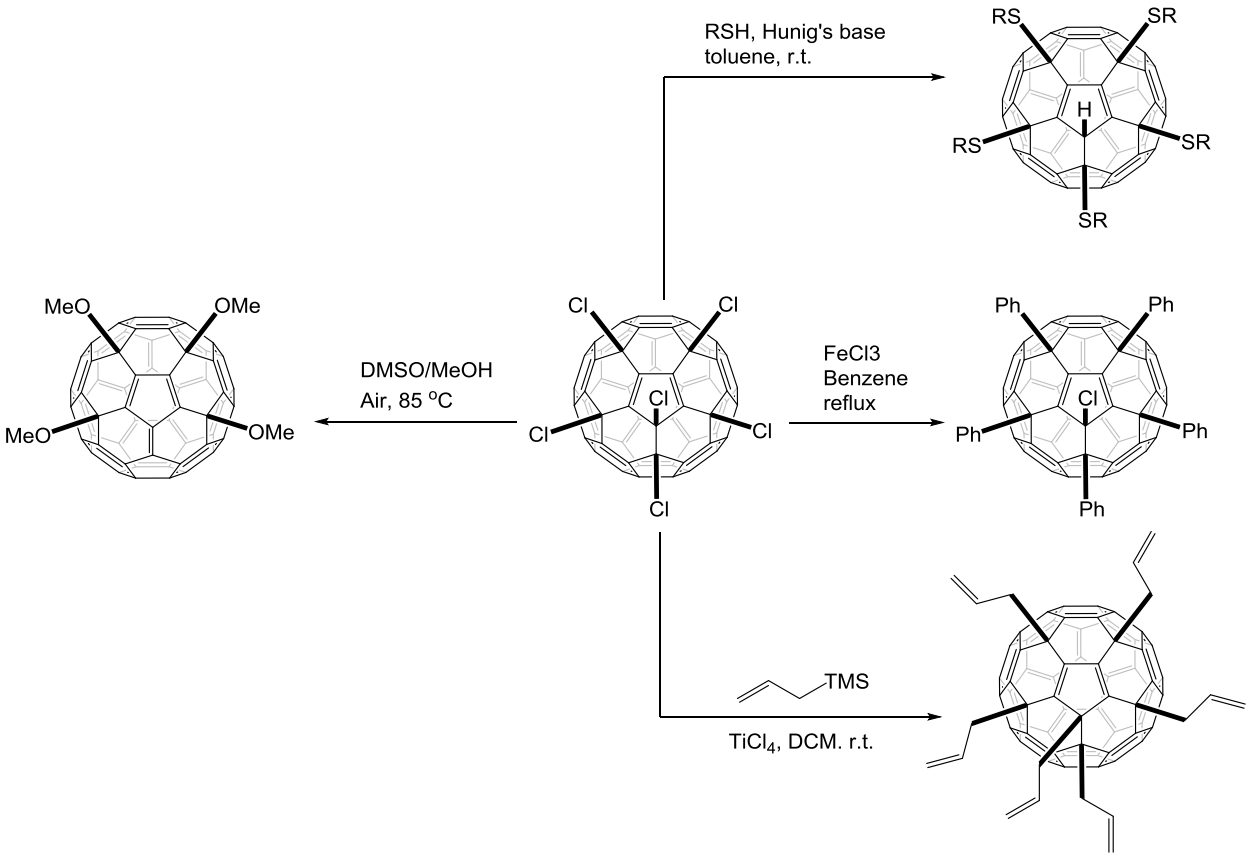

Figure 1.07. Reaction of various nucleophiles with $C_{60}Cl_6$.

Similar to the fluorenyl 4FSC, although by a different mechanism, the p-(diphenylamino)phenyl four-feathered epoxide **2** is generated when the anion of the five-feathered precursor **1** is exposed to oxygen, leading to the loss of one of the addends.[18] The reduction of a fullerene epoxide with triphenyl phosphine is known,[23] and it is conceivable that the four-feathered epoxide could also be reduced under similar conditions. However, the clean and high yielding, oxygen-induced defeathering seems to

be unique to the diphenylaminophenyl addend.[18] When the reaction conditions are attempted with other less electron-rich addends, a mixture of several oxidized products is formed in addition to both a symmetrical and asymmetrical four-feathered epoxide, Figure 1.08.[24]

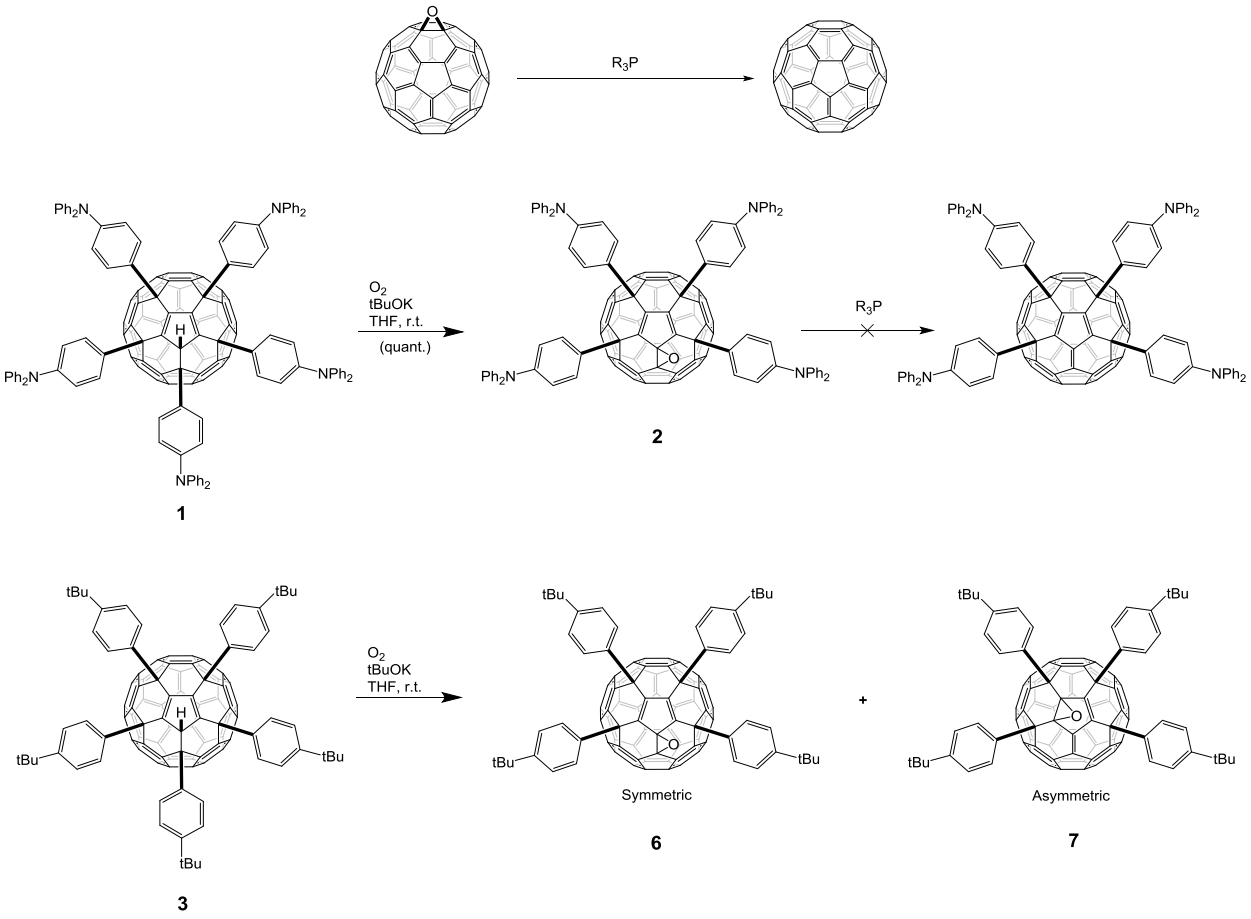

Figure 1.08. Synthesis of 4FSC epoxides and reduction of fullerene epoxide with Ph_3P.

The final class of four-feathered shuttlecocks discussed here, is that of the full or partial amino tetraadduct epoxides.[25,17] These tetraadducts are generated when pristine C_{60} or lower fullerene adducts are treated with a primary or secondary amine in DMSO/chlorobenzene in the presence of oxygen. The reaction is assumed to proceed

via a series of oxidation and single electron transfers. The amine will add up to four times, before the fulvene-containing tetradduct intermediate is oxidized by hydrogen peroxide (generated during the course of the reaction) or another oxidant. In principle, the epoxide formation is in competition with the addition of a fifth amino group; however, it is believed that the relative steric bulkiness of the amines favors reaction with the oxidant. In addition to this reaction being limited to an addend with a lone pair capable of single electron transfer with the fullerene, attempts at reduction of epoxide products results in at least partial removal of the amine addends.[26]

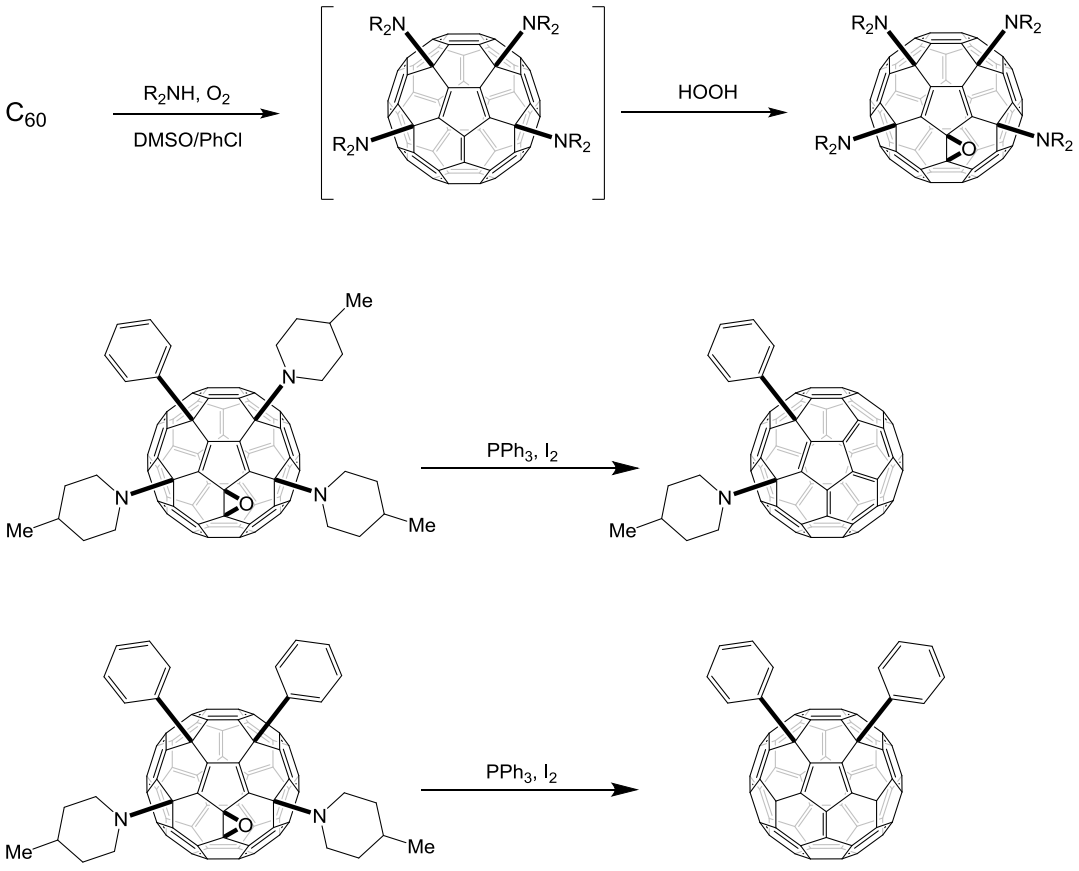

Figure 1.09. Synthesis of tetramino four-feathered epoxide and deamination of amino aryl tatra epoxide fullerene adducts in the presence of triphenyl phosphine and iodine.

Reactivity of the Fulvene Moiety in the Four-feathered Shuttlecocks

Not surprisingly, the known fulvenes containing four-feathered shuttlecocks react similarly to fulvene, with nucleophiles attacking the exocyclic methylene position and cycloadditions selectively reacting with the exocyclic double bond, Figure 1.10.5[15,19] When the tert-butylphenyl and tolyl 4FSCs were synthesized in our group, it was quickly discovered that they were unstable in air, light, and even methanol, oxidizing to form the corresponding 4FSC epoxides, or adding MeOH to form the methoxy addition product, respectively.[27]

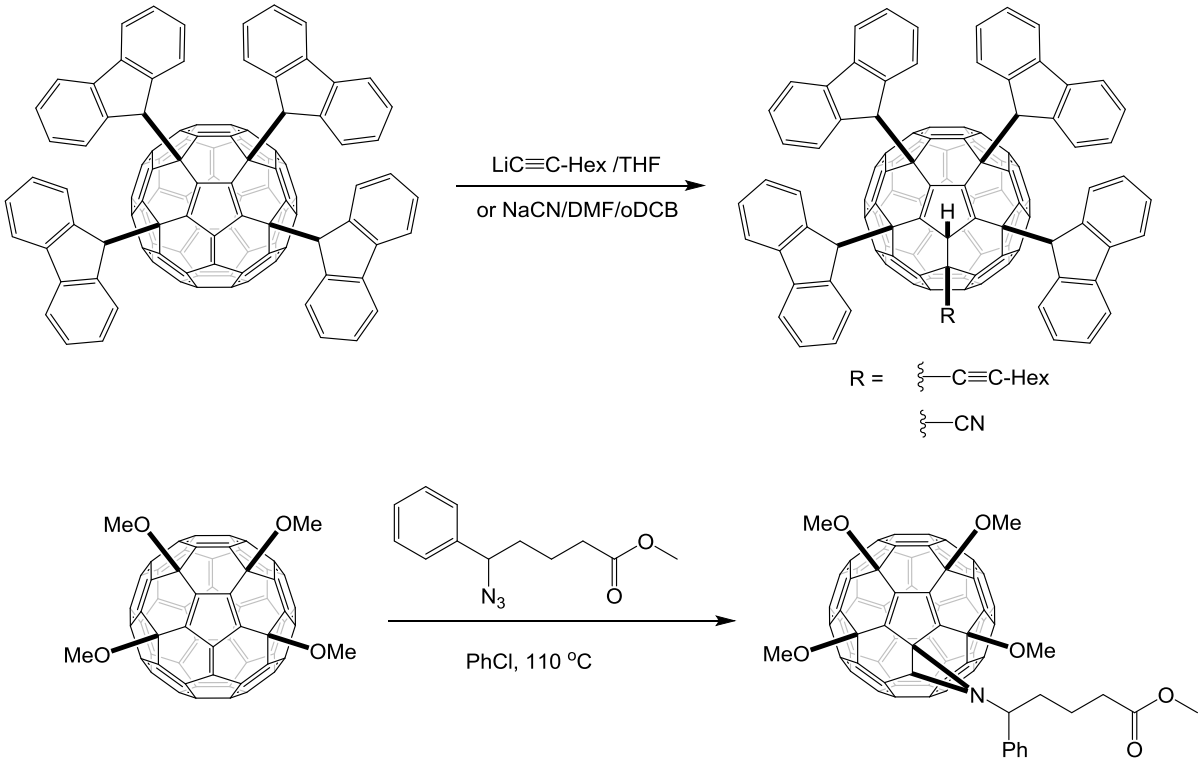

Figure 1.10. Nucleophilic and cycloaddition reactions of known 4FSCs showing a strong selectivity for the fulvene double bond position.

General Monoadduct/Protecting Group Strategy to Synthesize Four-feathered Shuttlecocks

Since it is known that aryl copper additions to either the fullerene mono-, bis-, and trisadduct derivatives produce the five-feathered shuttlecock addition pattern,[5] and that the addition is difficult to reliably terminate at the tetraaddition stage, and that certain addends can be coaxed to leave to produce four-feathered shuttlecocks from the pentaaddition stage, it was decided to pursue a strategy where the initial, single addition of a labile addend, before aryl copper addition, would act as a “protecting group.” After aryl copper addition, the labile addend of the mixed shuttlecock (MSC) intermediate could then be selectively defeathered to produce the desired four-feathered aryl shuttlecock, Figure 1.11.

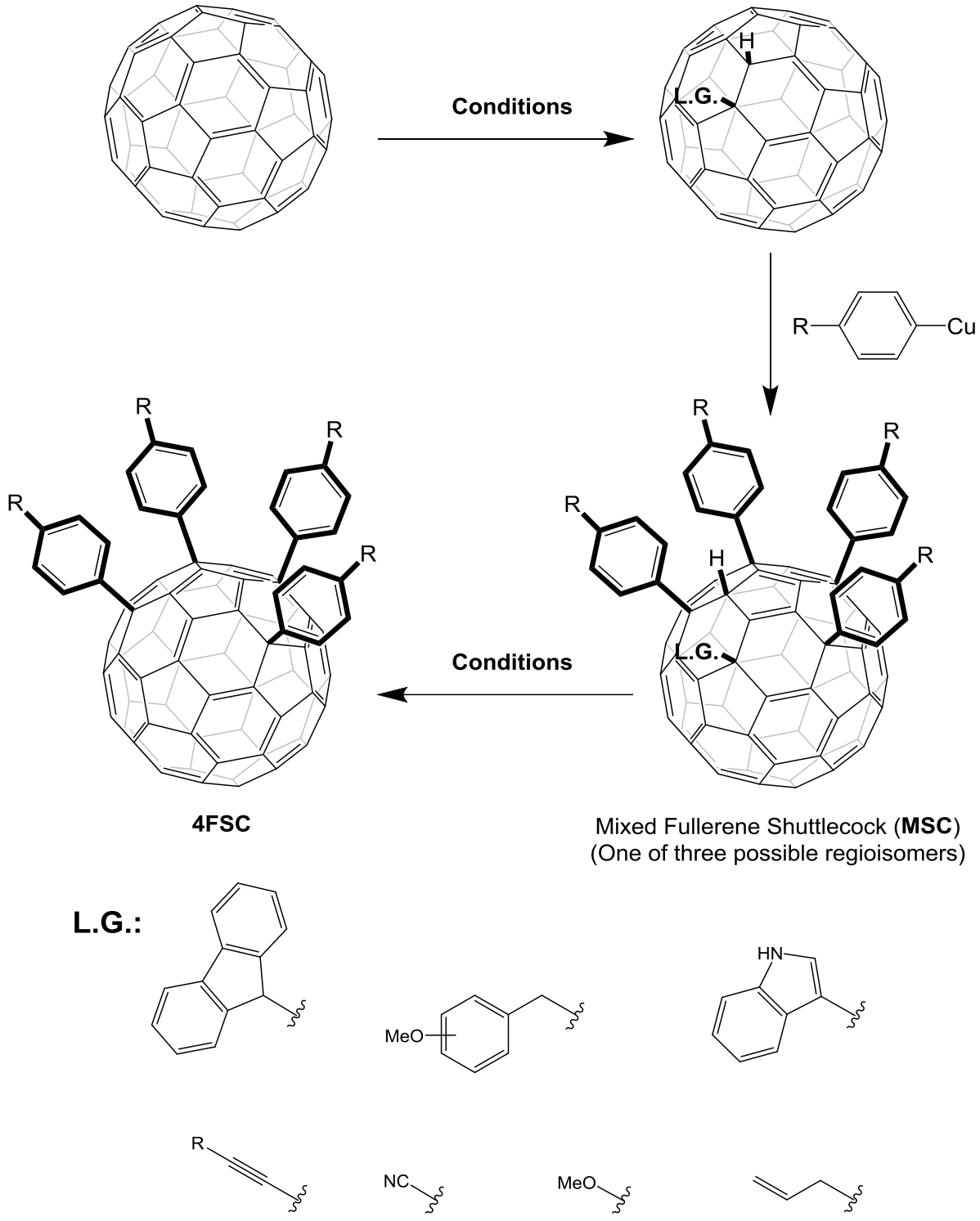

Figure 1.11. Mixed shuttlecock protecting group strategy.

In order to function as a protecting group, this addend must be stable enough to survive the conditions of the aryl-copper addition while also being labile enough to be selectively removed to produce the four-feathered shuttlecock, which is anticipated to be somewhat reactive/unstable at the newly formed alkene position. Hence a variety of potential protecting groups were synthesized and screened, Figure 1.11.

Analysis of Fullerene Shuttlecock Systems

Analysis of the fullerene SC structures is not a trivial task in itself, particularly in the case of MSCs, where more than one regioisomer is present. Ideally, for pure compounds, x-ray crystallographic data (if obtainable) greatly aids in the confirmation of the fullerene structure. However, when this is not achievable, one must glean what one can from the ^{1}H and ^{13}C NMR data, despite a woeful lack of protons directly attached to the fullerene cage. Nevertheless, consideration of the symmetry of the molecule as well as several characteristic SC peaks can often narrow down the possible structures to only a few choices, if not one choice, and can indicate the presence of one more isomers in more complex mixtures.

For example, in Figure 1.12, note the ^{1}H NMR spectra of three 5FSCs differing only in the substituent at the para position of their aryl rings (methoxy, methyl, and tert-butyl). The 5FSCs contain a single mirror plane and belong to the C_s point group. Therefore, the five aryl substituents can be divided into three chemically distinct groups differing only in their relative distance from the lone C_{60}-H in the SC aryl cavity with an integration ratio of 2:2:1. In more complex mixtures, the aryl region can often become indecipherable, but it is usually still possible to see distinct substituents on the aryl

feathers. Additionally, the lone C_{60}-H of the aryl SCs shows up in a relatively barren region of the spectrum between 5.0-5.5 ppm, and has a unique chemical shift for each SC, allowing it to be used as a "fingerprint" for the presence (or absence) of individual 5FSCs, even when the rest of the spectrum is muddied by the presence of multiple products.

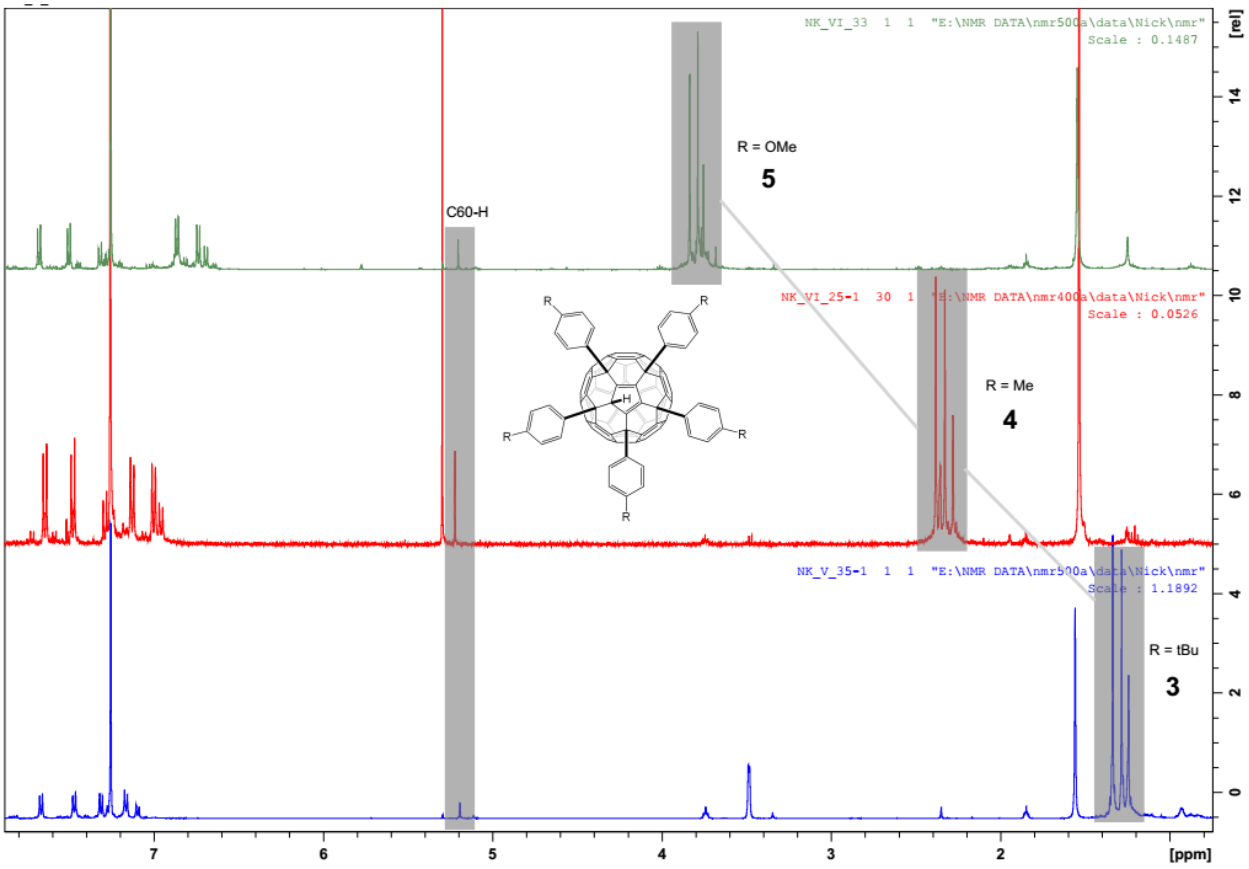

Figure 1.12. ^{1}H NMR comparison of the pentakis 4-anisyl (**5**), 4-tolyl (**3**), and 4-tBu-phenyl (**4**) 5FSCs. C_{60}-H and aryl substituent proton peaks are highlighted in grey.

Figure 1.13 shows a comparison of a 4FSC, and its two (symmetric and asymmetric) corresponding 4FSC epoxides. In contrast to the 5FSCs, the 4FSCs obviously lack the C_{60}-H. While the 4FSC and the symmetric 4FSC epoxide both share the C_s point group of the 5FSCs, the relative placement of the epoxide group in the

asymmetric 4FSC epoxide means that each substituent has a unique set of chemical shifts giving a 1:1:1:1 integration ratio. One can also see that the ^{1}H NMR spectra of the 4FSC and symmetric 4FSC epoxide, are very similar. However, comparison of the ^{13}C NMR spectra reveals the difference in the number of fullerene sp^3 carbons that appear between 60-80 ppm, the epoxide having an additional two lines due to the epoxide ring, Figure 1.14.

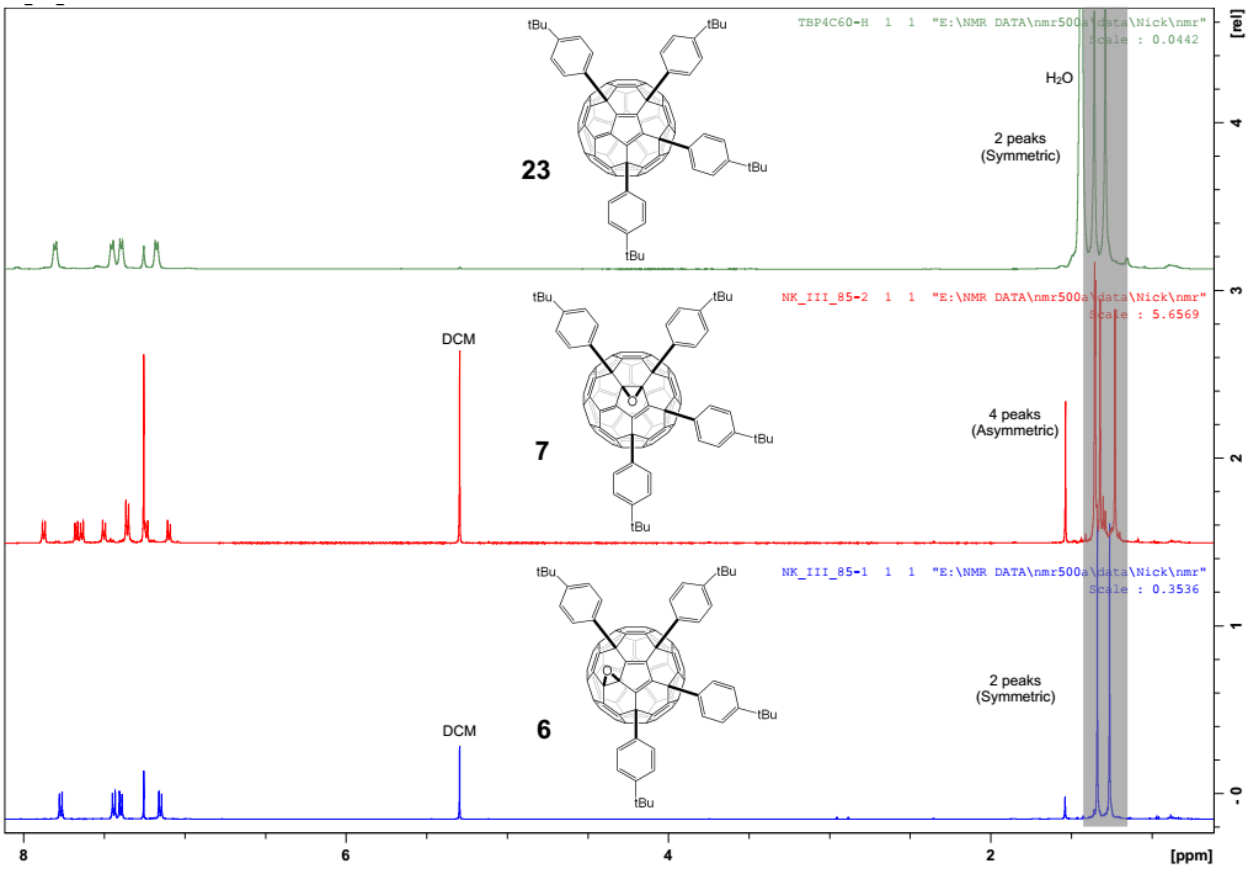

Figure 1.13. ^{1}H NMR comparison of the 4FSC (**23**), symmetric (**6**), and asymmetric (**7**) 4FSC epoxide. t-Butyl group proton signals are highlighted in grey.

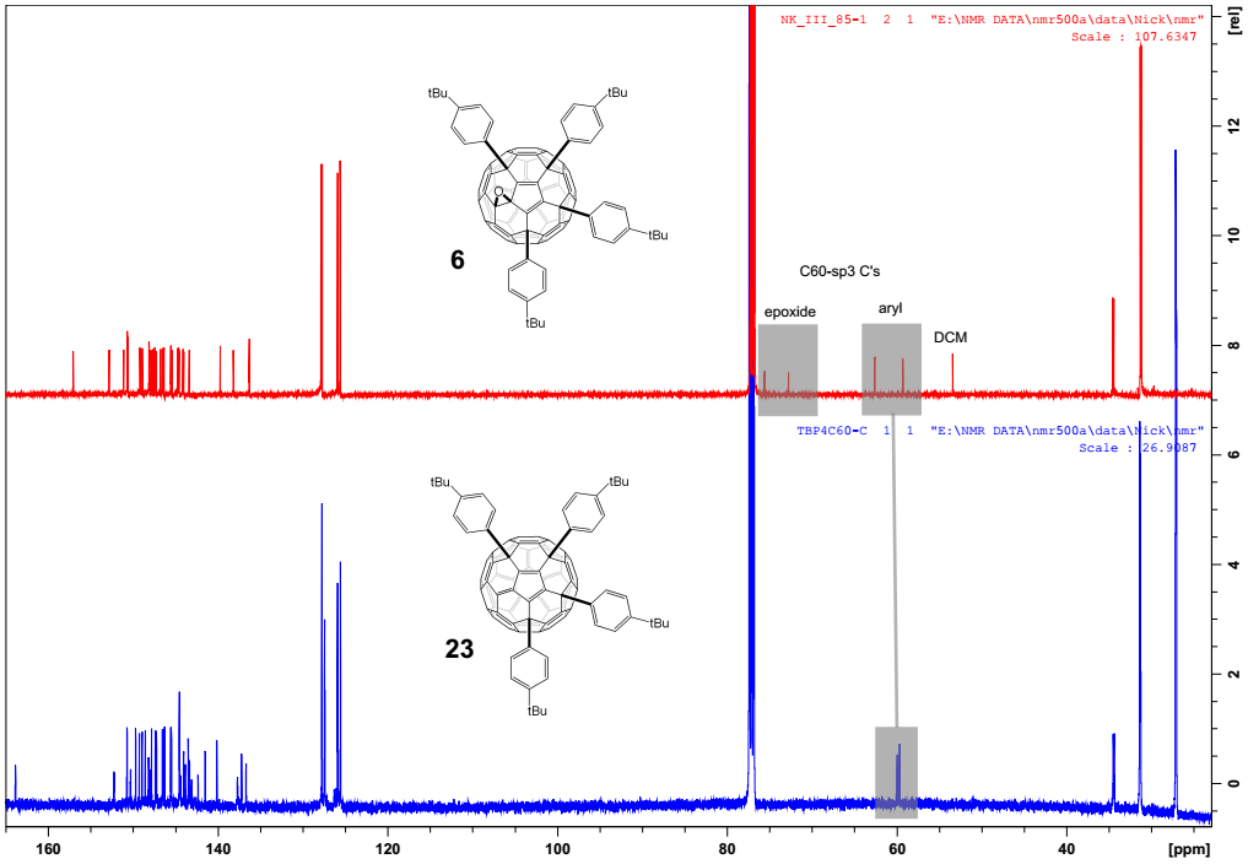

Figure 1.14. ^{13}C NMR comparison of the 4-t-butyphenyl 4FSC (**23**) and the symmetric 4-t-butylphenyl 4FSC epoxide (**6**).

Fluorenyl Group as a Potential Defeathering Element

It was thought that, analogously to the pentakis-fluorenyl fullerene prepared by Komatsu, a mixed shuttlecock containing a fluorenyl group would also show propensity to defeather under conditions similar to Komatsu's work,[28] to produce a fulvene-containing four-feathered shuttlecock. The hydro fluorenyl fullerene was synthesized by reacting pristine C_{60} with the fluorenyl anion produced in situ by reaction with n-butyl lithium (Figure 1.15). Consistent with other organolithium additions to C_{60}, the fluorenyl group selectively adds once, producing only the mono fluorenyl hydro fullerene **8** after quenching of the reaction with acid. However, attempts at organocopper additions with

the fluorenyl fullerene did not cleanly yield (if at all) any desired mixed fullerene products. Instead, a large number of inseparable isomers was produced, Figure 1.15.

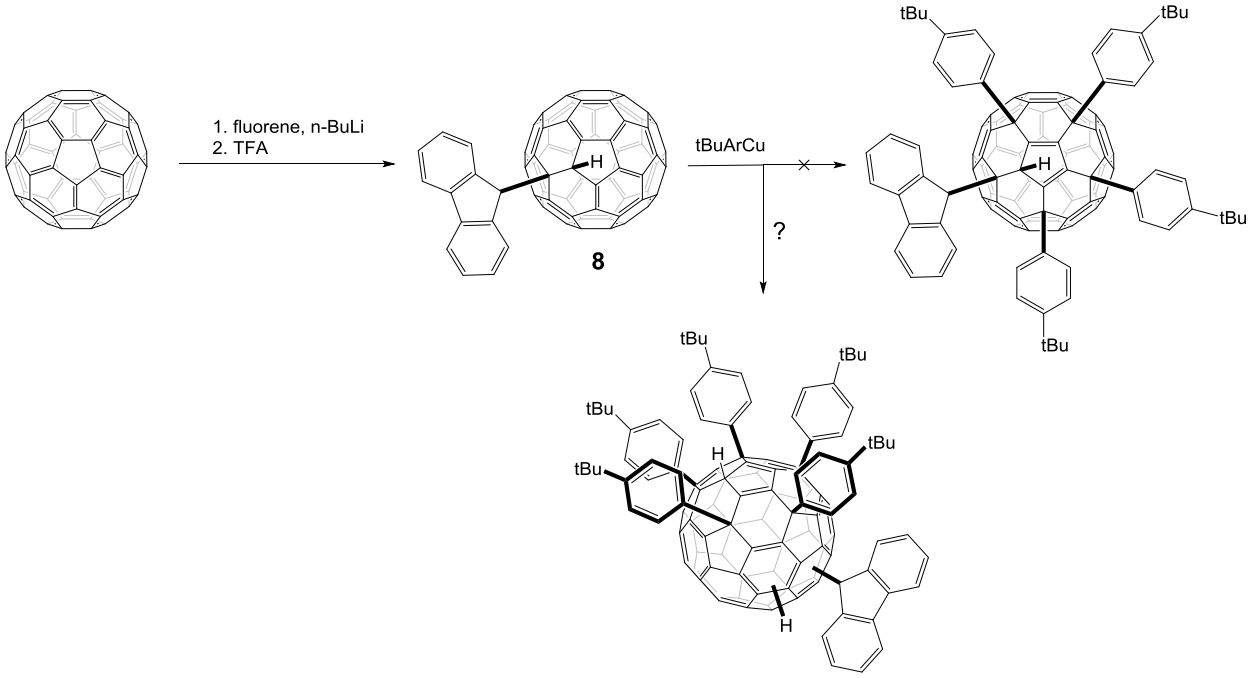

Figure 1.15. Attempted synthesis of the fluorenyl MSC and possible isomeric products.

While it is not feasible to determine the structure of each of these isomers, some basic information can still be gleaned from the ^{1}H NMR spectrum, Figure 16. The large number of peaks around 1.5 ppm corresponds to the aryl tert-butyl groups added to the fullerene. The three desired regioisomeric products should give a combined total of 10 peaks: 2 from the symmetric isomer, and 4 from each of the two asymmetric isomers. Instead, there appears to be more than 30 peaks. Likewise, the shuttlecock proton directly connected to the fullerene cage should appear around 5.3 ppm. There should be one for each of the three desired products and yet there are over 15 peaks in the mixture. Although the aromatic protons of the fluorenyl group cannot be seen over the vast number

of peaks in the aromatic region, it is likely that it is still attached, because otherwise, the five-feathered shuttlecock would likely be a dominant (or only) product. Unfortunately, without further information, it is impossible to know exactly why the 5FSC pattern is not observed. It is possible that the fluorenyl group, being simply too bulky, promotes the aryl copper addition to initiate at a different location of the cage. Whatever the reason, the fluorenyl protecting group did not produce the desired MSC, and was thus abandoned.

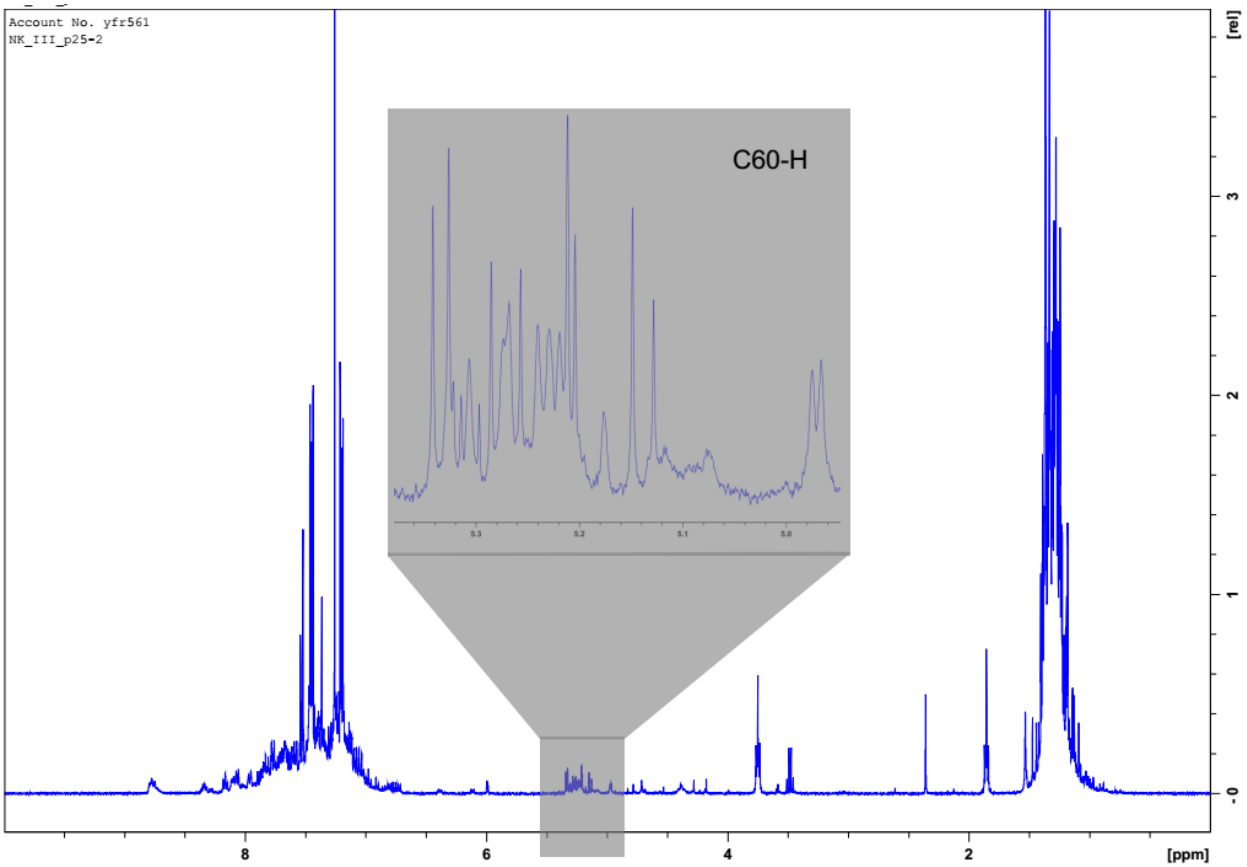

Figure 1.16. ^{1}H NMR of the mixture of inseparable products isolated from the reaction of the 9-fluorenyl-1-hydrofullerene with the t-butylaryl copper reagent.

Cyano Group as a Potential Defeathering Element

It was thought that, if a cyano-substituted mixed fullerene could be synthesized, the cyano group could then be hydrolyzed to the corresponding carboxylic acid and subsequently decarboxylated to give the dihydro 4FSC. This dihydro intermediate would then be oxidized with DDQ to yield the desired product. Cyanofullerene was already known and was synthesized according to the literature procedure.[29] Treatment of cyanofullerene with aryl copper reagents, however, yielded only the corresponding 5FSC, Figure 1.16. Since there was no C_{60} in the starting cyano fullerene, the cyano group must be removed at some point during the aryl additions, most likely by binding with copper(I) to give insoluble CuCN, and the reaction proceeds to the pentaaddition product without it. The cyano group was therefore deemed a poor protecting group due to this lability.

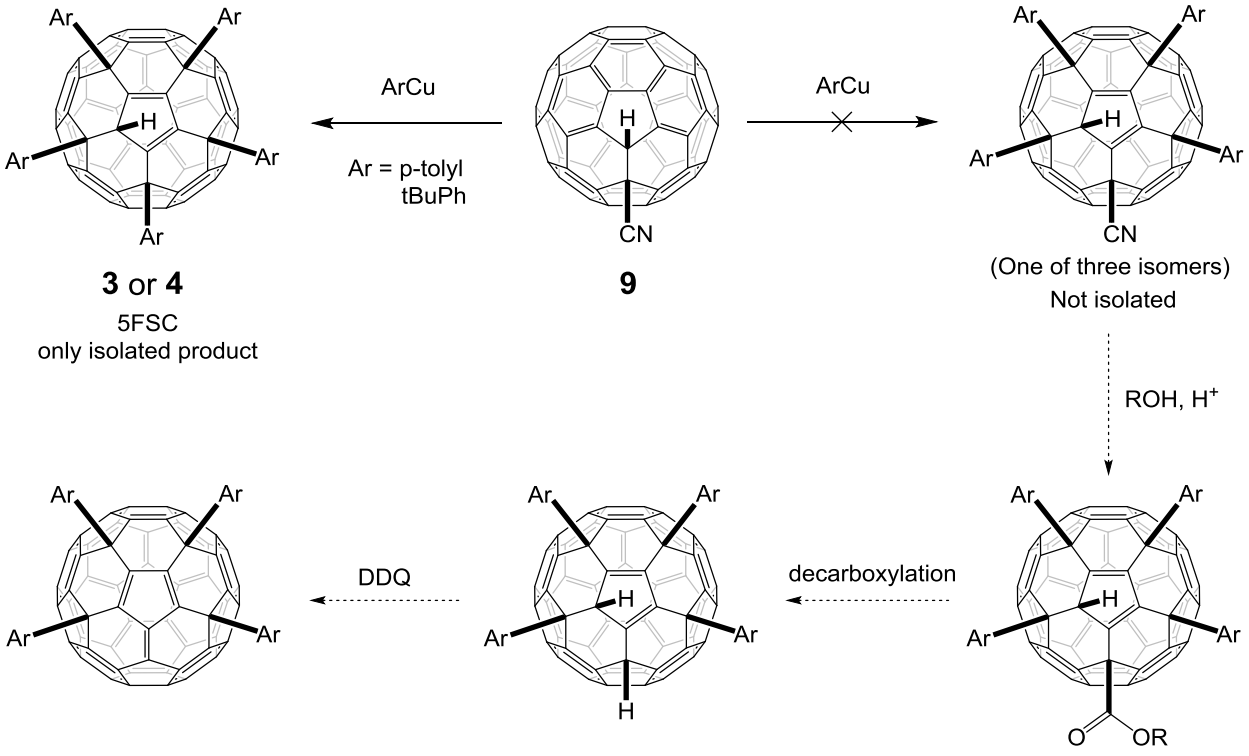

Figure 1.17. Attempted cyano MSC synthesis and deprotection.

Hydroxyl Group as a Potential Defeathering Element

An interesting reaction was found in the literature that installs both an aryl and a hydroxyl group in a 1,4-addition pattern.[30] Since the copper addition proceeds through the monoaryl intermediate, the aryl copper addition was attempted on this compound but, like the cyano group, resulted in only the 5FSC, being apparently too labile to survive the copper addition, Figure 1.18.

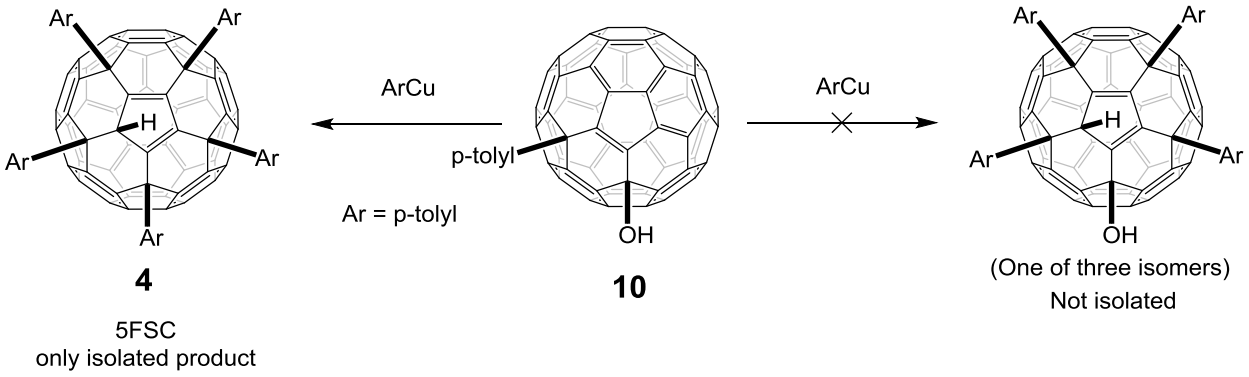

Figure 1.18. Reaction of p-tolylfullerenol (**10**) with aryl copper reagents.

Acetylene Group as a Potential Defeathering Element

The alkynyl fullerene adduct is also known in the literature. It was found that this adduct reverts back to pristine C_{60} in the presence of $Pd(OAc)_2$, $P(o\text{-}tol)_3$ and heat.[31] The alkynyl mixed shuttlecock was made cleanly in high yield but the mixed shuttlecock failed to de-alkynylate under the same conditions as the alkynyl monoadduct. Thus, further attempts with this deprotection route were not further pursued, Figure 1.19.

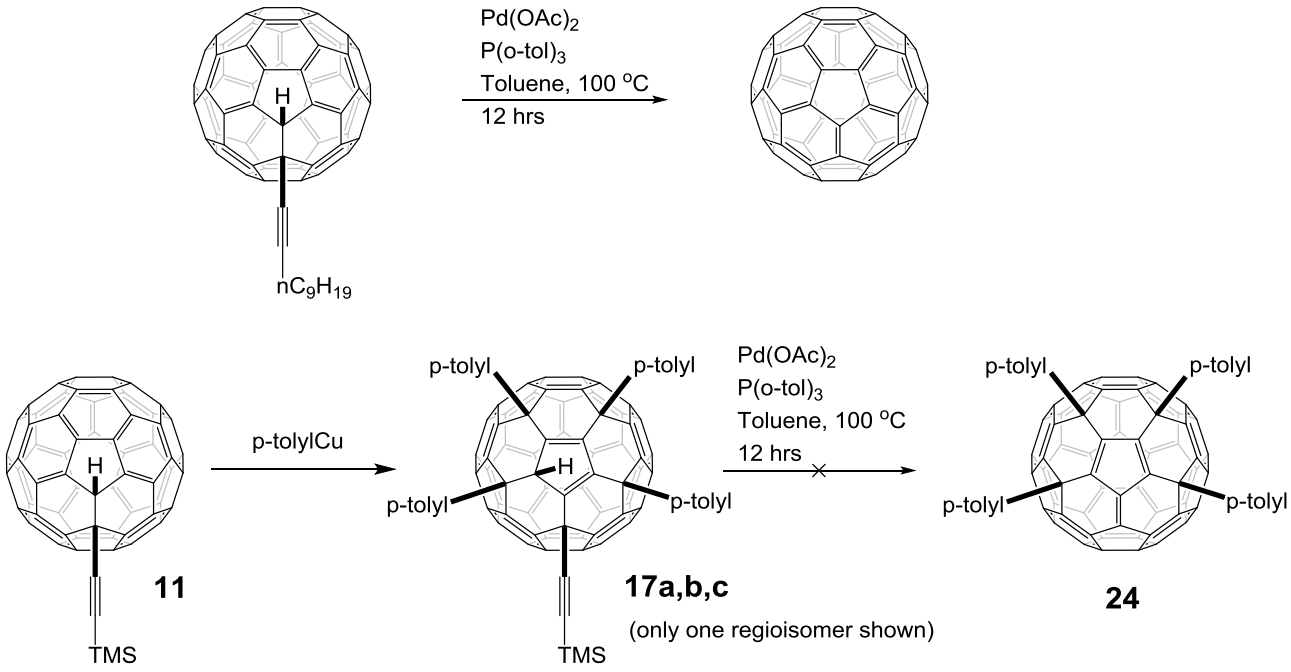

Figure 1.19. De-alkynylation of an alkynylfullerene, and synthesis of alkynyl MSCs.

Indole Group as a Potential Defeathering Element

The 1,2-(3-indole)(hydro)[60]fullerene **12** is also known in the literature.[32] Interestingly, while the reaction appears to also contain several side products, the C_{60}-H region of the ^{1}H NMR only has two, rather than the three major peaks one would expect for each of the three possible regioisomer, Figure 1.21. It's also possible that two of the regioisomers have nearly identical chemical shifts. This is corroborated by two sets of two peaks that appear to be, based on comparison to the starting indole fullerene, indole peaks of two isomers, Figure 1.22. There is also some of the corresponding 5FSC which, upon inspection of the starting material ^{13}C NMR, was due to residual C_{60}.

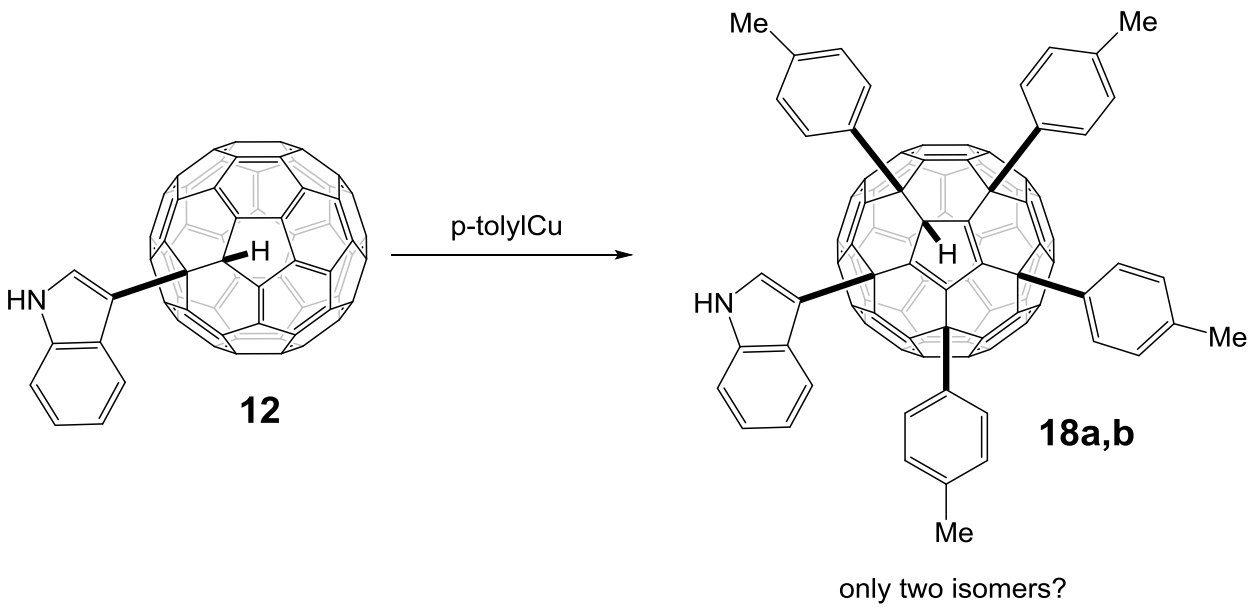

Figure 1.20. 1,2-(3-indole)(hydro)[60]fullerene **12** and corresponding MSCs **18a,b**.

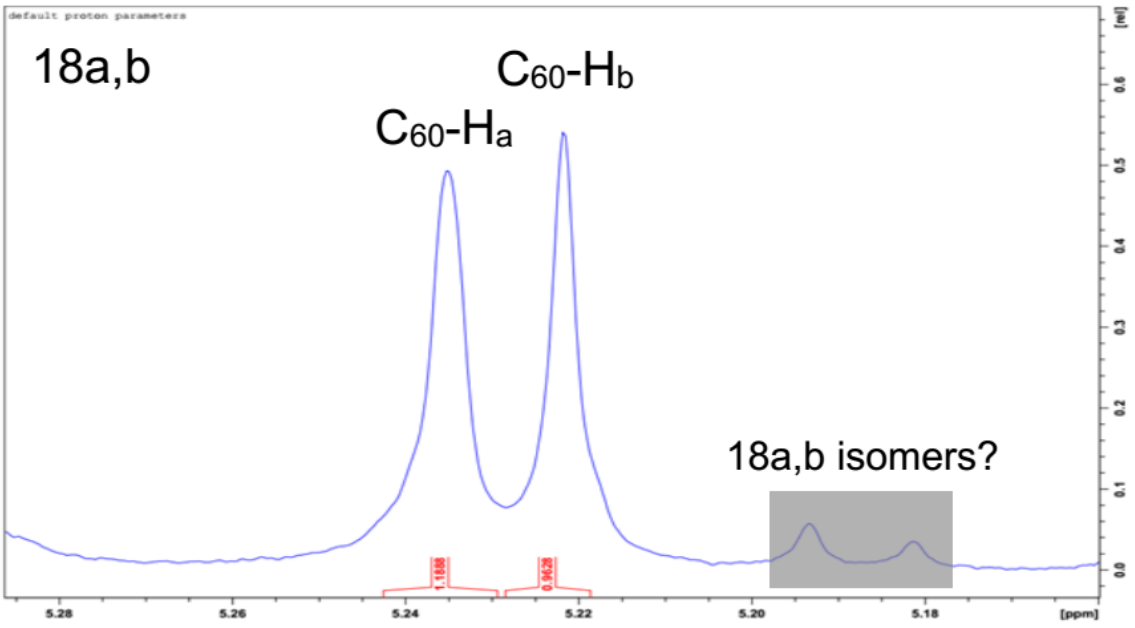

Figure 1.21. ^{1}H NMR of the C_{60}-H region (5.16–5.22 ppm) of a mixture of the 1,2-(3-indole)(hydro)[60]fullerene MSCs **18a,b.** Unlike the other MSCs, there are only two major peaks, instead of the expected three.

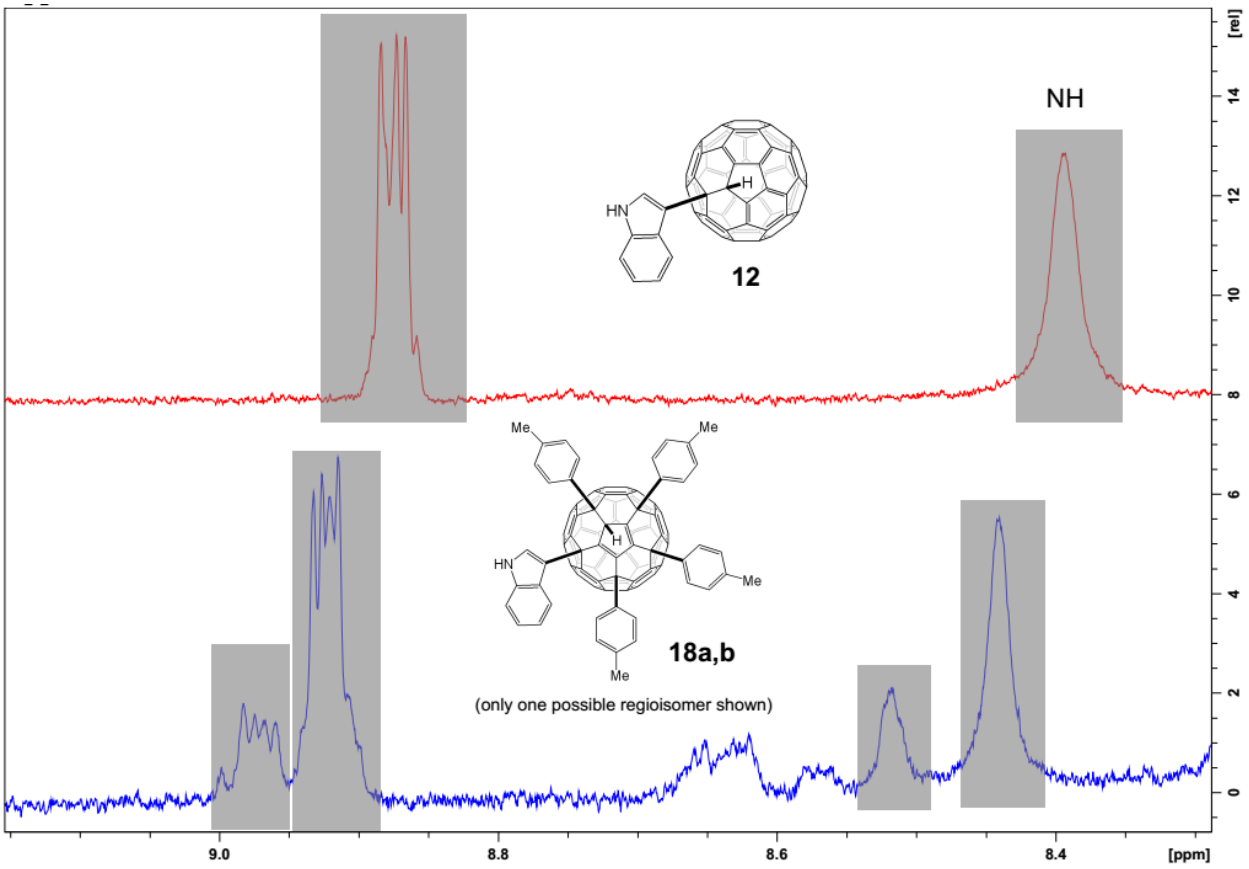

Figure 1.22. ^{1}H NMR comparison (8.3 to 10 ppm) of the indole fullerene **12** and its corresponding MSCs **18a,b.**

Indoles are well known for their addition-elimination chemistry at the 3-position of the indole ring.[33] It was envisioned that after addition of an electrophile to the indole ring of **12** or **18a,b**, the indole substituent would eliminate from the fullerene cage to produce the corresponding fullerene-alkene double bond, Figure 1.23. However, as of this writing, the chemistry of the indole-fullerenes has not been explored.

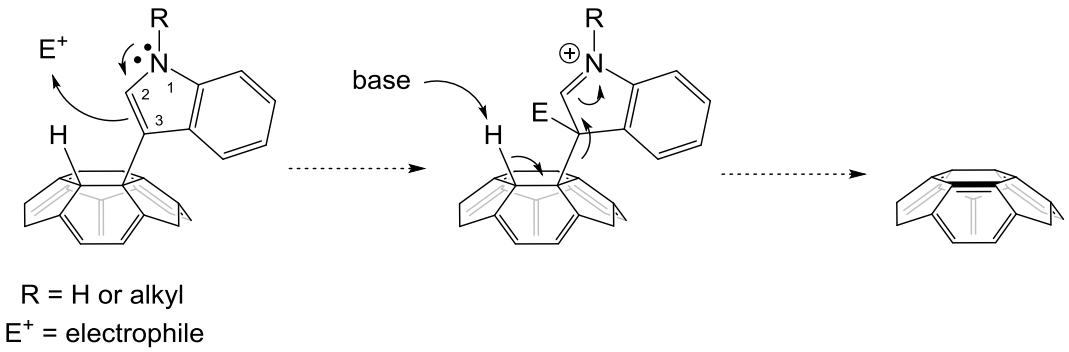

R = H or alkyl
E^+ = electrophile

Figure 1.23. Proposed electrophilic addition to the 3-postion of an indole-fullerene followed by a proposed elimination to from the corresponding alkene.

Allyl and Benzyl Groups as a Potential Defeathering Element

Unlike the other PGs above that are installed via nucleophilic addition to the fullerene cage, the allyl and benzyl substituents were added by first reducing the fullerene to its dianion, followed by nucleophilic substitution with the corresponding alkyl halide. One potential drawback of this approach is that, typically, a mixture of both the mono and bisadducts are formed, and depending on the polarity of the substituents, may not be easily separated, Figure 1.24.

The allyl group was envisioned to be removed thermally via a retro-ene reaction. Heating the allyl fullerene in refluxing *o*-DCB for 24 hours under inert atmosphere was not sufficient to induce the retro-ene reaction and this group was not pursued further. However, selective placement of electron donating/withdrawing groups on the allyl system or transition metal catalysts may help lower the reaction energy barrier.

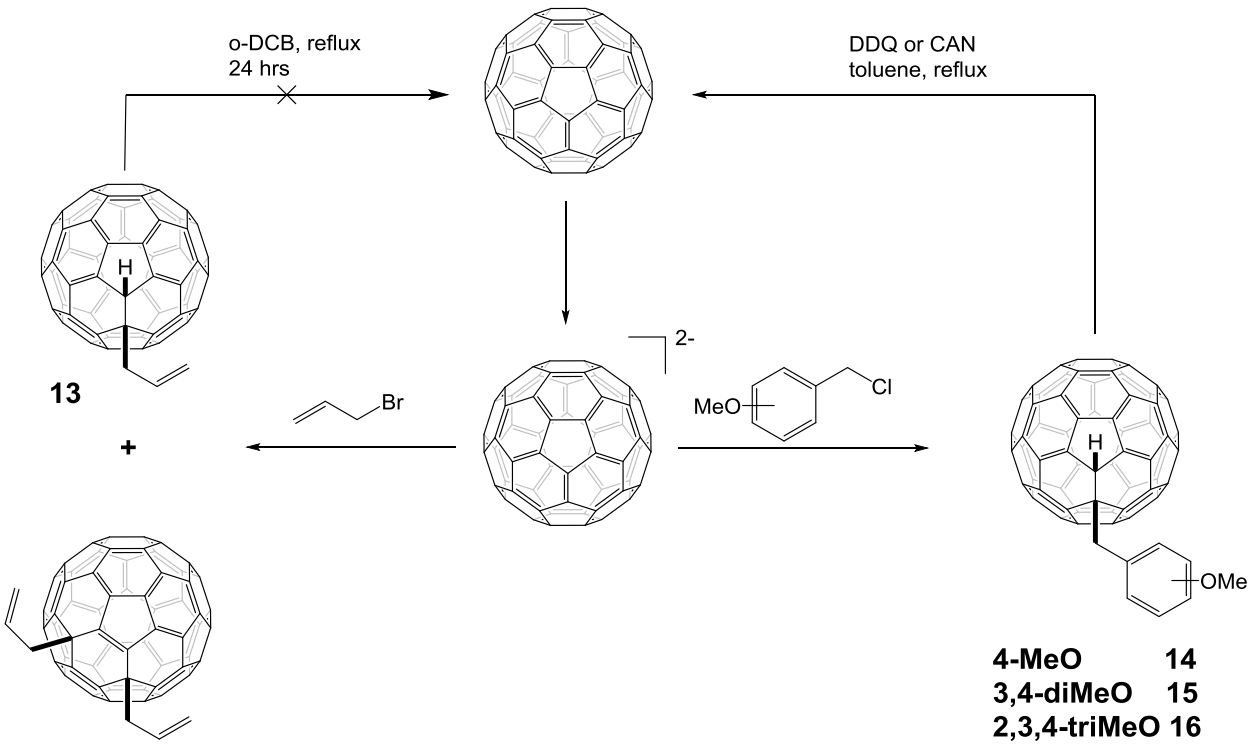

Figure 1.24. Synthesis of allyl and benzyl fullerenes via the fullerene dianion and removal of methoxybenzyl group to reproduce pristine C_{60}.

The most promising class of potential protecting groups were the methoxybenzyl adducts. These benzyl addends proved to be stable to both Grignard and arylcopper reagents, could be removed from benzylfullerene with DDQ or CAN to reproduce pristine C_{60} in high yield, and are available with a variety of different substituents that might be taken advantage of to give a wide range of reactivity/lability and other desirable properties, Figure 1.24.

Debenzylation Reaction

It was initially found that the p-methoxybenzyl adduct of the mixed shuttlecock could be removed, by heating in chloronaphthalene at 200 ^{o}C in a sealed tube with an excess of iodine to produce the desired 4FSC but in low yield (5-10%).[27] Not surprisingly, the 4FSC was not air or light stable, and would readily oxidize in air to the corresponding symmetric epoxide, as well as react with weak nucleophiles, such as methanol to from the addition product, Figure 1.25. Although demonstrating the proof of concept, these debenzylation conditions, being low yielding and difficult to scale, were less than ideal.

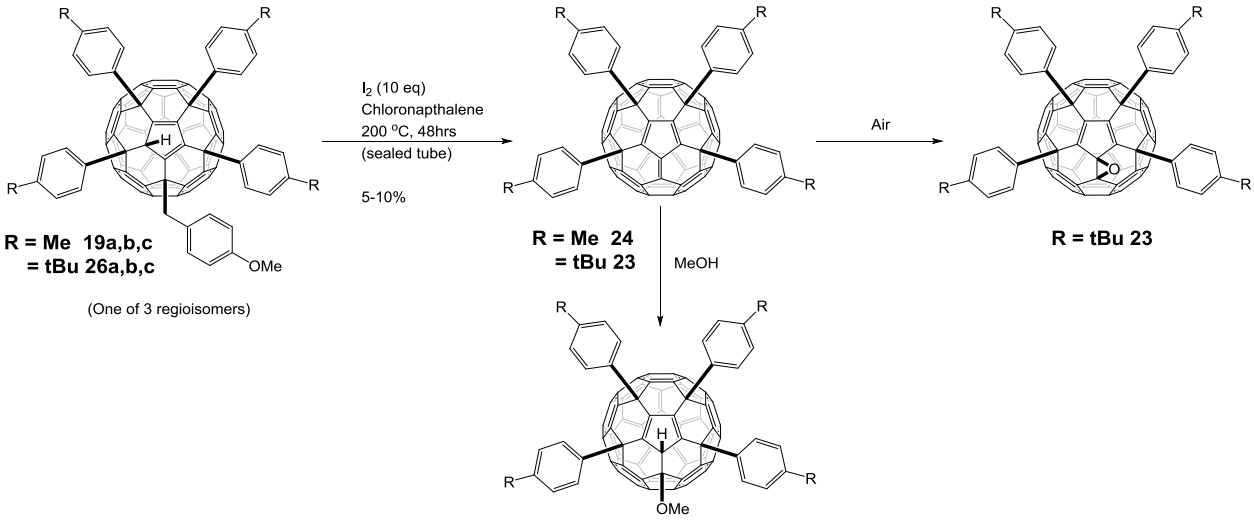

Figure 1.25. Debenzylation of p-methoxybenzyl MSCs to produce the 4FSCs. Aryl 4FSCs are unstable to air and react with weak nucleophiles.

In order to improve the yield of the debenzylation reaction, other oxidants as well as well as 3,4-dimethoxy- and 2,3,4-trimethoxy benzyl MSC were explored. Both DDQ and CAN have been commonly used to cleave benzyl ethers and it was promising to find that the 4-methoxy-, 3,4-dimethoxy-, and 2,3,4-trimethoxybenzyl-1-hydrofulleres were all

reverted to pristine C_{60} when treated with DDQ of CAN in refluxing toluene for 4 h in quantitative yield, Figure 24. However, under the same conditions, the benzyl MSCs did not produce any 4FSC, table 1.1.

When the p-methoxybenzyl MSCs were treated with an excess of DDQ at 25 ˚C, only starting material was recovered after 4 h. Surprisingly, when the reaction was refluxed for up to several hours, the corresponding 5FSC was recovered in 36 yield, table 1: rxn 1. While it was initially suspected that this was merely due to 5FSC impurity in the starting material, both its clear absence as well as relatively high yield (up to 38%), suggest instead that, after debenzylation, the 4FSC is being arylated by another SC in the solution.

When the 3,4-dimethoxybenzyl t-butylphenyl MSC was treated under the same conditions, three new TLC spots appeared. While the structure of some of the new compounds has not been determined, some information could still be gleaned from the ^{1}H NMR and ^{13}C NMR.

The most nonpolar spot is the corresponding tolyl 5FSC. It is interesting to note that the recovered yield of the corresponding 5FSC was only 5%, significantly lower than the same reaction with the monomethoxybenzyl MSC. One might expect that if the debenzylation was occurring via oxidation of the benzylic position, that the more electron-rich dibenzyl system would have at least a comparable yield.

Table 1.1. Debenzylation attempts on the benzyl MSCs.

Rxn	R	n	Solvent	oxidant	temp	time	Results
1	tBu	1	toluene	DDQ (10eq)	25 ˚C	4	No reaction
2	tBu	1	toluene	DDQ (10eq)	110	8	5FSC (36)
3	tBu	2	toluene	DDQ (10eq)	25 ˚C	2	No reaction
4	tBu	2	toluene	DDQ (10eq)	110	24	5FSC (5) Spot 2 (~17*) Spot 3 (17*)
5	tBu	2	toluene	CAN (10eq)	25 ˚C	2	No reaction
6	tBu	2	toluene	CAN (10eq)	110	8	degraded
7	tBu	2	ODCB	DDQ (10eq)	180	8	5FSC (30)
8	tBu	2	ODCB	None	180	2	No reaction
9	tBu	2	CH_2Cl_2	$KMnO_4$ (1eq)	25 ˚C	72	5FSC (10) S.M. (26)
10	tBu	3	chlorobenzene	DDQ (10eq)	25 ˚C	3	No reaction
11	tBu	3	chlorobenzene	DDQ (10eq)	80	48	5FSC (10)
12	Me	3	ODCB	DDQ (1eq)	180	12	5FSC (18) S.M. (28)
13	Me	3	ODCB	DDQ (10eq)	140	16	5FSC (38)
14	Me	3	ODCB	DDQ (1eq)	140	16	5FSC (20)
15	Me	3	ODCB	DDQ (2eq)	140	16	5FSC (50)
16	OMe	3	ODCB	DDQ (10eq)	140	16	5FSC (53)
17	OMe	3	ODCB	I_2 (10eq)	140	12	5FSC (26)
18	Me	1	1-chloronaphthalene	I_2 (10eq)	200	48	4FSC (5)
19	tBu	1	1-chloronaphthalene	I_2 (10eq)	200	48	4FSC (6)

*yield estimated by assuming mass for 5FSC.

The next most non-polar spot appears to be one compound that is an asymmetric SC that still contains the dimethoxy benzyl group. One can clearly see the two benzyl methoxy groups present in the ^{1}H NMR, Figure 1.26. Examination of the C_{60}-H chemical shifts also clearly shows that this is a new compound and not simply one of the asymmetric starting material regioisomers, Figure 1.27. Curiously, a distinct peak for the benzyl hydrogens is absent. However, one of the methoxy benzyl peaks has a relative integration of 4 H's, suggesting that there is a single benzylic hydrogen overlapping with the methoxy group at 3.74 ppm, Figure 1.26. This would be consistent with DDQ oxidation at the benzylic position, but it is not clear why this would lead to only one regioisomer. Furthermore, the most likely position of the C_{60}-H is at the position closest to the benzyl substituent, because placement at either of the other two possible positons would lead to a set of diastereomers, Figure 1.28.

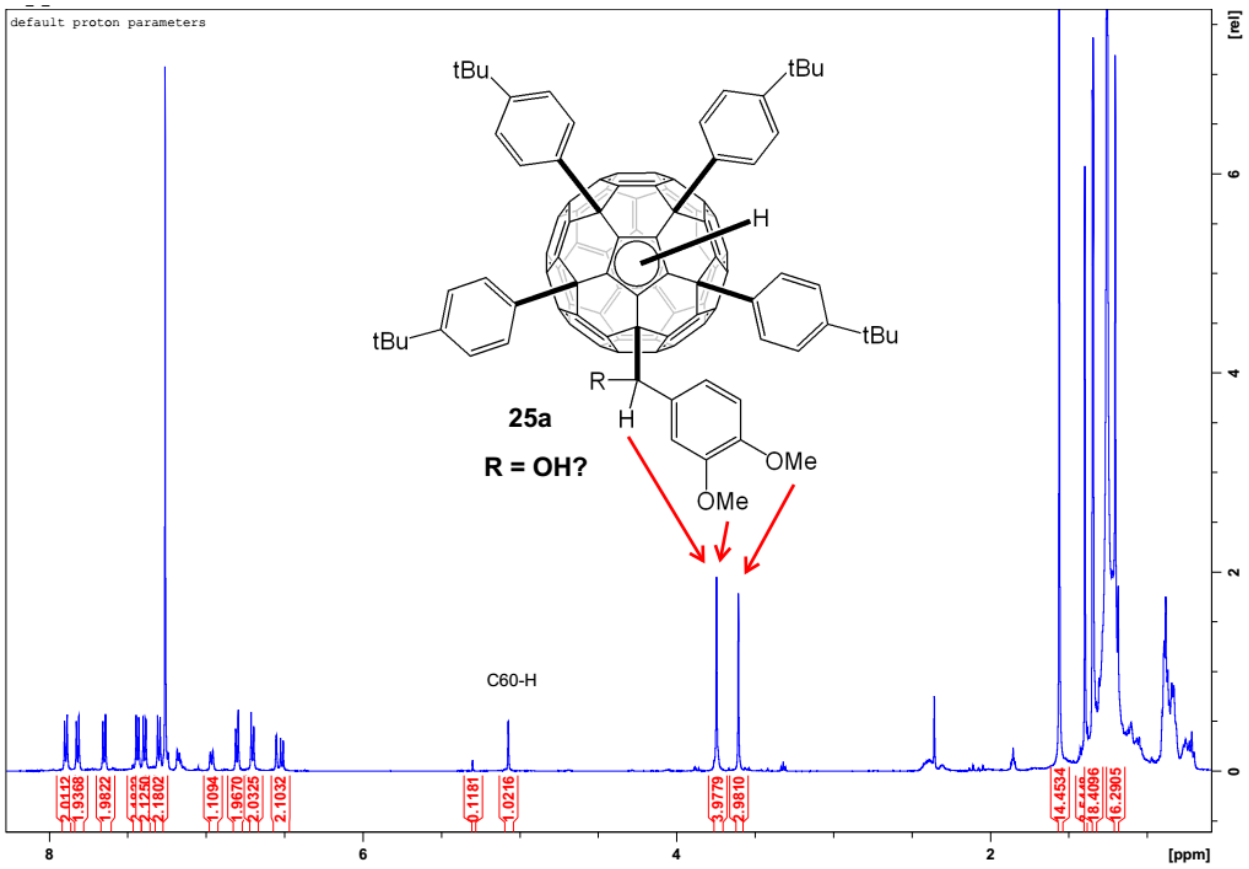

Figure 1.26. ^{1}H NMR of spot 2, showing proposed overlap of a single benzyl hydrogen peak with the methoxy peak at 3.74 ppm.

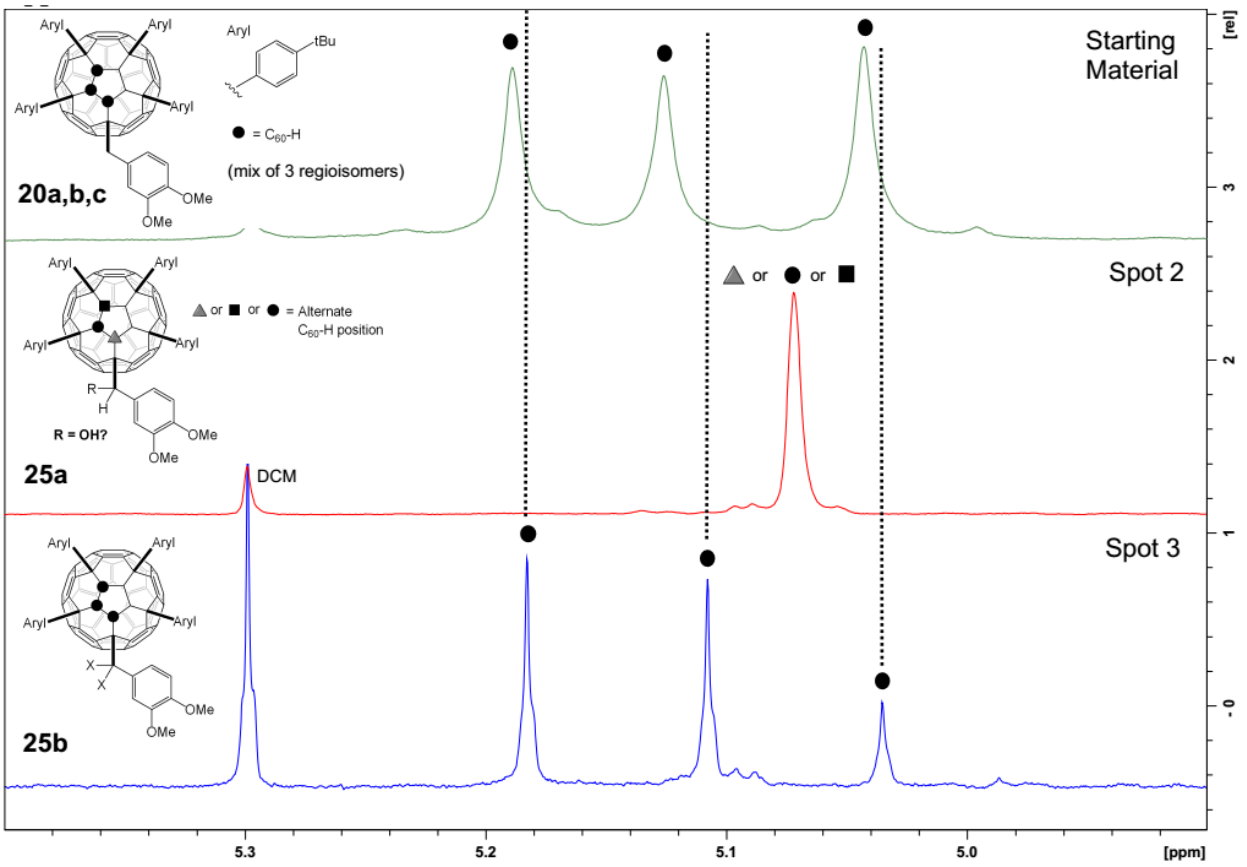

Figure 1.27. ^{1}H NMR comparison of the C_{60}-Hs of dimethoxybenzyl t-butylphenyl MSC, spot 2, and spot 3.

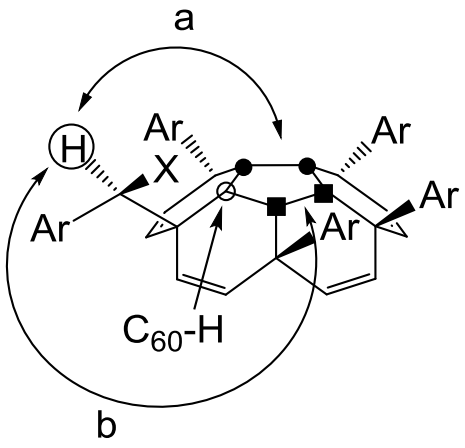

Figure 1.28. One of two possible enantiomers for spot 2 showing that any C_{60}-H position, other than the one closest to the benzyl substituent (open circle), would lead to a set of two diastereoisomers: 'a'-side (dark circle) vs. 'b'-side (dark square)

Examination the ^{13}C NMR also indicates that this is a single, asymmetric regioisomer with a new substituent at the benzylic position. In the aryl region, the 54 chemically distinct fullerene sp^2-C peaks, as well as the four unique sets of aryl “feather” peaks, confirms that compound is asymmetric, Figure 1.29. The methoxy, benzyl, and sp^3 fullerene carbons (indicating the number of substituents that are attached) all appear between 50-75 ppm, Figure 1.30. There is a total of nine peaks in this region, corresponding to the two methoxy carbons, one benzylic carbon, and the six fullerene carbons, which clearly shows that this new compound is not the result of a new addition to the fullerene cage, confirming that the alteration could only have occurred at the benzylic position. The absence of any additional unaccounted for aryl peaks eliminates DDQ or the solvent from being the new substituent, and it is proposed that this new substituent is most likely a hydroxy group from adventitious water, which is consistent with the DDQ benzyl ether cleavage mechanism.

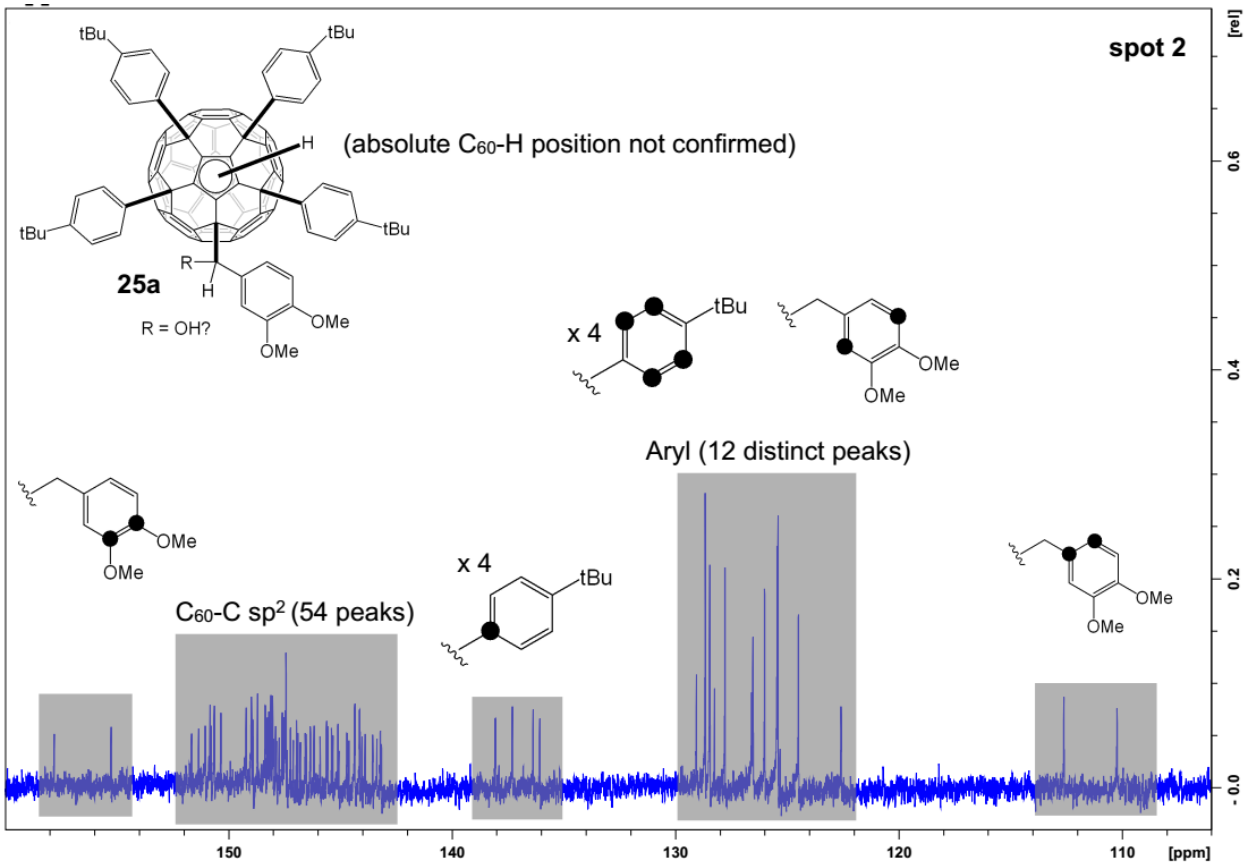

Figure 1.29. ^{13}C NMR (100-160 ppm) of spot 2 (**25a**) showing the expected number of aryl and sp^2-C_{60} signals for an asymmetric MSC and no addition carbon signals.

Finally, the most polar TLC spot, which has almost the same polarity as the starting material, appears to be a mixture of three isomers. Comparison of the aryl, C_{60}-H, benzyl/methoxy, and aryl tert-butyl ^1H NMR regions, shows that, while similar to the starting mixture of isomers, these isomers are not the same set of compounds, Figure 1.27. Unfortunately, a ^{13}C NMR could not be obtained, so with only the ^1H NMR available, it was not possible to determine what exact chemical change had occurred.

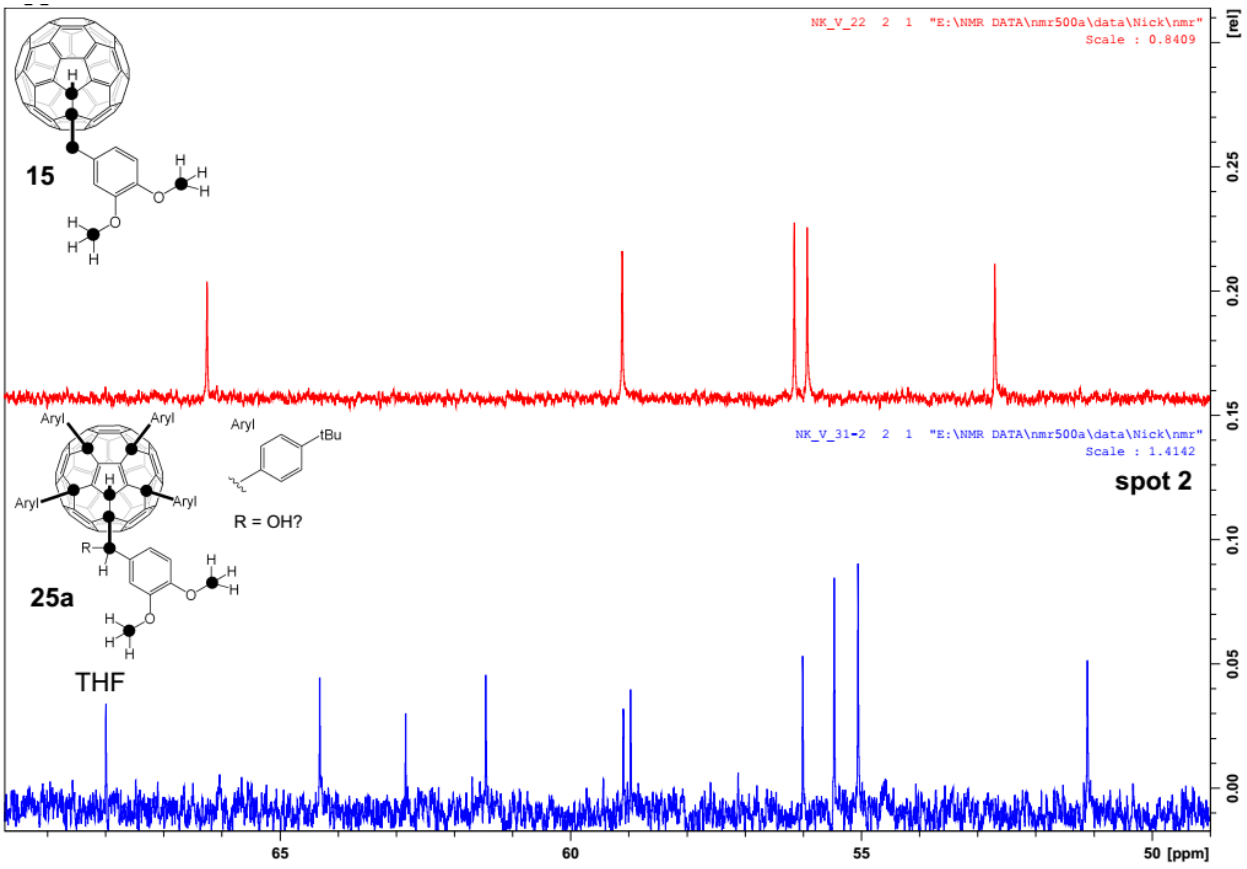

Figure 1.30. ^{13}C NMR Comparison of methoxy, benzyl, and sp^3-C_{60} carbon signals from 3,4-dimethoxybenzyl fullerene **15** (top) and spot 2, **25a** (bottom).

When the solvent was changed to *o*-DCB and the temperature was increased to 180 ºC, only the 5FSC was isolated, but now with a 30% yield, Table 1: rxn 7. Replacing the dimethoxy benzyl group with the 2,3,4,-trimethoxybenzyl group also gave similar results, Table 1.1, rxns 13-16.

In the absence of an oxidant under inert atmosphere, both the MSC and the 5FSCs do not react under the reaction conditions, Table 1.1: Rxn 8 and Table 2: Rxn 1 and 4. For the 5FSCs, when DDQ is present, most of the material degrades, Table 1.2: Rxn 2

and 4. The small amount of recoverable material appears by ^{1}H NMR to be a large mixture of products. MALDI-MS of the reaction shows a shift of the base peak from 1255 m/z (5FSC MW = 1257.33), Figure 31, to 1165 (4FSC epoxide MW = 1165.19), Figure 32, suggesting that the presence of DDQ induces loss of at least one aryl feather from the 5FSC. When the reaction was repeated in the presence of $C_{60,}$ Table 1.2: Rxn 3, about 20% of the 5FSC and 20% of pristine C_{60} were recovered, as well as a large mixture of other products. MALDI-MS of this mixture of products shows an increase in the relative intensity of the peaks at m/z 828 ($ArC_{60}H$ MW = 8282.8) and m/z 1041 ($Ar_3C_{60}H$ MW = 1043.06). While not conclusive, this is at least a consistent transfer of several aryl groups from the 5FSC to C_{60}.

Table 1.2. Reaction were carried out in *o*-DCB at 140° C for 6 h.

RXN	**SC**	**Conditions**	**Results**
1	Tolyl 5FSC	No oxidant	No Reaction
2	Tolyl 5FSC	DDQ (10eq)	Complex mixture of products
3	Tolyl 5FSC + C_{60}	DDQ (10eq)	Isolated C_{60} but no 5FSC
4	Anisoyl 5FSC	No oxidant	No reaction
5	Anisoyl 5FSC	DDQ (10eq)	Complex Mixture of Products (~10%)
6	Anisoyl 5FSC + C_{60} (1eq)	DDQ (10eq)	C_{60} (20%) 5FSC (20%) Other (16%)
7	Tolyl MSC + C_{60} (1eq)	DDQ (10eq)	C_{60} (18%) 5FSC (18%)
8	Tolyl MSC (1eq) Anisoly MSC (1eq)	DDQ (20eq)	Tolyl 5FSC (10%) Anisoyl 5FSC (10%)

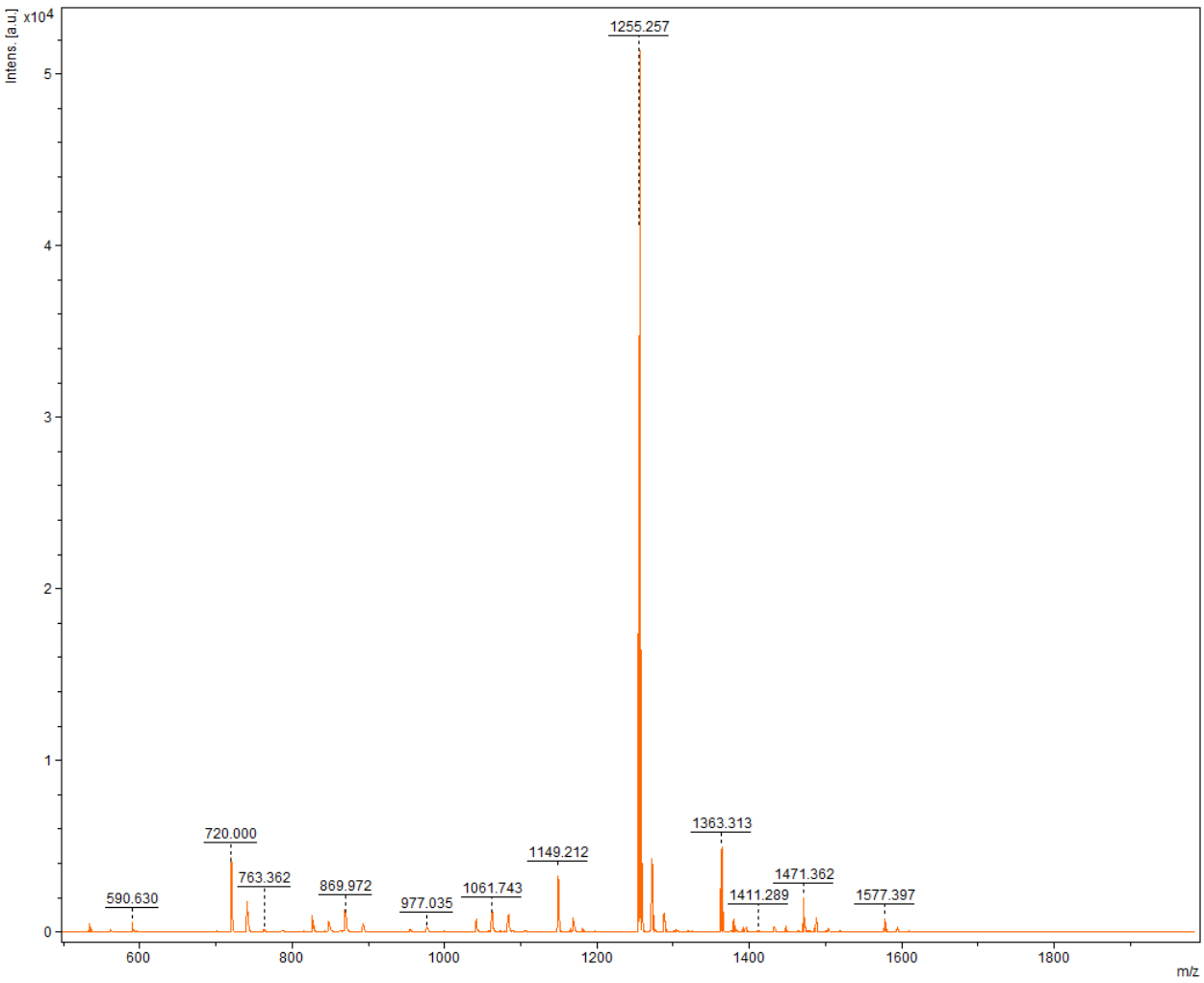

Figure 1.31. MALDI-MS spectrum of p-methoxy 5FSC, m/z 1255 (MW = 1257.33).

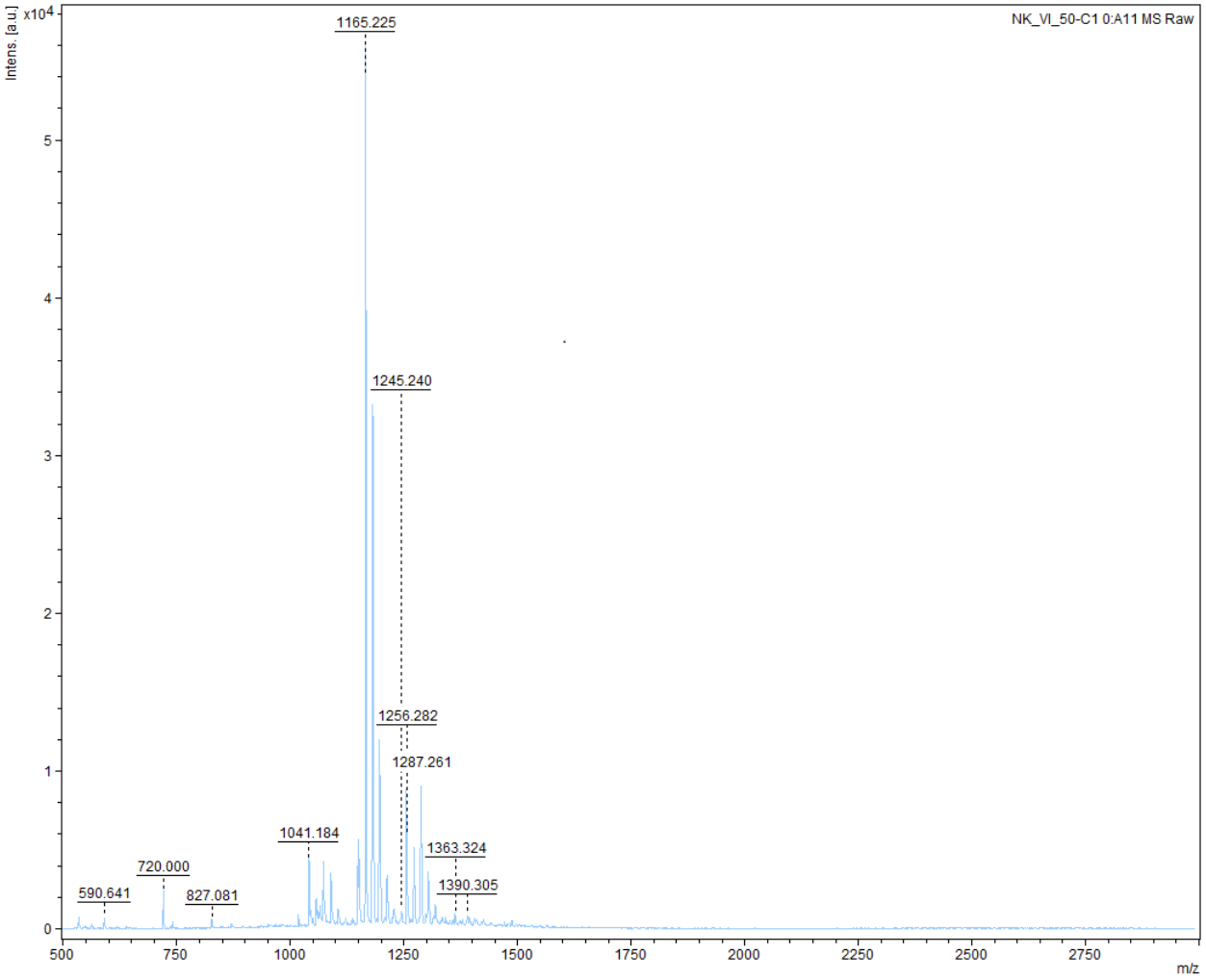

Figure 1.32. MALDI-MS of the reaction of p-methoxyphenyl 5FSC after being treated with DDQ (10eq) at 140° C in *o*-DCB for 16 h.

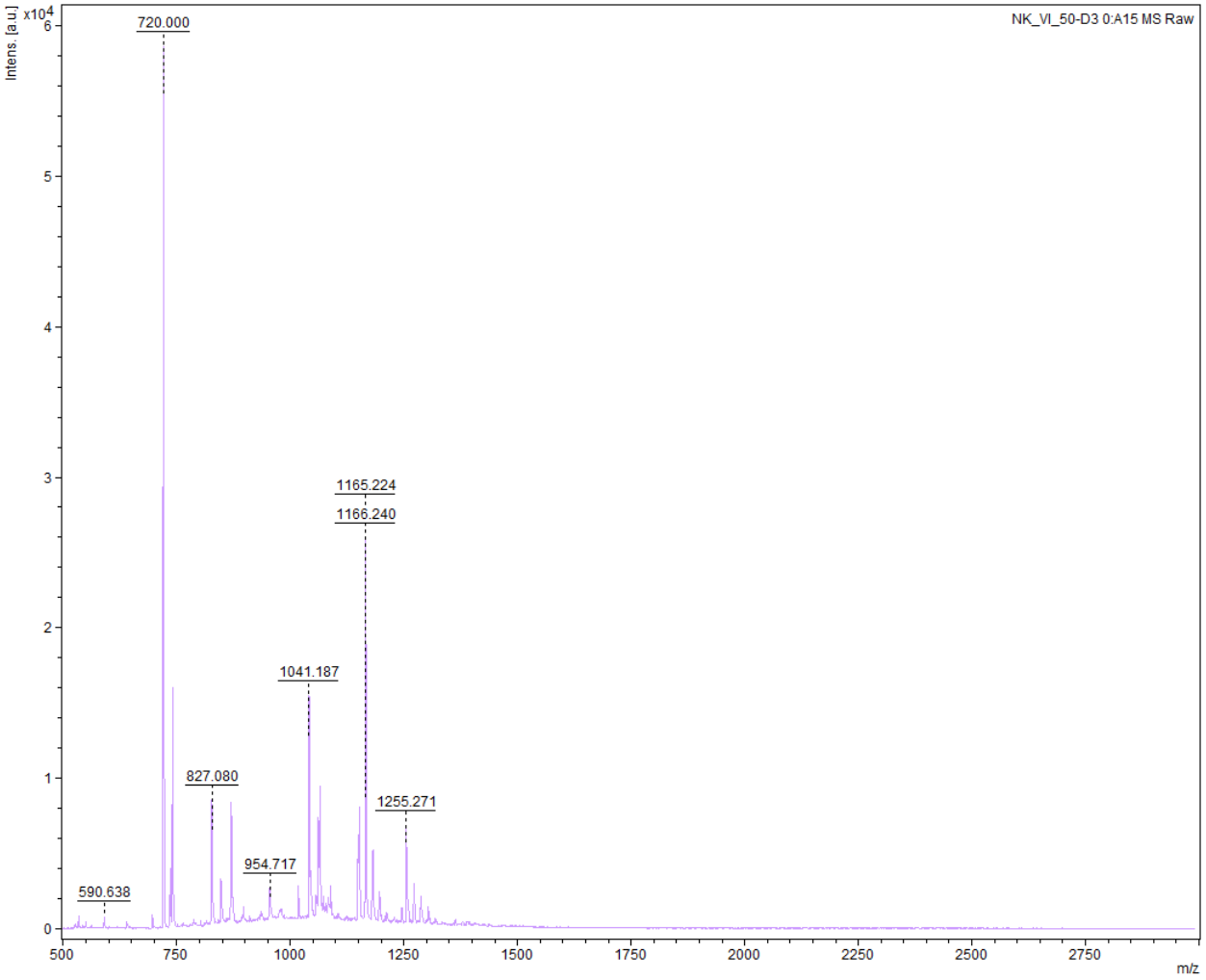

Figure 1.33. MALDI-MS of the reaction of p-methoxyphenyl 5FSC after being treated with DDQ (10eq) and C_{60} (1eq) at 140° C in *o*-DCB for 16 h.

Based on these results, a tentative general mechanism for the aryl debenzylation and aryl transfer reactions is proposed, Figure 1.34: DDQ (or another oxidant) induces the net loss of a hydride anion from the benzylic position of the MSC to produce a benzyl cation. Water or another nucleophile then adds to the benzylic position. The benzyl group is cleaved from the MSC to produce a dihydro 4FSC which is then oxidized by a second equivalent of DDQ to the 4FSC. The oxidant can also oxidize one of a fullerene's aryl

groups, producing an aryl radical cation. The aryl cation is then cleaved by elimination to an aryl radical and a dearylated fullerene SC. This aryl radical can then add to another fullerene. In the case of the 4FSC, this addition occurs selectively at the fulvene position, producing the 5FSC radical, which then abstracts a proton to product the 5FSC.

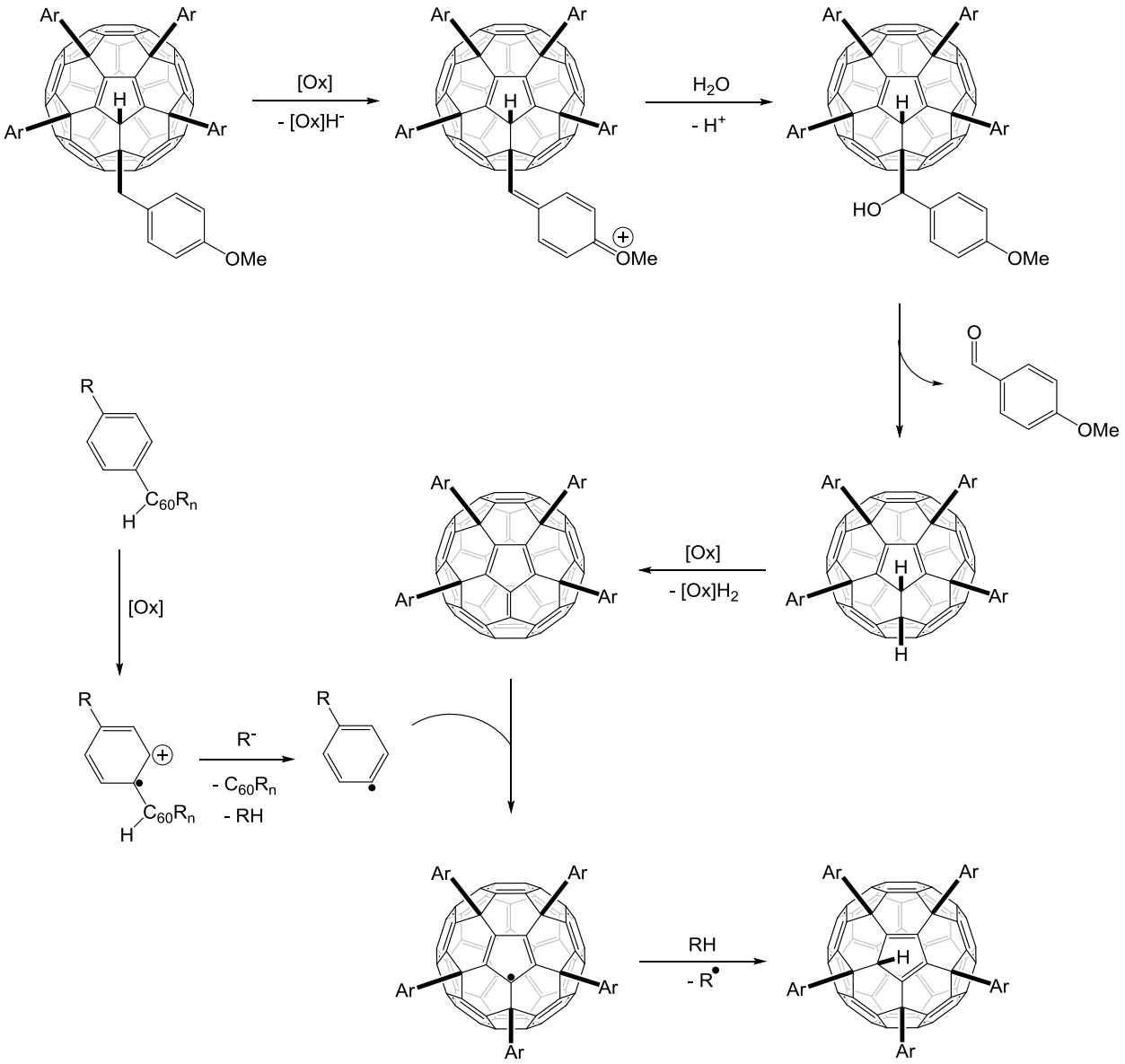

Figure 1.34. Proposed mechanism of SC fullerene aryl transfer in the presence of an oxidant.

To further test this mechanism, the reaction was repeated with a 1:1 mixture of the tolyl and anisoyl MSCs. If an aryl transfer is occurring, it would be expected that a mixture of MSCs with two different aryl groups should produce a mixture of 5FSCs, Figure 1.35. Unfortunately, while both the corresponding 5FSCs were produced, no mixed 5FSCs were detected. However, more experiments are needed before any conclusion can be drawn.

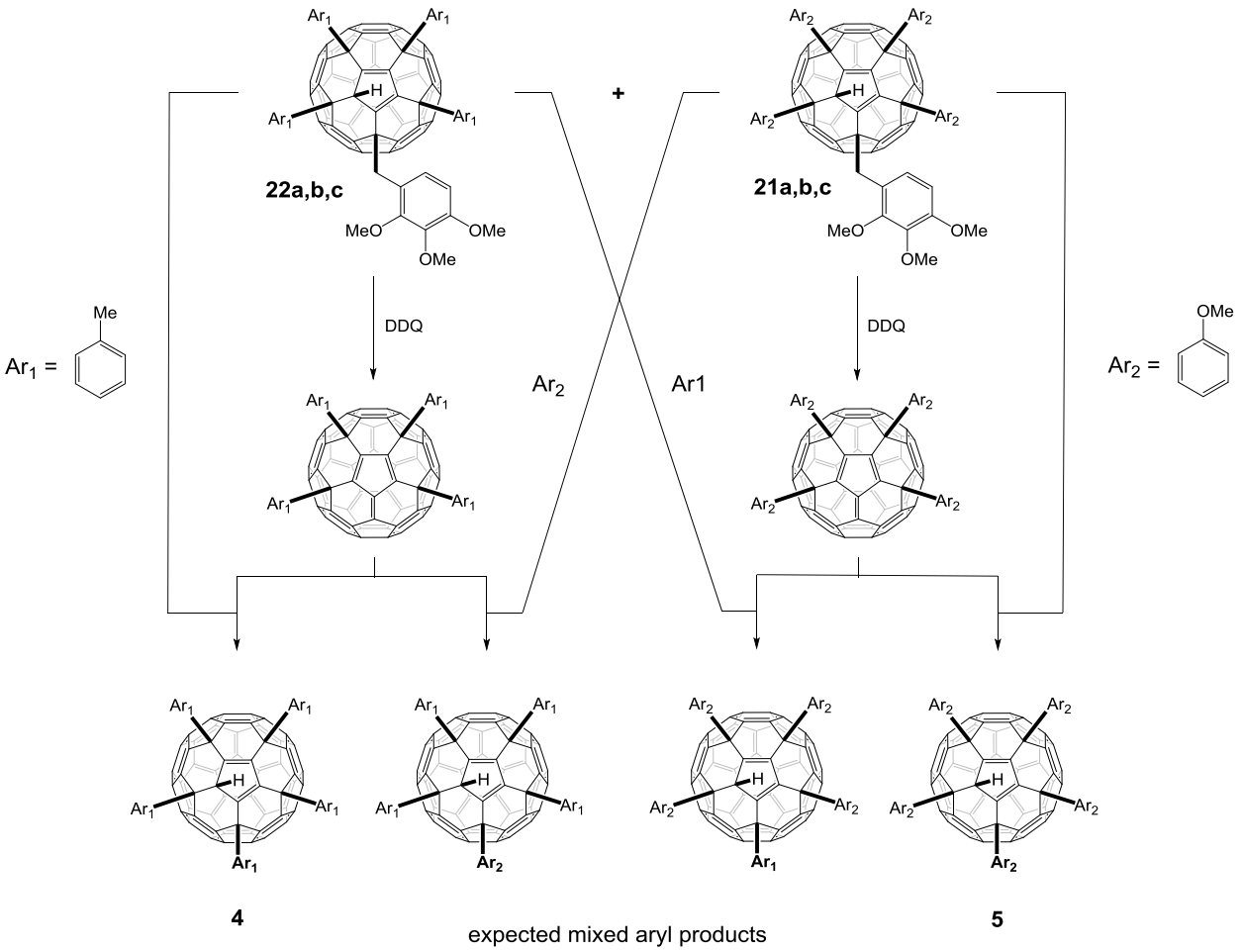

Figure 1.35. Diagram showing the four expected 5FSCs resulting from aryl mixing of two MSCs with different aryl groups.

Conclusion

It has been demonstrated here that certain addends, at least those that form carbon-carbon bonds with the fullerene cage, i.e. alkynyl, N-indolyl, allyl, and benzyl groups, are sufficiently stable to survive the aryl copper addition and produce MSC products. In the case of the methoxybenzyl MSC, the benzyl group can be removed at high temperature with iodine, and under the right conditions produces the corresponding 4FSC albeit in a very low yield. Unfortunately, due to the “mercurial” nature of many fullerene derivatives and the difficulty analyzing them, the DDQ induced debenzylation of benzyl MSCs remains inconclusive. While not ultimately producing the desired 4FSCs, oxidative cleavage does remove the benzyl group and potentially induces an unprecedented aryl transfer that should be explored further. Should removal of the benzyl system ultimately prove itself to be too difficult, removal of an alkynyl, indole or allyl group may not have been exhaustively explored, and may yield more fruitful results as a general method for synthesizing 4FSCs.

Experimental

General Experimental Details: All reactions were performed under argon unless otherwise stated. THF was dried by distillation over calcium hydride and stored over activated 4 Å Mol. Sieves. *o*-Dichlorobenzene was purchased anhydrous from Sigma-Aldrich. Proton and carbon nuclear magnetic resonance (1H and 13C) spectra were recorded in deuterated solvents on Bruker AV-500 (500 MHz) or DRX-400 (400 MHz) spectrometers at 298 K (20 ˚C) unless specified otherwise. Chemical shifts are reported in ppm, relative to residual $CHCl_3$ (δ 7.26). Mass spectra were recorded on a Bruker Ultraflex MALDI TOF-TOF.

MALDI-TOF MS data is only provided here for several compounds. The fullerene SCs are sensitive to choice of matric and produce widely different results with choice of matric. Often exchanging aryl groups to produce a wide range of masses, even with pure SCs (confirmed by NMR). It was found that the best matrix was 9-nitroanthracene, which was used to acquire all MALDI-TOF data.

6,9,12,15,18-Pentakis(N,N-diphenylamino-4-phenyl)-1-hydro[60]fullerene (1): The procedure given here for the synthesis of **1** deviates from the literature procedure due to difficulties forming the Grignard of 4-bromo-N,N-diphenylaniline.[18] It was found that bromo/lithium exchange using 2 eq of *tert*-Butyl lithium gave more reliable results. In a dry round-bottomed flask, 4-bromo-N,N-diphenylaniline (676 mg, 2.09 mmol, 15 eq) was dissolved in dry THF and cooled to -78 ^oC. tert-Butyl lithium (1.6 M pentane, 2.6 mL, 30 eq) was added dropwise and the reaction was allowed to stir at -78 ^oC for 1 h. The reaction was warmed to 0 ^oC and then added to a solution of $CuBr{\cdot}SMe_2$ (429 mg, 2.09 mmol, 15

eq) in 1 mL of THF. The reaction was allowed to stir for 30 min at 0 ºC, warmed to 25 ˚C and then a solution of C_{60} (100 mg, 0.139 mmol, 15 eq) dissolved in 5 mL of dry *o*-DCB was added. The reaction was allowed to stir for 8 h at 25 ˚C before being quenched with saturated ammonium chloride. The organic layer was separated and the crude product was precipitated with methanol. After filtration, purification through silica gel chromatography (hexane/toluene 1:1) afforded 122 mg (50%) of **1** as a red powder. ^{1}H NMR (500 MHz, $CDCl_3$) δ 7.64 (d, *J* = 8.5 Hz, 1H), 7.54 (d, *J* = 8.5 Hz, 1H), 7.39 (d, *J* = 8.6 Hz, 1H), 7.30 – 6.85 (m, 60H), 5.31 (s, 1H); ^{13}C NMR (126 MHz, $CDCl_3$) δ 156.05, 152.58, 152.26, 151.76, 148.72, 148.64, 148.62, 148.34, 148.21, 148.03, 147.81, 147.80, 147.67, 147.46, 147.44, 147.34, 147.19, 147.11, 147.03, 146.90, 146.81, 146.01, 145.94, 145.72, 145.38, 144.46, 144.33, 144.26, 144.16, 144.10, 144.04, 143.85, 143.13, 134.13, 133.93, 132.56, 130.50, 129.26, 129.22, 129.19, 129.16, 129.03, 129.00, 128.73, 128.20, 127.67, 127.27, 125.27, 124.41, 124.26, 124.20, 124.12, 124.05, 123.95, 123.82, 122.99, 122.84, 122.76, 122.62, 63.02, 60.51, 58.51, 58.33.

6,12,15,18-Tetrakis(N,N-diphenylamino-4-phenyl)-1,9-epoxy[60]fullerene (2). Synthesis of 2 followed the literature procedure.[18] Fullerene **1** (500 mg, 0.258 mmol, 1 eq) was dissolved in 20 mL of *o*-DCB. In air, potassium tert-butoxide (1M THF, 33 uL, 1.3 eq) was added and the reaction was allowed to stir for 8 h. The solvent was evaporated, the residue dissolved in carbon disulfide an purified through silica gel chromatography (carbon disulfide/DCM 9:1) to afford 220mg (100%) of **2** as a red powder. ^{1}H NMR (500 MHz, $CDCl_3$) δ 7.74 – 7.69 (m, 4H), 7.51 – 7.47 (m, 1H), 7.20 – 7.12 (m, 8H), 7.09 – 6.92 (m, 16H); ^{13}C NMR (126 MHz, $CDCl_3$) δ 156.81, 152.50, 151.14, 149.24, 148.95, 148.15, 147.96, 147.87, 147.80, 147.72, 147.62, 147.52, 147.46, 147.43, 147.28, 146.76, 146.49,

146.45, 146.36, 145.53, 145.27, 144.69, 144.66, 144.17, 144.04, 143.44, 139.85, 138.16, 133.27, 133.24, 129.31, 129.26, 129.12, 128.96, 124.36, 124.17, 124.16, 124.07, 123.04, 122.92, 75.58, 72.81, 62.42, 59.13.

General procedure for the synthesis of 6,9,12,15,18-pentakisaryl-1-hydro[60]fullerenes:[4] To a dry round-bottomed flask was added freshly ground magnesium turnings (15 eq). Dry THF (0.2M) and a small crystal of Iodine was added and the reaction vessel was flushed with argon. Phenyl bromide (15 eq) was added dropwise and heating was applied if necessary. The reaction was allowed to proceed until all of the magnesium turnings were consumed. The reaction mixture was then cannulated, slowly, into another dry round-bottomed flask containing $CuBr{\cdot}SMe_2$ in *o*-DCB (15 eq) cooled to 0 ^oC. The reaction was allowed to stir at 0 ^oC for 1 h, and then a sparged solution of C_{60} (1 eq) in *o*-DCB was added. The reaction was allowed to warn to room temperature stirred for 4-8 h before being quenched with saturated ammonium chloride. The organic layer was separated and either methanol or pentane was added to precipitate the crude product. After filtration, the crude solid was dissolved in carbon disulfide and purified through silica gel chromatography (pentane/DCM 1:1 to DCM 100%) to afford the desired shuttlecock as a red solid.

6,9,12,15,18-Pentakis(4-*tert*-butylphenyl)-1-hydro[60]fullerene (3): Synthesis of **3** follows the general procedure to afford (71%).[4] ^1H NMR (500 MHz, CDCl3) δ 7.67 (d, J = 8.6 Hz, 4H), 7.48 (d, J = 8.6 Hz, 4H), 7.32 (d, J = 8.6 Hz, 4H), 7.28 (d, J = 8.6 Hz, 2H), 7.17 (d, J = 8.6 Hz, 4H), 7.10 (d, J = 8.6 Hz, 2H), 5.20 (s, 1H), 1.34 (s, 18H), 1.29 (s, 18H), 1.25 (s, 9H); ^{13}C NMR (126 MHz, $CDCl_3$) δ 156.44, 152.41, 151.88, 150.57, 150.27, 149.92, 148.73, 148.67, 148.38, 148.23, 148.07, 148.05, 148.02, 147.72, 147.19, 147.08,

146.88, 146.35, 146.07, 145.79, 145.53, 144.65, 144.33, 144.28, 144.22, 144.10, 144.04, 144.00, 143.10, 142.86, 136.90, 132.56, 130.53, 128.00, 127.90, 127.70, 127.48, 125.62, 125.44, 125.34, 62.93, 60.71, 58.67, 58.56, 34.53, 34.43, 34.33, 31.31, 31.26, 31.20.

6,9,12,15,18-Pentakis(4-methylphenyl)-1-hydro[60]fullerene (4): Synthesis of **4** follows the general procedure to afford (71%). ^{1}H NMR (400 MHz, $CDCl_3$) δ 7.65 (d, *J* = 8.1 Hz, 4H), 7.48 (d, *J* = 8.2 Hz, 4H), 7.29 (d, *J* = 8.2 Hz, 2H), 7.13 (d, *J* = 7.9 Hz, 4H), 7.00 (d, *J* = 7.9 Hz, 4H), 6.96 (d, *J* = 8.0 Hz, 2H), 5.22 (s, 1H), 2.38 (s, 6H), 2.33 (s, *J* = 7.3 Hz, 6H), 2.28 (s, *J* = 8.0 Hz, 3H); ^{13}C NMR (126 MHz, $CDCl_3$) δ 156.24, 152.65, 152.45, 151.76, 148.70, 148.65, 148.36, 148.22, 148.05, 148.00, 147.72, 147.19, 147.09, 146.90, 146.29, 145.96, 145.76, 145.49, 144.55, 144.35, 144.29, 144.20, 144.07, 143.98, 143.82, 143.08, 142.92, 137.30, 137.03, 136.89, 136.84, 136.75, 132.16, 129.48, 129.38, 129.23, 129.10, 128.18, 128.00, 127.86, 127.60, 62.94, 60.73, 58.68, 58.61, 21.13, 21.06, 20.91. MALDI-TOF MS (1176)

6,9,12,15,18-Pentakis(4-methoxyphenyl)-1-hydro[60]fullerene (5): Synthesis of **5** follows the general procedure to afford (71%). ^{1}H NMR (500 MHz, $CDCl_3$) δ 7.68 (d, *J* = 8.7 Hz, 4H), 7.51 (d, *J* = 8.8 Hz, 4H), 7.32 (d, *J* = 8.7 Hz, 2H), 6.87 (d, *J* = 8.8 Hz, 4H), 6.74 (d, *J* = 8.8 Hz, 4H), 6.70 (d, *J* = 8.8 Hz, 2H), 5.21 (s, 1H), 3.84 (s, 6H), 3.79 (s, 6H), 3.76 (s, 3H); ^{13}C NMR (126 MHz, $CDCl_3$) δ 159.08, 158.89, 158.58, 156.25, 152.56, 152.40, 151.77, 148.73, 148.67, 148.65, 148.38, 148.23, 148.07, 147.93, 147.72, 147.19, 147.09, 146.19, 145.96, 145.71, 145.40, 144.49, 144.41, 144.31, 144.25, 144.11, 144.00, 143.78, 143.11, 138.08, 131.99, 131.90, 130.53, 129.26, 129.10, 128.82, 127.73, 127.70, 127.01, 114.22, 114.11, 113.96, 113.81, 113.72, 113.48, 113.41, 67.97, 63.01, 60.30, 58.31, 58.20, 55.44, 55.40, 55.37, 55.27. MALDI-TOF MS (m/z 1256)

9,12,15,18-Tetrakis(4-*tert*-butylphenyl)-1,9-epoxy[60]fullerene (6) and 6,9,12,18-tetratakis(4-*tert*-butylphenyl)-1,2-epoxy[60]fullerene (7): Synthesis of epoxides **6** and **7** followed the same procedure as the synthesis of compound **2** starting from compound **3** instead of compound **1**.[18] The crude mixture containing epoxides **6** and **7** was purified through silica gel chromatography (CS_2 100% to DCM 100%) eluting first **6** followed by **7** to afford:

Compound **6**, 14mg (8%) as a red solid. ^{1}H NMR (500 MHz, $CDCl_3$) δ 7.77 (d, *J* = 8.3 Hz, 4H), 7.45 (d, *J* = 8.4 Hz, 4H), 7.40 (d, *J* = 8.4 Hz, 4H), 7.16 (d, *J* = 8.4 Hz, 4H), 1.34 (s, 18H), 1.27 (s, 18H); ^{13}C NMR (126 MHz, $CDCl_3$) δ 157.07, 152.83, 151.11, 150.68, 150.62, 149.20, 148.93, 148.15, 148.12, 148.06, 147.84, 147.80, 147.61, 147.44, 147.27, 146.78, 146.54, 146.44, 146.37, 145.57, 145.54, 145.42, 144.76, 144.64, 144.59, 144.12, 144.03, 143.40, 139.73, 138.19, 136.32, 136.29, 127.86, 127.74, 125.91, 125.61, 75.61, 72.77, 62.62, 59.30, 53.44, 34.57, 34.45, 31.33, 31.22.

Compound **7**, 10 mg (5%) as a red solid. ^{1}H NMR (500 MHz, $CDCl_3$) δ 7.87 (d, *J* = 8.4 Hz, 2H), 7.67 (d, *J* = 8.4 Hz, 2H), 7.64 (d, *J* = 8.4 Hz, 2H), 7.50 (d, *J* = 8.4 Hz, 2H), 7.36 (d, *J* = 8.4 Hz, 2H), 7.24 (d, *J* = 8.5 Hz, 2H), 7.10 (d, *J* = 8.4 Hz, 2H), 1.35 (s, 9H), 1.35 (s, 9H), 1.32 (s, 9H), 1.23 (s, 9H); ^{13}C NMR (126 MHz, $CDCl_3$) δ 155.85, 154.73, 152.69, 152.31, 151.11, 150.98, 150.94, 150.25, 150.20, 149.31, 149.22, 149.18, 149.01, 148.88, 148.74, 148.42, 148.17, 148.05, 148.02, 147.89, 147.83, 147.77, 147.58, 147.49, 147.39, 147.33, 147.28, 147.09, 147.04, 146.99, 146.47, 146.43, 145.50, 145.43, 145.13, 145.04, 144.82, 144.63, 144.55, 144.29, 144.26, 143.99, 143.82, 143.75, 143.71, 143.61, 143.51, 143.05, 143.04, 142.84, 137.95, 137.43, 136.53, 136.44, 136.21, 135.70, 135.31, 128.48,

127.83, 127.48, 127.32, 126.14, 125.96, 125.91, 125.37, 73.27, 70.33, 60.17, 58.94, 58.92, 56.78, 53.44, 34.63, 34.58, 34.38, 31.37, 31.32, 31.31, 31.21.

1-(9*H*-Fluoren-9-yl)-9-hydro[60]fullerene (8):[11] To a dry solution of fluorene (23 mg, 0.139 mmol, 1 eq) in 5 mL of THF was added dropwise a solution of MeLi (1.6M Et_2O, 90 uL, 1 eq). The reaction was stirred for 30 minutes before a solution of C_{60} (100 mg, 0.139 mmol, 1 eq) in 10 mL *o*-DCB was added. The reaction was stirred for 1 h and eventually turned from purple to dark green. The reaction was quenched with saturated ammonium chloride. The organic layer was separated and the crude material was precipitated from solution with methanol. After filtration, the material was purified through silica gel chromatography (CS_2) to afford 41 mg (19%) **8** as a brown solid. ^{1}H NMR (500 MHz, $CDCl_3$) δ 8.41 (d, *J* = 7.6 Hz, 2H), 8.16 (d, *J* = 7.5 Hz, 2H), 7.72 (t, *J* = 7.4 Hz, 2H), 7.64 (dd, *J* = 10.8, 4.0 Hz, 2H), 5.63 (s, 1H), 5.36 (s, 1H). ^{13}C NMR (126 MHz, $CDCl_3$) δ 155.14, 154.77, 147.60, 147.34, 146.97, 146.52, 146.42, 146.31, 146.26, 146.19, 145.82, 145.69, 145.54, 145.48, 145.28, 144.82, 144.61, 143.38, 143.11, 142.63, 142.59, 142.44, 142.41, 142.06, 142.04, 141.77, 141.49, 141.43, 140.18, 140.02, 137.72, 136.17, 129.09, 127.78, 127.56, 120.56, 67.79, 59.54, 57.99, 55.07.

1-(Cyano)-9-hydro[60]fullerene (9):[29] odium cyanide (681 mg, 1.389 mmol, 20 eq) in 14 mL of DMF was added to a solution of C_{60} (500 mg, 0.694 mmol, 1 eq) in 40 mL of o-DCB. The reaction was stirred for 20 min and then quenched with 1 mL of trifluoroacetic acid. The crude solution was put directly onto a silica gel chromatography (hexanes/toluene 9:1) to afford **9** in 93 mg (18%) as a brown solid. ^{1}H NMR (500 MHz, $CDCl_3$) δ 7.20; ^{13}C NMR (126 MHz, $CDCl_3$) δ 149.19, 147.84, 147.51, 146.79, 146.59, 146.50, 146.37, 145.79, 145.76, 145.74, 145.54, 145.38, 145.08, 144.84, 144.41, 143.41,

143.17, 142.95, 142.84, 142.25, 142.20, 142.11, 141.92, 141.89, 141.32, 140.92, 140.55, 136.50, 135.47, 120.25, 59.22, 52.84, 50.92.

7-(4-Methylphenyl)-1-(hydroxyl)[60]fullerene (10): C_{60} (100 mg, 0.139 mmol, 1 eq), p-tolylhydrazine (44 mg, 0.278 mmol, 2 eq), and sodium nitrite (19 mg, 0.278, 2 eq) were dissolved in 70 mL of toluene/water (25:1). The reaction was heated to 50 ^{o}C for 48 h after which the solvent was evaporated. The crude material was dissolved in carbon disulfide and purified through silica gel chromatography (hexanes 100% to toluene 100%) to afford 92 mg (16%) of **10** as a brown solid. ^{1}H NMR (500 MHz, $CDCl_3$) δ 8.22 (d, *J* = 8.1 Hz, 2H), 7.47 (d, *J* = 8.3 Hz, 2H), 2.53 (s, 3H); ^{13}C NMR (126 MHz, $CDCl_3$) δ 154.16, 153.99, 152.46, 150.58, 149.09, 148.59, 147.96, 147.49, 147.43, 147.30, 147.09, 147.05, 146.82, 146.65, 145.93, 145.87, 145.78, 145.67, 145.16, 144.99, 144.66, 144.61, 144.41, 144.39, 144.31, 144.30, 144.26, 144.19, 144.18, 144.05, 143.95, 143.65, 143.57, 143.51, 143.48, 143.44, 143.42, 143.38, 143.25, 143.20, 143.18, 143.08, 143.04, 142.89, 142.84, 142.65, 142.52, 142.42, 142.25, 141.42, 141.14, 140.97, 140.02, 139.10, 138.41, 138.30, 137.60, 137.37, 130.48, 129.10, 128.33, 127.76, 125.42, 75.61, 61.36.

9-Hydro-((trimethylsilyl)ethynyl)-1-hydro[60]fullerene (11): To a dry solution of trimethylsilylacetylene (1.48 mL, 10.4 mmol, 15 eq) in 20 mL of dry THF, at -78 ^{o}C, was added dropwise 4.2 mL of n-butyl lithium (2.5 M pentane, 10.4, 15 eq). The reaction was stirred for 30 min at -78 ^{o}C before being allowed to warm to 0 ^{o}C and stirred for an additional 30 min. The solution was then added, dropwise, to a refluxing solution of C_{60} (500 mg, 0.694 mmol, 1 eq) in 500 mL of toluene. After the addition was complete, the reaction was cooled to 25 ˚C and quenched with 3 mL of trifluoroacetic acid. The crude

product was then precipitated from solution with methanol, filtered and purified through silica gel chromatography (pentane/CS_2 1:1) to afford 83 mg (15%) of **11** as a brown solid.

^{1}H NMR (500 MHz, $CDCl_3$) δ 7.04 (s, 1H), 0.48 (s, 9H); ^{13}C NMR (126 MHz, $CDCl_3$) δ 151.58, 151.41, 147.70, 147.44, 146.78, 146.53, 146.50, 146.35, 146.33, 145.93, 145.85, 145.79, 145.60, 145.55, 145.47, 144.81, 144.63, 143.34, 143.17, 142.74, 142.70, 142.21, 142.17, 142.15, 141.97, 141.81, 141.75, 140.47, 136.19, 135.23, 107.78, 88.48, 62.21, 55.61, 0.28.

9-Hydro-1-(1*H*-indole-3-yl)[60]fullerene (12):[32] C_{60} (500 mg, 0.694 mmol, 1 eq) and indole (98 mg, 0.833 mmol, 1.2 eq) were dissolved in 130 mL of *o*-DCB/DMSO 6:1. Under argon atmosphere, 1.735 mL of a solution of potassium tert-butoxide (1M THF, 2.5 eq) was added and the reaction was allowed to stir at 25 ˚C for 20 min. The reaction was quenched with 1 mL of trifuoroacetic acid, the crude material precipitated with methanol, and after filtering, purified through silica gel chromatography (CS_2/DCM 1:1) to afford 76 mg (13%) of **12** as brown solid. ^{1}H NMR (500 MHz, $CDCl_3$) δ 8.91 – 8.85 (m, 1H), 8.40 (s, 1H), 7.85 (d, *J* = 2.4 Hz, 1H), 7.64 (dd, *J* = 6.5, 2.7 Hz, 1H), 7.49 – 7.45 (m, 2H), 7.06 (s, 1H); ^{13}C NMR (126 MHz, $CDCl_3$) δ 154.09, 153.06, 147.35, 147.15, 146.74, 146.26, 146.23, 146.15, 146.07, 146.02, 145.72, 145.39, 145.36, 145.28, 144.62, 144.48, 143.12, 142.88, 142.48, 142.45, 142.13, 141.99, 141.90, 141.87, 141.59, 141.57, 140.34, 140.18, 137.25, 136.24, 135.30, 130.31, 127.40, 125.70, 124.14, 123.54, 121.85, 120.95, 119.41, 111.98, 62.37, 61.73.

General procedure for the allyl addition and benzylation of C_{60}. C_{60} (500 mg, 0.694 mmol, 1 eq), Ce_2CO_3 (950 mg, 2.917 mmol, 4.2 eq), and 100 mL of DMSO were added to a round-bottomed flask and sparged with argon. Propane thiol (265 uL, 2.917 mmol,

4.2 eq) was added and the reaction was allowed to stir at 25 ˚C for 2 h. The desired allyl or benzyl chloride/bromide (15eq) was added and the reaction was allowed to stir for up to 1.5 h. The reaction was then quenched with saturated ammonium chloride and the crude material was precipitated from solution with methanol. After filtration, the crude material was purified through silica gel chromatography (pentane 100 % to DCM 100%) to afford the desired product:

1-Allyl-9-hydro[60]fullerene (13): Synthesis of **13** followed the general procedure with allyl bromide. Recovered 24 mg (45%) of **13** as a brown solid. ^{1}H NMR (500 MHz, $CDCl_3$) δ 6.93 – 6.79 (m, 1H), 6.54 (s, 1H), 5.94 (d, *J* = 16.9 Hz, 1H), 5.80 (d, *J* = 10.0 Hz, 1H), 4.21 (d, *J* = 6.9 Hz, 2H); ^{13}C NMR (126 MHz, $CDCl_3$) δ 155.65, 155.50, 153.89, 147.11, 146.51, 146.34, 146.29, 146.26, 145.91, 145.64, 145.56, 145.51, 144.82, 144.68, 143.36, 142.68, 142.33, 142.15, 142.08, 142.04, 141.76, 140.39, 140.35, 137.67, 137.39, 136.47, 136.24, 135.60, 133.53, 129.11, 128.34, 125.44, 121.86, 64.41, 58.72, 51.25. MALDI-TOF MS (m/z 861).

1-(4-Methoxybenzyl)-9-hydro[60]fullerene (14): Synthesis of **14** followed the general procedure using 4-methoxybenzyl chloride. Recovered 114 mg (20%) of **14** as a brown solid. ^{1}H NMR (500 MHz, $CDCl_3$) δ 7.74 (d, *J* = 8.7 Hz, 2H), 7.11 – 7.02 (m, 2H), 6.62 (s, 1H), 4.71 (s, 2H), 3.89 (s, 3H); ^{13}C NMR (126 MHz, $CDCl_3$) δ 159.15, 155.62, 154.03, 147.51, 147.37, 147.06, 146.49, 146.46, 146.42, 146.29, 146.22, 145.86, 145.49, 145.43, 144.75, 144.62, 143.26, 143.11, 142.60, 142.28, 142.08, 142.02, 141.98, 141.68, 141.62, 140.19, 139.98, 136.40, 136.07, 132.52, 127.89, 114.15, 66.30, 59.08, 55.34, 52.25.

1-(3,4-Dimethoxybenzyl)-9-hydro[60]fullerene (15): Synthesis of **15** followed the general procedure using 3,4-dimethoxybenzyl chloride. Recovered 133 mg (15%) of **15**

as a brown solid. ^{1}H NMR (500 MHz, $CDCl_3$) δ 7.40 (d, *J* = 7.0 Hz, 1H), 7.32 (s, 1H), 7.04 (d, *J* = 8.1 Hz, 1H), 6.62 (s, 1H), 4.72 (s, 2H), 3.96 (d, *J* = 7.3 Hz, 6H); ^{13}C NMR (126 MHz, $CDCl_3$) δ 155.61, 154.01, 148.84, 148.62, 147.48, 147.32, 147.02, 146.42, 146.41, 146.27, 146.19, 145.82, 145.46, 145.41, 145.37, 144.72, 144.57, 143.24, 142.58, 142.22, 142.04, 141.99, 141.87, 141.65, 141.59, 141.56, 140.18, 139.91, 136.30, 135.94, 128.36, 123.79, 114.51, 111.20, 66.21, 59.07, 56.11, 55.89, 52.66.

1-(2,3,4-trimethoxybenzyl)-9-hydro[60]fullerene (16): Synthesis of **16** followed the general procedure using 2,3,4-trimethoxybenzyl chloride. Recovered 272 mg (30%) of **16** as a brown solid. ^{1}H NMR (500 MHz, CDCl3) δ 7.40 (d, *J* = 8.5 Hz, 1H), 6.79 (d, *J* = 8.6 Hz, 1H), 6.75 (s, 1H), 4.73 (s, 2H), 4.08 (s, 3H), 3.94 (s, 3H), 3.93 (s, 3H); ^{13}C NMR (126 MHz, $CDCl_3$) δ 156.03, 154.33, 153.48, 152.81, 147.46, 147.30, 147.14, 146.51, 146.39, 146.34, 146.21, 146.16, 145.87, 145.38, 145.35, 145.34, 144.71, 144.60, 143.23, 142.53, 142.25, 142.08, 142.03, 141.98, 141.95, 141.63, 141.54, 140.11, 139.82, 136.43, 135.75, 127.24, 121.52, 106.86, 66.34, 61.16, 60.84, 59.27, 55.96, 46.31.

6,12,15,18-Tetrakis(4-*tert*-butylphenyl)-9-((trimethylsilyl)ethynyl)-1-hydro[60]fullerene (17a), 6,12,15,18-tetrakis(4-*tert*-butylphenyl)-9-((trimethylsilyl)ethynyl)-2-hydro[60]fullerene (17b), and 6,12,15,18-tetrakis(4-*tert*-butylphenyl)-9-((trimethylsilyl)ethynyl)-3-hydro[60]fullerene (17c): Synthesis of **17a,b,c** follows the same general procedure as the aryl copper pentaaddition starting from ethynyl fullerene **11** to afford a mixture of **17a,b,c** (20%) as a red solid. ^{1}H NMR (500 MHz, $CDCl_3$) δ 8.01 (d, *J* = 8.1 Hz, 3H), 7.90 (t, *J* = 7.8 Hz, 5H), 7.81 (d, *J* = 8.2 Hz, 3H), 7.79 – 7.74 (m, 5H), 7.56 (d, *J* = 8.1 Hz, 4H), 7.50 (d, *J* = 8.2 Hz, 3H), 7.45 – 7.42 (m, 4H), 7.40 (d, *J* = 8.2 Hz, 3H), 7.28 (s, 4H), 7.22 (d, *J* = 7.9 Hz, 4H), 7.20 – 7.18 (m, 4H),

7.16 (d, *J* = 7.8 Hz, 6H), 7.09 (d, *J* = 7.9 Hz, 4H), 7.03 (d, *J* = 7.9 Hz, 3H), 6.99 – 6.95 (m, 7H), 6.93 (d, *J* = 7.9 Hz, 3H), 5.49 (s, 1H), 5.15 (s, 1H), 4.95 (s, 1H), 2.42 (s, 5H), 2.41 (s, 5H), 2.40 (s, 4H), 2.38 (s, 6H), 2.37 (s, 4H), 2.36 (s, 6H), 2.31 (s, 4H), 2.30 (s, 9H), 2.24 (s, 4H), 0.37 (s, 9H), 0.37 (s, 9H), 0.33 (s, 9H), 0.33 (s, 9H), 0.32 (s, 13H), 0.32 (s, 12H); ^{13}C NMR (126 MHz, CDCl3) δ 157.44, 157.44, 157.42, 156.37, 156.37, 154.18, 154.18, 153.74, 153.74, 153.69, 153.69, 153.34, 153.34, 152.93, 152.93, 152.89, 152.74, 152.74, 152.02, 151.98, 151.98, 151.94, 151.74, 151.74, 150.90, 150.90, 150.86, 149.48, 149.30, 149.30, 149.01, 149.01, 148.90, 148.90, 148.79, 148.79, 148.70, 148.70, 148.63, 148.63, 148.55, 148.55, 148.44, 148.44, 148.39, 148.39, 148.29, 148.29, 148.22, 148.22, 148.13, 148.13, 148.06, 148.06, 148.02, 148.02, 147.97, 147.97, 147.89, 147.89, 147.77, 147.77, 147.64, 147.64, 147.27, 147.16, 147.16, 147.15, 147.14, 147.11, 147.09, 147.09, 147.07, 147.01, 147.01, 146.97, 146.90, 146.90, 146.86, 146.82, 146.82, 146.20, 146.18, 146.18, 146.15, 146.08, 145.91, 145.91, 145.89, 145.84, 145.84, 145.82, 145.79, 145.79, 145.75, 145.75, 145.72, 145.44, 145.39, 145.39, 145.35, 145.23, 145.23, 145.11, 145.11, 144.82, 144.82, 144.74, 144.74, 144.71, 144.70, 144.64, 144.64, 144.57, 144.57, 144.45, 144.45, 144.44, 144.42, 144.40, 144.39, 144.37, 144.36, 144.30, 144.30, 144.27, 144.27, 144.26, 144.20, 144.20, 144.18, 144.13, 144.13, 144.11, 144.11, 143.95, 143.95, 143.89, 143.89, 143.79, 143.79, 143.64, 143.64, 143.61, 143.57, 143.57, 143.48, 143.48, 143.38, 143.38, 143.20, 143.20, 143.06, 143.06, 142.97, 142.95, 142.95, 142.88, 142.88, 142.78, 142.78, 142.50, 142.50, 141.07, 141.07, 137.62, 137.62, 137.55, 137.55, 137.40, 137.40, 137.37, 137.37, 137.27, 137.27, 137.22, 137.22, 137.20, 137.20, 137.16, 137.16, 137.07, 137.07, 137.04, 137.02, 137.02, 136.98, 136.98, 136.81, 136.81, 136.75, 136.75, 136.71, 136.71, 136.52, 136.52, 136.46, 136.46, 136.44, 129.69, 129.69, 129.58, 129.58, 129.52,

129.52, 129.49, 129.49, 129.47, 129.47, 129.43, 129.43, 129.29, 129.29, 128.30, 128.30, 128.00, 128.00, 127.94, 127.94, 127.87, 127.87, 127.74, 127.74, 127.71, 127.71, 127.61, 127.61, 127.56, 127.56, 127.32, 127.32, 87.87, 87.72, 87.43, 77.27, 77.02, 76.76, 62.19, 62.19, 61.87, 61.87, 60.93, 60.93, 60.83, 60.83, 60.70, 60.70, 60.67, 60.67, 58.91, 58.71, 58.71, 58.58, 58.58, 47.45, 46.72, 45.93, 34.68, 34.53, 31.60, 29.71, 26.92, 25.29, 22.67, 21.24, 21.19, 21.15, 21.14, 21.08, 20.89, 20.71, 14.14.

6,12,15,18-Tetrakis(4-*tert*-butylphenyl)-9-(1*H*-indole-3-yl)-1-hydro[60]fullerene (17a), 6,12,15,18-tetrakis(4-*tert*-butylphenyl)-9-(1*H*-indole-3-yl)-2-hydro[60]fullerene (17b), and 6,12,15,18-tetrakis(4-*tert*-butylphenyl)-9-(t1*H*-indole-3-yl)-3-hydro[60]fullerene (18c): Synthesis of **18a,b** follows the same general procedure as the aryl copper pentaaddition starting from ethynyl fullerene **11** to afford a mixture of **18a,b** (15%) as a red solid. ^{1}H NMR (500 MHz, $CDCl_3$) δ 9.01 – 8.88 (m), 8.48 (d, *J* = 38.7 Hz), 8.33 – 7.98 (m), 7.87 – 7.47 (m), 7.41 – 7.22 (m), 7.16 – 6.81 (m), 5.24 (s), 5.22 (s), 2.46 – 2.18 (m). ^{13}C NMR (126 MHz, $CDCl_3$) δ 156.26, 154.44, 152.68, 152.47, 151.79, 148.67, 148.38, 148.25, 148.08, 147.74, 147.23, 147.11, 147.00, 146.48, 146.32, 146.25, 145.99, 145.79, 145.58, 145.52, 144.57, 144.31, 144.22, 144.10, 144.01, 143.10, 142.11, 141.80, 137.33, 137.06, 136.92, 136.87, 136.79, 132.58, 130.55, 129.51, 129.44, 129.26, 129.14, 129.05, 128.23, 128.17, 128.02, 127.89, 127.72, 127.63, 126.81, 123.52, 122.16, 120.96, 119.52, 115.16, 114.52, 113.08, 112.28, 72.53, 62.96, 61.87, 60.76, 58.71, 58.64, 58.10, 53.44.

6,12,15,18-Tetrakis(4-*tert*-butylphenyl)-9-(4-methoxybenzyl)-1-hydro[60]fullerene (19a), 6,12,15,18-tetrakis(4-*tert*-butylphenyl)-9-(4-methoxybenzyl)-2-hydro[60]fullerene (19b), and 6,12,15,18-tetrakis(4-*tert*-butylphenyl)-9-(4-

methoxybenzyl)-3-hydro[60]fullerene (19c): Synthesis of **19a,b,c** follows the same general procedure as the aryl copper pentaaddition starting from 4-methoxybenzyl fullerene **14** to afford a mixture of **19a,b,c** (58%) as a red solid. ^{1}H NMR (500 MHz, $CDCl_3$) δ 7.89 (d, *J* = 8.6 Hz), 7.81 (d, *J* = 8.6 Hz), 7.78 (d, *J* = 8.6 Hz), 7.72 (dd, *J* = 11.7, 8.6 Hz), 7.61 (d, *J* = 8.6 Hz), 7.48 (dd, *J* = 8.5, 5.8 Hz), 7.45 – 7.42 (m), 7.42 – 7.38 (m), 7.35 (dt, *J* = 4.5, 2.5 Hz), 7.33 – 7.28 (m), 7.23 (dd, *J* = 7.8, 4.4 Hz), 7.18 (ddd, *J* = 5.8, 3.9, 1.7 Hz), 7.17 – 7.14 (m), 7.12 – 7.09 (m), 7.03 (ddd, *J* = 11.7, 6.9, 3.6 Hz), 6.71 – 6.61 (m), 6.59 – 6.54 (m), 5.19 (s), 5.12 (s), 4.99 (s), 3.80 – 3.68 (m), 3.63 (d, *J* = 13.4 Hz), 3.49 (s), 1.41 (s), 1.39 (q, *J* = 2.5 Hz), 1.37 – 1.36 (m), 1.35 (d, *J* = 1.4 Hz), 1.30 (s), 1.29 (t, *J* = 2.5 Hz), 1.26 (d, *J* = 4.5 Hz); ^{13}C NMR (126 MHz, CDCl3) δ 158.54, 158.42, 158.35, 157.09, 156.61, 156.21, 153.43, 153.20, 152.89, 152.86, 152.78, 152.76, 152.35, 152.01, 151.99, 151.68, 151.64, 151.60, 151.58, 151.55, 150.71, 150.62, 150.57, 150.56, 150.42, 150.27, 150.25, 150.16, 149.90, 149.88, 148.71, 148.70, 148.66, 148.64, 148.60, 148.59, 148.58, 148.55, 148.51, 148.47, 148.32, 148.27, 148.24, 148.20, 148.16, 148.14, 148.10, 148.02, 147.99, 147.77, 147.71, 147.67, 147.63, 147.19, 147.13, 147.10, 147.05, 147.01, 146.97, 146.83, 146.78, 146.73, 146.46, 146.45, 146.34, 146.23, 146.07, 145.95, 145.85, 145.82, 145.77, 145.72, 145.62, 145.56, 145.48, 145.42, 145.25, 144.64, 144.63, 144.61, 144.60, 144.43, 144.39, 144.37, 144.25, 144.19, 144.14, 144.13, 144.11, 144.09, 144.07, 144.03, 144.00, 143.96, 143.93, 143.91, 143.87, 143.80, 143.66, 143.56, 143.09, 143.05, 142.94, 142.92, 142.88, 142.87, 142.70, 137.41, 137.16, 136.96, 136.88, 136.60, 131.71, 131.38, 131.28, 130.03, 128.59, 128.53, 128.35, 128.10, 128.05, 127.92, 127.56, 127.46, 127.34, 127.28, 127.08, 126.41, 126.00, 125.84, 125.82, 125.68, 125.47, 125.31, 113.54, 113.42, 113.37, 67.97, 62.80, 62.54, 60.73, 60.66, 60.60, 60.56, 59.48, 58.92, 58.70,

58.60, 58.56, 58.54, 58.39, 58.29, 57.22, 56.70, 55.07, 55.04, 55.00, 53.41, 49.19, 44.70, 44.60, 34.63, 34.58, 34.55, 34.51, 34.44, 34.33, 31.58, 31.52, 31.37, 31.34, 31.31, 31.27, 31.21, 29.70, 25.60, 25.27, 22.65, 14.12.

6,12,15,18-Tetrakis(4-*tert*-butylphenyl)-9-(3,4-dimethoxybenzyl)-1-hydro[60]fullerene (20a), 6,12,15,18-tetrakis(4-*tert*-butylphenyl)-9-(3,4-dimethoxybenzyl)-2-hydro[60]fullerene (20b), and 6,12,15,18-tetrakis(4-*tert*-butylphenyl)-9-(3,4-dimethoxybenzyl)-3-hydro[60]fullerene (20c): Synthesis of **19a,b,c** follows the same general procedure as the aryl copper pentaaddition starting from 3,4-dimethoxybenzyl fullerene **15** to afford a mixture of **20a,b,c** (46%) as a red solid. ^{1}H NMR (500 MHz, $CDCl_3$) δ 7.91 (d, *J* = 8.0 Hz), 7.83 (d, *J* = 7.9 Hz), 7.79 (d, *J* = 8.1 Hz), 7.71 (m), 7.61 (d, *J* = 8.0 Hz), 7.53 – 7.38 (m), 7.33 (m), 7.25 – 7.13 (m), 7.10 (d, *J* = 8.0 Hz), 6.85 (d, *J* = 7.9 Hz), 6.73 (m), 6.66 (m), 6.54 (d, *J* = 23.3 Hz, 1H), 5.19 (s), 5.13 (s), 5.04 (s), 3.86 – 3.63 (m), 3.54 (m), 1.35 (m); ^{13}C NMR (126 MHz, $CDCl_3$) δ 157.08, 156.53, 156.29, 155.26, 154.66, 153.31, 153.15, 153.04, 152.77, 152.68, 152.36, 152.04, 151.94, 151.72, 151.66, 151.59, 151.43, 151.25, 150.70, 150.61, 150.54, 150.46, 150.35, 150.23, 150.16, 149.98, 149.87, 148.72, 148.63, 148.56, 148.50, 148.48, 148.35, 148.31, 148.27, 148.23, 148.18, 148.16, 148.10, 148.05, 147.99, 147.98, 147.90, 147.87, 147.82, 147.77, 147.70, 147.64, 147.60, 147.51, 147.09, 147.06, 147.04, 147.00, 146.96, 146.81, 146.78, 146.71, 146.57, 146.42, 146.39, 146.23, 146.15, 146.08, 145.93, 145.81, 145.76, 145.71, 145.68, 145.55, 145.50, 145.49, 145.43, 145.40, 145.24, 145.22, 145.05, 144.65, 144.60, 144.53, 144.44, 144.37, 144.28, 144.19, 144.12, 144.08, 144.06, 144.03, 144.00, 143.92, 143.89, 143.87, 143.84, 143.78, 143.73, 143.62, 143.47, 143.13, 143.07, 142.94, 142.89, 142.81, 142.67, 137.36, 137.12, 136.95, 136.92, 136.90, 136.57, 132.54, 131.01,

130.52, 129.18, 129.04, 128.93, 128.05, 127.88, 127.69, 127.52, 127.49, 127.41, 127.35, 127.23, 127.07, 125.99, 125.83, 125.81, 125.67, 125.64, 125.48, 125.32, 123.26, 122.62, 122.29, 113.83, 113.74, 113.55, 110.75, 110.69, 110.44, 67.96, 62.78, 62.45, 60.74, 60.65, 60.54, 59.23, 58.95, 58.70, 58.54, 58.37, 58.18, 56.90, 56.56, 55.74, 55.65, 55.62, 55.60, 55.56, 55.54, 49.73, 45.03, 44.89, 34.63, 34.57, 34.55, 34.53, 34.50, 34.42, 34.39, 34.32, 31.34, 31.30, 31.26, 31.20, 30.92.

6,12,15,18-Tetrakis(4-methylphenyl)-9-(2,3,4-trimethoxybenzyl)-1-hydro[60]fullerene (21a), 6,12,15,18-tetrakis(4-methylphenyl)-9-(2.3,4-trimethoxybenzyl)-2-hydro[60]fullerene (21b), and 6,12,15,18-tetrakis(4-methylphenyl)-9-(2,3,4-trimethoxybenzyl)-3-hydro[60]fullerene (21c): Synthesis of **21a,b,c** follows the same general procedure as the aryl copper pentaaddition starting from 2,3,4-trimethoxybenzyl fullerene **16** to afford a mixture of **21a,b,c** (58%) as a red solid. ^{1}H NMR (500 MHz, $CDCl_3$) δ 7.89 – 6.81 (m), 6.74 – 6.55 (m), 5.24 (s), 5.22 (s), 5.17 (s), 4.05 – 3.61 (m), 2.47 – 2.19 (m); ^{13}C NMR (126 MHz, $CDCl_3$) δ 157.02, 156.67, 153.49, 153.14, 152.94, 152.77, 152.72, 152.69, 152.64, 152.21, 151.76, 151.72, 151.47, 149.38, 148.73, 148.62, 148.59, 148.56, 148.31, 148.21, 148.16, 148.13, 148.09, 148.00, 147.95, 147.68, 147.16, 147.07, 146.99, 146.81, 146.38, 146.19, 145.98, 145.90, 145.82, 145.70, 145.49, 144.62, 144.50, 144.36, 144.18, 144.13, 144.01, 143.93, 143.84, 143.02, 141.38, 137.89, 137.45, 137.31, 137.25, 137.11, 136.95, 136.92, 136.87, 136.82, 136.68, 132.58, 130.56, 129.71, 129.62, 129.57, 129.55, 129.52, 129.50, 129.44, 129.39, 129.33, 129.25, 129.22, 129.16, 129.13, 129.06, 128.25, 128.20, 128.17, 128.11, 127.95, 127.88, 127.84, 127.77, 127.74, 127.65, 127.61, 127.57, 127.53, 127.46, 127.44, 127.42, 126.44, 125.32, 121.96, 106.78, 106.61, 106.50, 106.27, 68.00, 61.11, 61.00, 60.94, 60.80, 60.66,

60.64, 60.55, 60.52, 60.37, 59.01, 58.73, 58.60, 58.07, 57.04, 57.01, 56.05, 55.93, 55.60, 55.53, 55.33, 53.46, 21.20, 21.15, 21.11, 20.99, 20.96.

6,12,15,18-Tetrakis(4-methoxyphenyl)-9-(2,3,4-trimethoxybenzyl)-1-hydro[60]fullerene (22a), 6,12,15,18-tetrakis(4-methyoxyphenyl)-9-(2.3,4-trimethoxybenzyl)-2-hydro[60]fullerene (21b), and 6,12,15,18-tetrakis(4-methyoxyphenyl)-9-(2,3,4-trimethoxybenzyl)-3-hydro[60]fullerene (22c): Synthesis of **21a,b,c** follows the same general procedure as the aryl copper pentaaddition starting from 2,3,4-trimethoxybenzyl fullerene **16** to afford a mixture of **21a,b,c** (58%) as a red solid. ^{1}H NMR (500 MHz, $CDCl_3$) δ 7.88 – 7.10 (m), 7.10 – 6.55 (m), 5.24 (s), 5.17 (s), 5.15 (s), 4.05 – 3.60 (m); ^{13}C NMR (126 MHz, $CDCl_3$) δ 159.18, 158.96, 158.81, 158.68, 158.58, 158.45, 156.78, 156.19, 155.55, 154.91, 153.33, 153.16, 153.01, 152.86, 152.75, 152.56, 152.11, 151.82, 151.62, 150.13, 148.89, 148.62, 148.58, 148.53, 148.31, 148.22, 148.15, 148.00, 147.76, 147.65, 147.46, 147.12, 147.07, 146.97, 146.92, 146.84, 146.78, 146.14, 145.97, 145.75, 145.69, 145.46, 145.38, 145.32, 145.03, 144.70, 144.42, 144.22, 144.17, 144.02, 143.98, 143.93, 143.82, 143.67, 143.04, 142.72, 141.91, 141.61, 141.34, 138.12, 137.89, 136.38, 132.57, 132.48, 132.11, 131.85, 131.64, 130.55, 129.54, 129.49, 129.35, 129.24, 129.16, 129.13, 129.05, 129.01, 128.99, 128.86, 128.75, 128.62, 128.24, 127.76, 127.74, 127.23, 126.37, 125.32, 122.09, 121.85, 114.32, 114.28, 114.23, 114.14, 114.02, 113.98, 113.93, 113.88, 113.85, 113.83, 113.78, 106.76, 106.45, 106.26, 100.04, 67.99, 67.05, 63.37, 63.10, 62.85, 61.30, 61.12, 60.94, 60.79, 60.74, 60.58, 60.54, 60.51, 60.21, 59.29, 58.38, 58.33, 58.15, 57.58, 57.03, 56.64, 55.94, 55.42, 55.39, 55.35, 55.30, 55.23, 55.10.

Debenzylation of methoxybenzyl fullerenes

6,9,12,15-Tetrakis(4-*tert*-butylphenyl)[60]fullerene (23): The mixture of **19a,b,c** (60 mg, 0.044 mmol, 1 eq) Iodine (60 mg, 0.236 mmol, 5.3 eq) were dissolved in 12 mL of 1-chloronaphthalene, sparged thoroughly with argon and then heated in a sealed pressure tube at 200 ºC for 48 h. The reaction was allowed to cool to 25 ˚C and the crude material was precipitated from solution with methanol. After filtration, the crude material was purified through silica gel chromatography (pentane/CS_2 1:1) to afford **3** mg (5%) as a brown solid. ^{1}H NMR (500 MHz, $CDCl_3$) δ 7.80 (d, *J* = 7.9 Hz, 4H), 7.45 (d, *J* = 8.0 Hz, 4H), 7.39 (d, *J* = 8.1 Hz, 4H), 7.18 (d, *J* = 8.1 Hz, 4H), 1.36 (s, *J* = 16.0 Hz, 18H), 1.29 (s, 18H). ^{13}C NMR (126 MHz, $CDCl_3$) δ 163.88, 152.25, 150.72, 150.30, 149.71, 149.26, 148.96, 148.58, 148.19, 148.01, 147.83, 147.38, 147.26, 146.56, 146.44, 146.33, 146.28, 145.56, 145.50, 144.55, 144.44, 144.05, 143.86, 143.51, 143.37, 143.12, 142.36, 141.52, 140.15, 137.70, 137.24, 136.69, 127.76, 127.44, 125.91, 125.58, 59.98, 59.69, 34.51, 34.39, 31.39, 31.29, 27.16, 27.07.

6,9,12,15-Tetrakis(4-methylphenyl)[60]fullerene (24): Compound **24** was synthesized using the same debenzylation conditions used to synthesize compound **23**, from a mixture of regioisomers **20a,b,c** to afford compound **24** (8%) as a brown solid. ^{1}H NMR (500 MHz, $CDCl_3$) δ 7.85 – 7.74 (m, 4H), 7.51 – 7.42 (m, 4H), 7.24 – 7.17 (m, 4H), 7.03 (dd, *J* = 19.4, 8.8 Hz, 4H), 2.38 (d, *J* = 10.0 Hz, 6H), 2.32 (s, 6H); ^{13}C NMR (126 MHz, $CDCl_3$) δ 164.08, 151.82, 151.01, 149.69, 149.23, 148.91, 148.52, 148.04, 147.99, 147.72, 147.34, 147.21, 146.53, 146.44, 146.30, 146.25, 145.57, 145.43, 144.56, 144.50, 144.47, 144.29, 143.93, 143.79, 143.42, 143.32, 142.37, 141.49, 140.31, 137.79, 137.61, 137.19, 137.07, 136.70, 129.66, 129.41, 127.63, 127.44, 60.04, 59.71, 21.17, 21.08.

General debenzylation procedure using DDQ. Benzyl fullerenes **14, 15** or **16** (0.036 mmol, 1 eq) and DDQ (82 mg, 0.36 mmol, 10 eq) was dissolved in 4 mL of toluene, sparged with argon and then refluxed for 4-6 h or until starting material (monitored by TLC) was gone. The reaction was then cooled to 25 ˚C and methanol was added to precipitate the crude product. After filtration, the crude material was purified through silica gel chromatography (pentane/toluene 9:1) to afford 20-22 mg (~77%) of pristine C_{60}.

Synthesis of unconfirmed spot 2 (25a) and spot 3 (25b). Following the general debenzylation procedure using DDQ, the mixture of regioisomers **20a,b,c** (55 mg) afforded three products after purification through silica gel chromatography:

The first product to elute was the 5FSC **3** 2 mg (4%).

The next product was “spot 2” **25a**, 9 mg (~16%). ^{1}H NMR (500 MHz, $CDCl_3$) δ 7.89 (d, *J* = 8.4 Hz, 2H), 7.82 (d, *J* = 8.3 Hz, 2H), 7.65 (d, *J* = 8.3 Hz, 2H), 7.44 (d, *J* = 8.4 Hz, 2H), 7.39 (d, *J* = 8.3 Hz, 2H), 7.30 (d, *J* = 8.4 Hz, 2H), 6.80 (d, *J* = 8.4 Hz, 2H), 6.70 (d, *J* = 8.4 Hz, 2H), 6.55 (s, 1H), 6.52 (d, *J* = 8.3 Hz, 1H), 5.08 (d, *J* = 8.5 Hz, 1H), 3.75 (d, *J* = 7.7 Hz, 4H), 3.60 (s, 3H), 1.40 (s, 9H), 1.34 (d, *J* = 2.2 Hz, 18H), 1.20 (s, 9H); ^{13}C NMR (126 MHz, $CDCl_3$) δ 157.78, 155.23, 151.63, 151.31, 151.01, 150.80, 150.75, 150.61, 150.31, 149.18, 148.95, 148.89, 148.67, 148.33, 148.23, 148.17, 148.07, 148.00, 147.86, 147.82, 147.70, 147.57, 147.51, 147.44, 147.40, 147.35, 147.20, 147.07, 146.93, 146.87, 146.75, 146.54, 146.51, 146.31, 146.14, 145.87, 145.58, 145.54, 145.36, 145.30, 145.07, 145.03, 144.67, 144.58, 144.32, 144.11, 144.00, 143.86, 143.52, 143.33, 143.18, 143.13, 138.03, 137.27, 136.33, 136.04, 129.03, 128.63, 128.43, 128.22, 127.75, 126.55, 126.49, 125.97, 125.42, 125.37, 125.29, 124.46, 122.55, 112.58, 110.20, 64.29, 62.81, 61.44, 59.07, 58.94, 55.98, 55.44, 55.03, 51.09, 34.60, 34.57, 34.52, 34.09, 31.37, 31.33, 31.31, 31.08.

The next set of products “spot 3” **25b**, 9 mg (~16%). ^{1}H NMR (500 MHz, $CDCl_3$) δ 7.90 (t, *J* = 7.8 Hz), 7.83 (t, *J* = 7.5 Hz), 7.78 (d, *J* = 8.5 Hz), 7.72 (m), 7.61 (d, *J* = 8.5 Hz), 7.44 (m), 7.32 (m), 7.24 – 7.20 (m, 2H), 7.16 (m), 7.10 (m), 7.06 (d, *J* = 7.2 Hz), 6.93 (s), 6.87 – 6.82 (m), 6.81 – 6.69 (m), 6.69 – 6.62 (m), 6.55 (m), 5.18 (s), 5.11 (s), 5.04 (s), 3.86 – 3.49 (m), 1.42 – 1.27 (m).

6,12,15,18-Tetrakis(4-Methylphenyl)-9-(4-Methoxybenzyl)-1-hydro[60]fullerene (26a), 6,12,15,18-tetrakis(4-Methylphenyl)-9-(4-methoxybenzyl)-2-hydro[60]fullerene (26b), and 6,12,15,18-tetrakis(4-Methylphenyl)-9-(4-methoxybenzyl)-3-hydro[60]fullerene (26c): Synthesis of **26a,b,c** follows the same general procedure as the aryl copper pentaaddition starting from 4-methoxybenzyl fullerene **14** to afford a mixture of **26a,b,c** (58%) as a red solid. ^{1}H NMR (500 MHz, $CDCl_3$) δ 7.83 – 7.79 (m), 7.77 – 7.67 (m), 7.55 (d, *J* = 8.1 Hz), 7.37 (d, *J* = 8.2 Hz), 7.18 – 6.95 (m), 6.61 (s), 6.61 – 6.57 (m), 6.47 (d, *J* = 8.6 Hz), 5.23 (s), 5.10 (s), 5.01 (s), 4.70 (s), 3.90 – 3.54 (m), 2.45 (s), 2.43 (s), 2.41 (s), 2.40 (s), 2.39 (s), 2.34 (s), 2.33 (s), 2.33 (s), 2.29 (s).

NMR Spectra

Unless otherwise stated, all spectra were acquired in $CDCl_3$.

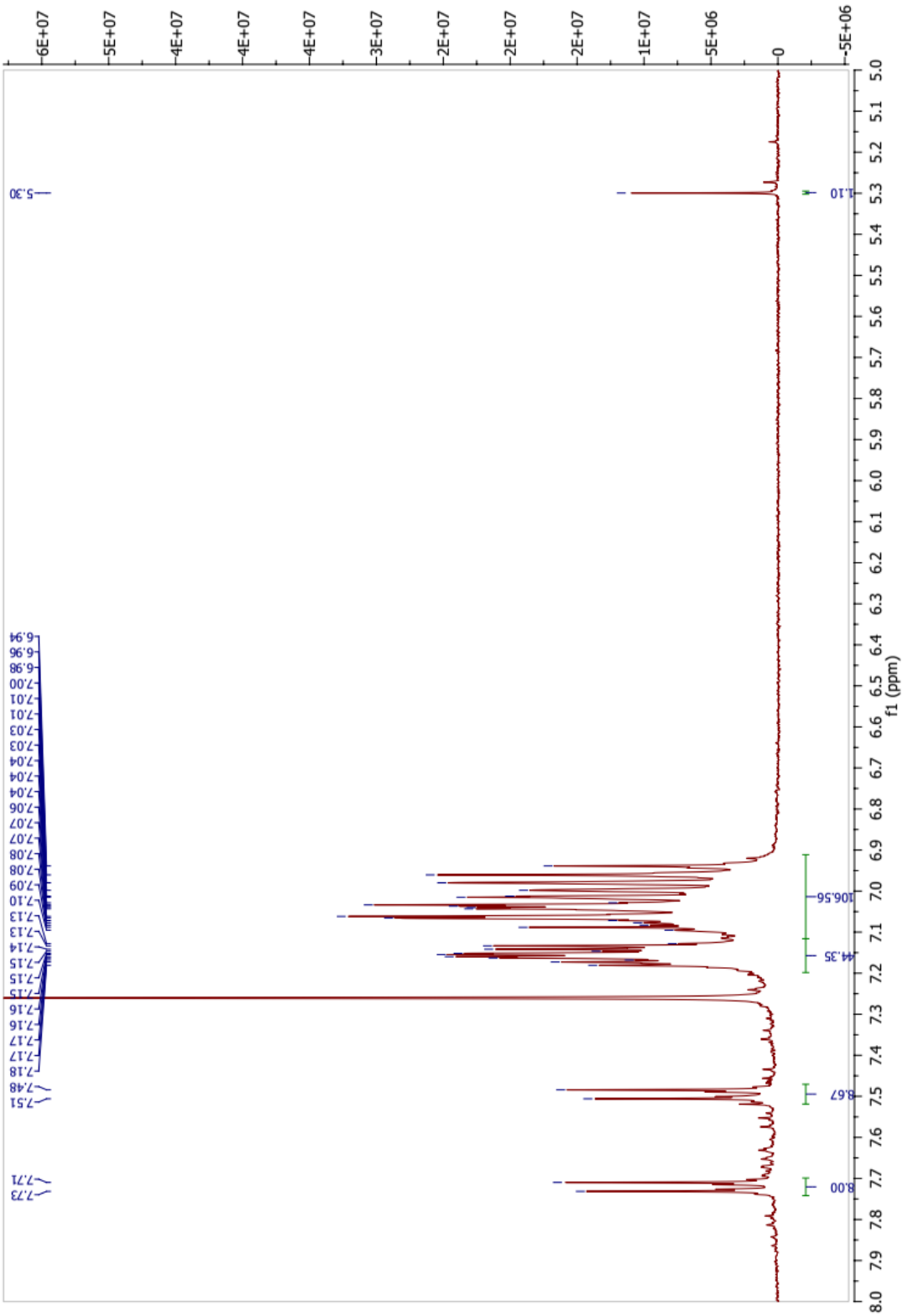

Fig. 1.36. ^{1}H NMR of compound **1** ($CDCl_3$)

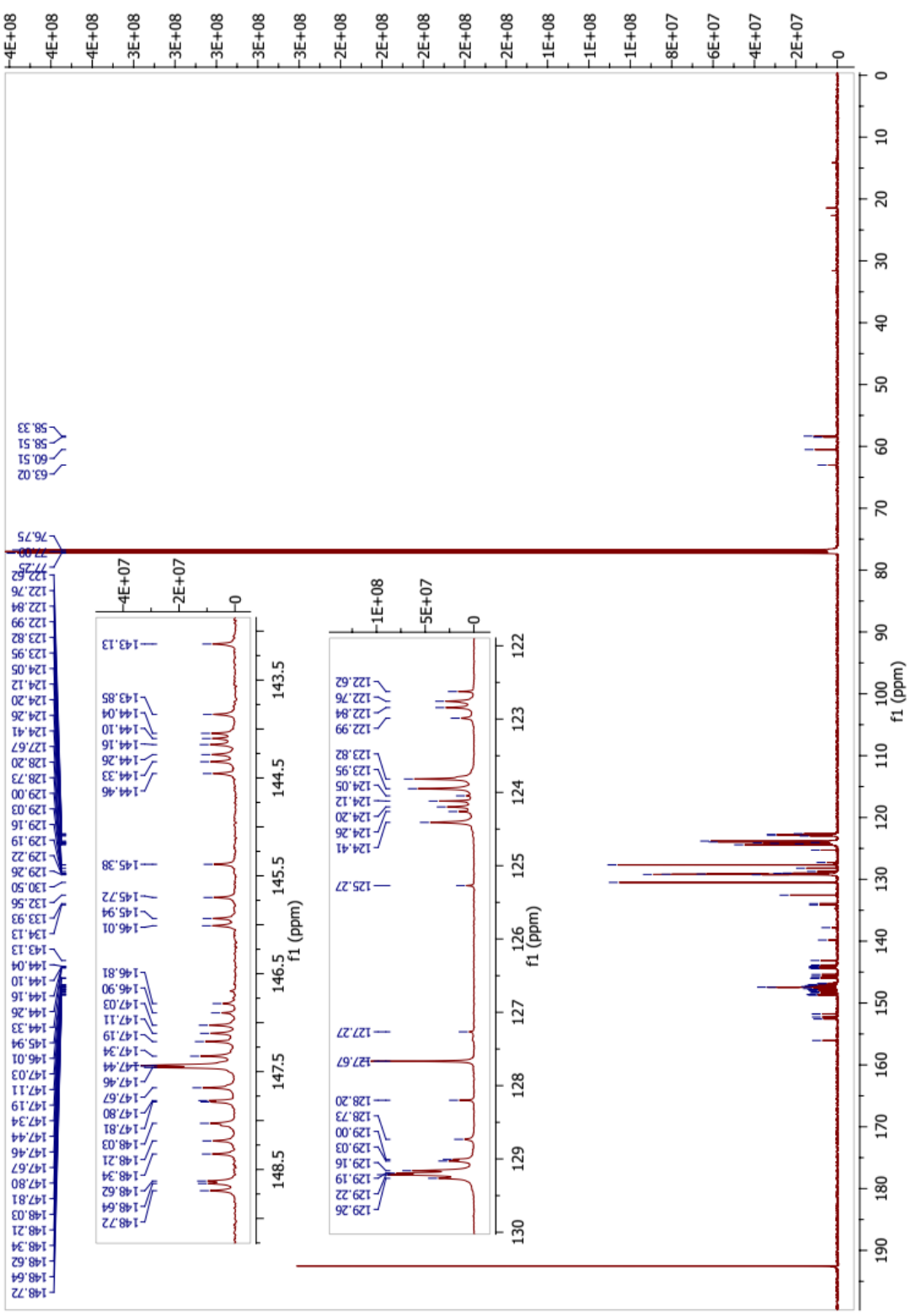

Fig. 1.37. ^{13}C NMR of compound **1** ($CDCl_3$)

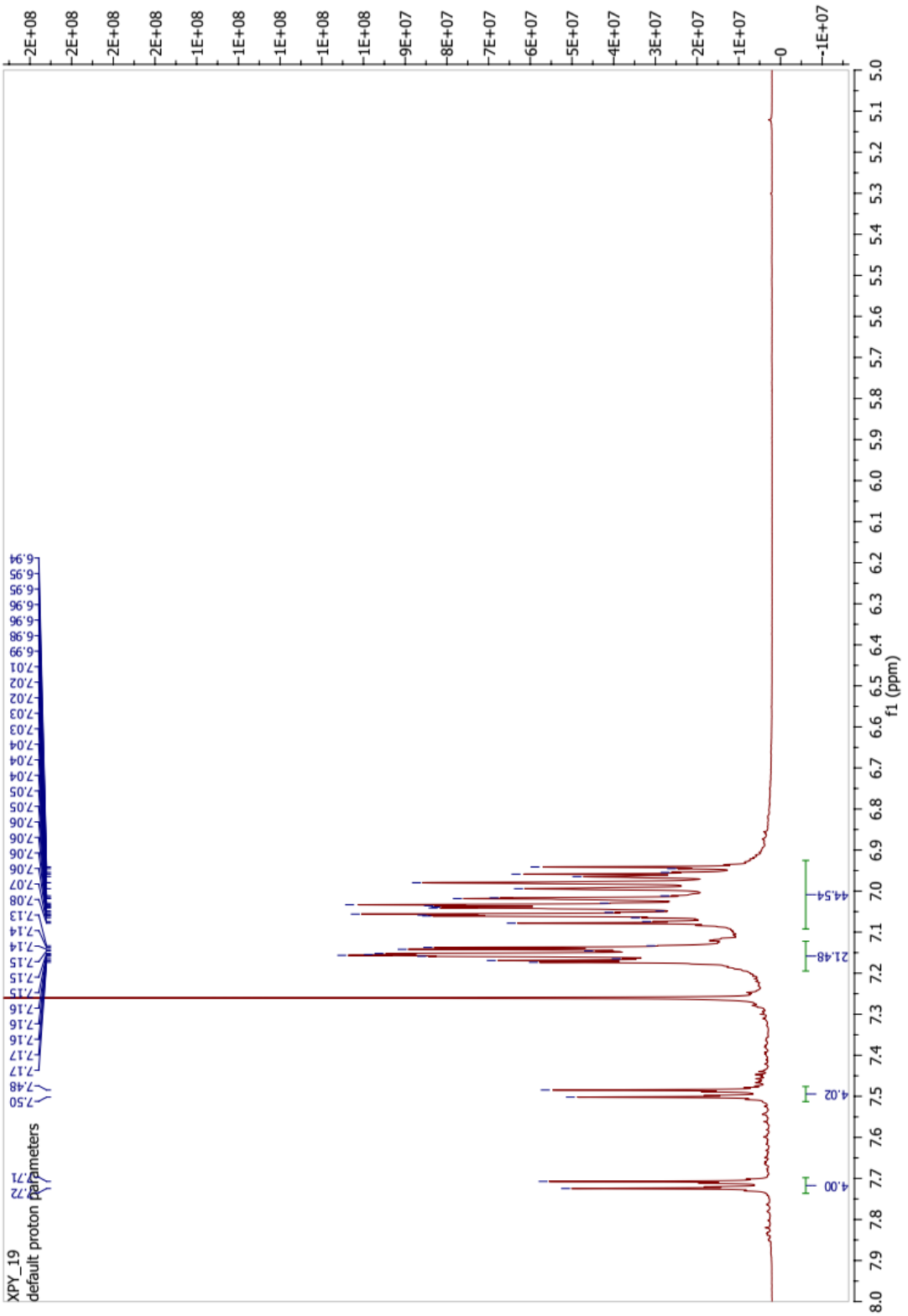

Fig. 1.38. ^{1}H NMR of Compound **2** ($CDCl_3$).

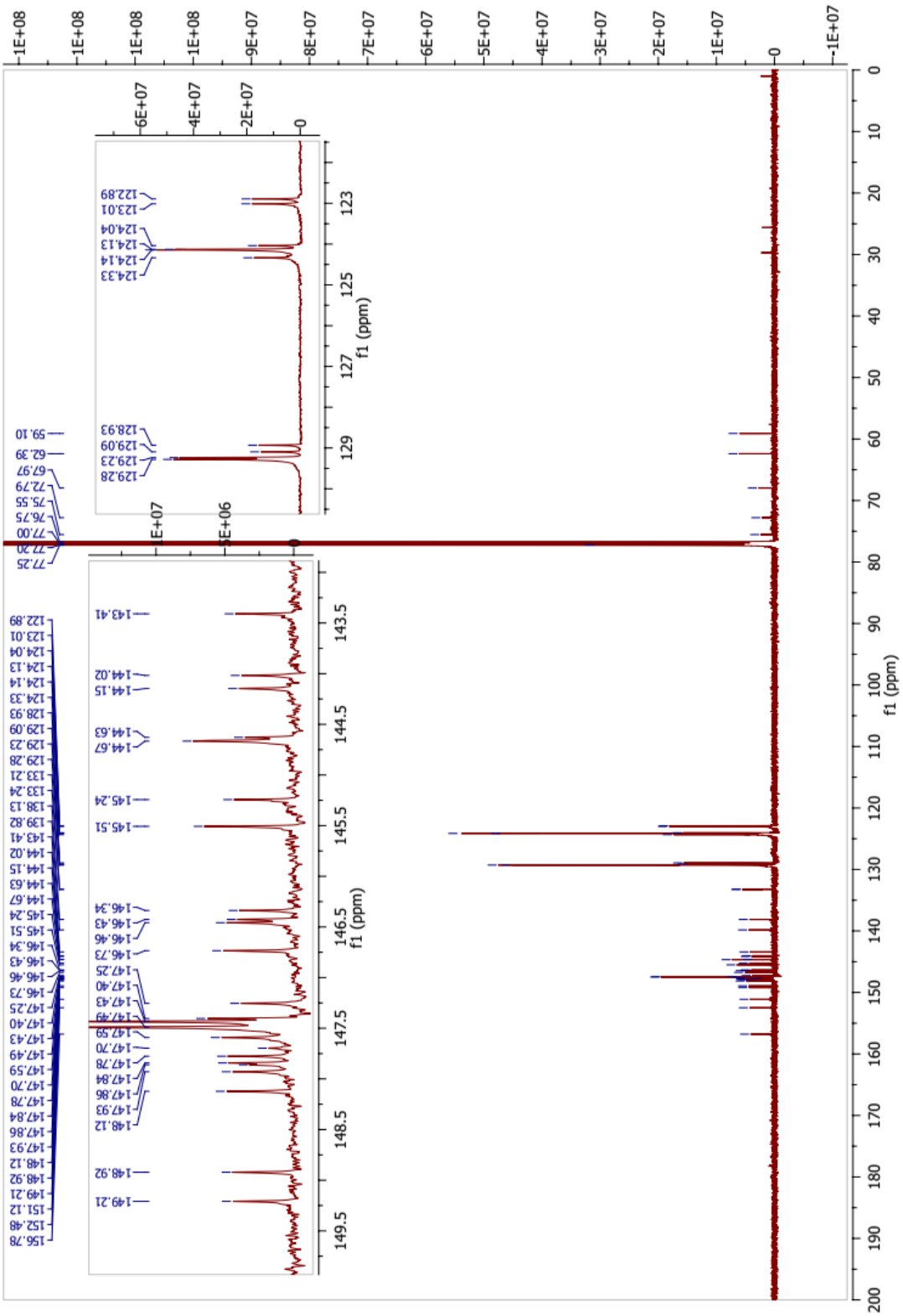

Fig. 1.39. ^{13}C NMR of compound **2** ($CDCl_3$)

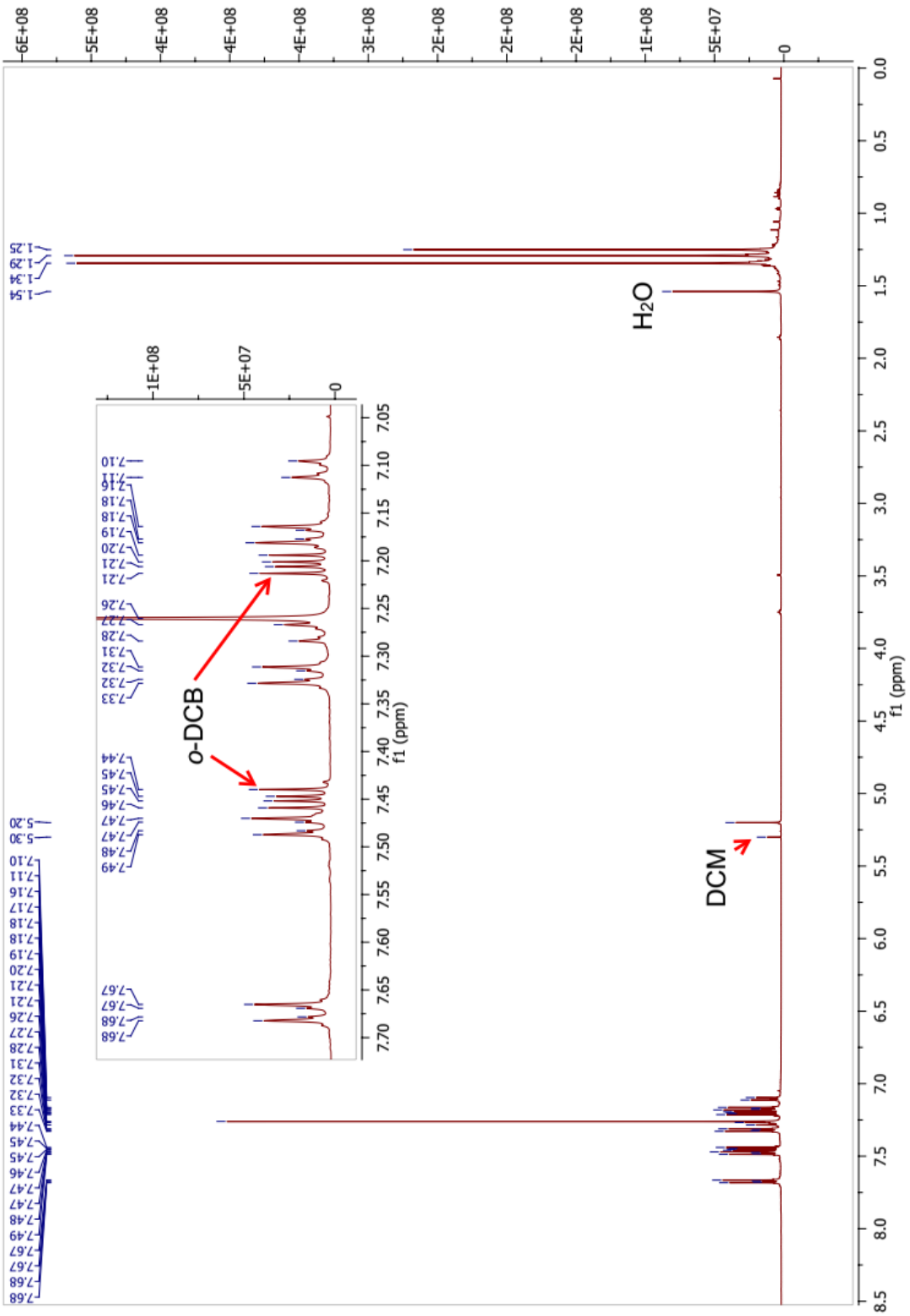

Fig. 1.40. ^{1}H NMR of Compound **3** ($CDCl_3$)

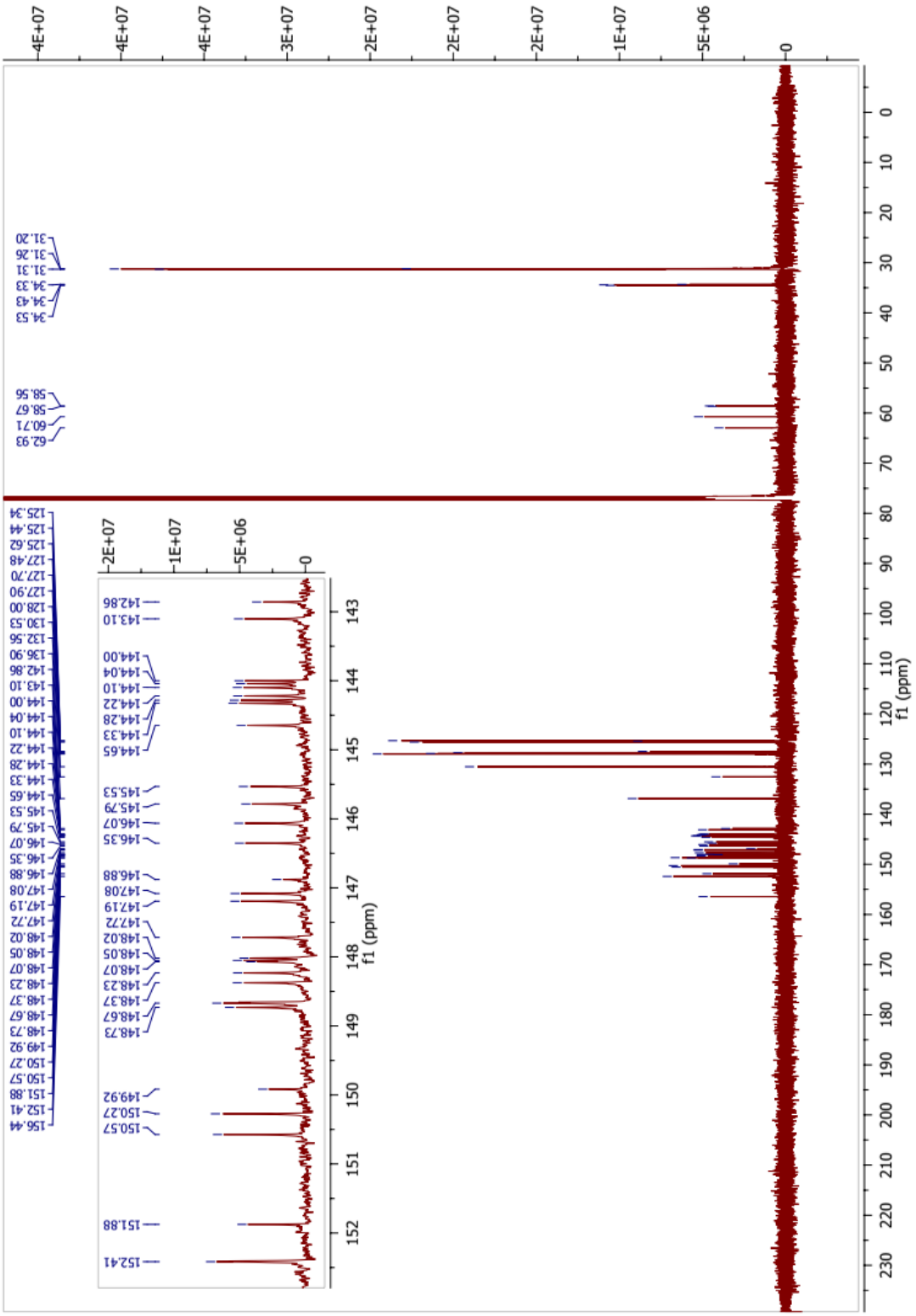

Fig. 1.41. ^{13}C NMR of compound **3** ($CDCl_3$)

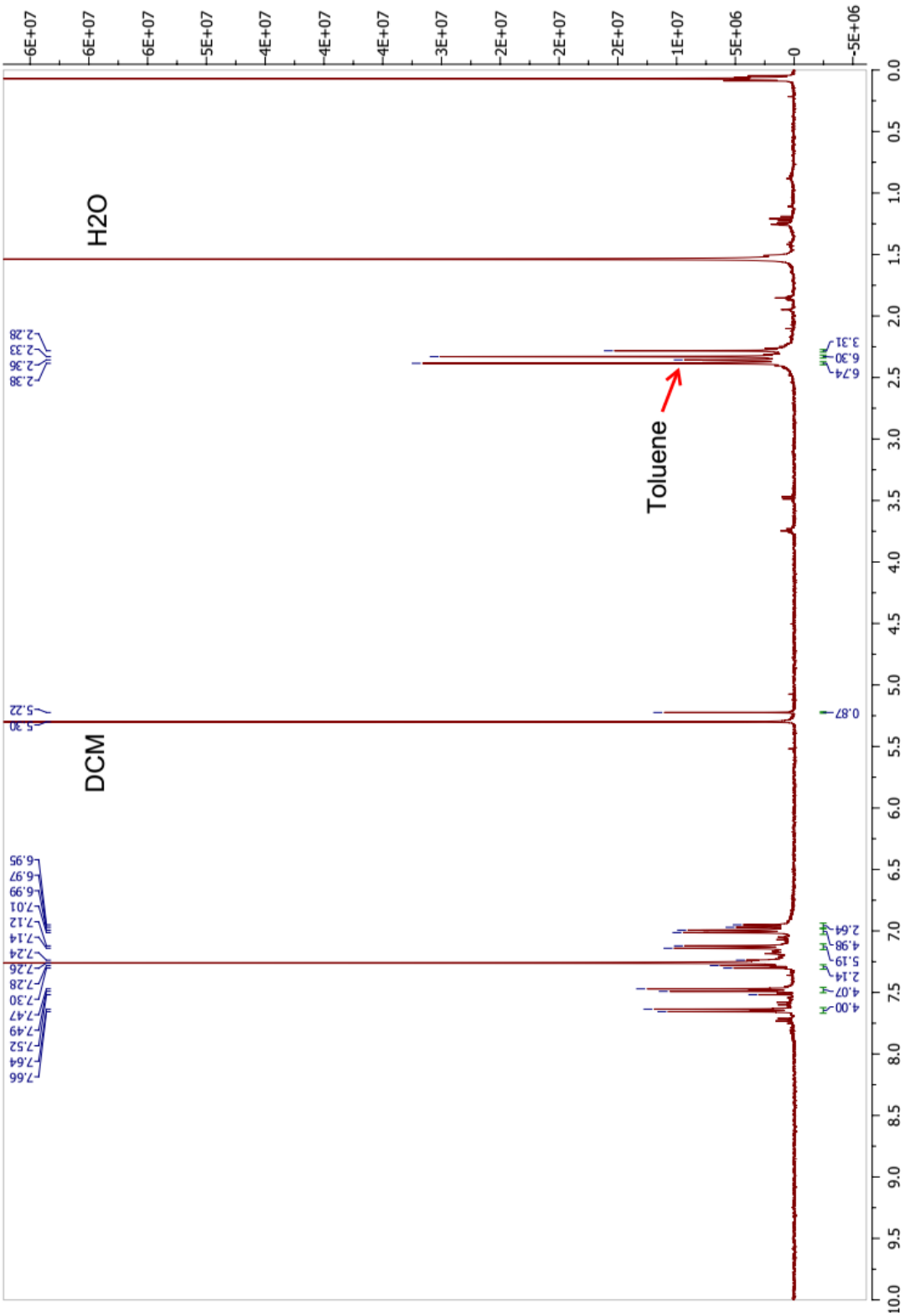

Fig. 1.42. ^{1}H NMR of Compound **4** ($CDCl_3$)

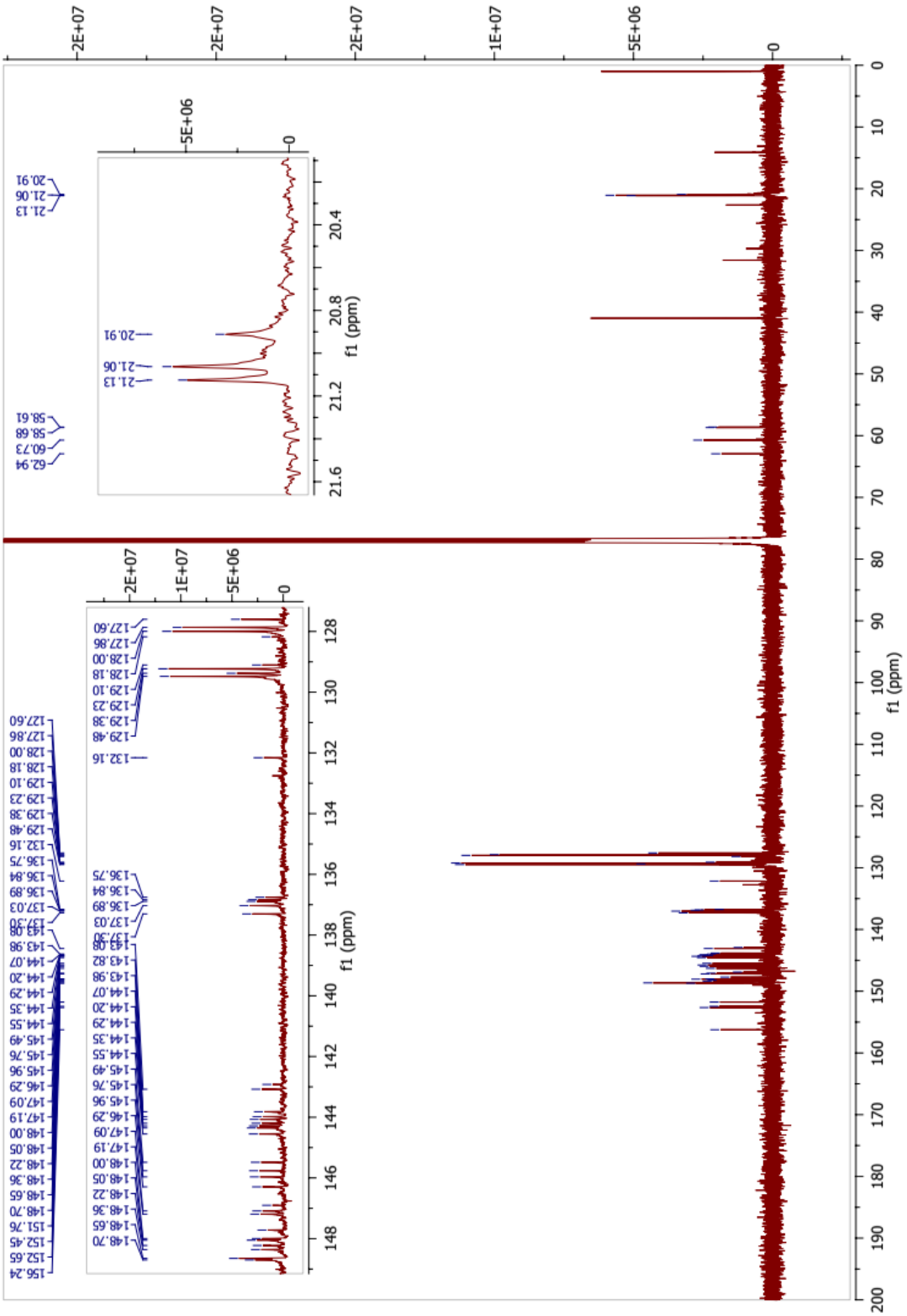

Fig. 1.43. ^{13}C NMR of compound **4** ($CDCl_3$)

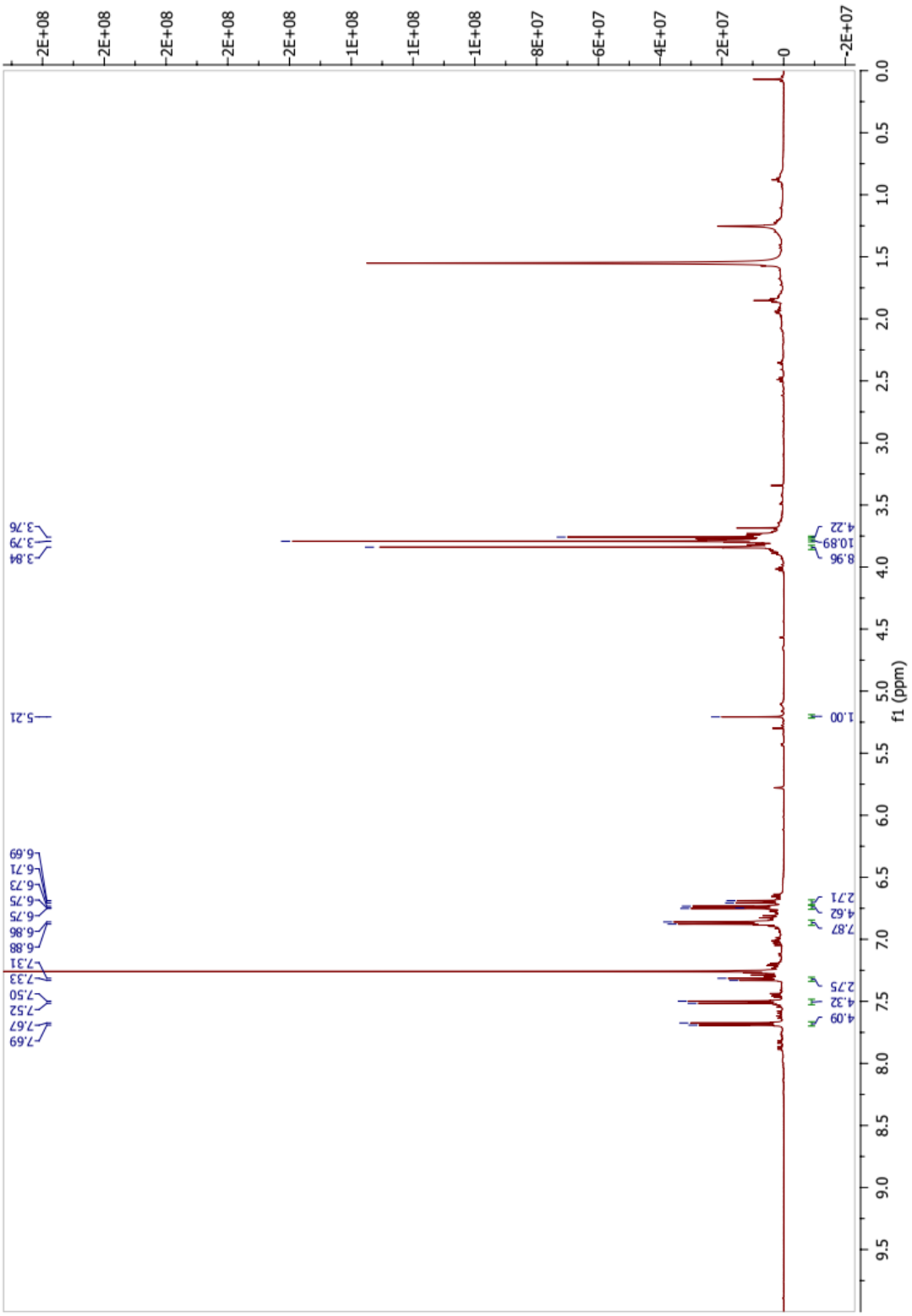

Fig. 1.44. ^{1}H NMR of Compound **5** ($CDCl_3$)

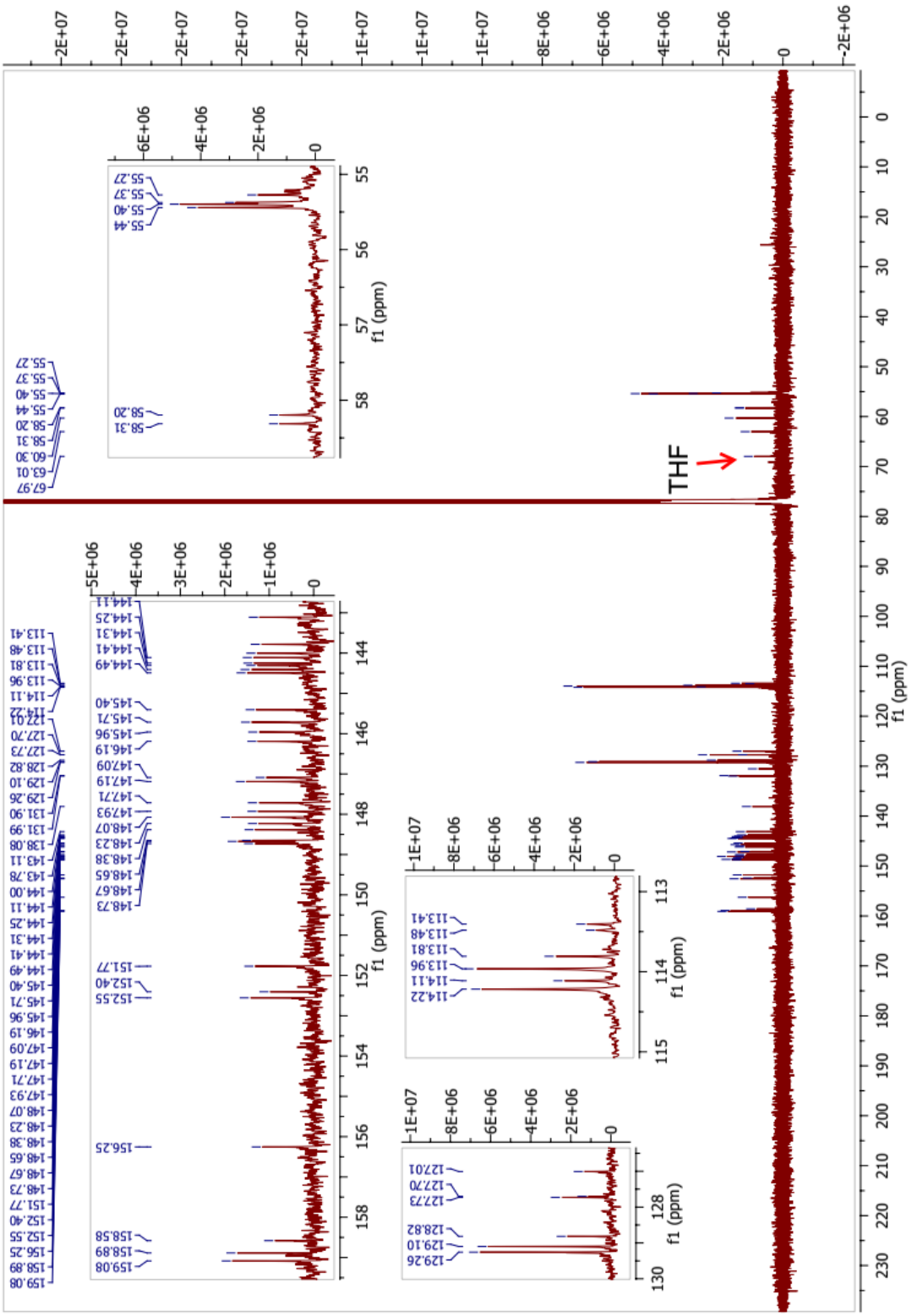

Fig. 1.45. ^{13}C NMR of compound **5** ($CDCl_3$)

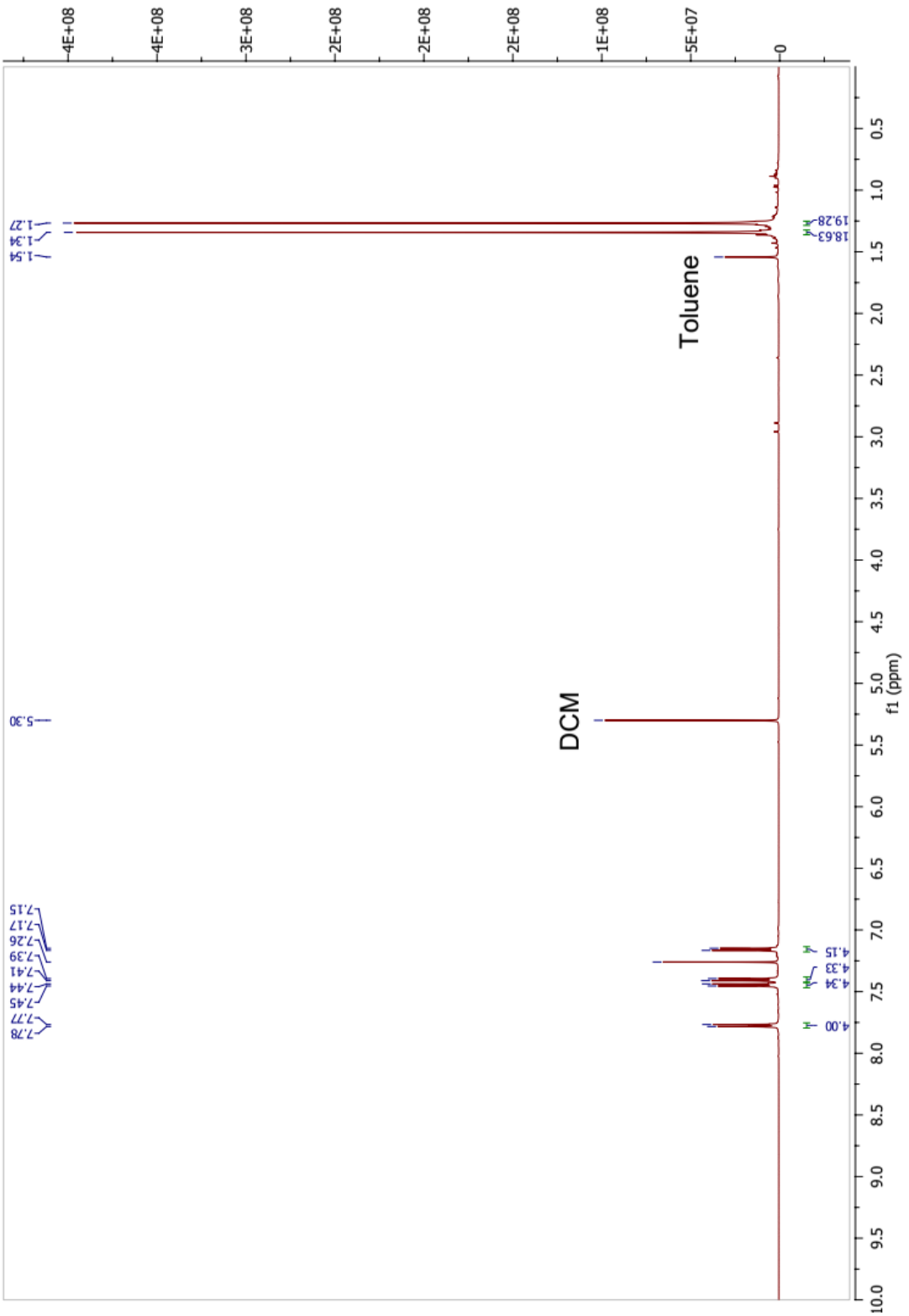

Fig. 1.46. ^{1}H NMR of Compound **6** ($CDCl_3$)

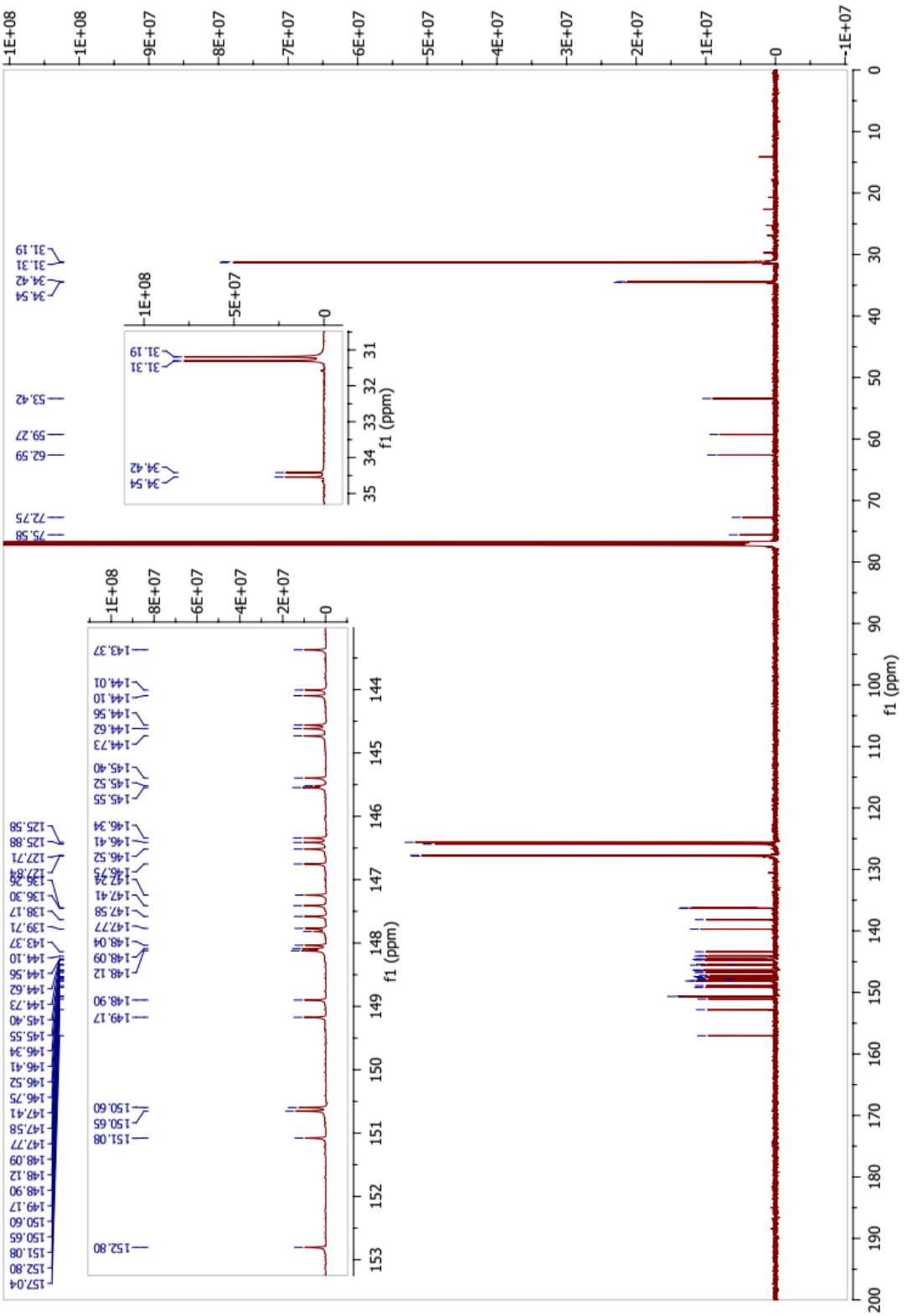

Fig. 1.47. ^{13}C NMR of compound **6** ($CDCl_3$)

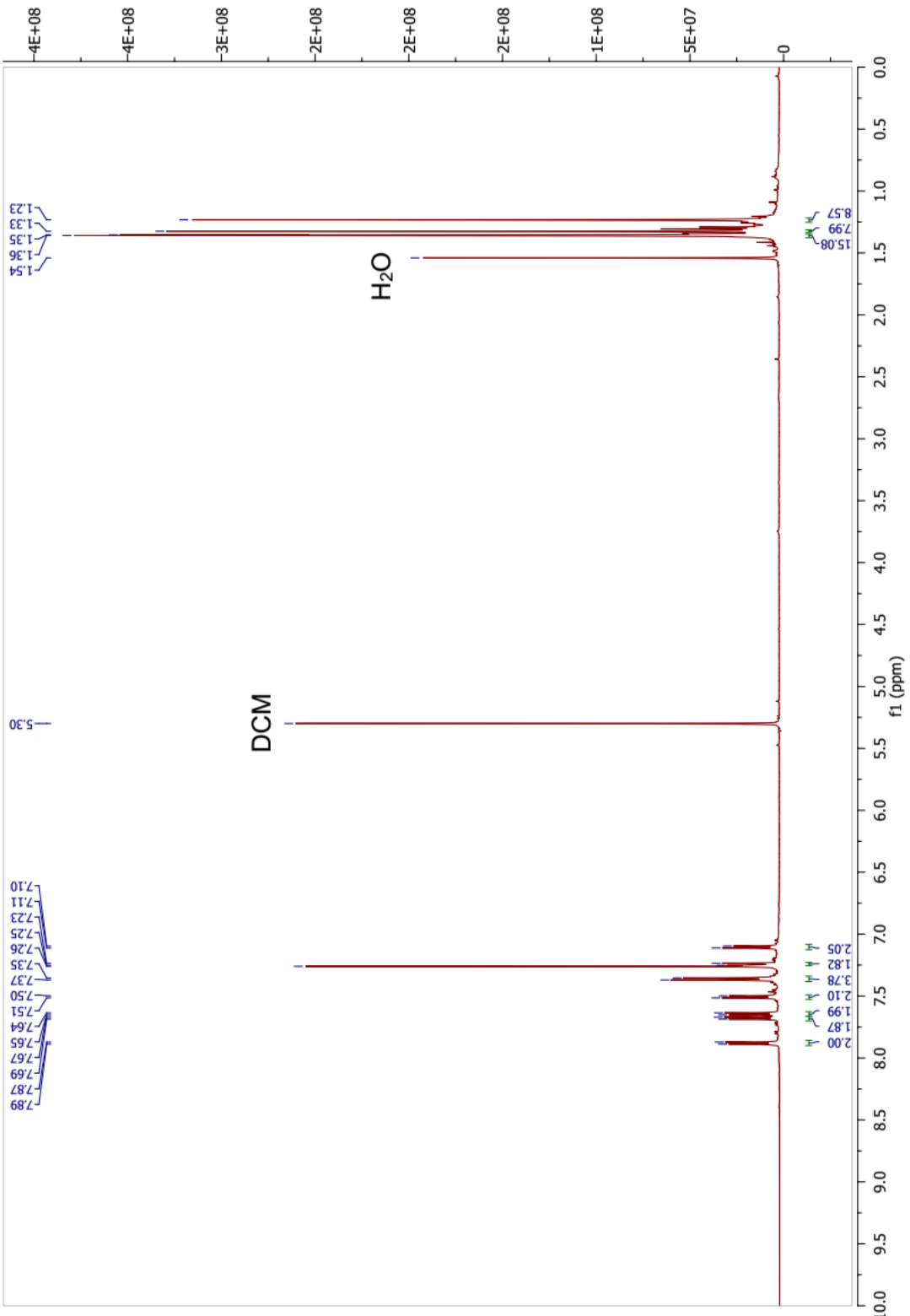

Fig. 1.48. ^{1}H NMR of Compound **7** ($CDCl_3$)

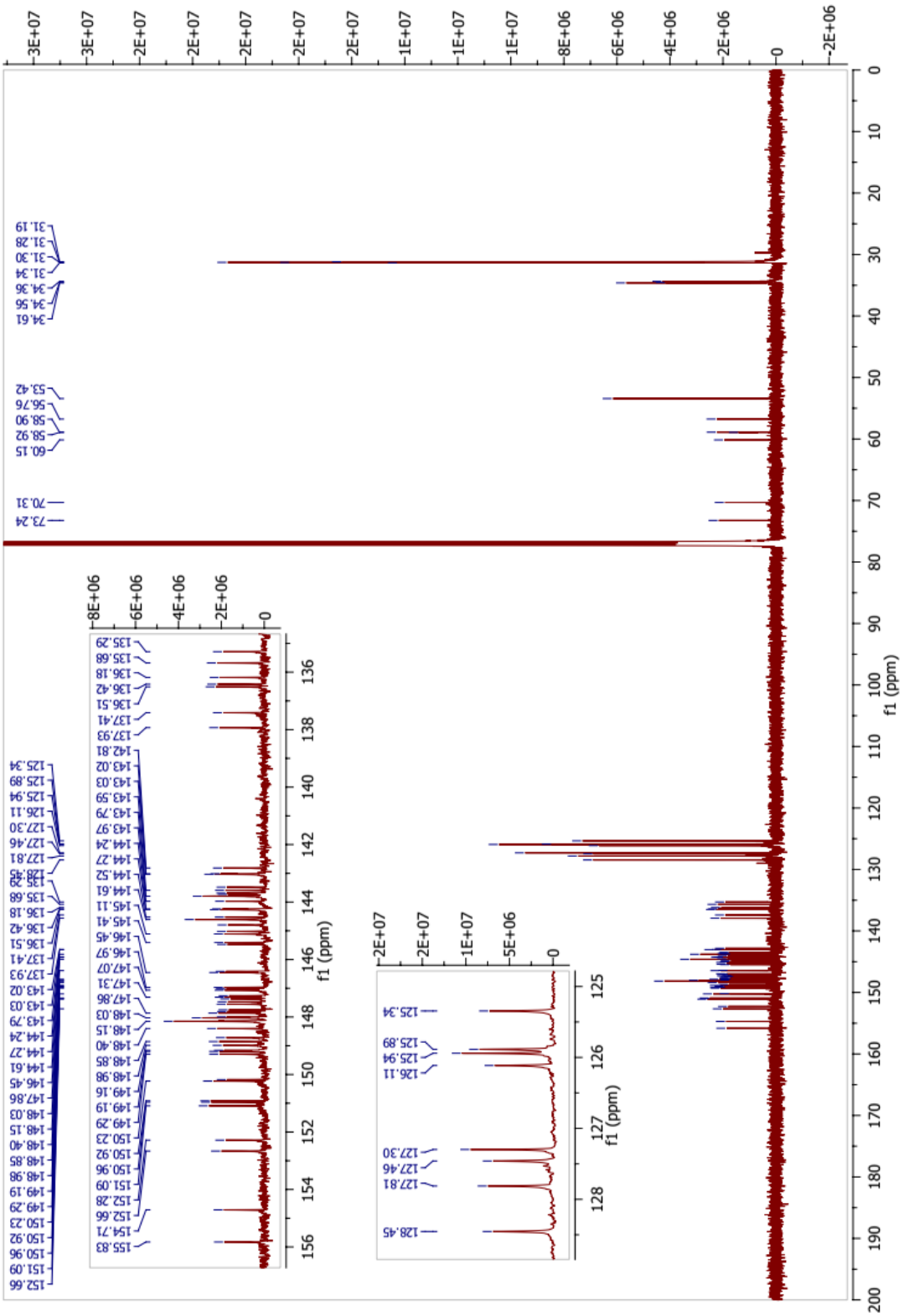

Fig. 1.49. ^{13}C NMR of compound **7** ($CDCl_3$)

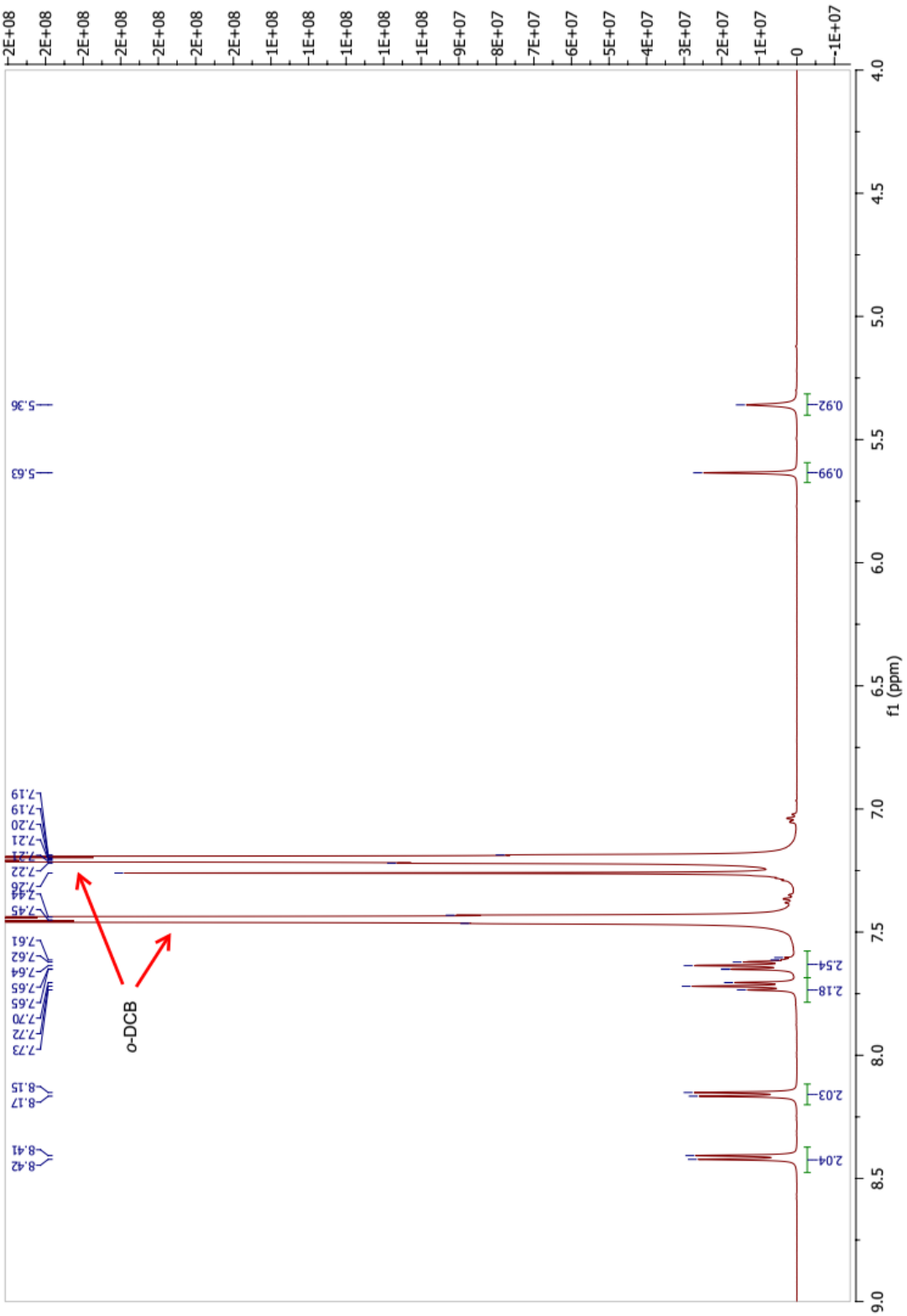

Fig. 1.50. ^{1}H NMR of Compound **8** ($CDCl_3$)

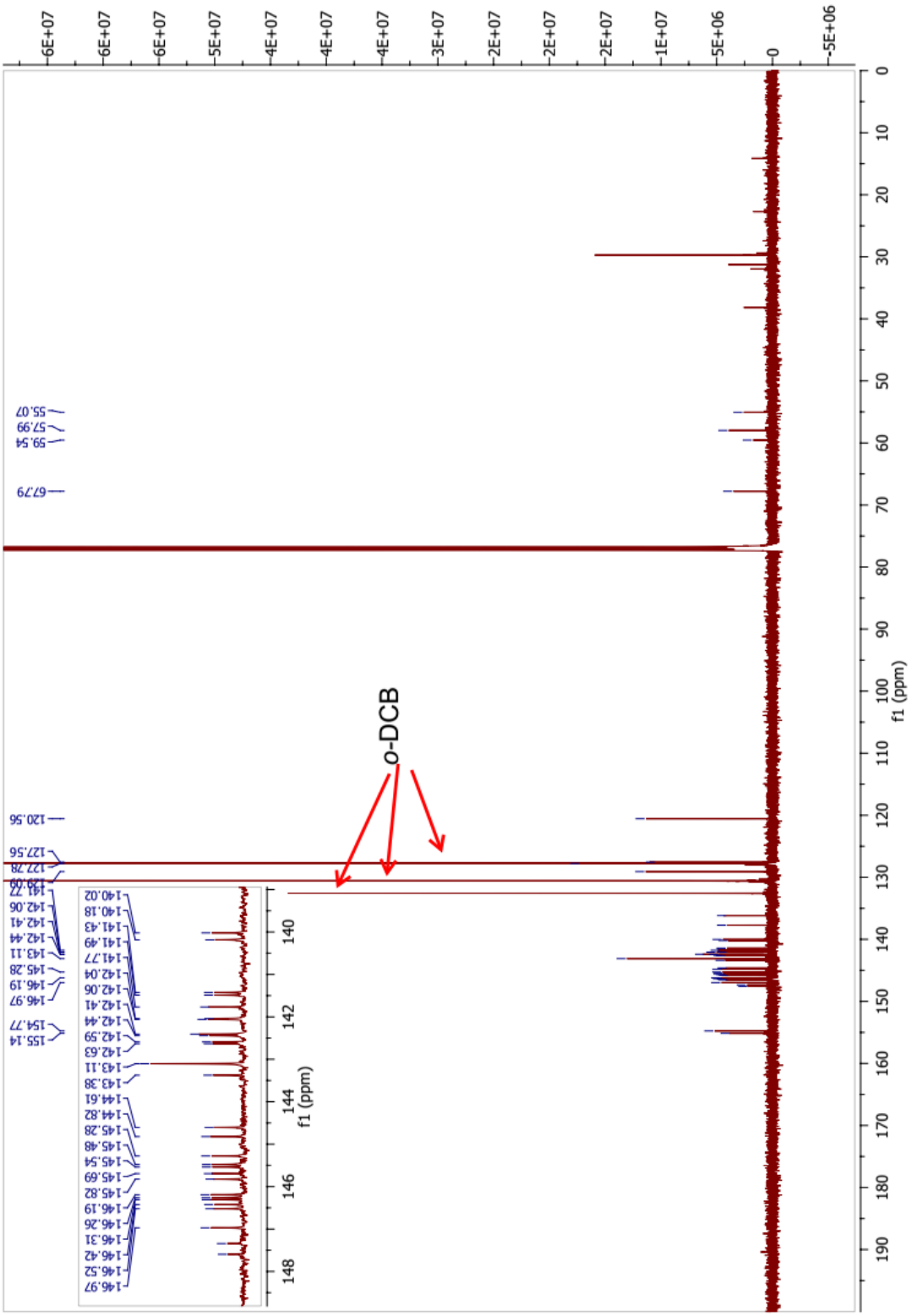

Fig. 1.51. ^{13}C NMR of compound **8** ($CDCl_3$)

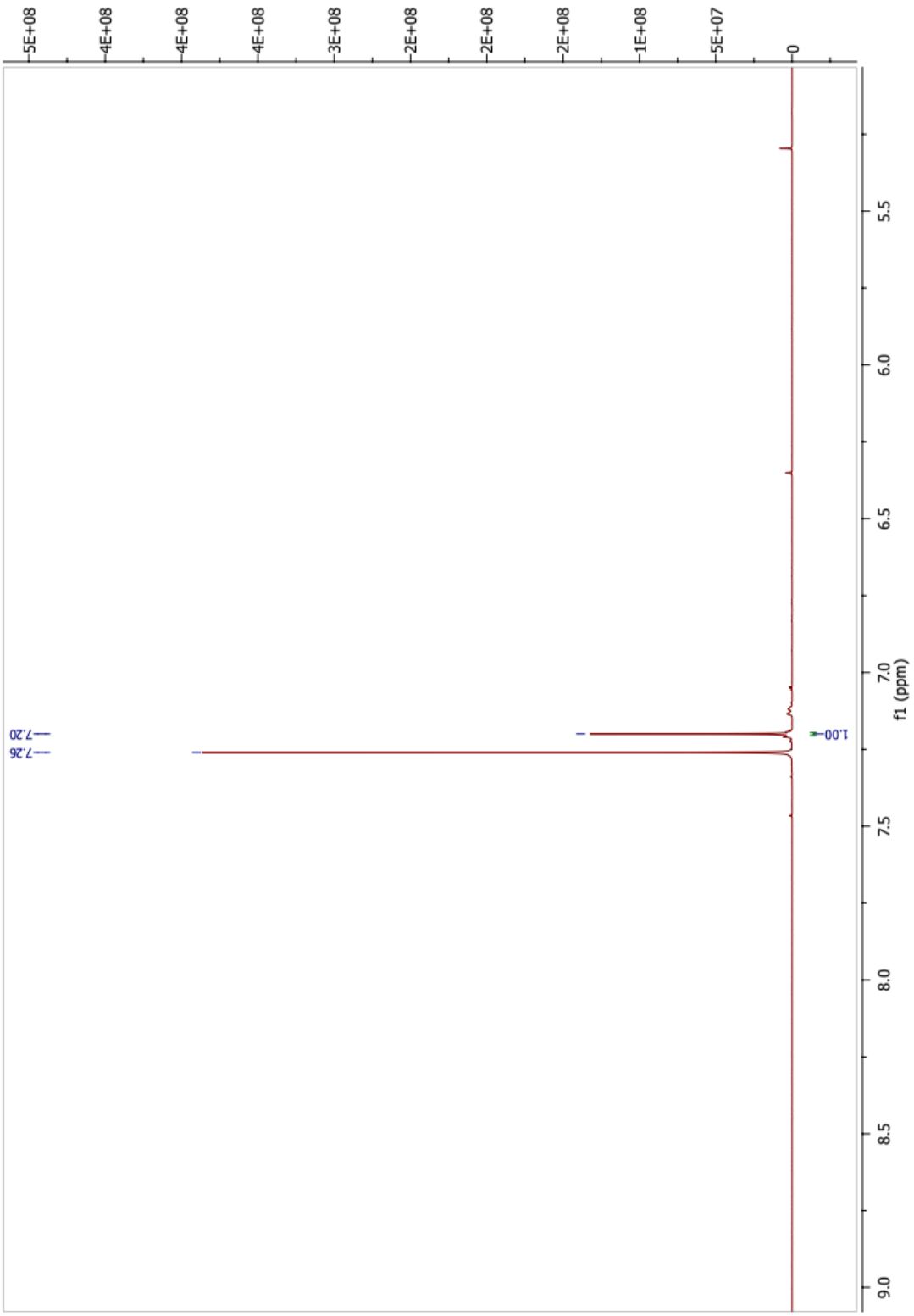

Fig. 1.52. ^{1}H NMR of Compound **9** ($CDCl_3$)

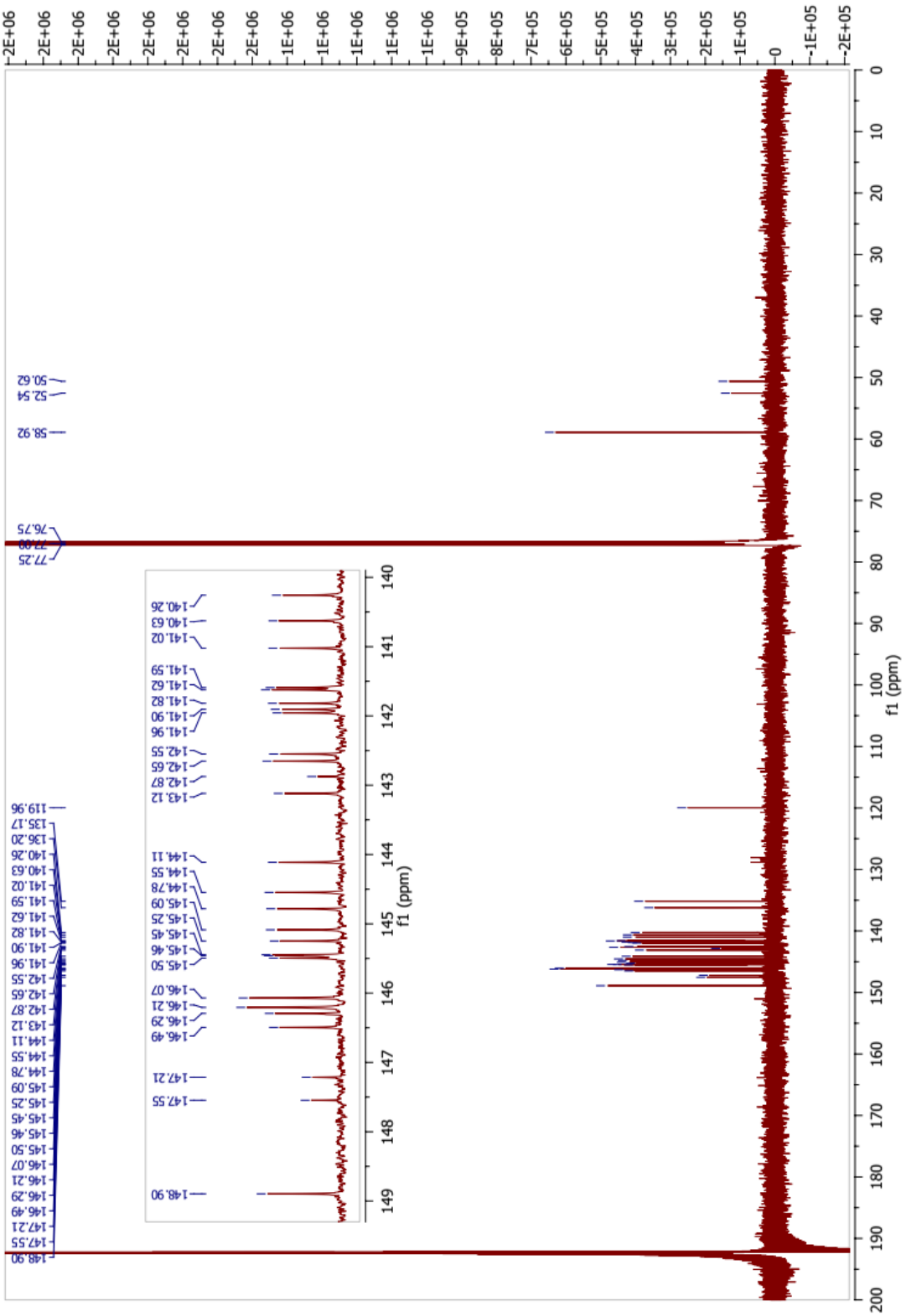

Fig. 1.53. ^{13}C NMR of compound **9** ($CDCl_3$)

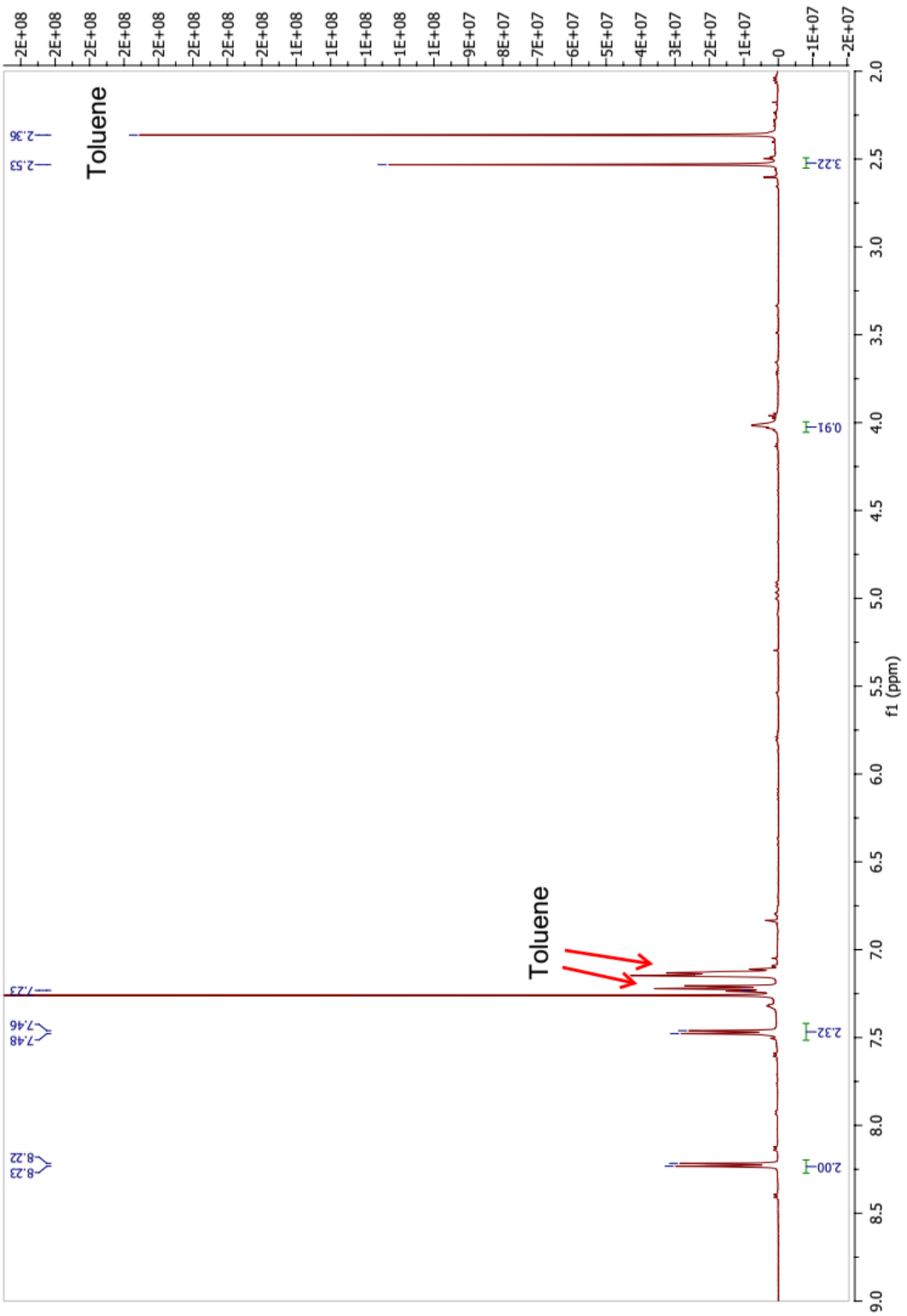

Fig. 1.54. ^{1}H NMR of Compound **10** ($CDCl_3$)

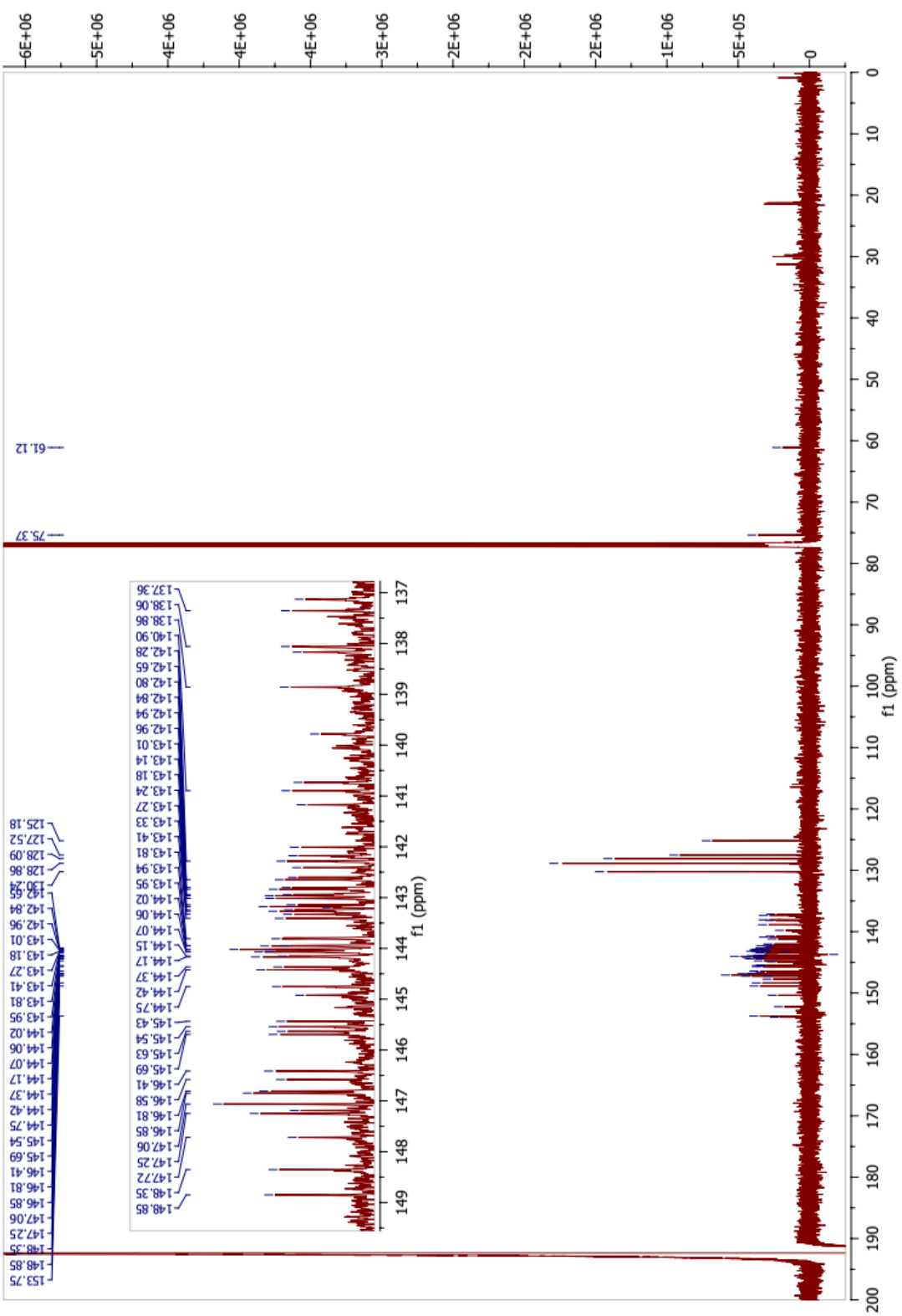

Fig. 1.55. ^{13}C NMR of compound **10** ($CDCl_3$).

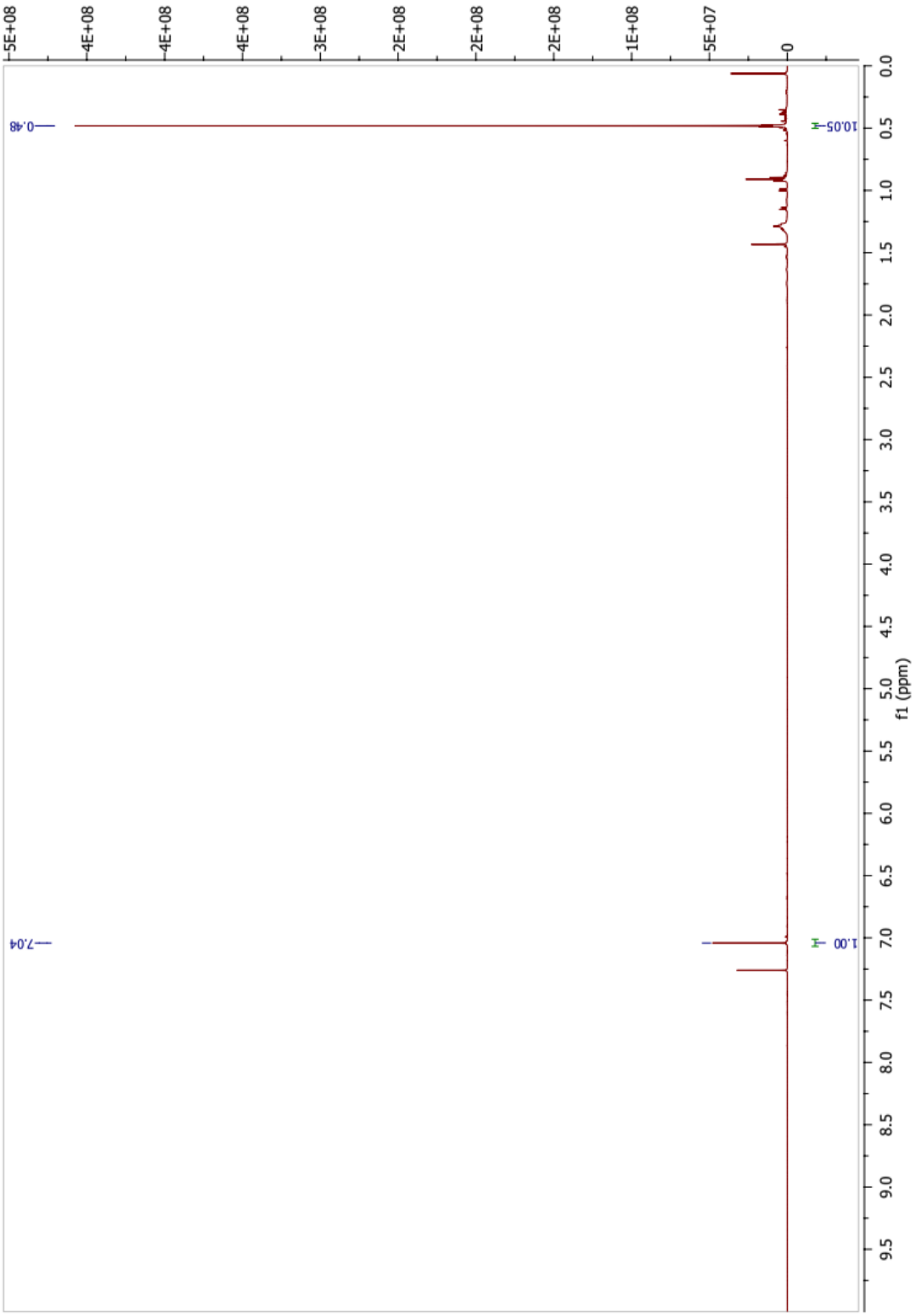

Fig. 1.56. ^{1}H NMR of compound **11** ($CDCl_3$)

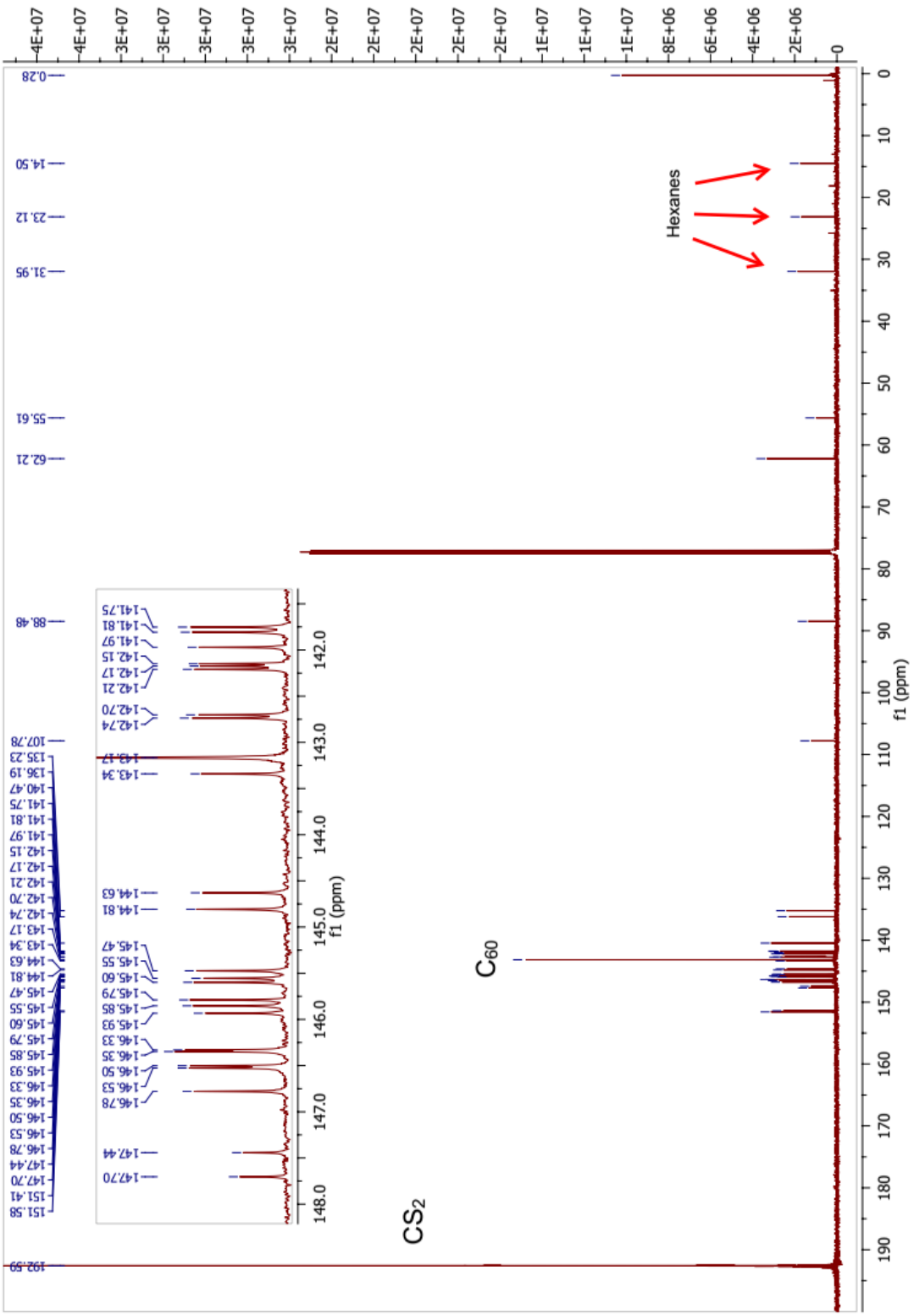

Fig. 1.57. ^{13}C NMR of compound **11** ($CDCl_3$)

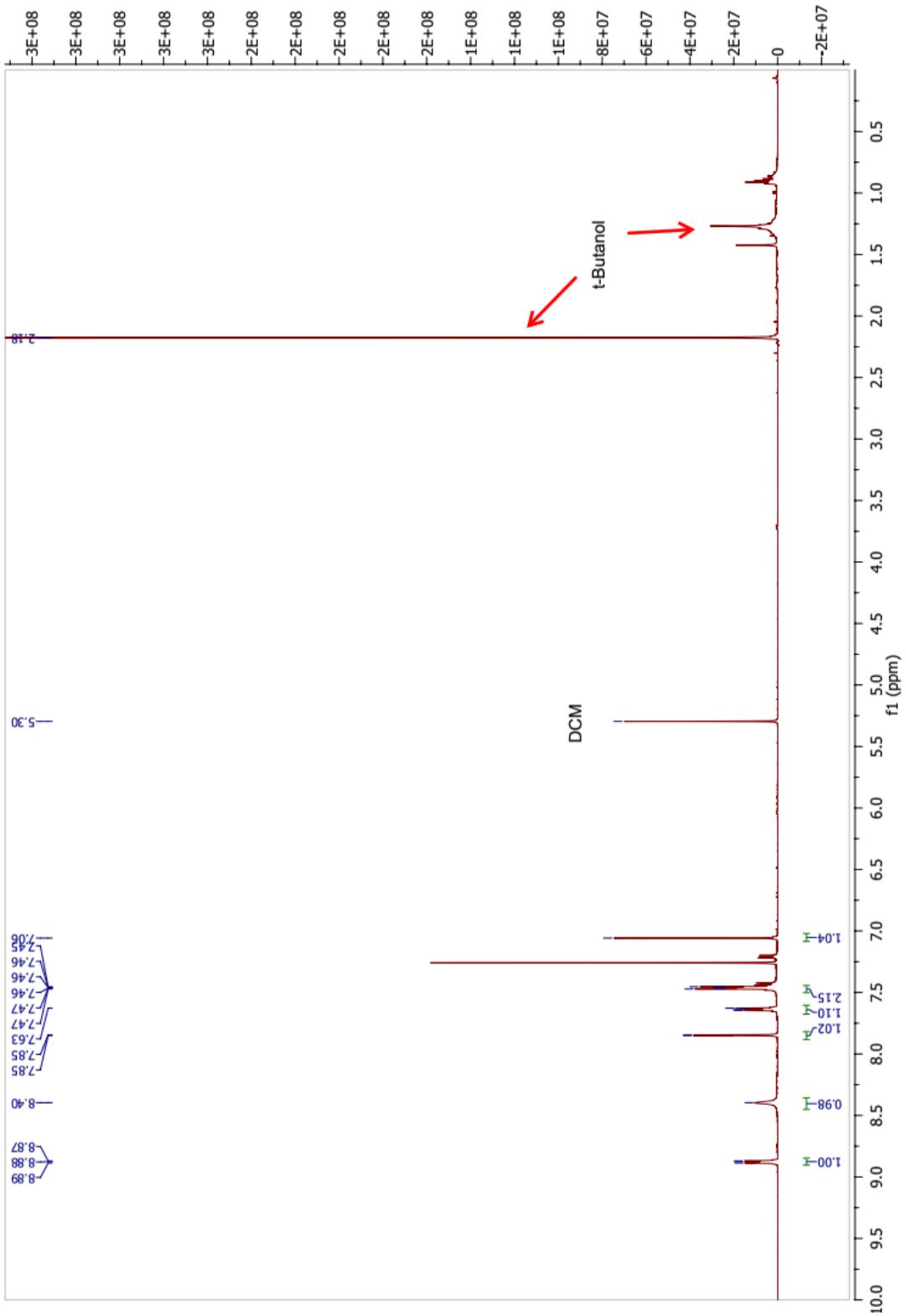

Fig. 1.58. ^{1}H NMR of compound **12** ($CDCl_3$)

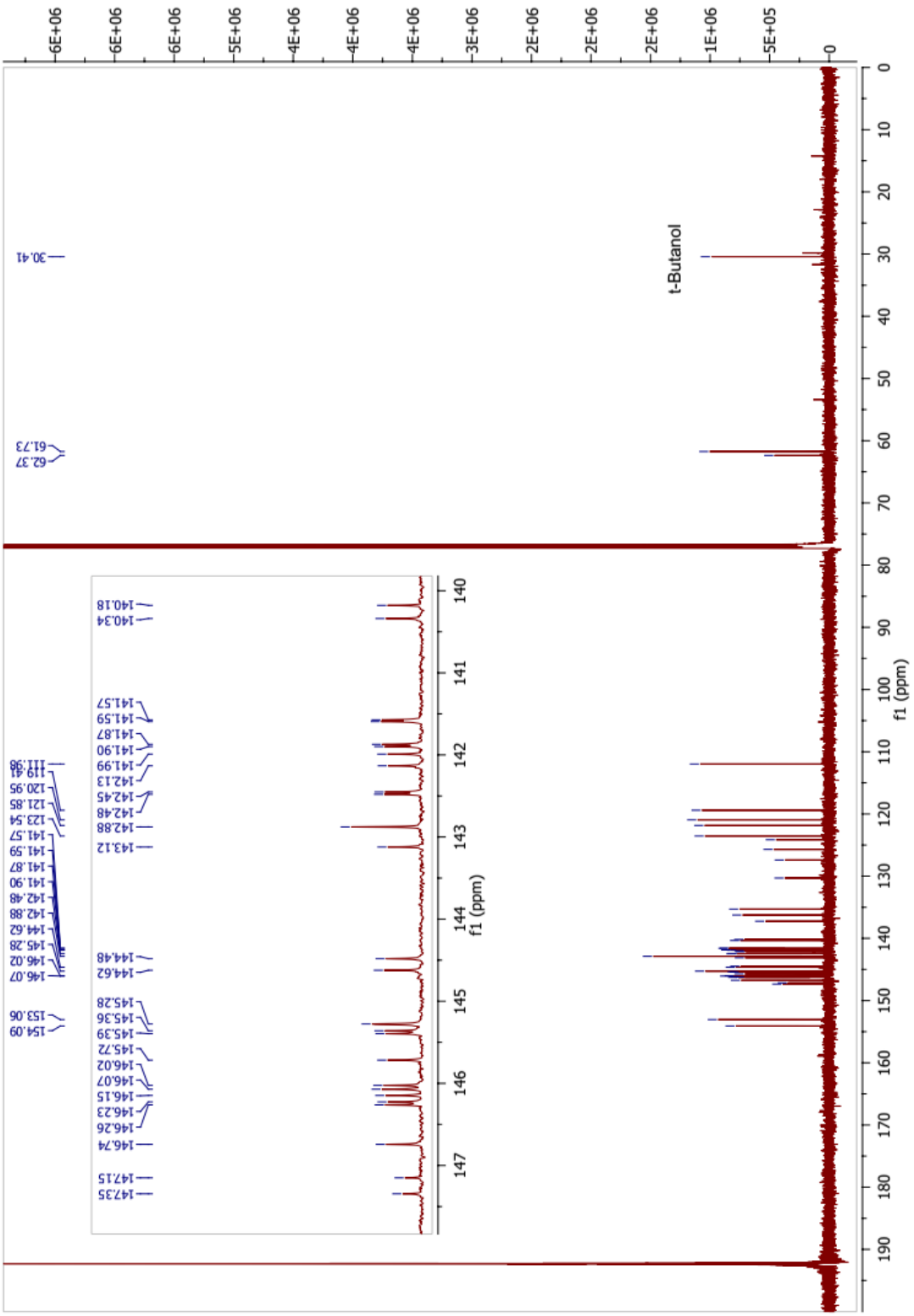

Fig. 1.59. ^{13}C NMR of compound **12** ($CDCl_3$)

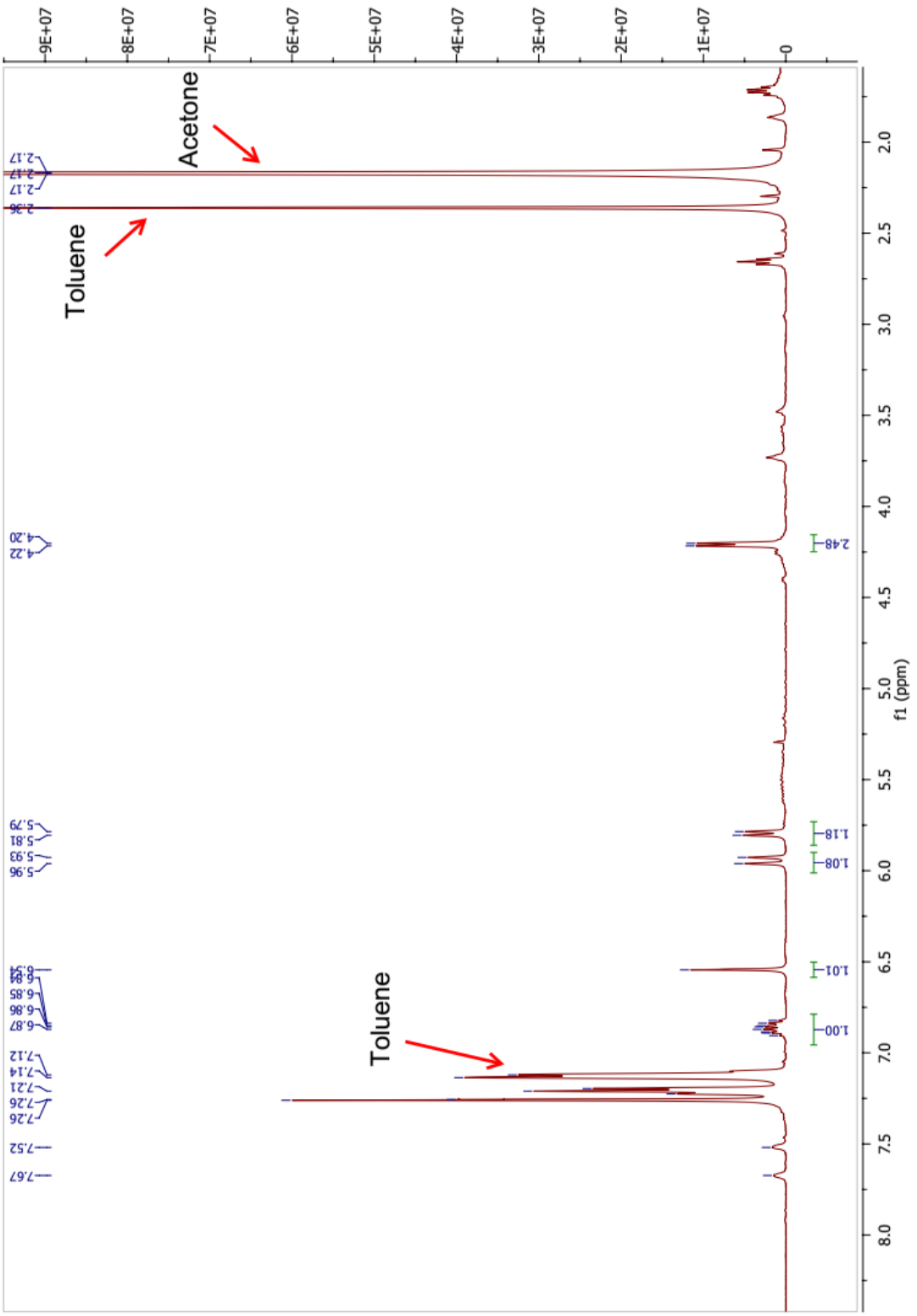

Fig. 1.60. ^{1}H NMR of compound **13** ($CDCl_3$)

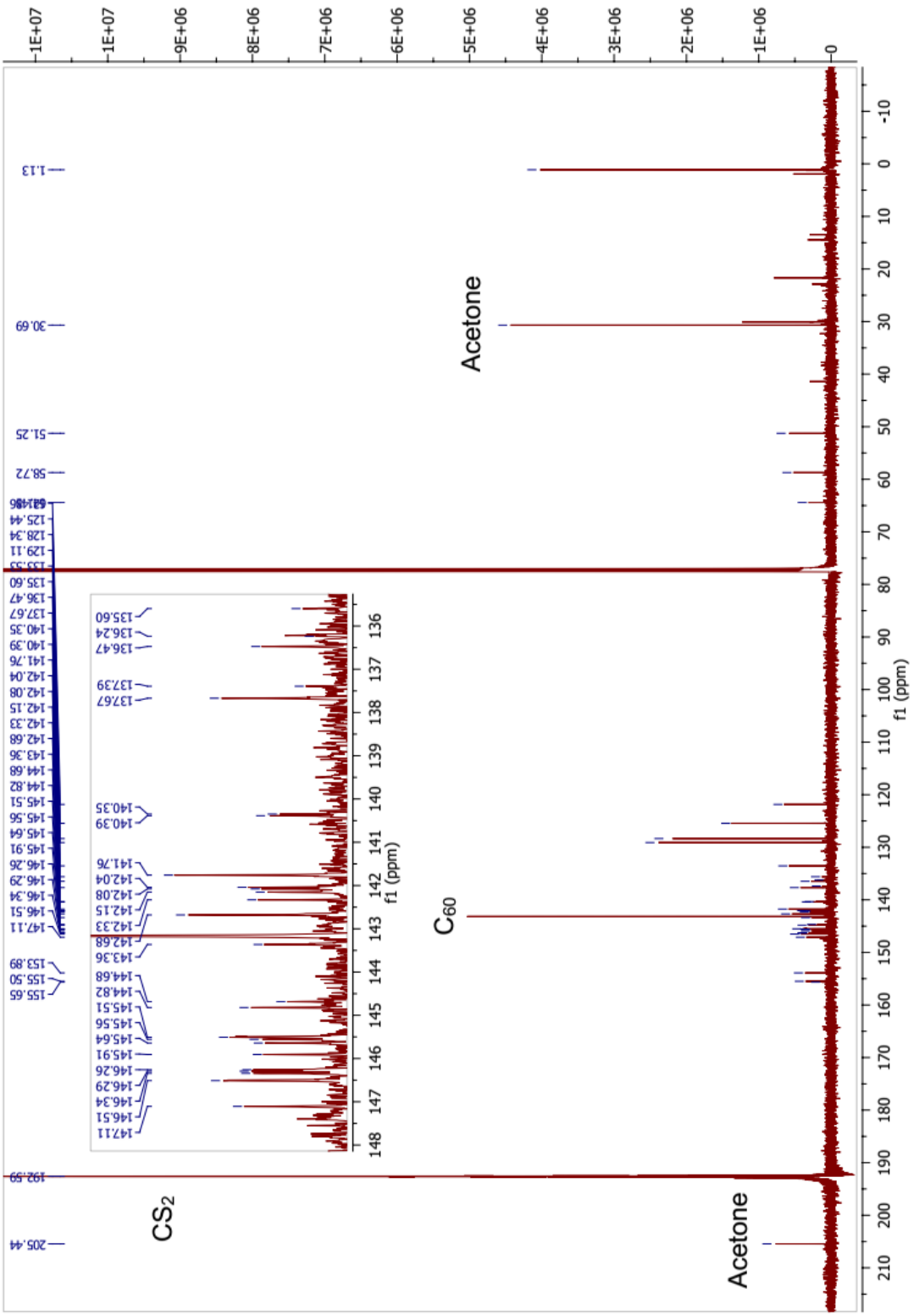

Fig. 1.61. ^{13}C NMR of compound **13** ($CDCl_3$)

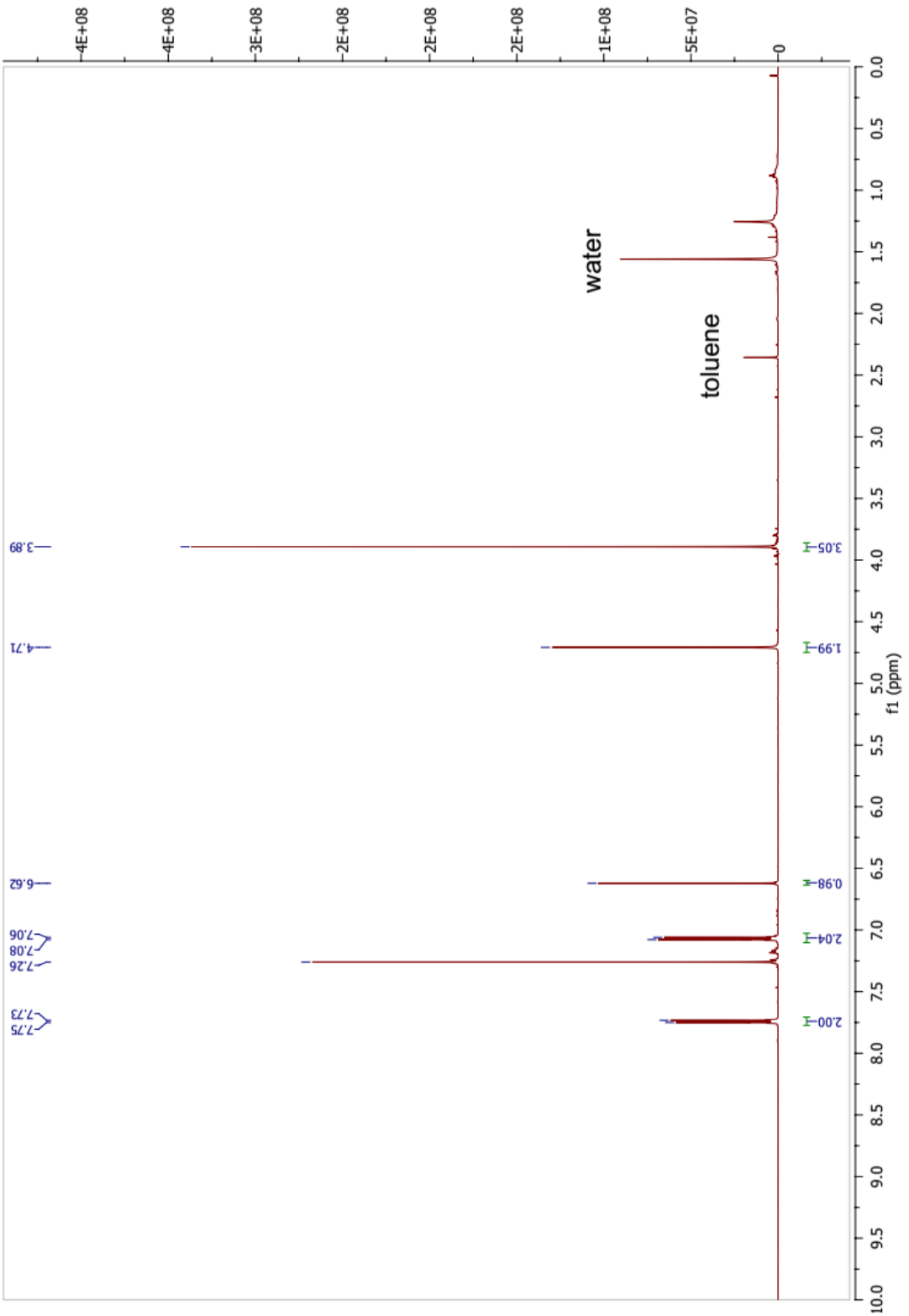

Fig. 1.62. ^{1}H NMR of compound **14** ($CDCl_3$)

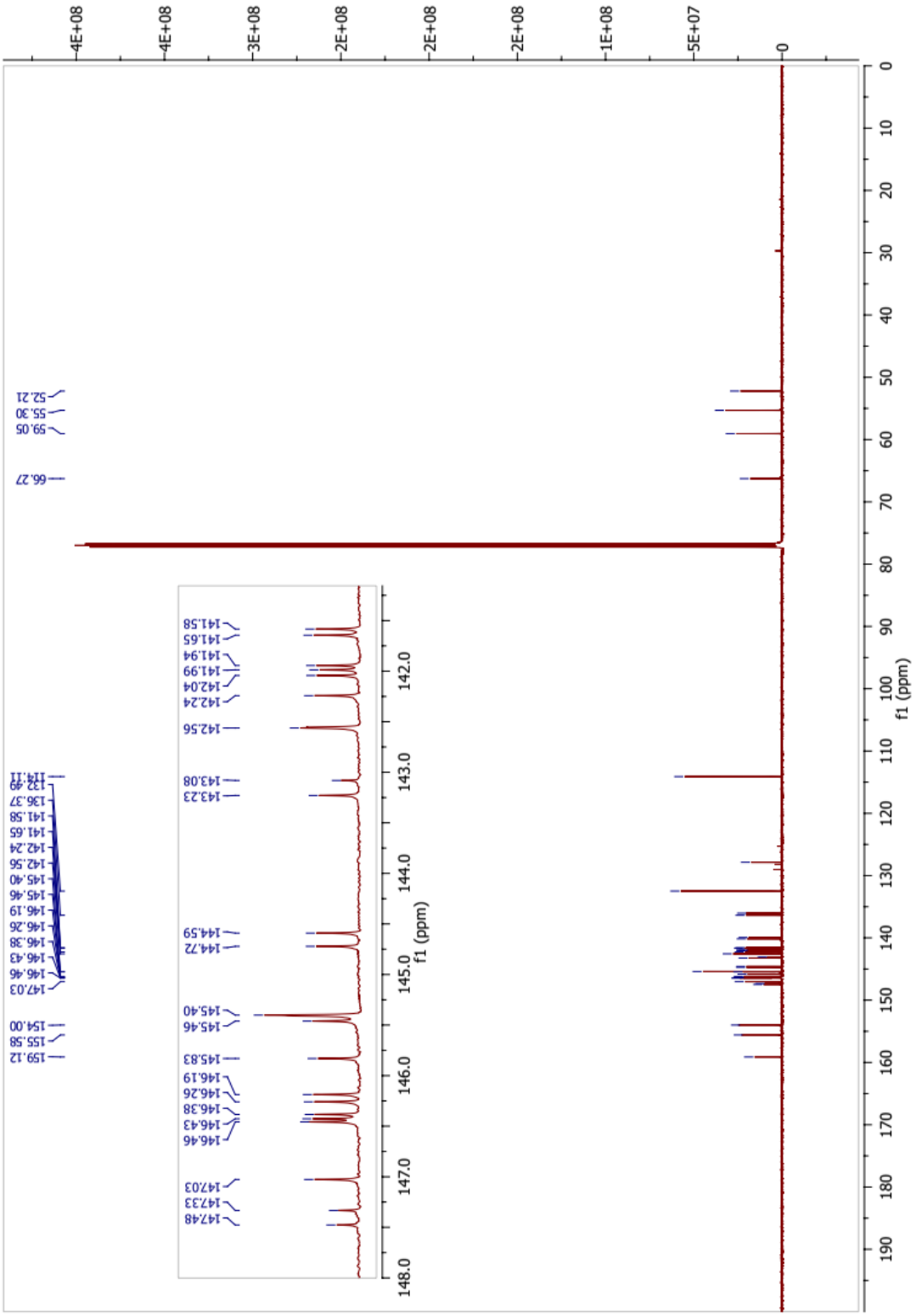

Fig. 1.63. ^{13}C NMR of compound **14** ($CDCl_3$)

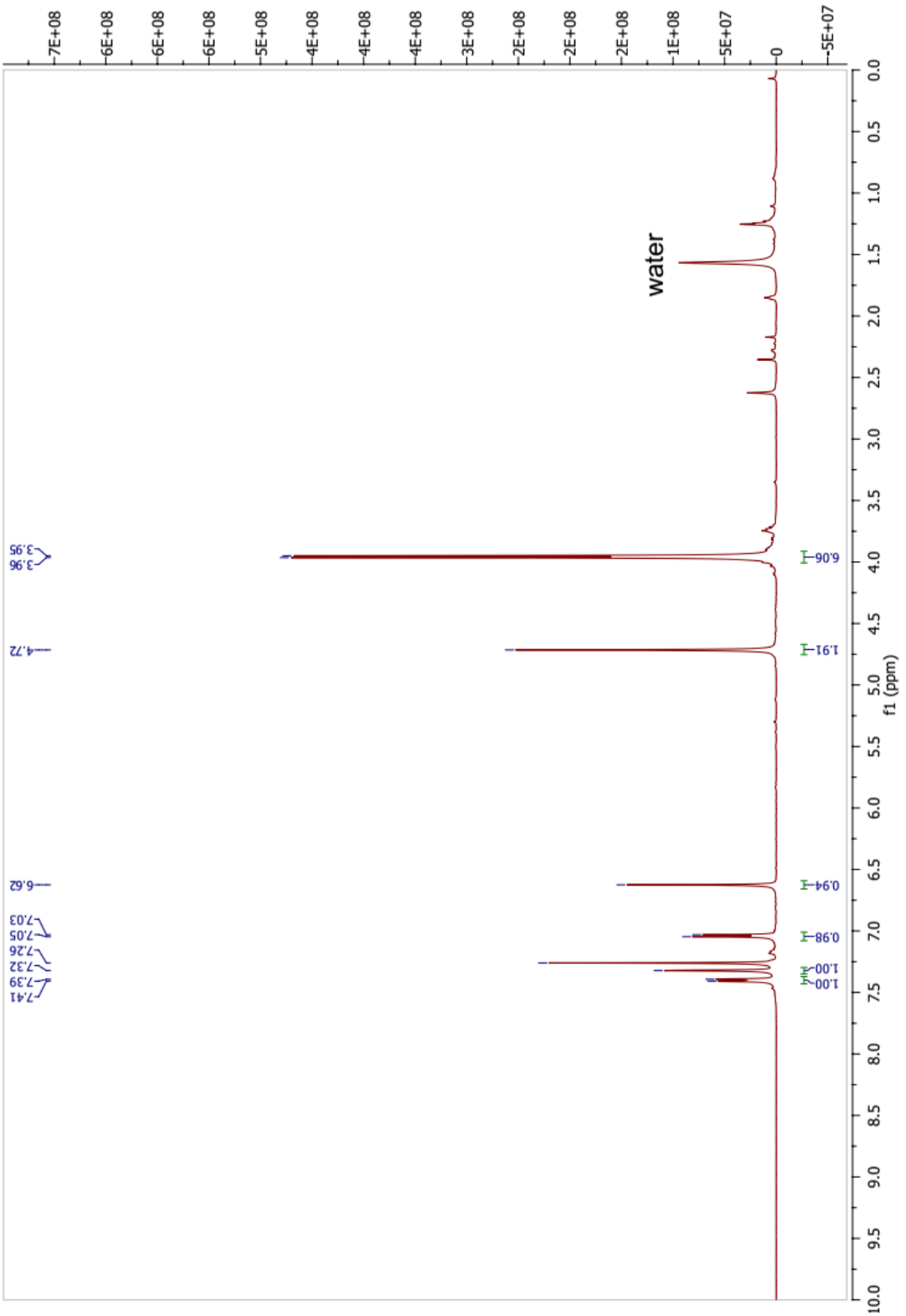

Fig. 1.64. ^{1}H NMR of compound **15** ($CDCl_3$)

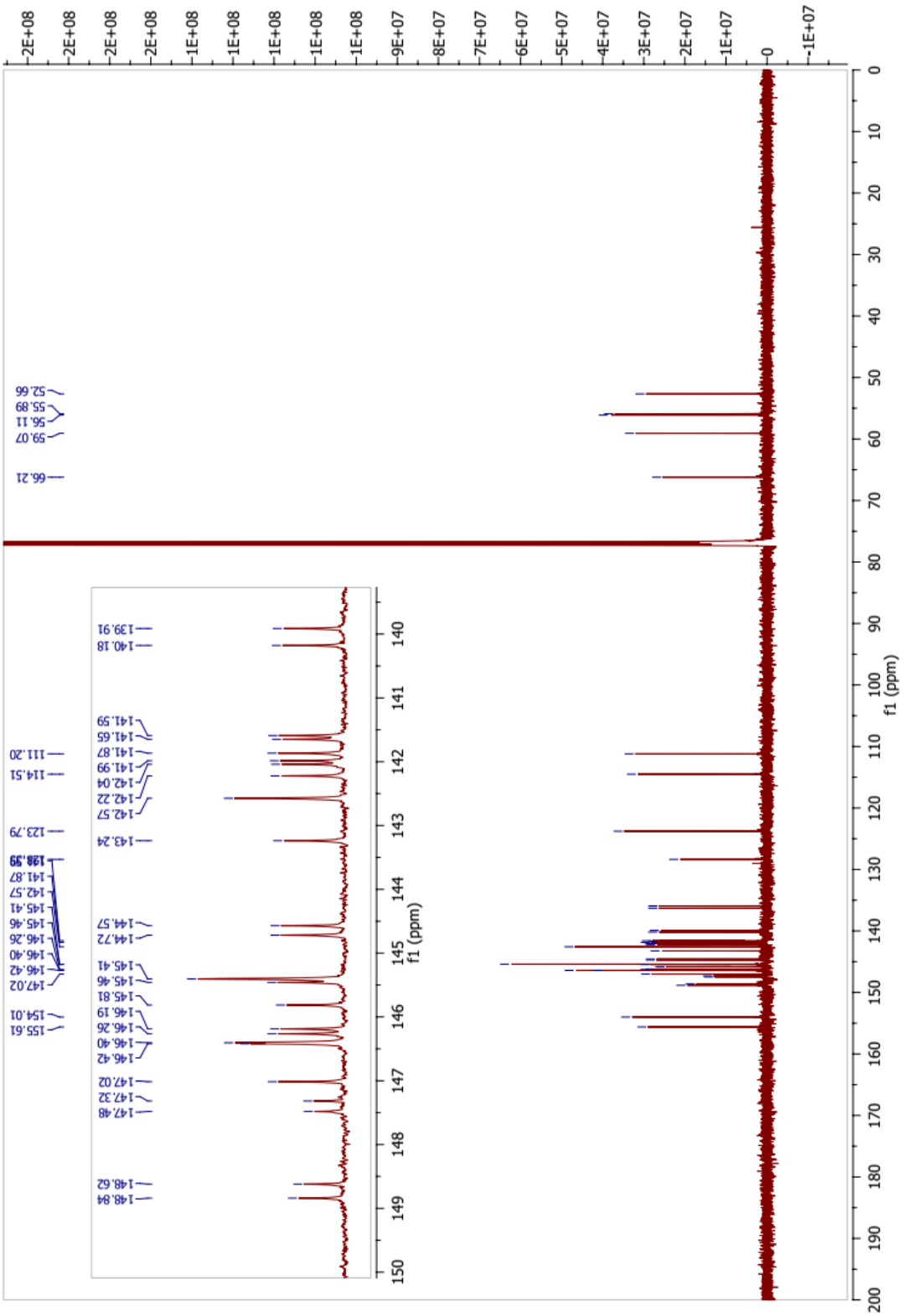

Fig. 1.65. ^{13}C NMR of compound **15** ($CDCl_3$)

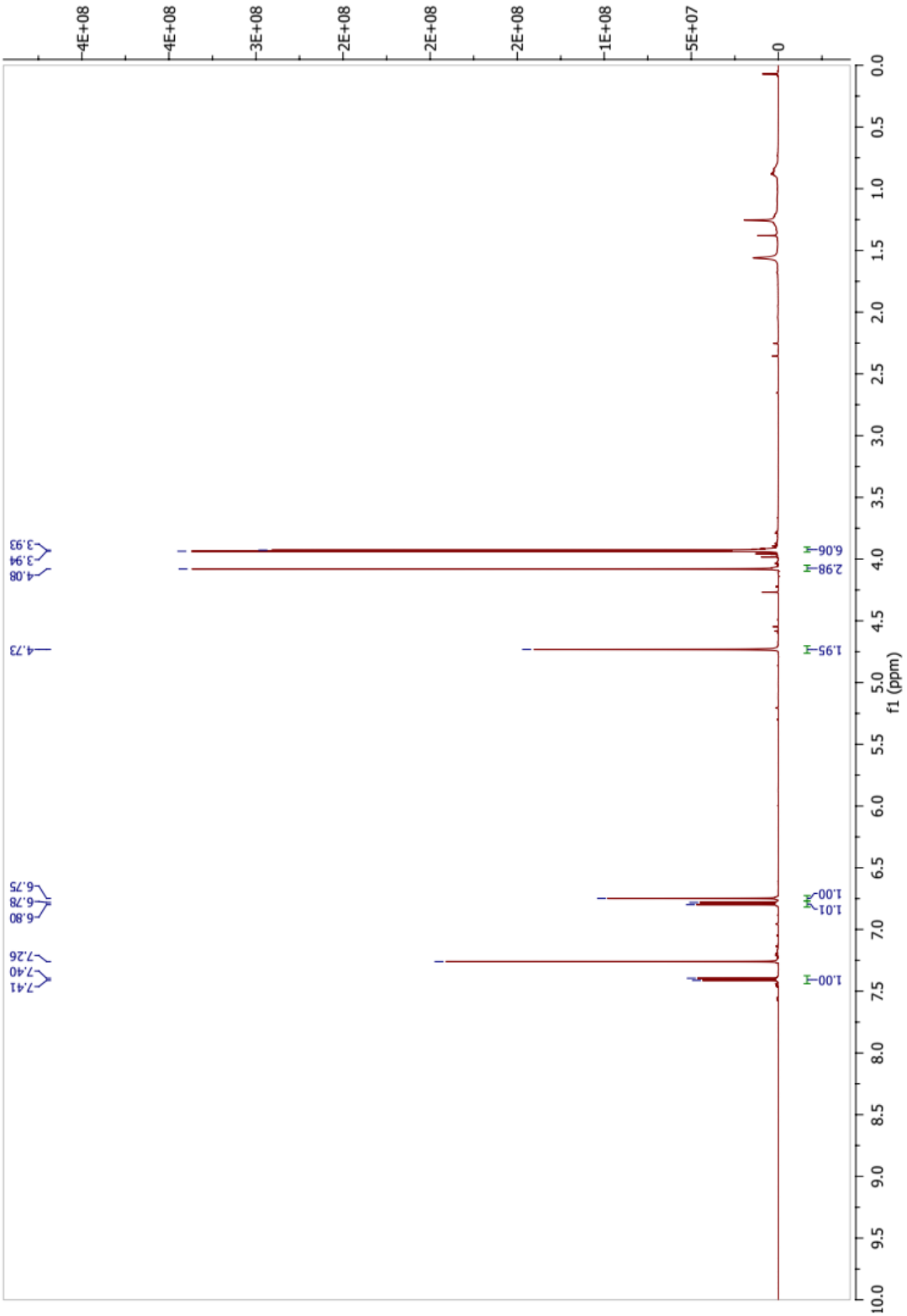

Fig. 1.66. ^{1}H NMR of compound **16** ($CDCl_3$)

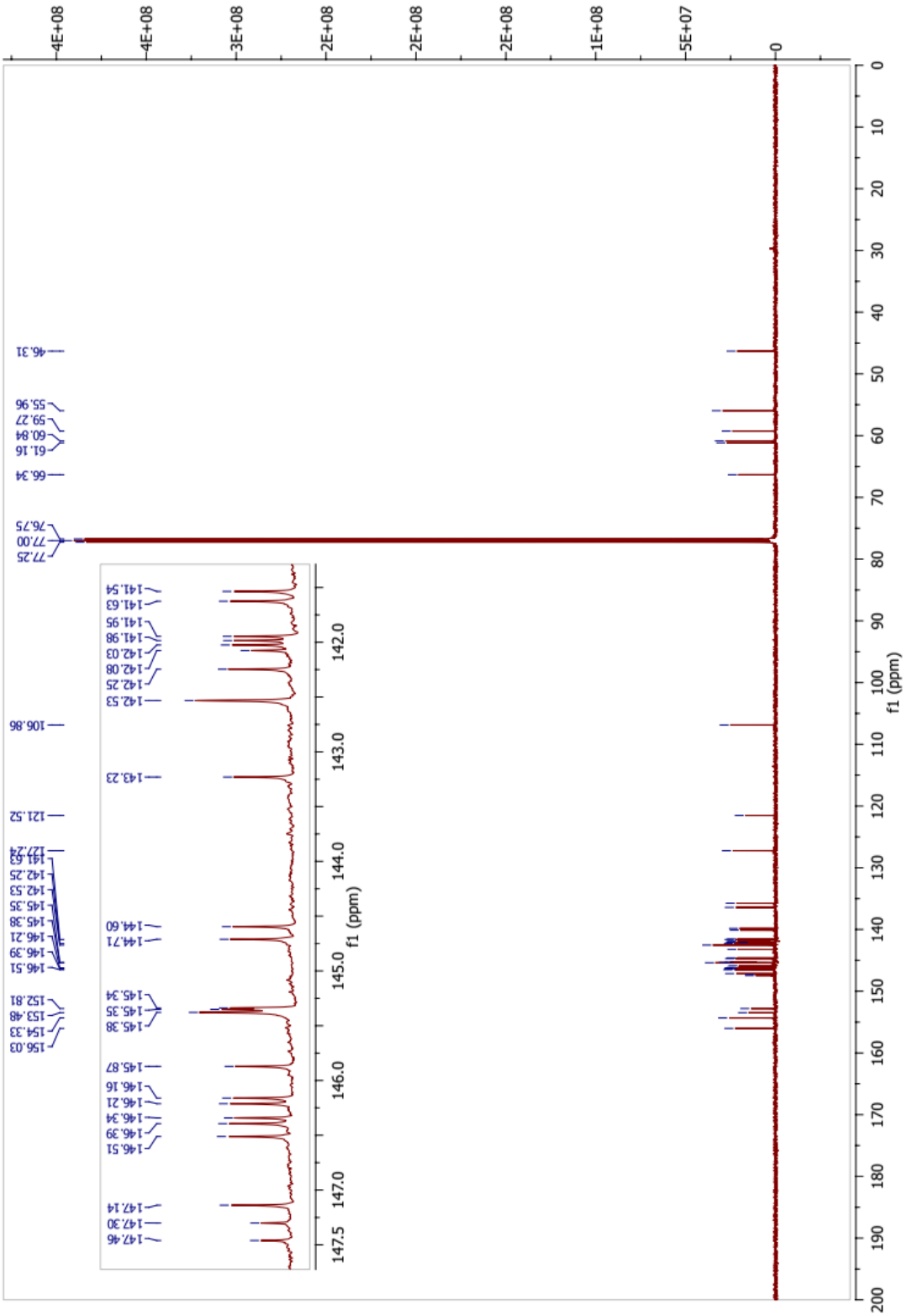

Fig. 1.67. ^{13}C NMR of compound **16** ($CDCl_3$)

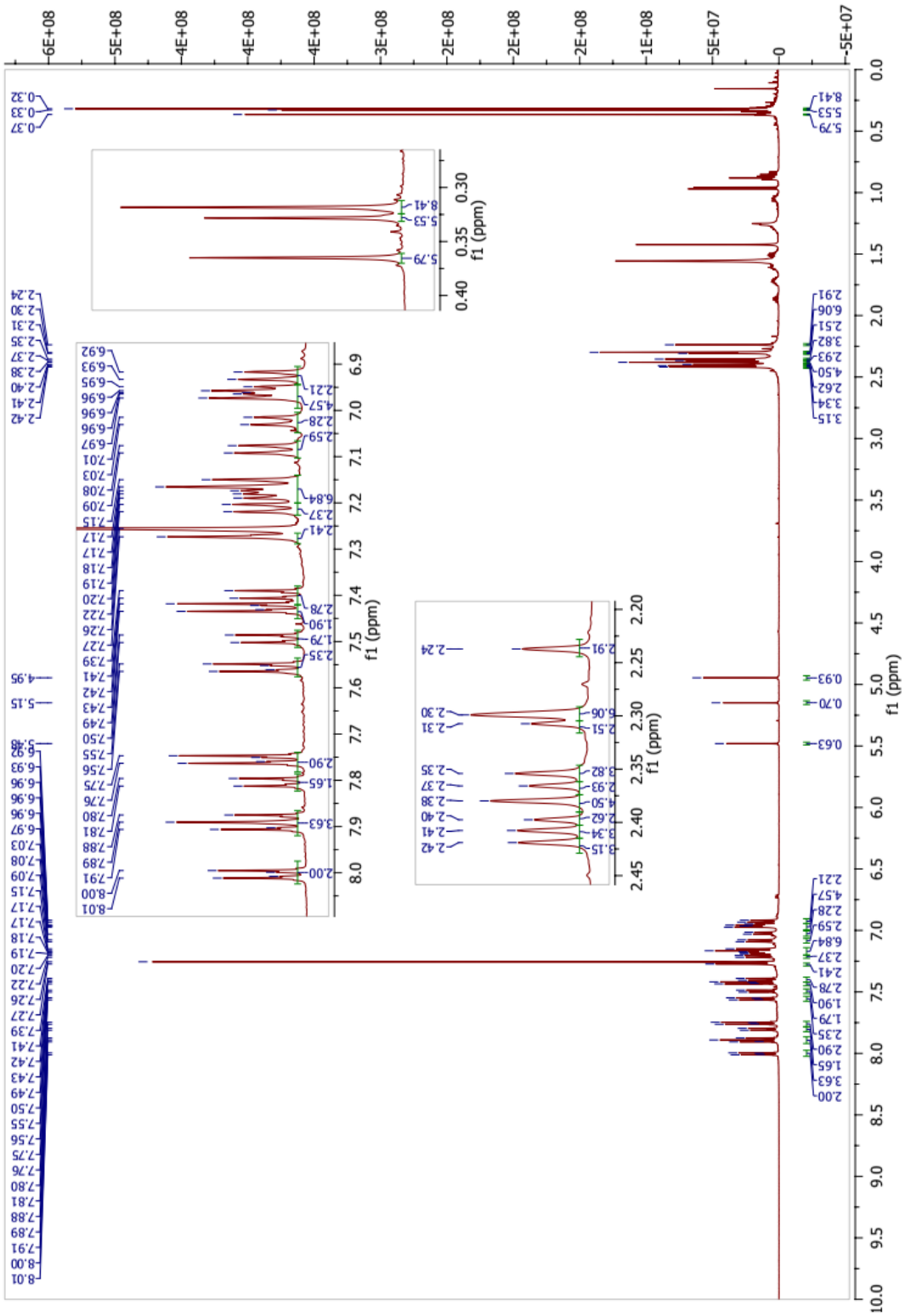

Fig. 1.68. 1H NMR of compound **17a,b,c** ($CDCl_3$)

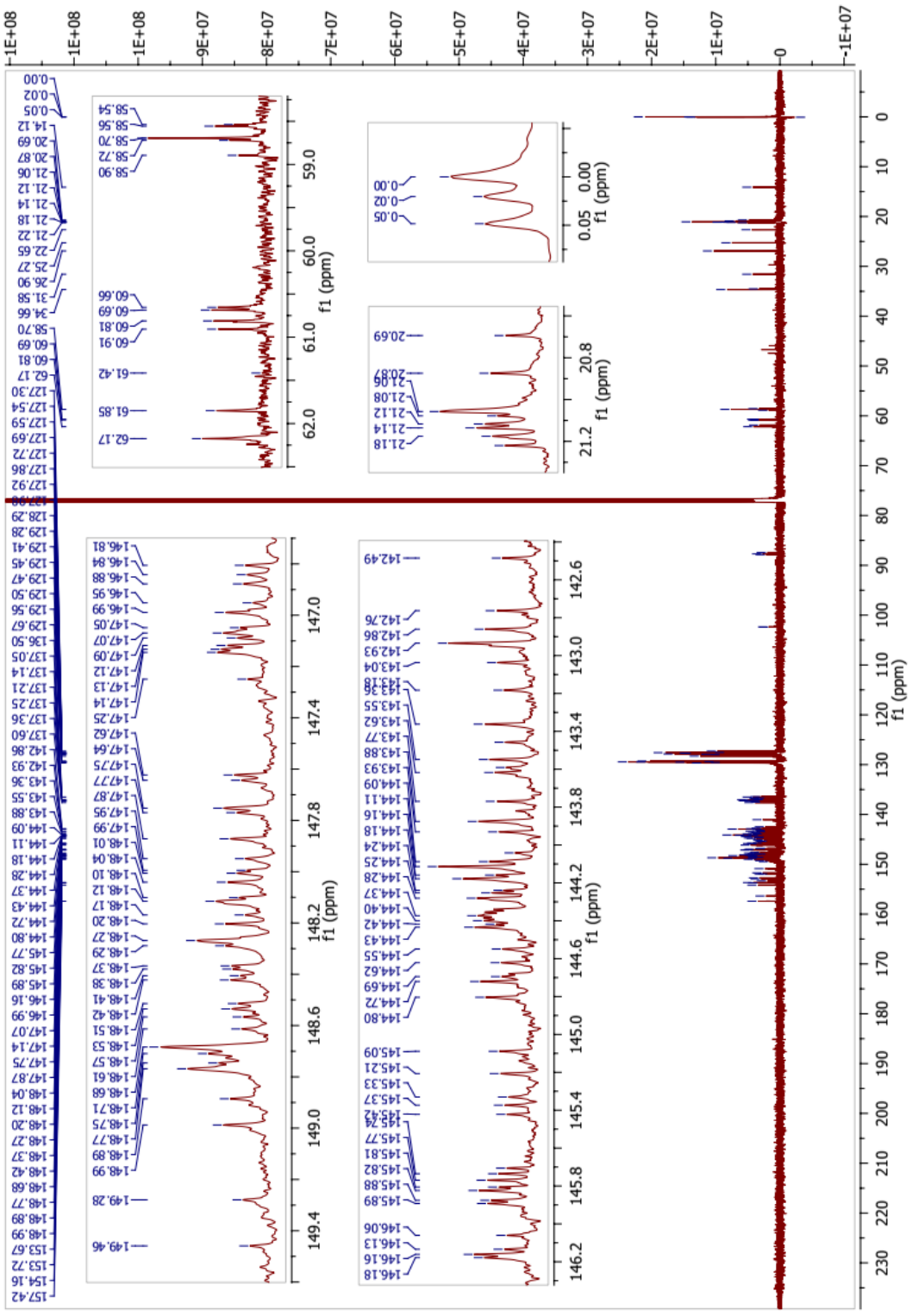

Fig. 1.69. ^{13}C NMR of compound **17a,b,c** ($CDCl_3$)

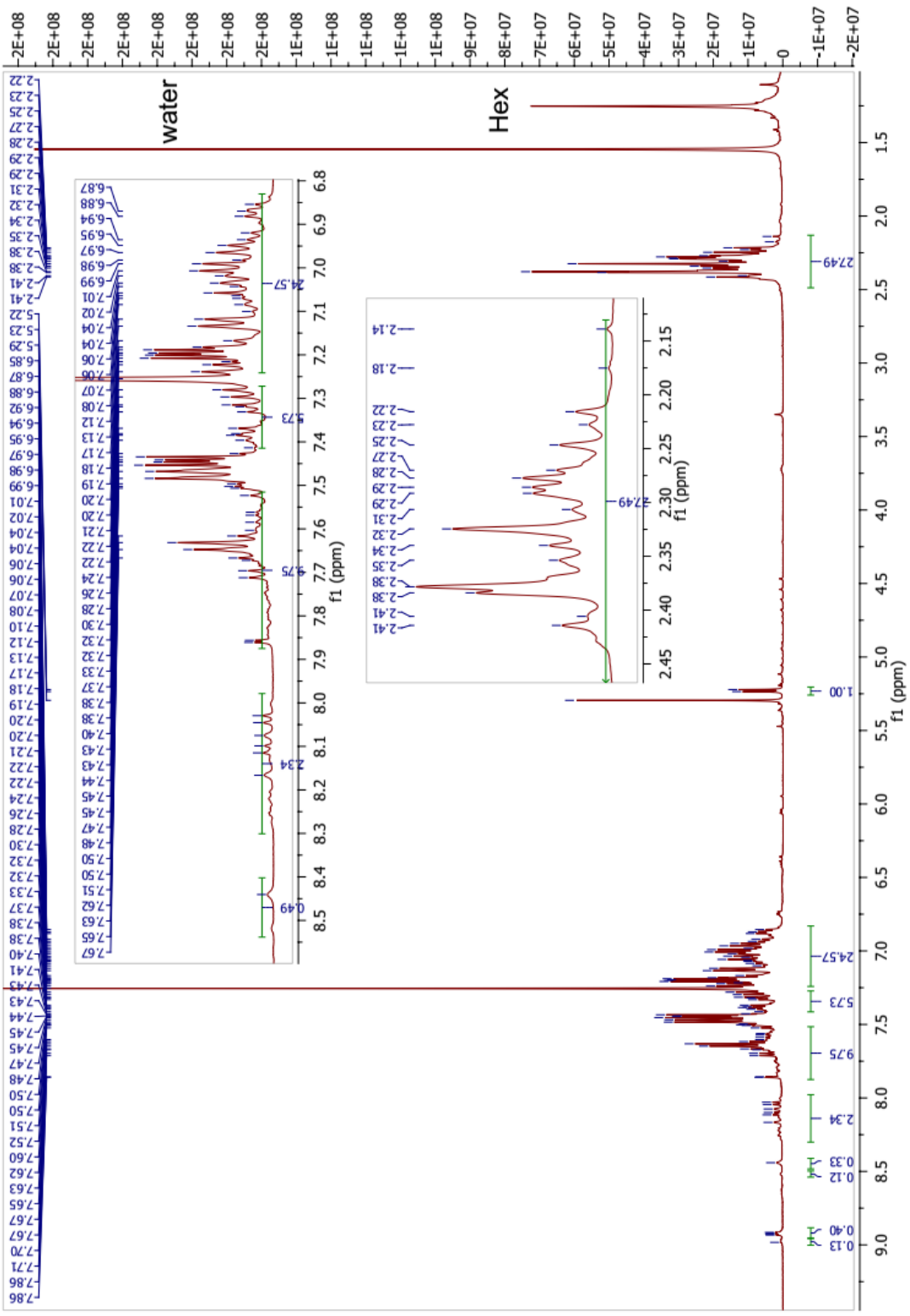

Fig. 1.70. ^{1}H NMR of compound **18a,b** ($CDCl_3$)

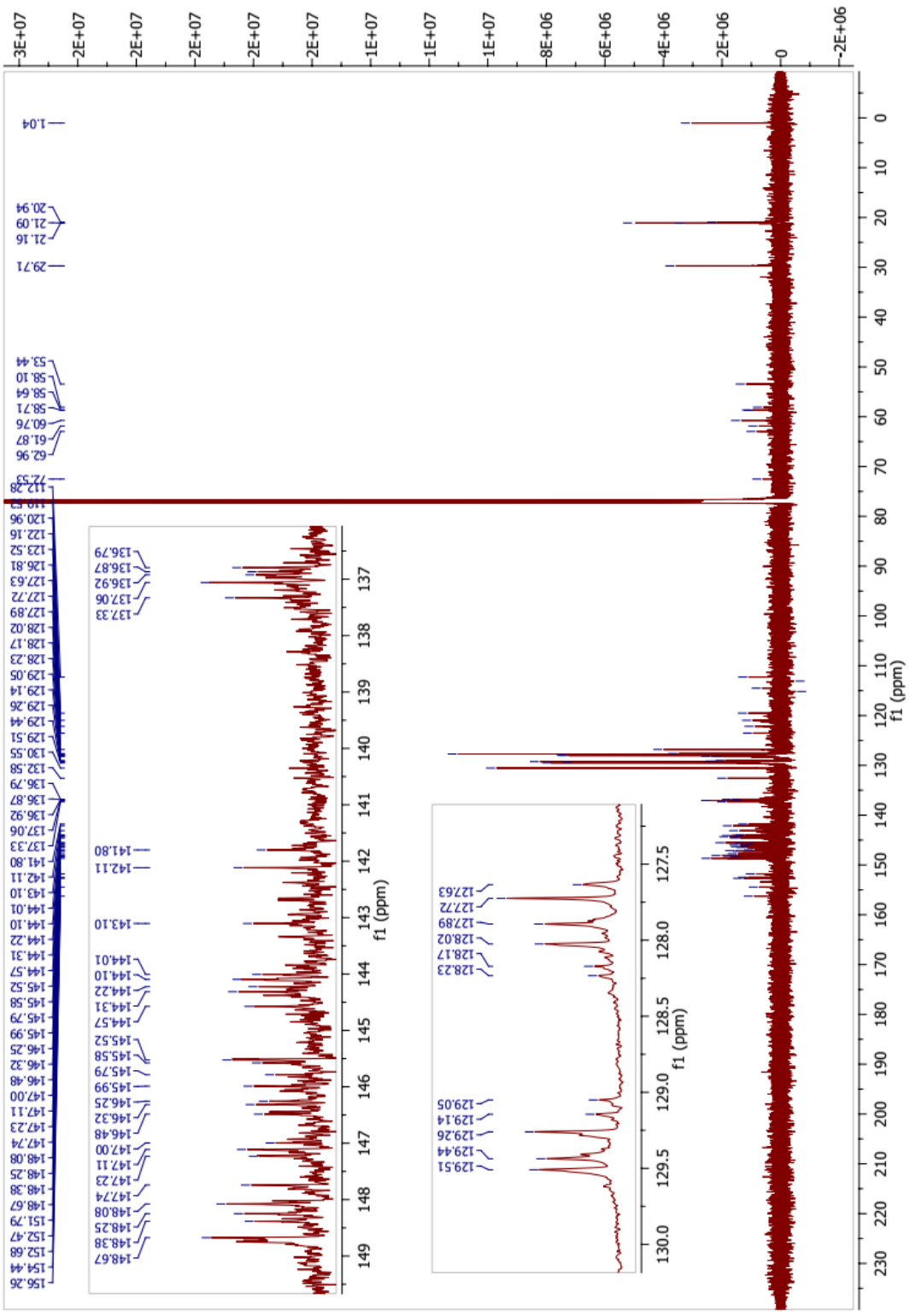

Fig. 1.71 ^{13}C NMR of compound **18a,b** ($CDCl_3$)

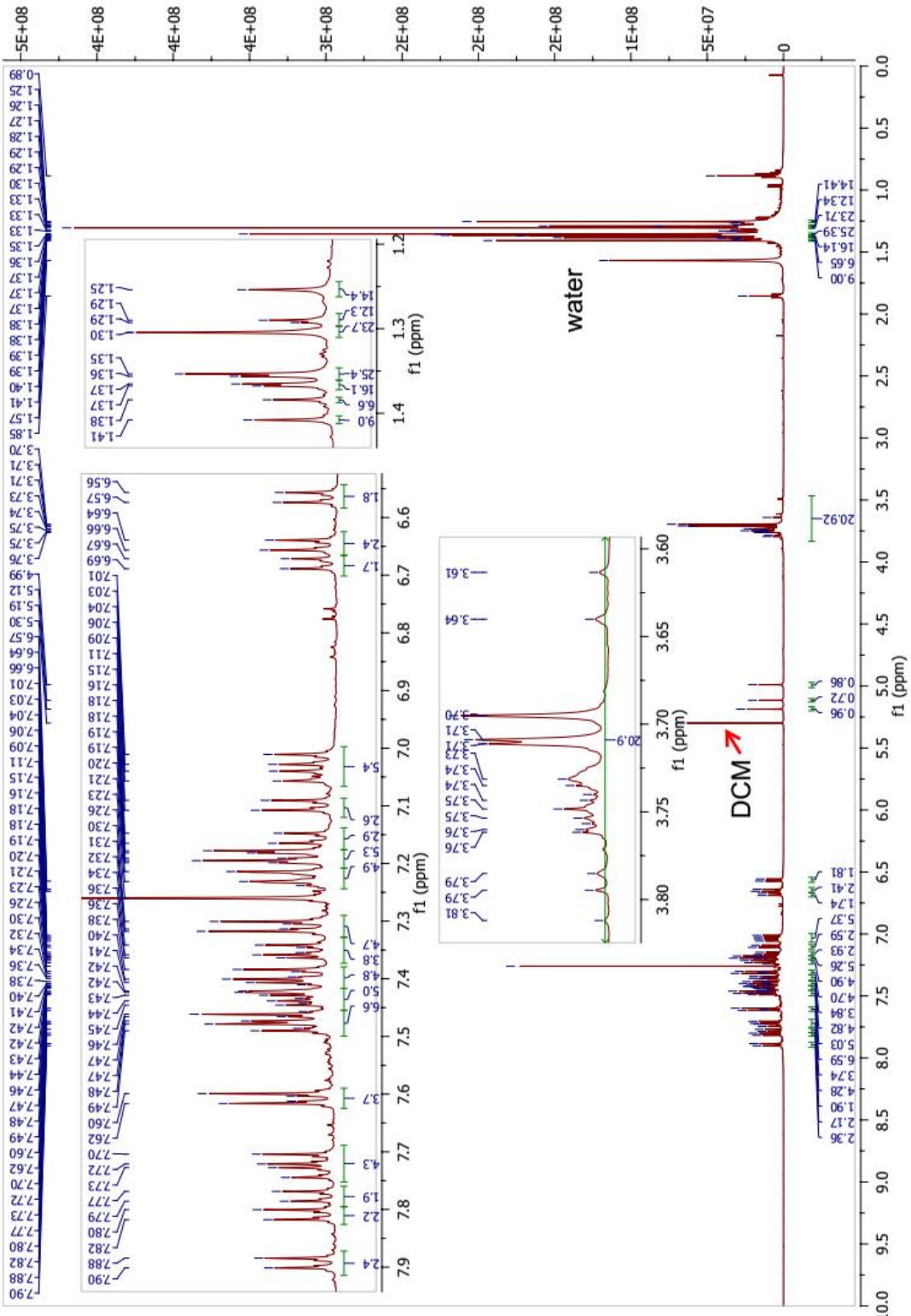

Fig. 1.72. ^{1}H NMR of compound **19a,b,c** ($CDCl_3$)

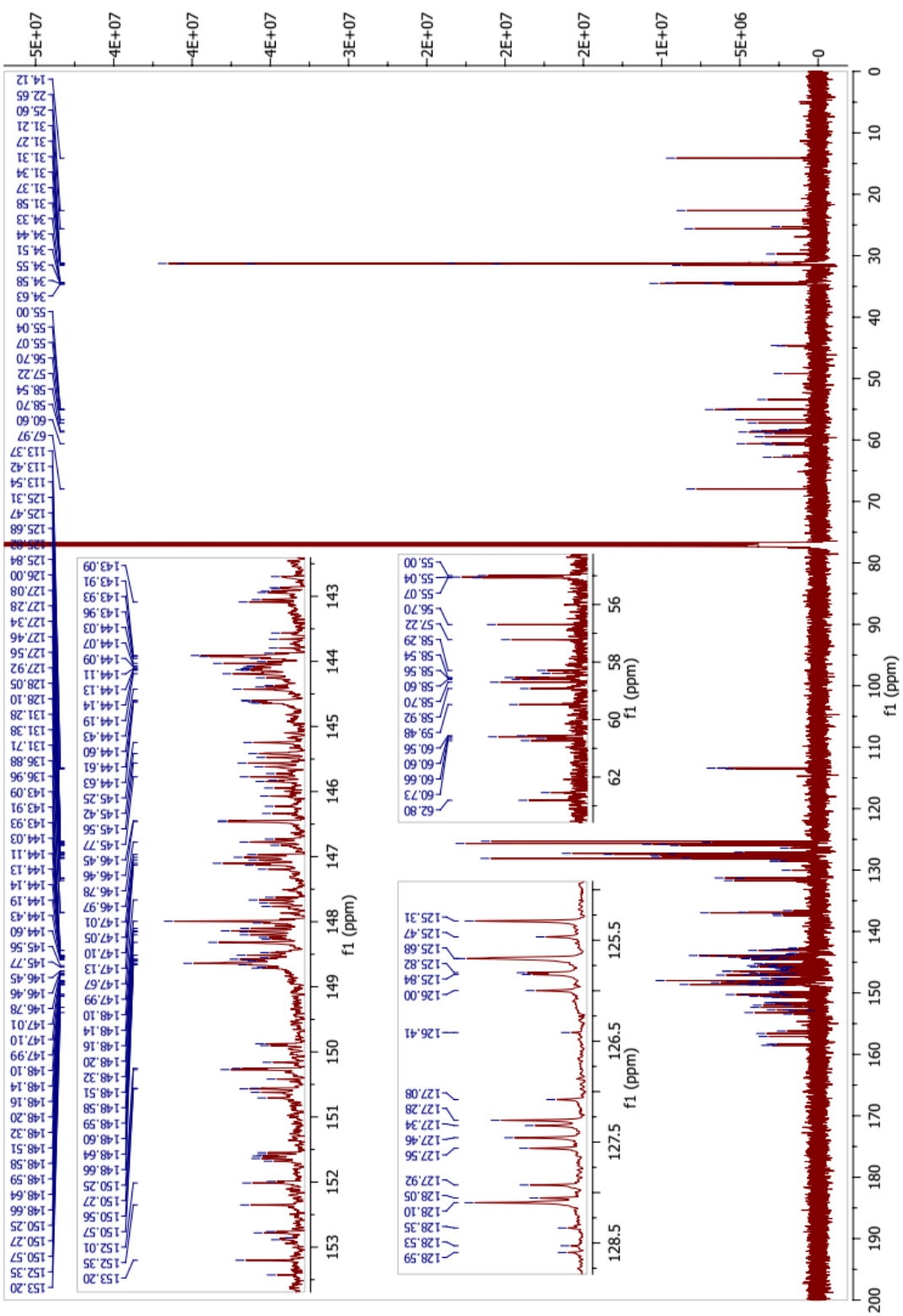

Fig. 1.73. ^{13}C NMR of compound **19a,b,c** ($CDCl_3$)

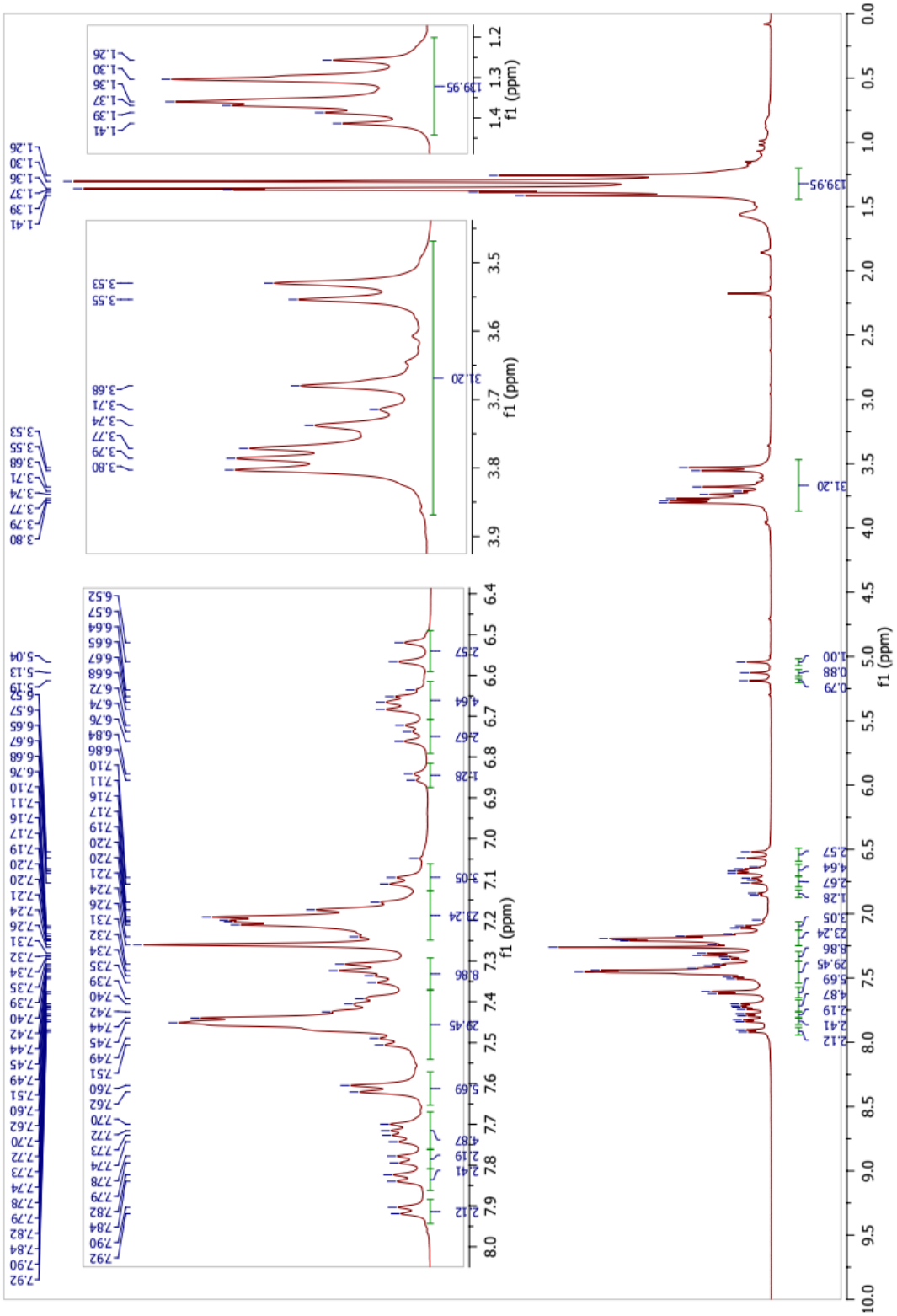

Fig. 1.74. ^{1}H NMR of compound **20a,b,c** ($CDCl_3$)

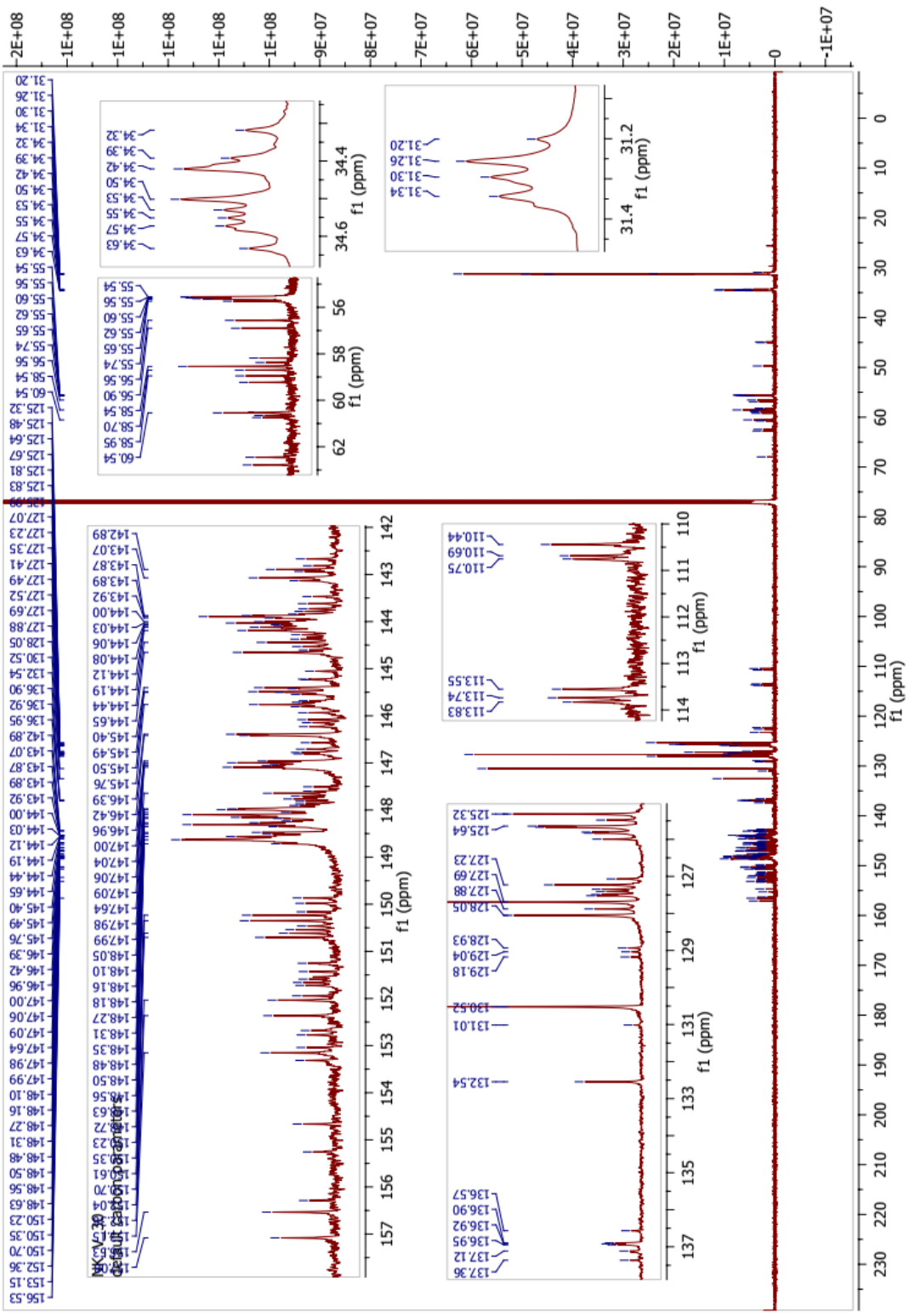

Fig. 1.75. ^{13}C NMR of compound **20a,b,c** ($CDCl_3$)

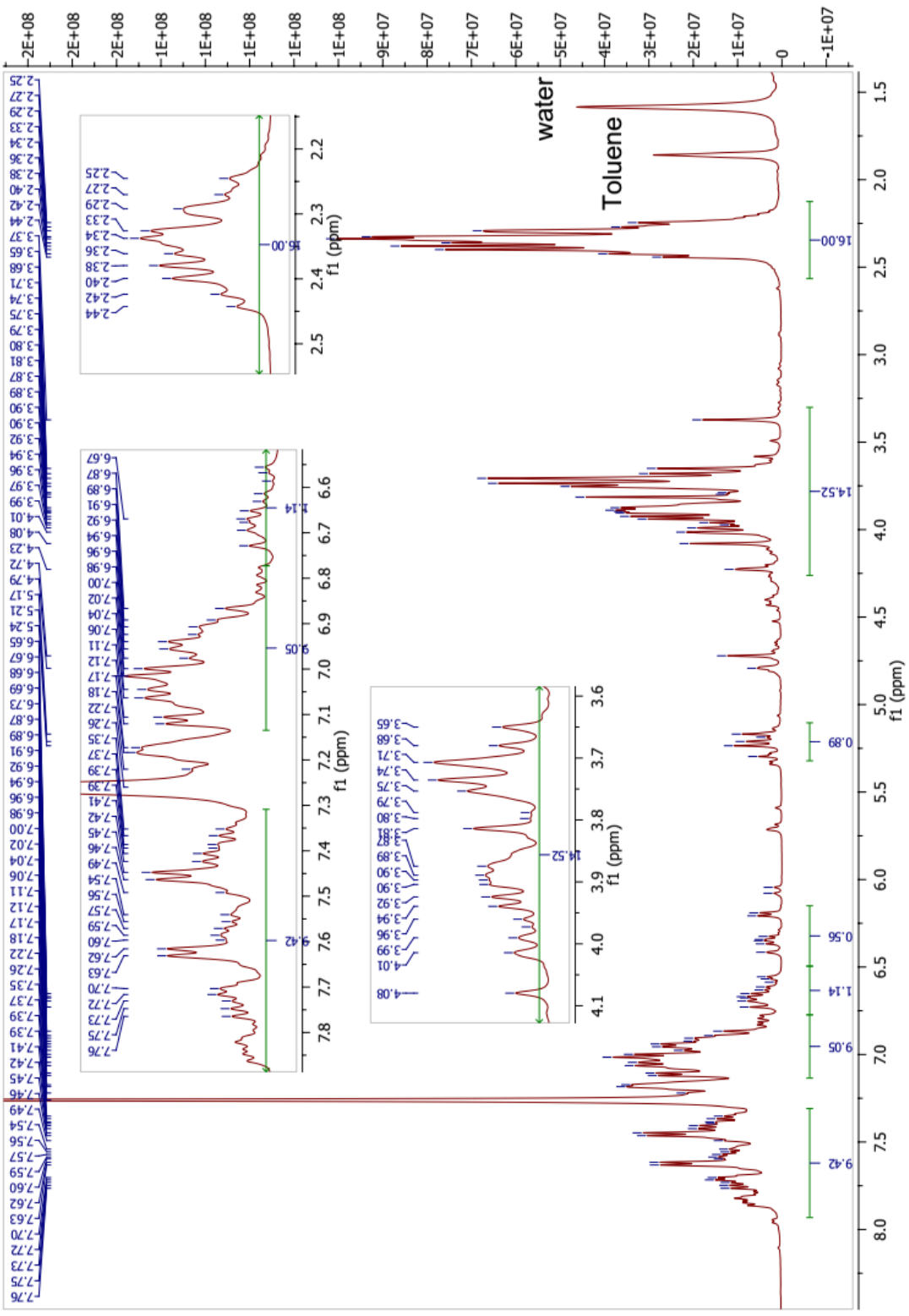

Fig. 1.76. ^{1}H NMR of compound **21a,b,c** ($CDCl_3$)

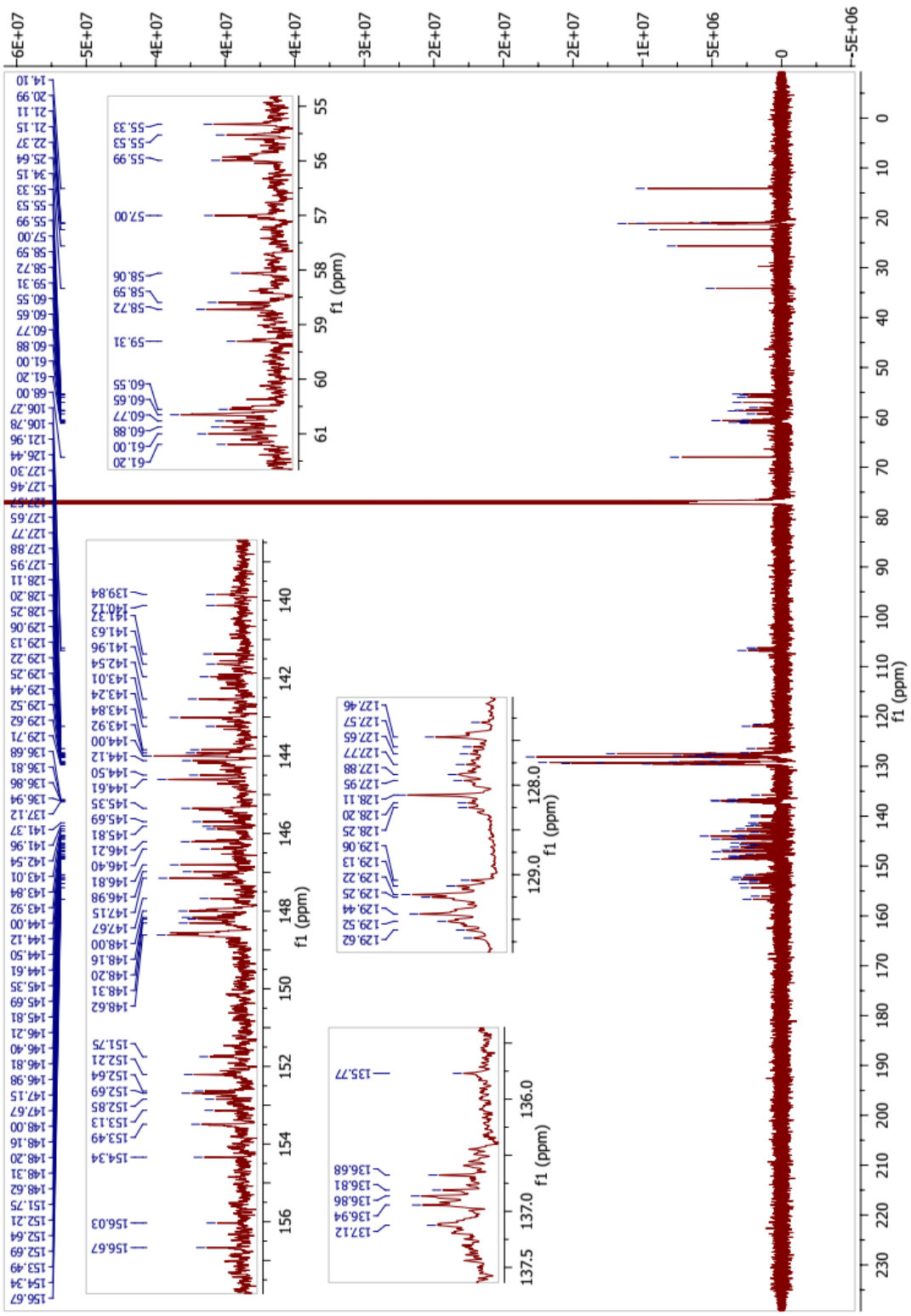

Fig. 1.77. ^{13}C NMR of compound **21a,b,c** ($CDCl_3$)

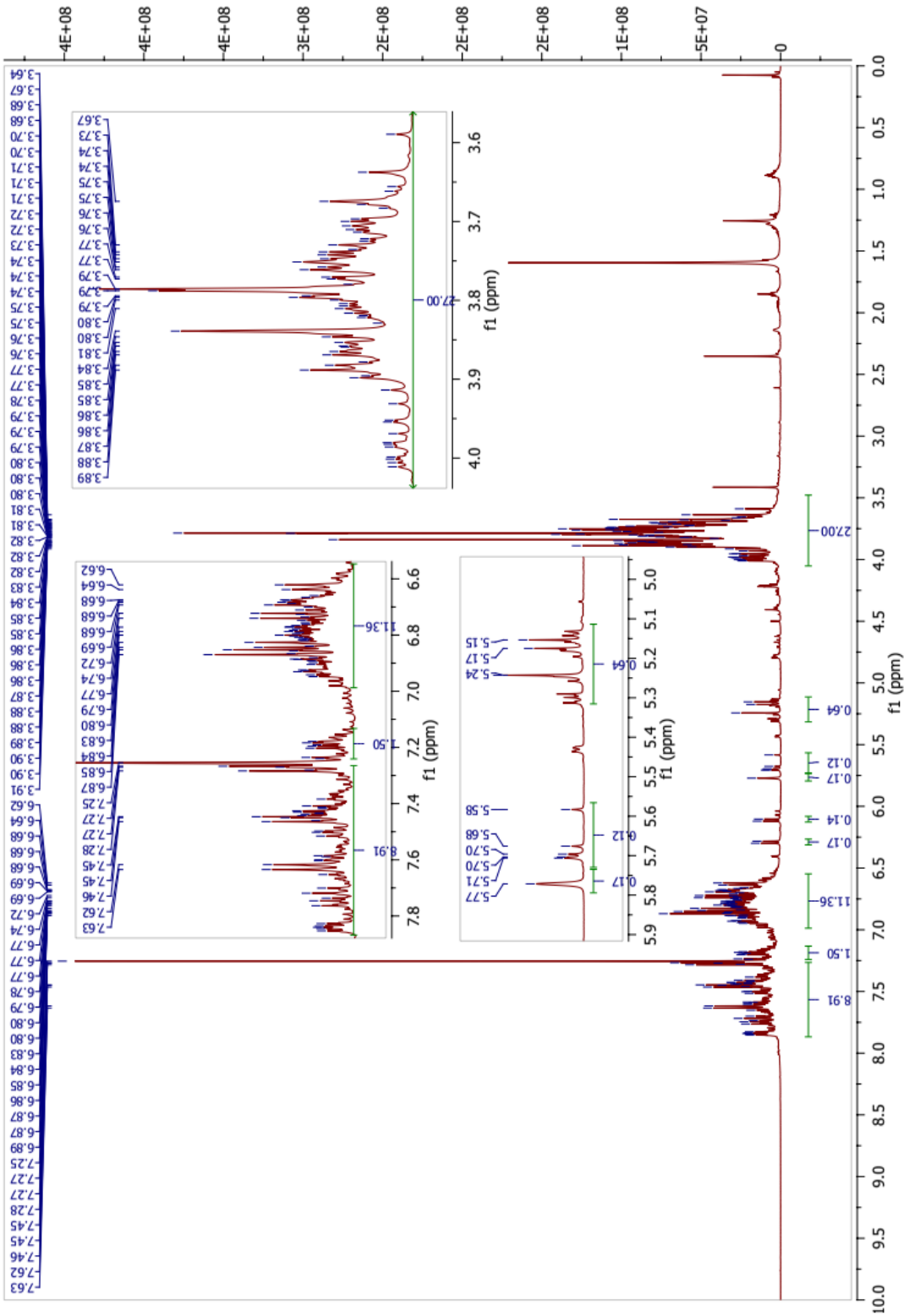

Fig. 1.78. ^{1}H NMR of compound **22a,b,c** ($CDCl_3$)

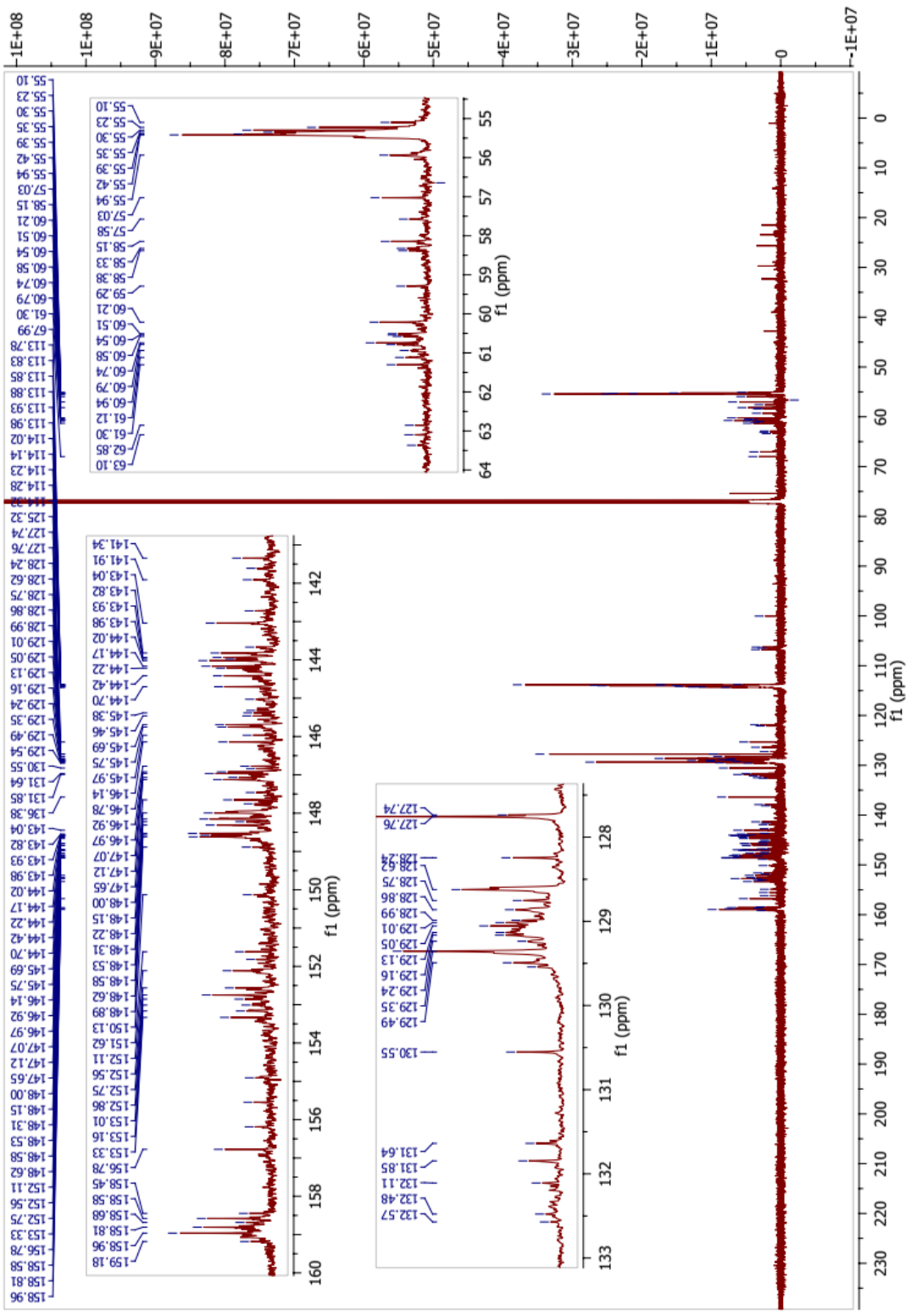

Fig. 1.79. ^{13}C NMR of compound **22a,b,c** ($CDCl_3$)

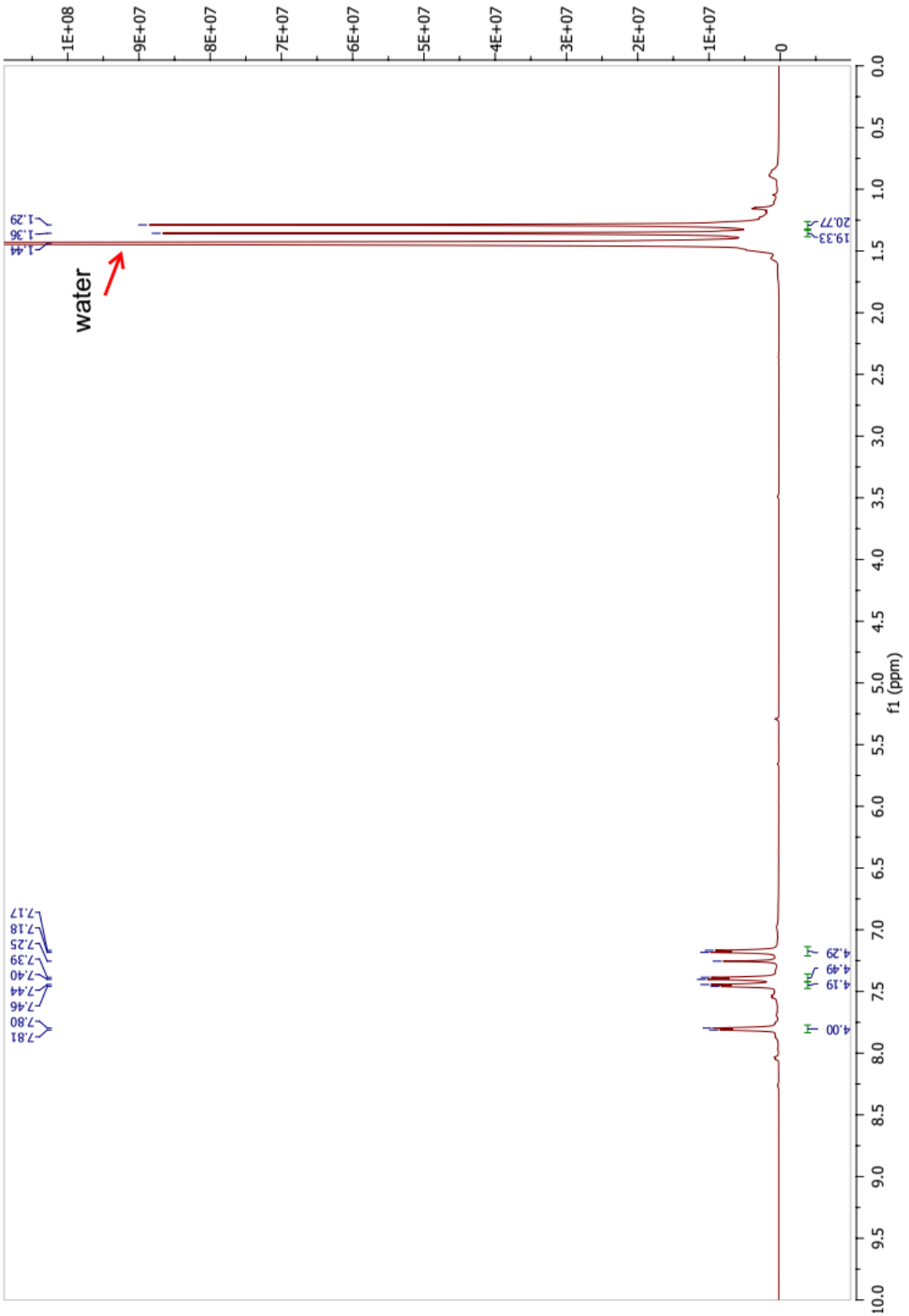

Fig. 1.80. ^{1}H NMR of compound **23** ($CDCl_3$)

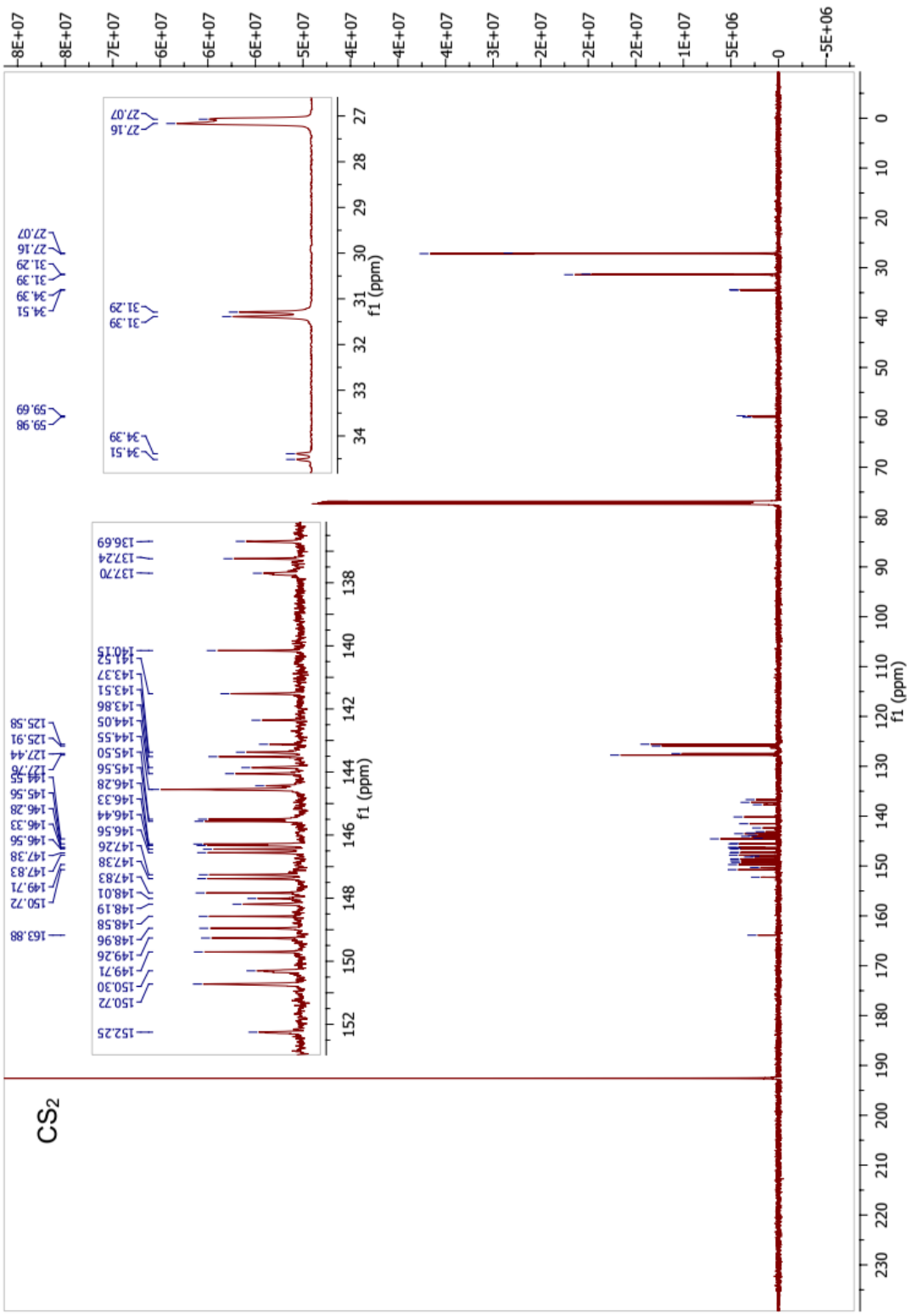

Fig. 1.81. ^{13}C NMR of compound **23** ($CDCl_3$)

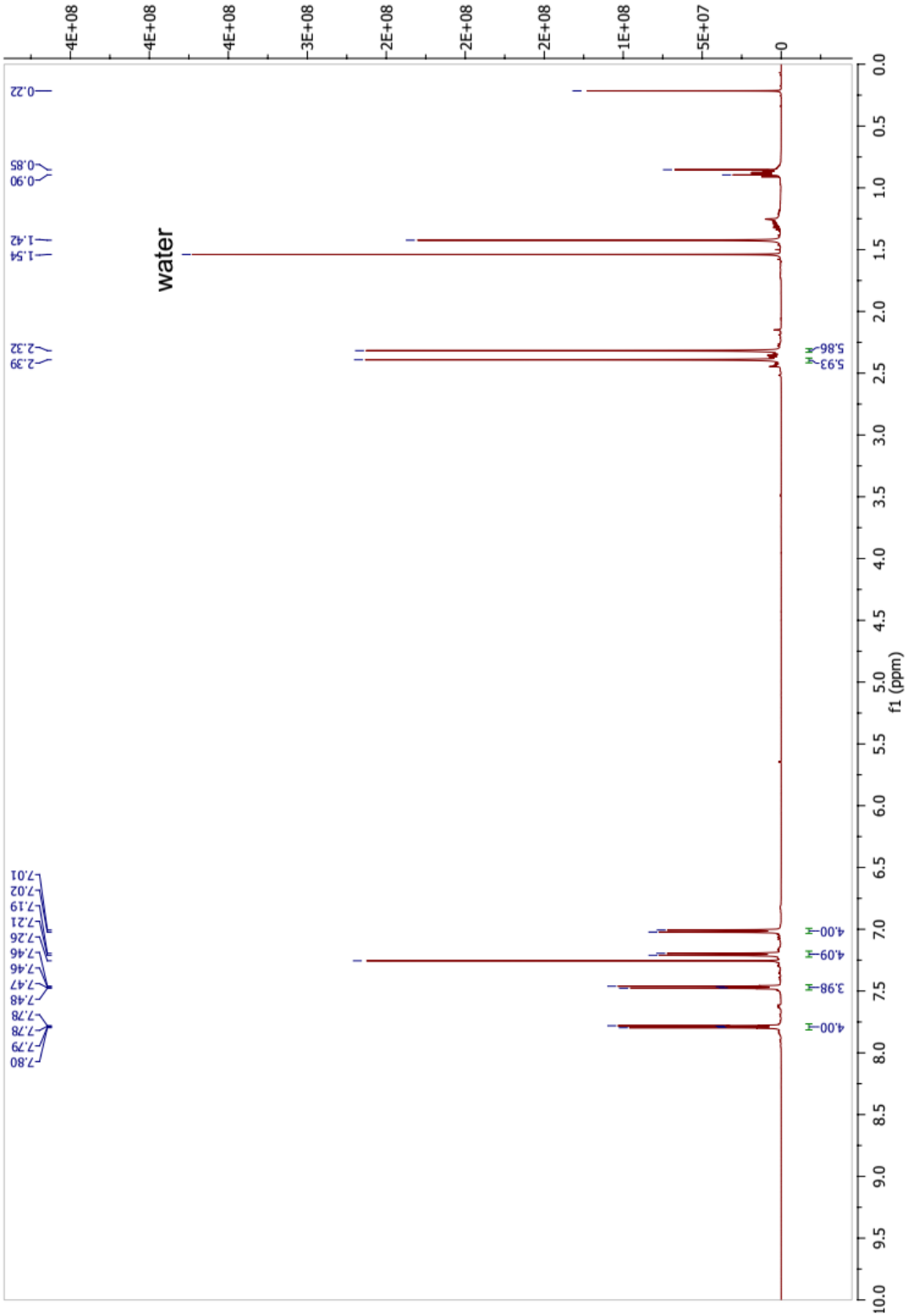

Fig. 1.82. ^{1}H NMR of compound **24** ($CDCl_3$)

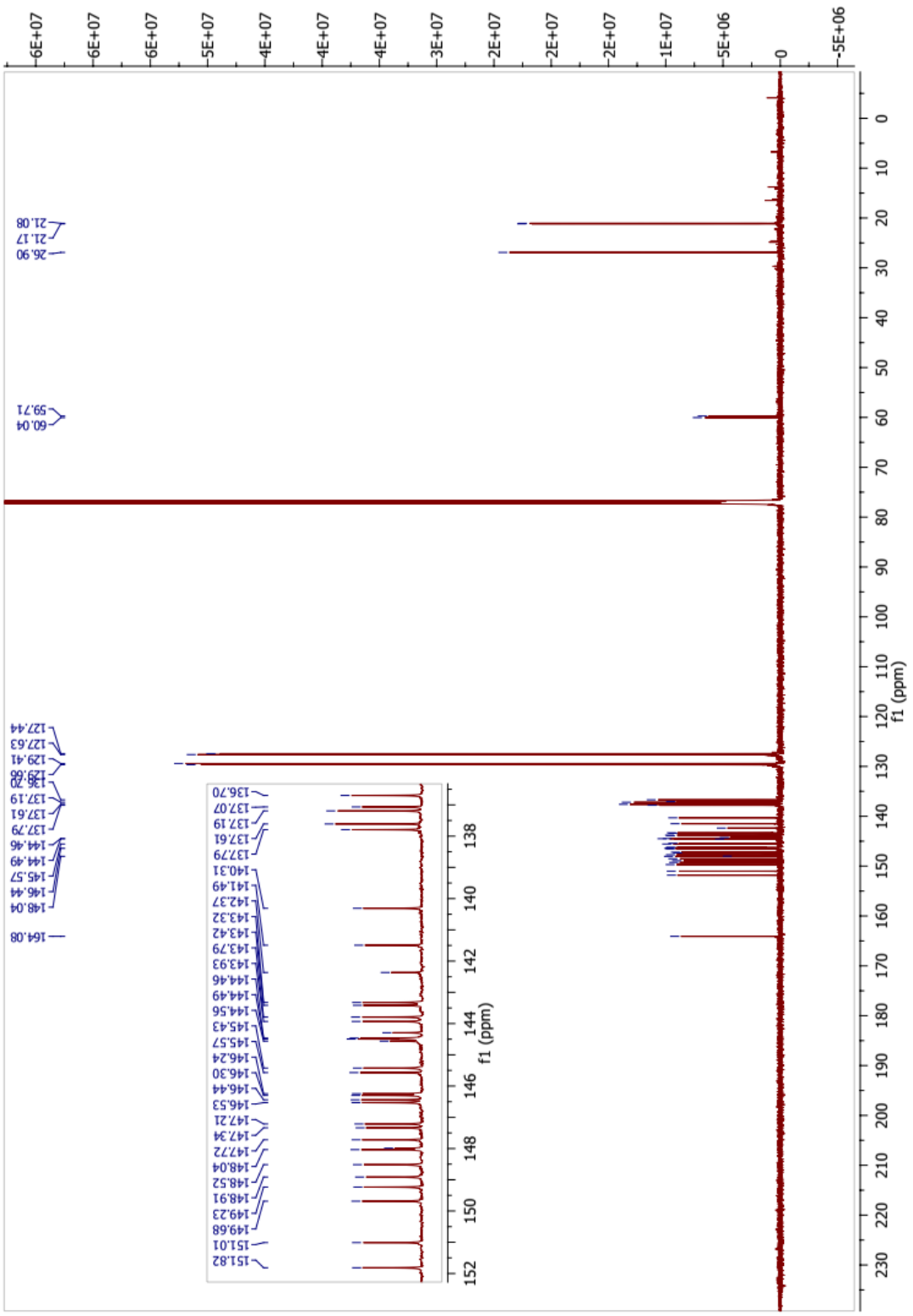

Fig. 1.83. ^{13}C NMR of compound **24** ($CDCl_3$)

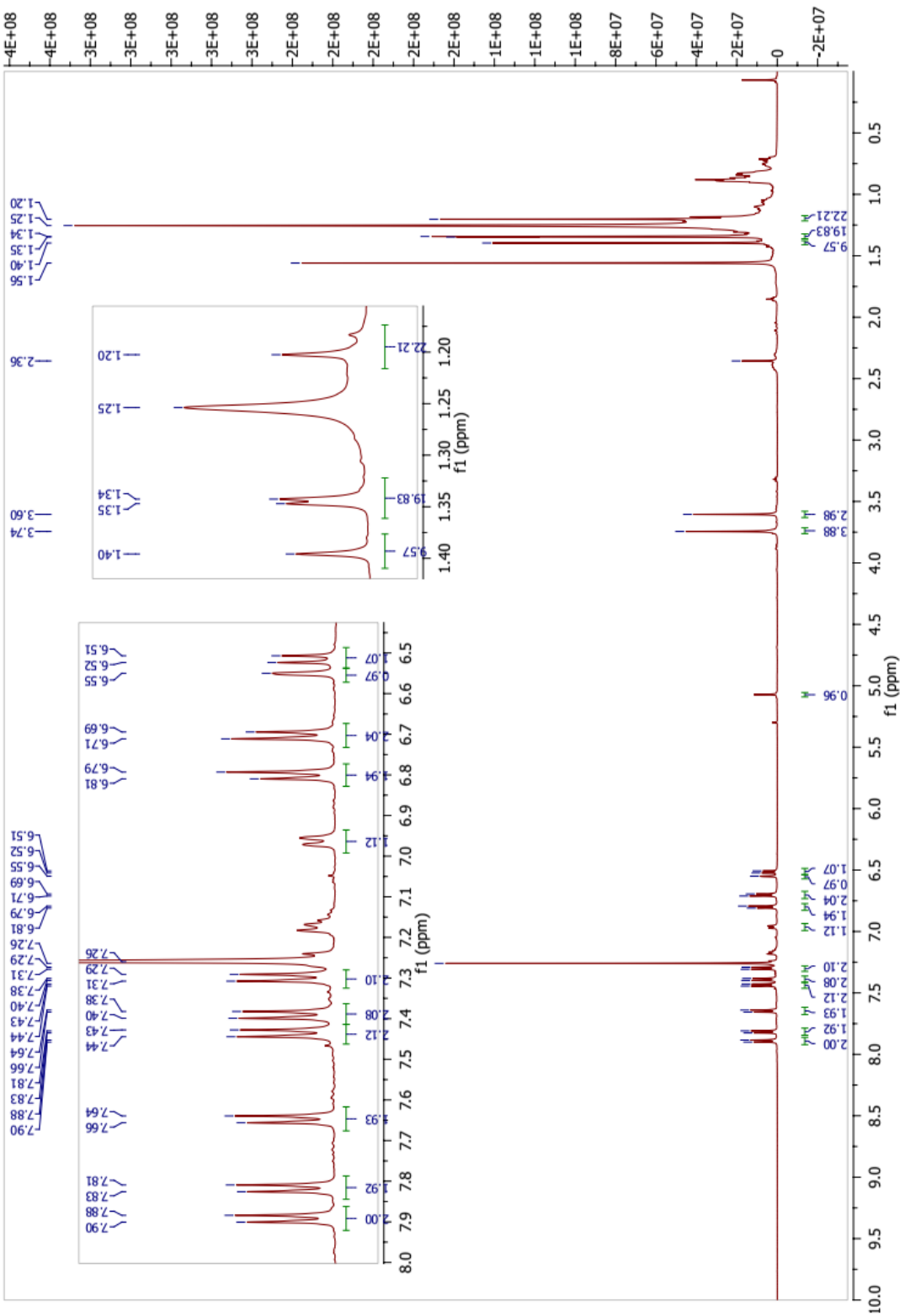

Fig 1.84. ^{1}H NMR of compound **25a** ($CDCl_3$)

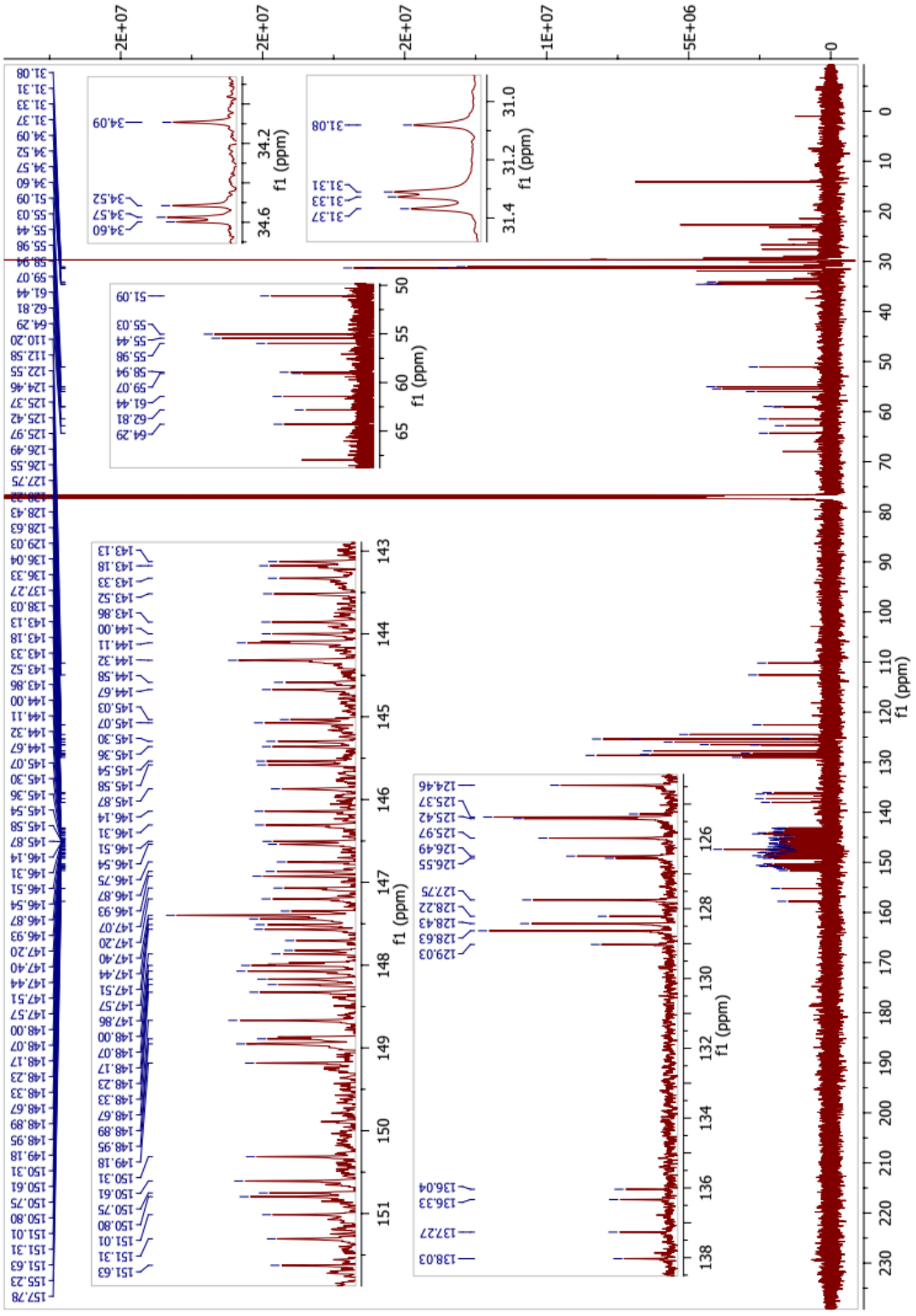

Fig. 1.85. ^{13}C NMR of compound **25a** ($CDCl_3$)

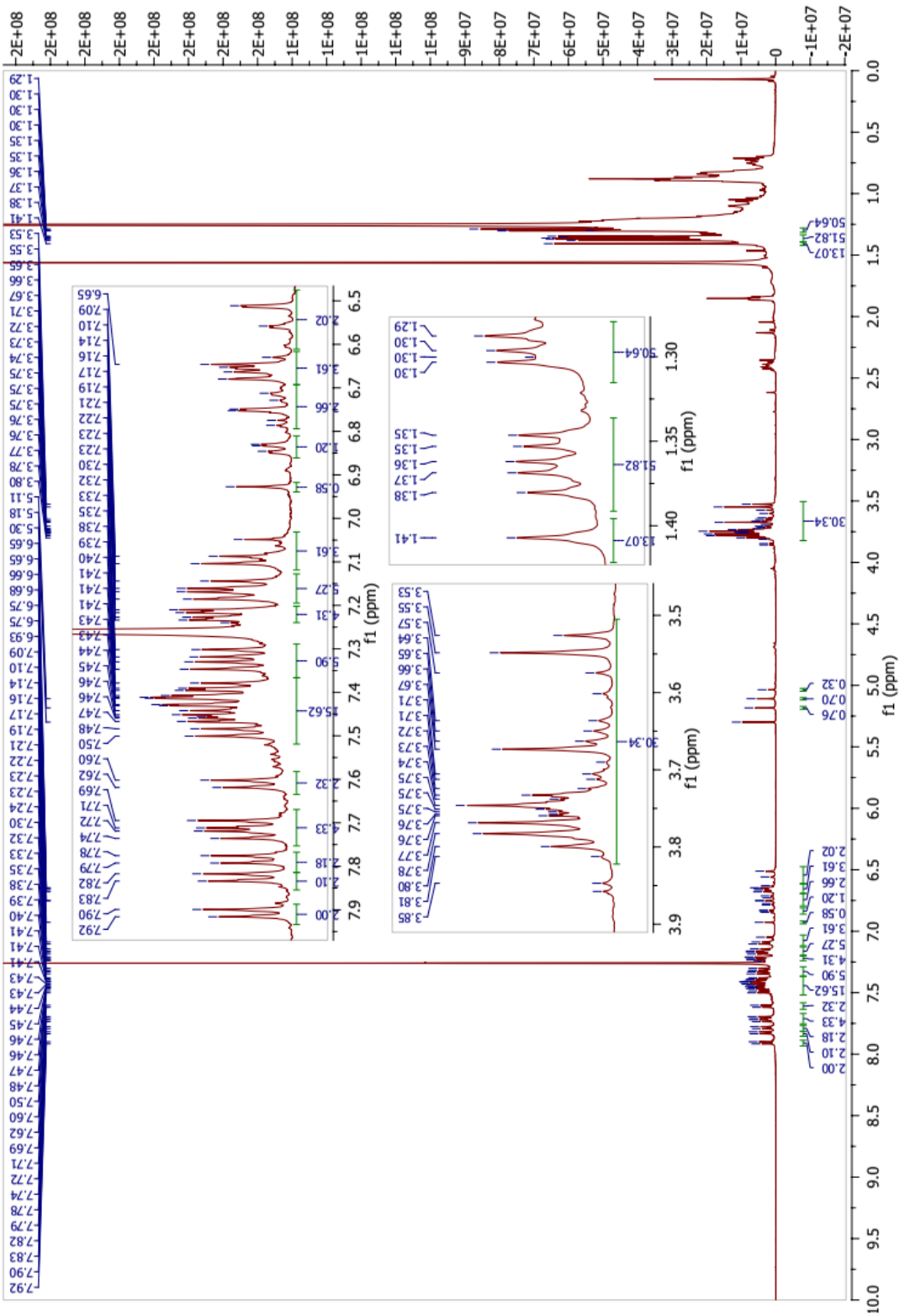

Fig 1.86. ^{1}H NMR of compound **25b** ($CDCl_3$)

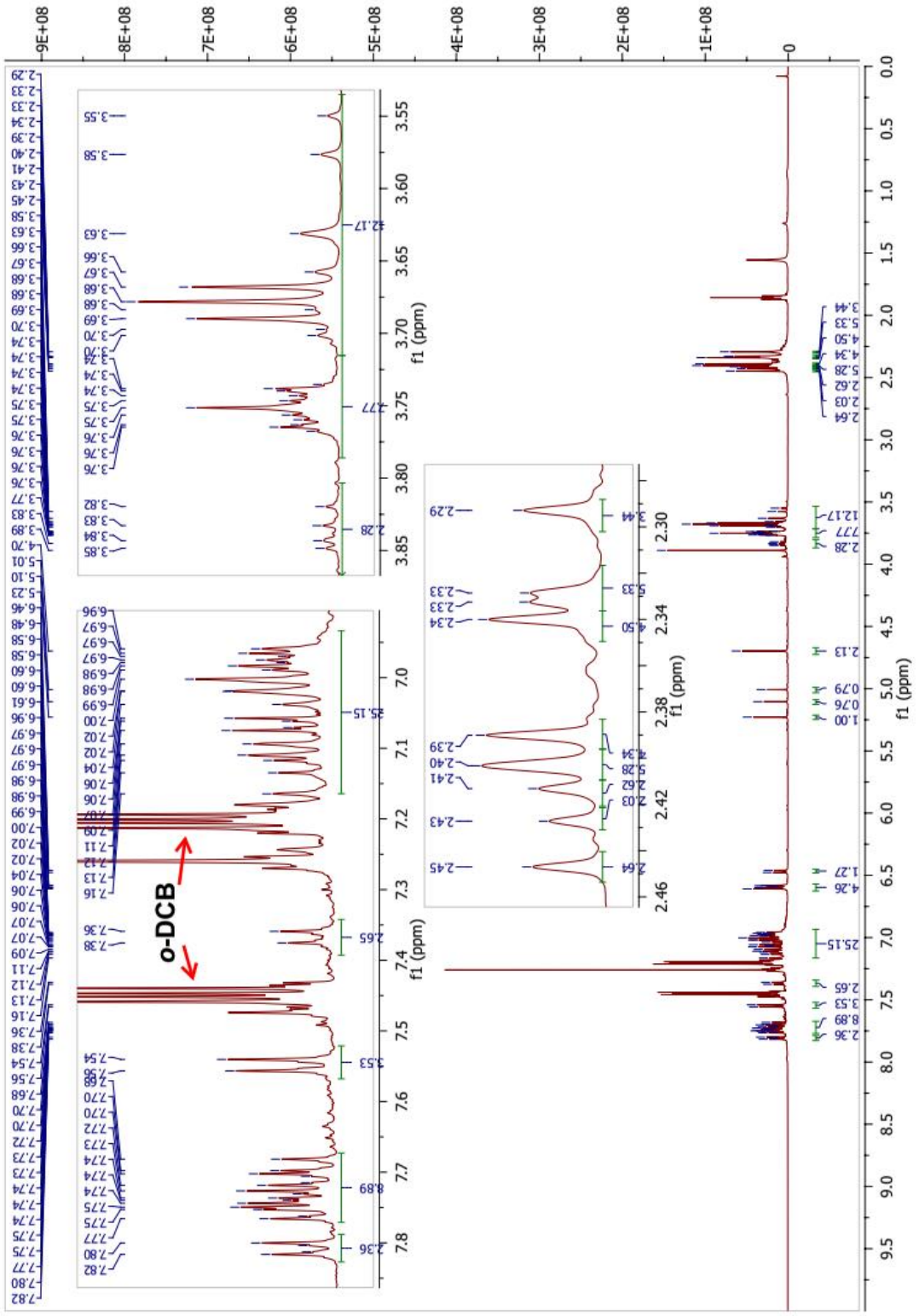

Fig. 1.87. ^{1}H NMR of compound **26a,b,c** ($CDCl_3$)

MALDI Data

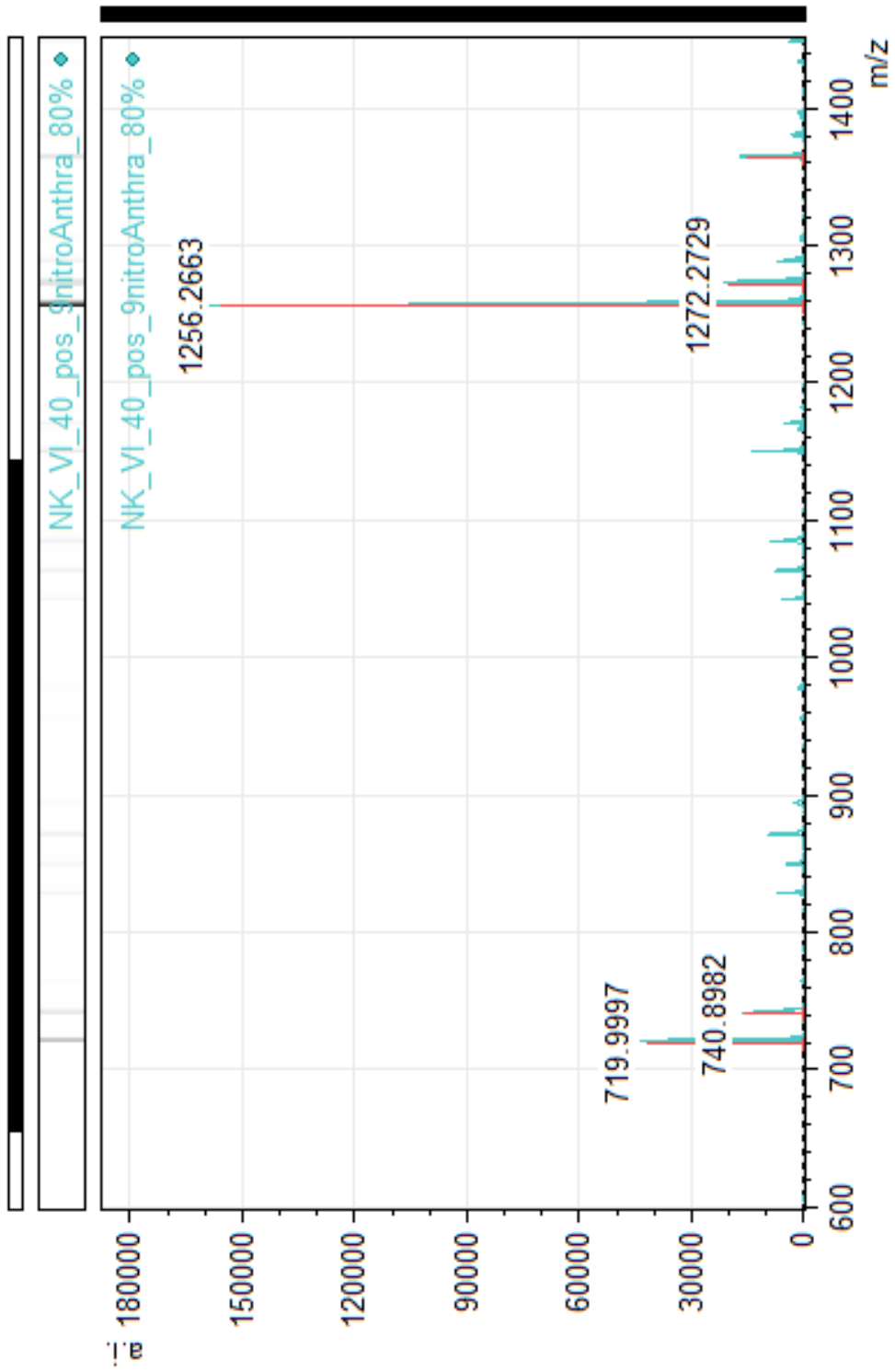

Fig. 1.88. MALDI-TOF MS of **5** (matrix: 9-nitroanthracene)

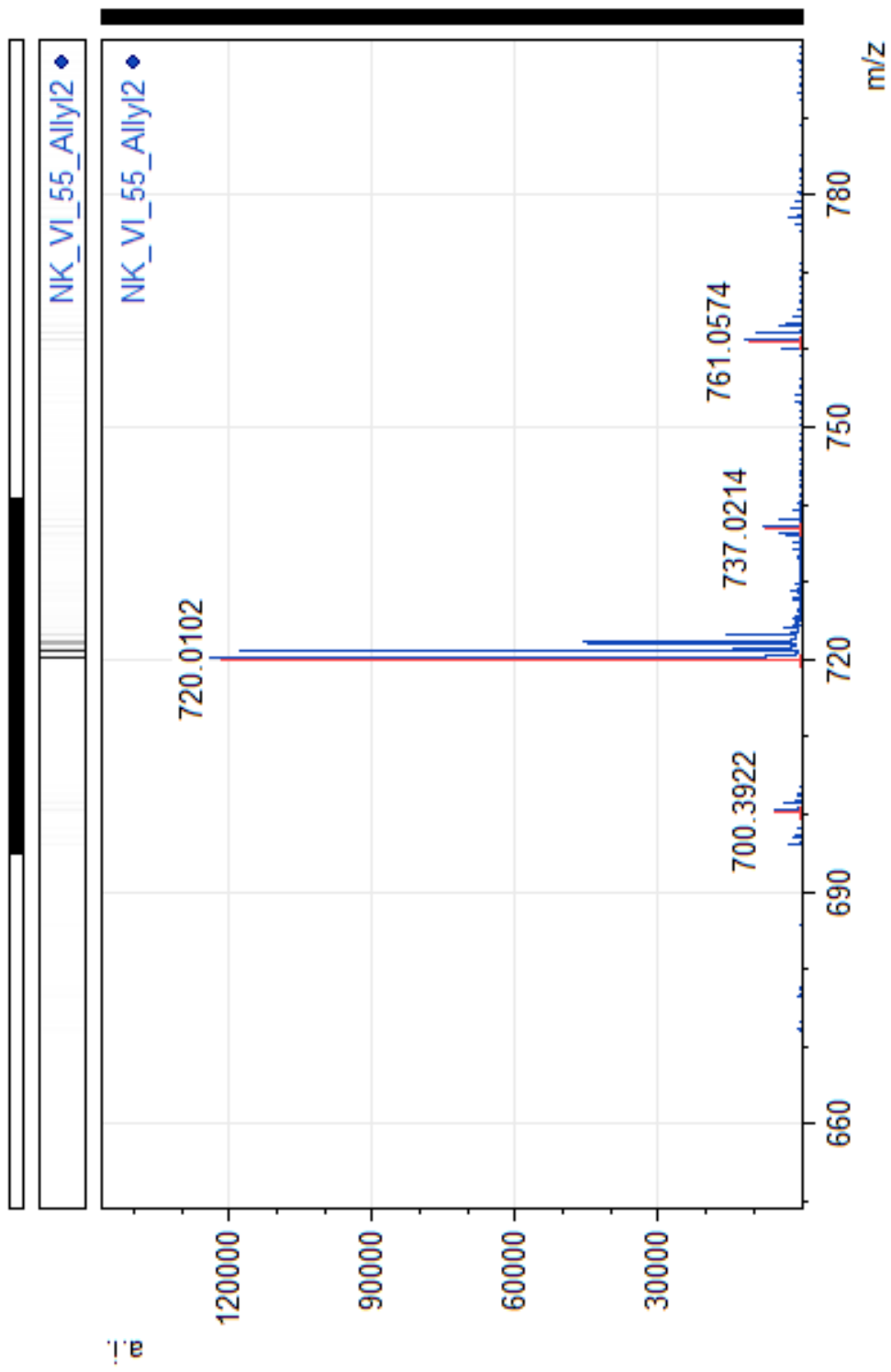

Figure 1.89. MALDI-TOF MS of **13** (matrix: 9-nitroanthracene)

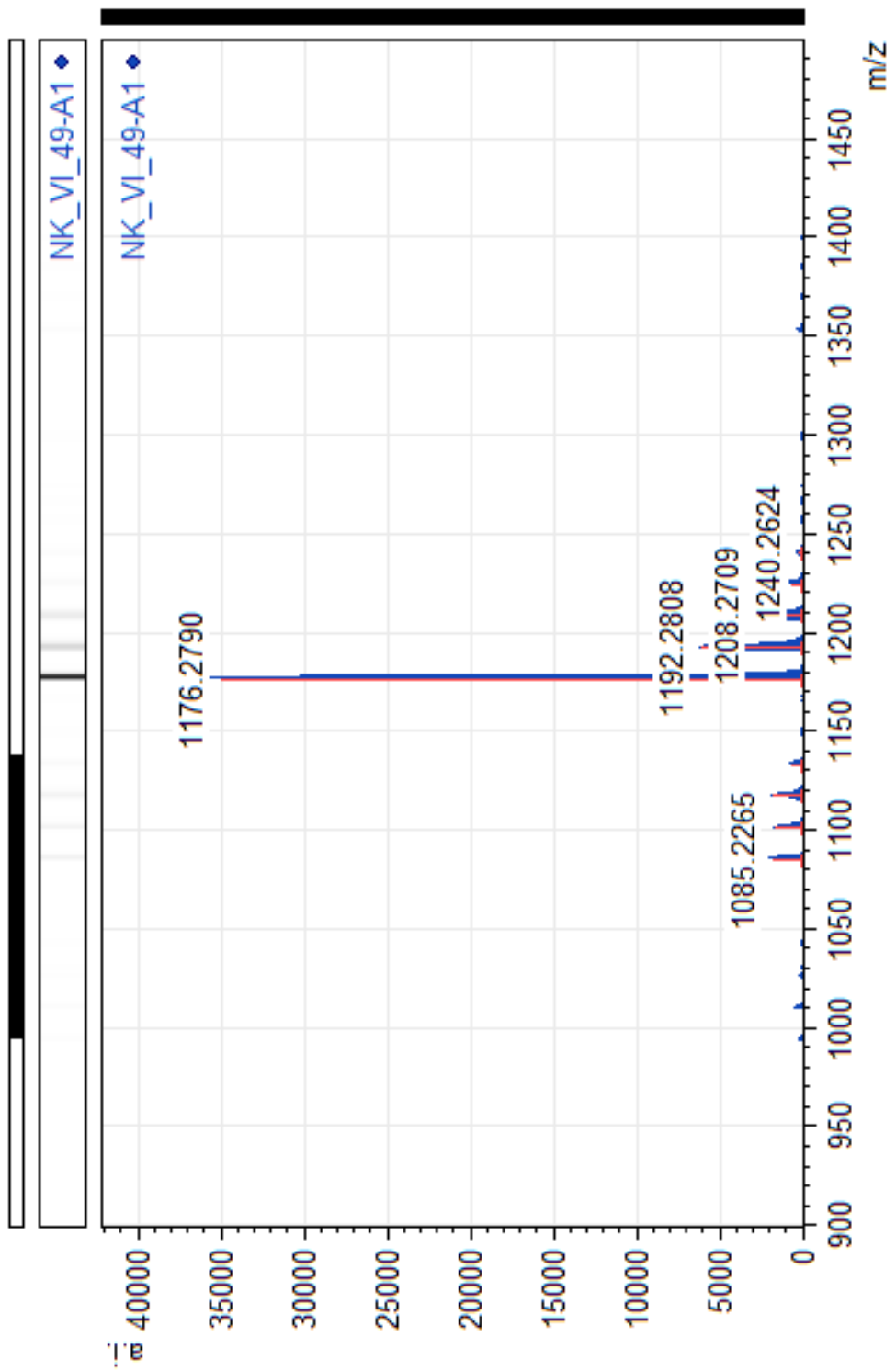

Fig. 1.90. MALDI-TOF MS of **4** (matrix: 9-nitroanthracene)

References

1. Matsuo, Y. and Nakamura, E. "**Selective Multiaddition of Organocopper Reagents to Fullerenes.**" *Chem. Rev.*, 108, no. 8, **2008**, 3016–28. doi:10.1021/cr0684218, Available at http://www.ncbi.nlm.nih.gov/pubmed/18652514.

2. Nakamura, E. and Sawamura, M. "**Chemistry of η 5 -Fullerene Metal Complexes***" 73, no. 2, **2001**, 355–359.

3. Sawamura, M.; Iikura, H.; and Nakamura, E. "**The First Pentahaptofullerene Metal Complexes**" *J. Am. Chem. Soc.*, 118, no. 50, **1996**, 12850–12851. doi:10.1021/ja962681x, Available at http://pubs.acs.org/doi/abs/10.1021/ja962681x.

4. Sawamura, M.; Nagahama, N.; Toganoh, M.; and Nakamura, E. "**Regioselective Penta-Addition of 1-Alkenyl Copper Reagent to [60]fullerene. Synthesis of Penta-Alkenyl FCp Ligand**" *J. Organomet. Chem.*, 652, no. 1–2, **2002**, 31–35. doi:10.1016/S0022-328X(02)01305-0.

5. Matsuo, Y. and Nakamura, E. "**Selective Multiaddition of Organocopper Reagents to Fullerenes**" *Chem. Rev.*, 108, no. 8, **2008**, 3016–3028. doi:10.1021/cr0684218.

6. Champeil, E.; Crean, C.; Larraya, C.; Pescitelli, G.; Proni, G.; and Ghosez, L. "**Functionalization of C60 via Organometallic Reagents**" *Tetrahedron*, 64, no. 45, **2008**, 10319–10330. doi:10.1016/j.tet.2008.08.017, Available at

http://linkinghub.elsevier.com/retrieve/pii/S004040200801466X.

7. Kennedy, R. D.; Ayzner, A. L.; Wanger, D. D.; Day, C. T.; Halim, M.; Khan, S. I.; Tolbert, S. H.; Schwartz, B. J.; and Rubin, Y. "**Self-Assembling Fullerenes for Improved Bulk-Heterojunction Photovoltaic Devices.**" *J. Am. Chem. Soc.*, 130, no. 51, **2008**, 17290–2. doi:10.1021/ja807627u, Available at http://www.ncbi.nlm.nih.gov/pubmed/19053441.

8. Kennedy, R. D.; Halim, M.; Khan, S. I.; Schwartz, B. J.; Tolbert, S. H.; and Rubin, Y. "**Crystal-Packing Trends for a Series of 6,9,12,15,18-Pentaaryl-1-hydro[60]fullerenes.**" *Chemistry*, 18, no. 24, **2012**, 7418–33. doi:10.1002/chem.201103400. Available at http://www.ncbi.nlm.nih.gov/pubmed/22573530

9. Ganesamoorthy, R.; Sathiyan, G.; and Sakthivel, P. "**Review: Fullerene Based Acceptors for Efficient Bulk Heterojunction Organic Solar Cell Applications**" *Sol. Energy Mater. Sol. Cells*, 161, no. August 2016, **2017**, 102–148. doi:10.1016/j.solmat.2016.11.024. Available at http://linkinghub.elsevier.com/retrieve/pii/S0927024816304998

10. **LUMO and LUMO Desnsity, as Well as Figues, of Four and Five Feathered Shuttlecocks Were Calculated by Dr. Yves Rubin**

11. Champeil, E.; Crean, C.; Larraya, C.; Pescitelli, G.; Proni, G.; and Ghosez, L. "**Functionalization of C60 via Organometallic Reagents**" *Tetrahedron*, 64, no. 45, **2008**, 10319–10330. doi:10.1016/j.tet.2008.08.017.

12. Sawamura, M.; Toganoh, M.; Suzuki, K.; Hirai, A.; Iikura, H.; and Nakamura, E. "**Stepwise Synthesis of Fullerene Cyclopentadienide R 5 C 60 - and Indenide R 3 C 60 - . An Approach to Fully Unsymmetrically Substituted Derivatives**" *Org. Lett.*, 2, no. 13, **2000**, 1919–1921. doi:10.1021/ol005993k, Available at http://pubs.acs.org/doi/abs/10.1021/ol005993k.

13. Iwashita, A.; Matsuo, Y.; and Nakamura, E. "**AlCl3-Mediated Mono-, Di-, and Trihydroarylation of [60]fullerene**" *Angew. Chemie - Int. Ed.*, 46, no. 19, **2007**, 3513–3516. doi:10.1002/anie.200700062.

14. Tassone, C. J.; Ayzner, A. L.; Kennedy, R. D.; Halim, M.; So, M.; Rubin, Y.; Tolbert, S. H.; and Schwartz, B. J. "**Using Pentaarylfullerenes to Understand Network Formation in Conjugated Polymer-Based Bulk-Heterojunction Solar Cells**" *J. Phys. Chem. C*, 115, no. 45, **2011**, 22563–22571. doi:10.1021/jp207382f, Available at http://pubs.acs.org/doi/abs/10.1021/jp207382f.

15. Murata, Y.; Shiro, M.; and Komatsu, K. "**Synthesis, X-Ray Structure, and Properties of the First Tetrakisadduct of Fullerene C60 Having a Fulvene-Type π-System on the Spherical Surface**" *J. Am. Chem. Soc.*, 119, no. 34, **1997**, 8117–8118. doi:10.1021/ja971456s.

16. Lemiègre, L.; Tanaka, T.; Nanao, T.; Isobe, H.; and Nakamura, E. "**Synthesis of Oxy Aminated [60] and [70]Fullerenes with Cumene Hydroperoxide as Oxidant**" *Chem. Lett.*, 36, no. 1, **2007**, 20–21. doi:10.1246/cl.2007.20, Available at http://joi.jlc.jst.go.jp/JST.JSTAGE/cl/2007.20?from=CrossRef.

17. Isobe, H.; Tanaka, T.; Nakanishi, W.; Lemiègre, L.; and Nakamura, E.

"**Regioselective Oxygenative Tetraamination of [60]Fullerene. Fullerene-Mediated Reduction of Molecular Oxygen by Amine via Ground State Single Electron Transfer in Dimethyl Sulfoxide**" *J. Org. Chem.*, 70, no. 12, **2005**, 4826–4832. doi:10.1021/jo050432y, Available at http://pubs.acs.org/doi/abs/10.1021/jo050432y.

18. Clavaguera, S.; Khan, S. I.; and Rubin, Y. "**Unexpected de-Arylation of a Pentaaryl Fullerene.**" *Org. Lett.*, 11, no. 6, **2009**, 1389–91. doi:10.1021/ol900224w, Available at http://www.ncbi.nlm.nih.gov/pubmed/19245246.

19. Deng, L.; Xie, S.; Yuan, C.; Liu, R.; Feng, J.; Sun, L.; Lu, X.; Xie, S.; Huang, R.; and Zheng, L. "**Solar Energy Materials & Solar Cells High LUMO Energy Level C 60 (OCH 3) 4 Derivatives : Electronic Acceptors for Photovoltaic Cells with Higher Open-Circuit Voltage**" *Sol. Energy Mater. Sol. Cells*, 111, **2013**, 193–199. doi:10.1016/j.solmat.2012.12.026, Available at http://dx.doi.org/10.1016/j.solmat.2012.12.026.

20. Troyanov, S. I.; Trush, V. V; Vovk, A. I.; Mumyatov, A. V; Martynenko, V. M.; and Troshin, P. A. "**ChemComm Highly Selective Reactions of C 60 Cl 6 with Thiols for the Synthesis of Functionalized [60] Fullerene Derivatives W**" **2012**, 7158–7160. doi:10.1039/c2cc32517a.

21. Abdul-Sada, A. K.; Avent, A. G.; Birkett, P. R.; Kroto, H. W.; Taylor, R.; and Walton, D. R. M. "**A hexaallyl[60]fullerene, C60(CH2CH□CH2)6**" *J. Chem. Soc. Perkin Trans. 1*, 60, no. 3, **1998**, 393–396. doi:10.1039/a708197i. Available at

http://xlink.rsc.org/?DOI=a708197i.

22. Birkett, P. R.; Avent, A. G.; Darwish, A. D.; Kroto, H. W.; Taylor, R.; and Walton, D. R. M. "**Preparation and Characterisation of Unsymmetrical C60Ph4 and Symmetrical C60Ph2: The Effect of Regioselective Nucleophilic Attack upon C60Cl6**" *J. Chem. Soc. Perkin Trans. 2*,no. 3, **1997**, 457–462. doi:10.1039/a606717d, Available at http://xlink.rsc.org/?DOI=a606717d.

23. Hashiguchi, M.; Nagata, K.; Tanaka, K.; and Matsuo, Y. "**Facile Purification of C 60O-Containing [60]fullerene Using Trialkylphosphines at Room Temperature**" *Org. Process Res. Dev.*, 16, no. 4, **2012**, 643–646. doi:10.1021/op200376w.

24. **Merissa Halim and Yves Rubin, Unpublished Results.**

25. Lemiègre, L.; Tanaka, T.; Nanao, T.; Isobe, H.; and Nakamura, E. "**Synthesis of Oxy Aminated [60] and [70]Fullerenes with Cumene Hydroperoxide as Oxidant**" *Chem. Lett.*, 36, no. 1, **2007**, 20–21. doi:10.1246/cl.2007.20, Available at http://joi.jlc.jst.go.jp/JST.JSTAGE/cl/2007.20?from=CrossRef.

26. Liang, S.; Xu, L.; and Gan, L. "**Synthesis and Chemical Reactivity of tetrahydro[60]fullerene Epoxides with Both Amino and Aryl Addends**" *J. Org. Chem.*, 80, no. 8, **2015**, 3957–3964. doi:10.1021/acs.joc.5b00287.

27. **Shaohua Huang, Nicholas Knutson, Yves Rubin, Unpublished Results**.

28. Murata, Y.; Shiro, M.; and Komatsu, K. "**Synthesis, X-Ray Structure, and Properties of the First Tetrakisadduct of Fullerene C 60 Having a Fulvene-**

Type π-System on the Spherical Surface" *J. Am. Chem. Soc.*, 119, no. 34, **1997**, 8117–8118. doi:10.1021/ja971456s, Available at http://pubs.acs.org/doi/abs/10.1021/ja971456s.

29. Keshavarz-k, M.; Knight, B.; Srdanov, G.; and Wudl, F. "**Cyanodihydrofullerenes and Dicyanodihydrofullerene: The First Polar Solid Based on C60**" *J. Am. Chem. Soc.*, 117, **1995**, 11371–11372.

30. Wang, G.; Lu, Y.; and Chen, Z. "**1, 4-Fullerenols C 60 ArOH : Synthesis and Functionalization**" *Org. Lett.*, 11, no. 7, **2009**, 1507–1510. doi:10.1021/ol900110g.

31. Nambo, M. and Itami, K. "**Palladium-Catalyzed Carbon-Carbon Bond Formation and Cleavage of Organo(hydro)fullerenes**" *Chem. - A Eur. J.*, 15, no. 19, **2009**, 4760–4764. doi:10.1002/chem.200900022.

32. Li, F.; Haj Elhussin, I. E.; Li, S.; Zhou, H.; Wu, J.; and Tian, Y. "**KOtBu-Mediated Coupling of Indoles and [60]Fullerene: Transition-Metal-Free and General Synthesis of 1,2-(3-Indole)(hydro)[60]fullerenes**" *J. Org. Chem.*, 80, no. 21, **2015**, 10605–10610. doi:10.1021/acs.joc.5b01725.

33. Bartoli, G.; Bencivenni, G.; and Dalpozzo, R. "**Organocatalytic Strategies for the Asymmetric Functionalization of Indoles.**" *Chem. Soc. Rev.*, 39, no. 11, **2010**, 4449–4465. doi:10.1039/b923063g.

2. Beyond PCBM: Methoxylated 1,4-Bisbenzyl [60]Fullerene Adducts for Efficient Organic Solar Cells

Introduction

Organic solar cells have received great attention in recent years as a potential alternative to silicon solar cells because of their ability to be inexpensively solution-processed and because they can be lightweight and flexible.[1–5] The key component of an organic-based photovoltaic system is its active layer, wherein a *p*-type conjugated polymer and an *n*-type acceptor material mix to form a bicontinuous interpenetrating network that is referred to as a bulk heterojunction (BHJ).[6,7] Fullerene derivatives have been used extensively as the acceptors in BHJ solar cells thanks to their high electron affinities and electron mobilities.[8] The power conversion efficiency (PCE) of polymer/fullerene BHJ solar cells can be as high as 10.8%,[9] with most of the recent advances coming from the design of new polymer donors and/or the use of new device architectures.[10,11] In contrast, progress on the design and synthesis of novel fullerene acceptors for high-efficiency organic photovoltaics has been much less rapid. Most of the highest performing devices[9,12] still utilize the classic fullerene derivative [6,6]-phenyl-C-61-butyric acid methyl ester (PCBM), synthesized more than twenty years ago,[13] or its expensive C_{70} analogue, $PC_{71}BM$.[14]

The PCE of a solar cell is proportional to the product of the short-circuit current (J_{sc}), open-circuit voltage (V_{oc}) and fill factor (*FF*). Thus, one strategy for improving device efficiency is to increase the V_{oc}, which is directly related to the

difference between the energy of the highest occupied molecular orbital (HOMO) of the polymer donor and that of the lowest unoccupied molecular orbital (LUMO) of the fullerene acceptor. As long as the LUMO of the fullerene is lower than that of the polymer by an amount sufficient to promote charge separation, raising the fullerene LUMO level should increase the V_{oc} and thus the PCE.

To this end, several research groups have synthesized fullerene derivatives where two or more double bonds of the fullerene cage are saturated.[15–24] Although V_{oc} has been demonstrated to increase with this method, devices based on most of these new fullerenes fail to maintain high J_{sc} and/or *FF*, and as a result, the overall device efficiency suffers.[19,25–27] This is because altering the chemical structure of a fullerene addend can have detrimental effects on device performance for two reasons: first, the size and pattern of the addends can dramatically influence the electronic coupling between adjacent fullerenes through steric and/or electronic effects, causing a significant decrease in local electron mobility;[27] and second, changes in the fullerene addends can alter the degree of phase separation from the polymer, sometimes caused by a reduction in fullerene crystallinity due to packing constraints or mixtures of isomers. In cases where fullerene crystallization drives phase separation, this can dramatically change the morphology of the bulk heterojunction.[27]

There are a few select fullerene derivatives, such as the bisadduct of PCBM (*bis*-PCBM)[28], indene C_{60} bisadduct (ICBA)[15] and its C_{70} congeners,[29] dihydronaphthyl-based C_{60} bisadduct (NCBA)[30] and di(4-methyl-

phenyl)methano-C_{60} bisadduct (DMPCBA),[31] that have shown good photovoltaic performance when used in combination with the classic crystalline semiconducting polymer poly(3-hexylthiophene-2,5-diyl) (P3HT). However, when these fullerene derivatives are used in combination with less crystalline state-of-the-art low-bandgap polymers, the performance of the solar cells is typically low, with greatly decreased J_{sc} and *FF*.[25,26,32–34] Therefore, despite the aforementioned efforts to increase the V_{oc}, PCBM (and its C_{70} analogue) are still the most successful fullerene acceptors for high-performance polymer-based photovoltaics to date.

In order to design new fullerene acceptors for high performance polymer-based solar cells, the following factors need to be considered: 1) The LUMO level of the fullerene derivative should be carefully tuned so that when paired with the polymer of choice, an ideal energy level offset between the fullerene donor and polymer acceptor is attained. Although still under debate,[34,35] the generally accepted range of this offset is about 0.3 eV, depending on the materials.[26,36,37] 2) Size-suitable addends are needed to assist close contacts between fullerene balls, thereby facilitating favorable electronic coupling to facilitate charge transport within the fullerene domains.[27,38] 3) Derivatives must possess good solubility in organic solvents for solution processing, and must form reasonable BHJ structures with a variety of polymers. In this paper, we thus present the synthesis of a series of new fullerene derivatives that satisfy all of these requirements. We find that when carefully designed, fullerenes with higher LUMOs can be prepared that produce devices with higher V_{oc}'s – without significant loss of J_{sc} or *FF* – and thus higher power conversion efficiencies.

Our new derivatives are methoxylated 1,4-bisbenzyl fullerene adducts (MeO-BBF, Table 2.1), i.e. two addends are located at the *"para"* positions of a six-membered ring on the fullerene cage.[39] These derivatives have a smaller *π*-conjugated system with reduced symmetry[40–43] resulting in a slightly higher LUMO level than the corresponding 1,2-fullerene bisadducts. The LUMO level, side chain nature and solubility of the 1,4-fullerene bisadducts can be further tuned by altering each addend independently.[39] The molecules we focus on bear electron-donating methoxy group(s) on the benzyl ring(s). Since these electron-rich methoxy substituents are not conjugated with the fullerene π-system, they would be expected to have negligible electronic interaction. However, we find through experiments that are supported by DFT calculations that the relative position and number of methoxy groups can have a dramatic effect on the performance of these fullerene derivatives in polymer-based solar cells.

Table 2.1. Synthesis of symmetric and asymmetric 1,4-bisbenzyl fullerene C_{60} adducts **1a–k**.

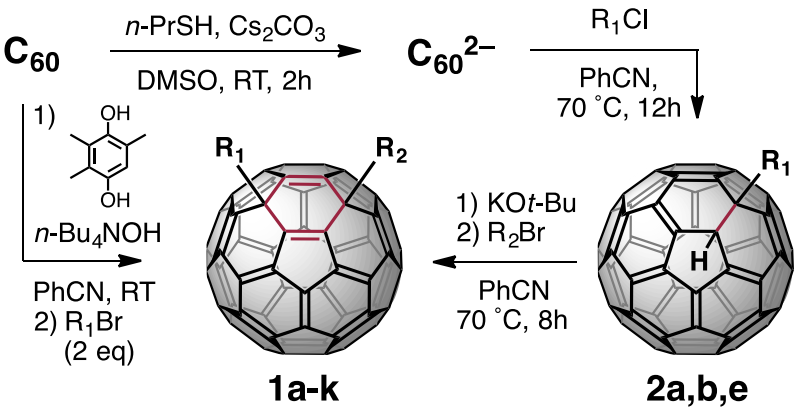

$R_1 = R_2$	$R_1 \neq R_2$
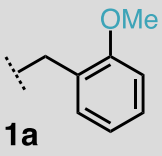 **1a**	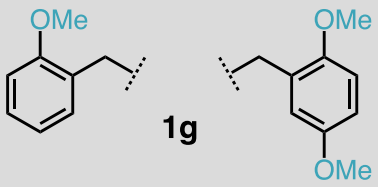 **1g**
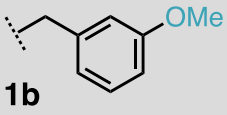 **1b**	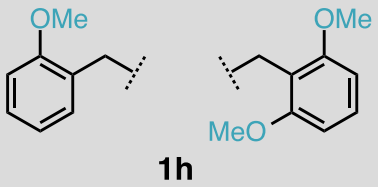 **1h**
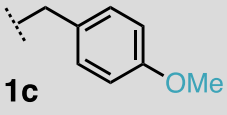 **1c**	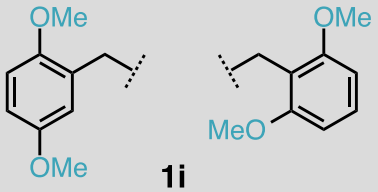 **1i**
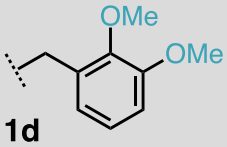 **1d**	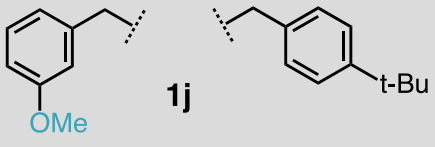 **1j**
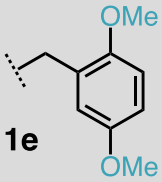 **1e**	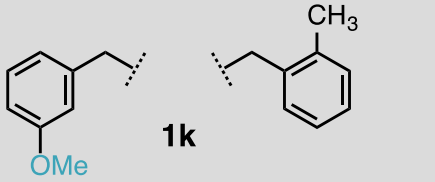 **1k**
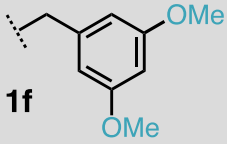 **1f**	

We have investigated the performance of these fullerenes in combination with both P3HT and the low-bandgap polymer PTB7.[44] The best PCE based on P3HT:1-(2',5'-dimetho-xybenzyl)-4-(2",6"-dimethoxybenzyl)[60]fullerene bisadduct (**1i**) is 4.1%, which is a > 20% enhancement relative to devices made from P3HT:PCBM.

Furthermore, devices based on PTB7:**1e** show a V_{oc} of 0.83 V, a respectable *FF* (53%) and a J_{sc} (12.3 mA/cm^2) that is higher than that for devices based on PTB7:PCBM, resulting in a PCE of 5.4%. Perhaps more importantly, our results clearly show that the precise nature and degree of substitution of the methoxy group(s), even on a single benzyl addend, greatly influences both the V_{oc} and PCE of the BHJ photovoltaic devices. Moreover, the higher conformational flexibility of the benzyl vs. an aryl substituent in these 1,4-bisadducts appears to play a significant role in obtaining high PCE values.[39,43]

Experimental

Synthesis

Our ability to synthesize the MeO-BBF bisadducts is a direct result of the ease of alkylating the C_{60} dianion.[45–50] As shown in Table 1, C_{60}^{2-} can be generated readily in dry degassed PhCN when treated with hydroquinone and base (SI).[51] By adding a large excess of a substituted benzyl bromide to a dark red solution of C_{60}^{2-}, we produced the symmetric 1,4-dibenzyl C_{60} bisadducts in relatively good yields (Table 2.1).

The synthesis of asymmetric 1,4-dibenzyl C_{60} bisadducts involves a stepwise alkylation procedure (SI). As shown in Table 2.1, C_{60} also can be

reduced to C_{60}^{2-} with *n*-$PrS^{-}Cs^{+}$ generated *in situ* through the reaction of *n*-propanethiol and Cs_2CO_3 in DMSO.[52] C_{60}^{2-} reacts with substituted benzyl chlorides to provide monoadducts **2a,b** or **2e** in 50-60% yields. The lower reactivity of benzyl chlorides relative to benzyl bromides towards S_N2 is likely at the origin of the different outcomes of these two reaction conditions.[49] The subsequent benzylation of deprotonated monoadducts **2a,b** or **2e** with a benzyl bromide provides the asymmetric 1,4-bisadducts **1j–k**, which bear two different addends.

The synthesis details of each fullerene derivative and their NMR, mass-spectrometry and cyclic voltammetry character-istics can be found in the Supporting Information (SI).

Photovoltaic Device and Active Layer Fabrication Procedures

We fabricated polymer:fullerene BHJ solar cells by starting with prepatterned tin-doped indium oxide (ITO)-coated substrates (TFD Inc.) and cleaning them by successive sonication in detergent solution, deionized water, acetone and isopropanol for ~10 min each. After drying in vacuum for at least an hour, we treated the ITO substrates with an air plasma (200 mTorr, 15 min). A thin layer of poly(ethylene-dioxythiophene):poly(styrenesulfonic acid) (PEDOT:PSS) (Clevios™ P VP AI 4083) was then spin-coated onto the clean substrates in air at 5000 rpm for 20 s, and the PEDOT:PSS-covered substrate was then baked at 150 ºC for 20 min in air.

P3HT:fullerene blend solutions were prepared by dissolving solid P3HT (Rieke Metal Inc. P100) and solid fullerene derivatives in *o*-dichlorobenzene (*o*-DCB) with a weight ratio of 1:0.8. The concentration was 20 mg/mL with respect

to P3HT. The solutions were stirred at 55 ºC overnight on a hot plate in a nitrogen glovebox before being cooled down to room temperature. The solutions were spun onto the PEDOT:PSS-covered substrates at 1160 rpm for 20 s. The active layers were still wet when the samples were taken off the spin-coater. Without covering or any other form of solvent annealing, the wet films became dry in the nitrogen glovebox after ~2 min. All of the films were then thermally annealed at 150 ºC for 20 min on a hot plate under an argon atmosphere. The thickness of the polymer:fullerene layers were ~160–180 nm, as measured with a Dektak 150 Stylus Surface Profiler.

PTB7:fullerene solutions were prepared by dissolving solid PTB7 (Solarmer Energy Inc.) and solid fullerene derivatives in a mixture of 95% chlorobenzene (CB)/5% 1,8-diiodooctane (DIO) v/v with a polymer:fullerene weight ratio of 1:1.5 for the fullerene bisadducts and 1:1.34 for PCBM (the change in weight ratio accounts for molecular weight differences to ensure that all polymer:fullerene blends were equimolar). The concentration was 10 mg/mL with respect to PTB7. The solutions were stirred at 55 ºC overnight prior to being spun at 1000 rpm for 60 s onto PEDOT:PSS-covered substrates. The films were then transferred to the antechamber of the glovebox and held under vacuum for ~1 hr. Pure methanol was then spun onto the films at a speed of 2500 rpm for 40 s to remove residual DIO. No further treatments were performed after this step before the deposition of the metal cathode. Cathode deposition consisted of ~10 nm of Ca evaporated at a rate of ~0.5 Å/s followed by 70 nm of Al at rates below 1 Å/s. The resulting device active areas were 7.2 mm^2.

Current density–applied voltage (*J*–*V*) measurements were performed in an argon atmosphere using a Keithley 2400 source meter. A xenon arc lamp and 1-sun-calibrated AM-1.5 filter were used as the excitation source.

External quantum efficiency (EQE) measurements were taken using a home-built set-up that has been detailed in previous publications by our group.[53]

Films for non-device measurements were prepared using identical procedures to those described above but without deposition of a top electrode.

Structural and Optical Characterization

UV-Visible absorption spectra were collected using a Perkin-Elmer Lambda 25 UV/Vis Spectrophotometer.

The 2-D grazing incidence wide angle X-ray scattering (GIWAXS) experiments were performed at the Stanford Synchrotron Radiation Lightsource on beamline 11-3 using a wavelength of 0.9742 Å. Figure 3c in the next section was obtained by radially-integrating the full 2-D diffractograms. Each data curve in Fig. 3c is the average of at least three different samples prepared using the same conditions. The 2-D images were collected on a plate with the detector 400 mm away from the center of the measured sample. The beam spot had a width of ~150 μm. A helium chamber was used to reduce the noise. The software package WxDiff was used to analyze the GIWAXS data.

Results and discussion

Material properties

Fullerene derivatives **1a–k** all have good solubility in common organic solvents for solar cell fabrication, such as $CHCl_3$, CS_2, CB and *o*-DCB. The products were

characterized by mass spectrometry, ^{1}H-NMR and ^{13}C-NMR (SI) spectroscopy. The ^{1}H-NMR spectra show that the peaks of methylene groups are split into AB quartets for the symmetrical 1,4-bisadducts **1a–f**, and mostly split into four doublets for unsymmetrical **1g–k** (see SI), which implies the 1,4-addition pattern. Single crystals of **1c** and **1e** were obtained through slow diffusion of EtOH into a CS_2 solution, providing the X-ray structures shown in Fig. 1. Their structures show a number of short intermolecular C–C contact distances between fullerene carbons, as shown in Fig. 1b,e; these short packing distances should favor electron mobility through increased intermolecular orbital interactions. The shortest contacts are 3.301 Å and 3.028 Å for **1c** and **1e**, respectively. Despite the different short-contact distances, both structures have a similar 2-D layered structure and an interpenetrating network of methoxylated benzyl groups. The opposite side of the interpenetrated network of methoxylated benzyl groups is a fullerene bilayer displaying a number of fullerene-fullerene close-contacts (Fig. 2.1c,f).

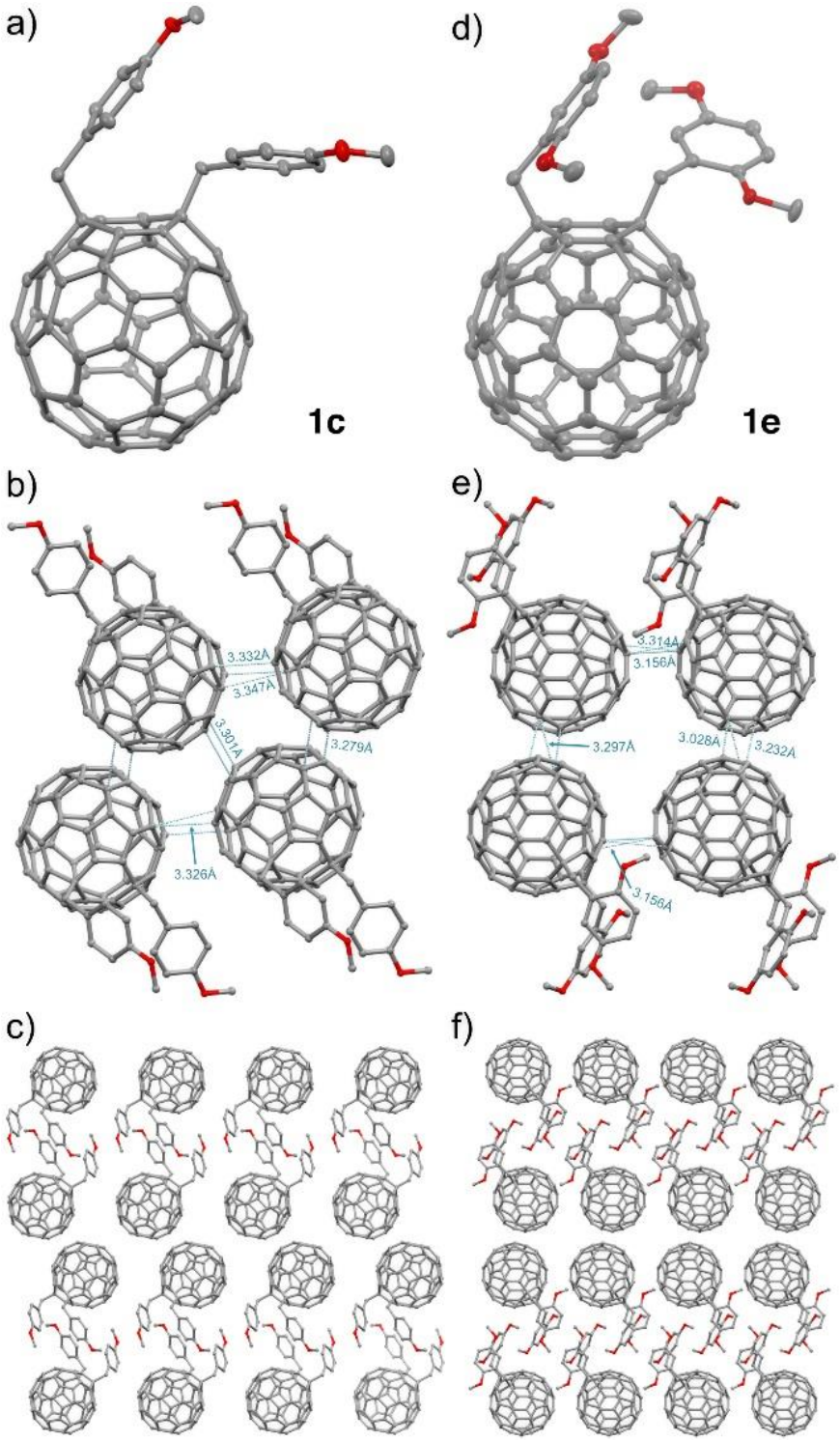

Fig. 2.01 a,d) ORTEP representations of the single crystal structures for 1,4-bisadducts **1c** and **1e**, respectively. b,e) Packing modes and intermolecular C–C contacts shorter than van der Waals distances (≤ 0.05 Å) for **1c** and **1e**, respectively. c,f) Packing structures for **1c** down the crystallographic *a*-axis, and **1e** down the crystallographic *b*-axis, respectively. Both are 2-D layered structures. Hydrogens and CS_2 cocrystallization solvent molecules are omitted for clarity.

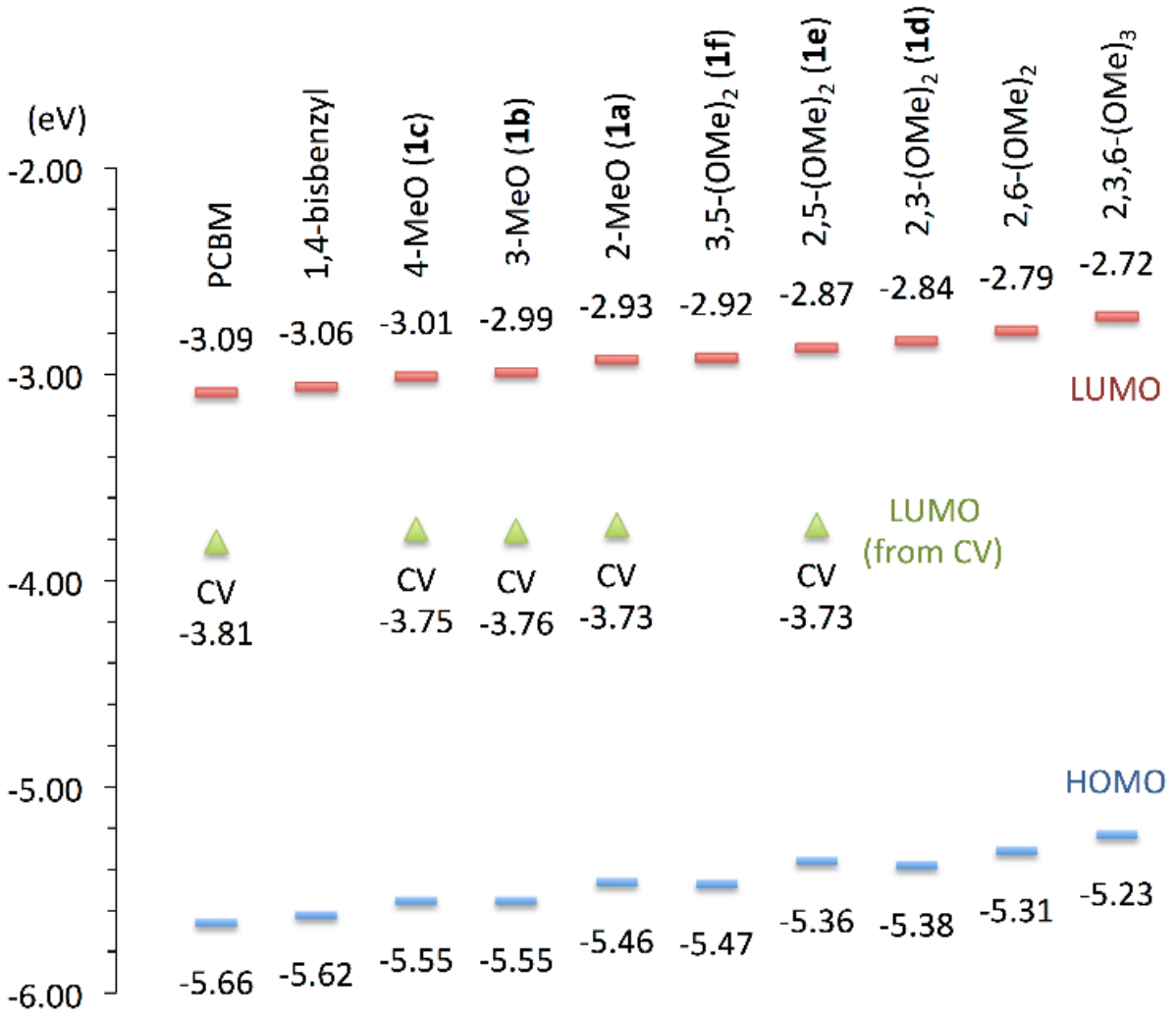

Fig. 2.02 DFT (B3LYP/6-31G(d)) calculated HOMO (red dash) and LUMO (blue dash) energies and selected LUMOs from experimental CV data (green triangle) for PCBM and symmetrically substituted 1,4-bisbenzyl [60]fullerene adducts (i.e. R_1=R_2 in Table 1) where the compound legend after PCBM and 1,4-bisbenzyl indicates the relative position(s) of methoxy group(s) on the benzyl substituents.

The green triangles in Fig. 2 show the electrochemical properties of several selected MeO-BBFs. These cyclic voltammetry (CV) measurements show that the LUMO levels of our MeO-BBFs are higher than that of PCBM by ~0.05–0.09 eV, depending on the position of the methoxy substituent. Methoxy substitution at the 2-position results in a slightly higher LUMO level than substitution at the 3- or 4-positions.

DFT calculations (B3LYP/6-31G(d)) of the HOMO and LUMO levels of MeO-BBFs **1a–f** also show the same trend in increasing HOMO and LUMO energies as the relative placement of the methoxy group changes from the 2- to the 3- and 4-positions (Fig. 2.02), although the absolute values do not agree with experiment, as expected for a calculation of this type. Furthermore, increasing the number of methoxy substituents also steadily raises both the HOMO and LUMO energies. This effect of substitution can be explained by the Wheeler-Houk model:[54–56] since there can be only negligible overlap between the π-systems of the benzyl substituents and the fullerene, the interaction between them is primarily electrostatic. Thus, proximal oxygen lone pairs can increase electron density on the fullerene π-system. A methoxy group at the 2-position has its lone pairs closest to the fullerene π-system, while methoxy groups at the 3- or 4-positions show less interaction as the average distance increases. Similarly, increasing the number of methoxy groups from one (**1a–c**) to two (**1d–f** or 1,4-bis[2,6-dimethoxybenzyl]) or three (1,4-bis[2,3,6-trimethoxybenzyl]) results in easier ionization and makes reduction become more difficult (Fig. 2.02).

Photovoltaic device performance and structural characterization

To examine the performance of the MeO-BBF **1a–k** in BHJ solar cells, we first blended our new fullerene derivatives with P3HT and fabricated photovoltaic devices with a structure glass/ITO/PEDOT:PSS (30 nm)/1:0.8 polymer:fullerene (~160-180 nm)/Ca(10 nm)/Al (70 nm). All of the performance comparisons and conclusions we draw are based on the study of devices with composition- and thickness-matched active layers. All active layers were thermally annealed at

150 °C for 20 min prior to deposition of the cathode, and *J*–*V* curves were measured under AM 1.5G illumination.

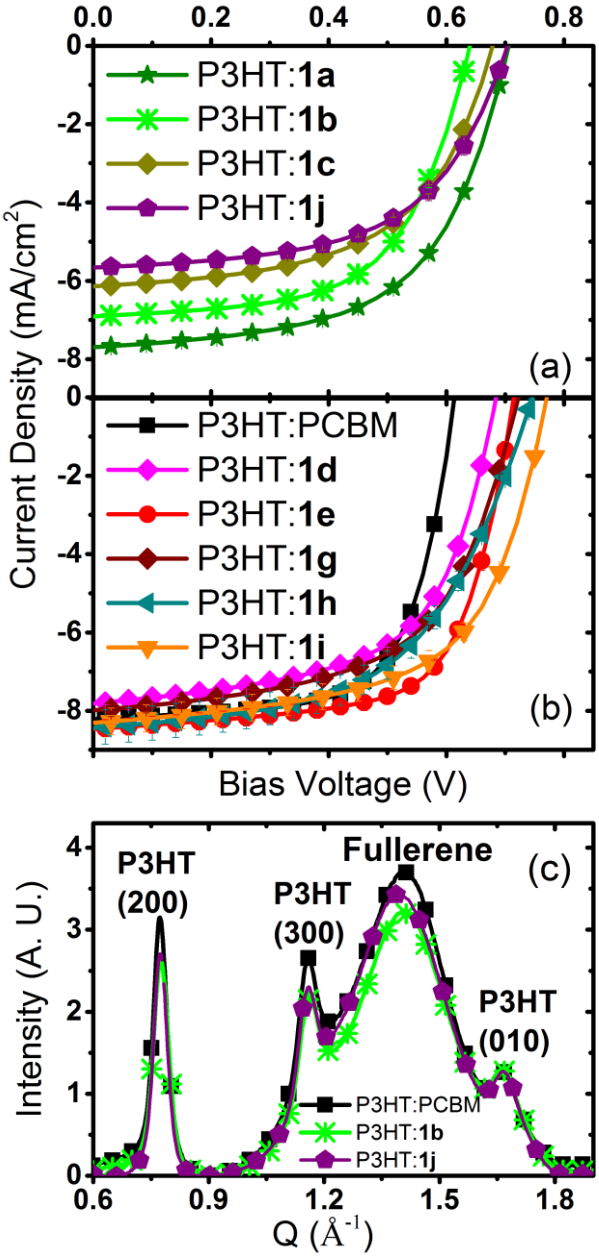

Fig. 2.03 (a) and (b): Current density versus applied bias for photovoltaic devices based on P3HT:MeO-BBFs where each of the benzyl rings in the MeO-BBFs are substituted with one side group (a) and two methoxy groups (b). The *J*-*V* curve of a standard P3HT:PCBM-based control device is plotted in (b) as the black curve/squares. The error bars show 1 standard deviation for measurements over at least 6 independent devices. (c): Example of radially-integrated 2-D GIWAXS intensities for three P3HT:fullerene active layers processed on silicon substrates.

Figure 2.03a and Table 2.2 summarize the performance of P3HT:MeO-BBF-based devices where the benzyl rings connected to the fullerene ball have substituents with a single side group (**1a**–**1c, 1j, 1k**). We find that non-methoxy substituents on even one of the benzyl rings resulted in either lower *FF*s (P3HT:**1k**) or lower J_{SC}'s (P3HT:**1j**) than benzyl groups with methoxy substitution; the PCE's for devices based on non-methoxylated 1,4-bisadducts were in the relatively low range of 2.2 to 2.4%. In contrast, methoxy substitution led to higher-performing devices (PCE's ranging from 2.3 to 3.1% for P3HT:**1a**) depending on the exact position at which the methoxy groups were substituted.

Table 2.2. Summary of Photovoltaic Device Parameters

BHJ	V_{oc} (mV)	J_{sc} (mA/cm^2)	*FF* (%)	*PCE* (%)
P3HT:PCBM	613 ± 2	8.2 ± 0.2	66.6 ± 0.4	3.4 ± 0.1
P3HT:**1a**	716 ± 5	7.6 ± 0.3	57.6 ± 1.1	3.1 ± 0.1
P3HT:**1b**	640 ± 4	6.9 ± 0.2	59.4 ± 0.6	2.6 ± 0.1
P3HT:**1c**	679 ± 2	6.1 ± 0.2	55.4 ± 1.6	2.3 ± 0.1
P3HT:**1d**	680 ± 1	7.8 ± 0.1	59.7 ± 1.1	3.2 ± 0.1
P3HT:**1e**	715 ± 1	8.5 ± 0.2	66.3 ± 0.7	3.9 ± 0.1
P3HT:**1f**	588 ± 5	6.0 ± 0.1	55.4 ± 1.3	2.0 ± 0.1
P3HT:**1g**	720 ± 1	8.0 ± 0.2	57.5 ± 0.1	3.3 ± 0.1
P3HT:**1h**	740 ± 1	8.4 ± 0.5	55.0 ± 0.1	3.4 ± 0.2
P3HT:**1i**	771 ± 2	8.3 ± 0.3	60.1 ± 0.8	3.9 ± 0.2
P3HT:**1j**	704 ± 1	5.7 ± 0.3	56.1 ± 1.5	2.2 ± 0.1
P3HT:**1k**	667 ± 4	7.2 ± 0.1	49.2 ± 1.1	2.4 ± 0.1
PTB7:PCBM	760 ± 1	12.1 ± 0.2	64.4 ± 0.1	5.9 ± 0.3
PTB7:**1e**	825 ± 9	12.3 ± 0.2	53.3 ± 0.1	5.4 ± 0.1

To understand why such subtle variations in the substitution pattern of our 1,4-bisadducts led to such widely varying device performance, we studied the morphology of the solar cell active layers using GIWAXS. The experiments were performed at the Stanford Synchrotron Radiation Light Source on

beamline 11−3 with a wavelength of 0.9742 Å. For these experiments, we focused on three selected polymer:fullerene systems: P3HT:PCBM, P3HT:**1b** and P3HT:**1j** (Fig. 3c).

In pure films, P3HT orients with the chains edge-on to the substrate,[57–60] and based on the relative in-plane and out-of plane scattering intensities, we see that this preferred chain orientation is maintained upon addition of either MeO-BBF or PCBM (see SI). However, both the characteristic fullerene diffraction observed at ~1.4 $Å^{-1}$ and the crystallinity of the P3HT (as measured by the intensity of the (200) peak) are smaller when **1b** or **1j** are used in the active layer compared to when PCBM is used. Lower crystallinity materials should have a poorer carrier mobility, which could explain the lower J_{sc} and *FF* of the photovoltaic devices based on these active layers.[60] Another notable difference is that for P3HT:**1j**, the fullerene peak is shifted towards lower *Q*, which corresponds to an increased spacing between fullerenes. Fullerene **1j** contains a bulky *t*-butyl group substituted on one benzyl ring, which likely hinders close packing of the fullerene molecules. Consequently, this increase in inter-fullerene spacing leads to a decreased electronic coupling between fullerenes and therefore to a decrease in carrier mobility.[27] This is also consistent with **1j** having the lowest J_{sc} among all the MEO-BBFs.

Figure 2.03a and Table 2.2 also show that when the methoxy group is at the 2-position of the benzyl group (**1a**), the corresponding device has a greater PCE (3.1%) compared to the 3-position (2.6%, **1b**), which in turn is greater than with the 4-position (2.3%, **1c**). The changes in V_{oc} (Table 2.2) of these three

devices track the changes in experimental (CV) and DFT-calculated LUMO levels of MeO-BBFs **1a–f** (Fig. 2.2).

Although electrostatic interactions can explain the changes in V_{oc}, the variation in the J_{sc} of the devices cannot be easily explained by the electrochemical or computational results. There are two potential reasons for the sensitivity of the photocurrent to the substitution position. First, the position of the methoxy group can affect the fullerene-to-fullerene contact distance and thus the electronic coupling and local carrier mobility. Second, the way the fullerene interacts with the polymer could be altered by the structure of the benzyl side chain, which would alter the resultant BHJ morphology. Finally, the propensity of the fullerene to crystallize could alter the polymer/fullerene phase separation, again changing the overall BHJ morphology.

To investigate this, we measured the diode ideality factor, n_{ideal}, for each of the MeO-BBF-based devices by fitting their dark *J*–*V* curves (Table 2.3); n_{ideal} provides an indicator of the charge carrier recombination mechanism.[61,62] Table 3 in the SI shows that devices with P3HT:**1a** have the most ideal (i.e., closest to bimolecular rather than trap-dominated) recombination among fullerene derivatives **1a**–**c**, suggesting that the variations in J_{sc} predominantly reflect changes in BHJ morphology.

Table 2.3. Summary of Photovoltaic Device Parameter

BHJ	n_{ideal}	R_{seires} (Ω-cm^2)	R_{shunt} ($\times 10^5$ Ω-cm^2)
P3HT:PCBM	1.34 ± 0.03	3.2 ± 0.1	2.0 ± 0.1
P3HT:**1a**	1.40 ± 0.02	4.4 ± 0.4	29 ± 7
P3HT:**1b**	1.80 ± 0.15	3.5 ± 0.2	1.2 ± 0.6
P3HT:**1c**	1.44 ± 0.03	6.0 ± 0.6	14 ± 0.8
P3HT:**1d**	1.39 ± 0.03	4.0 ± 0.3	8.0 ± 0.2
P3HT:**1e**	1.31 ± 0.01	3.3 ± 0.1	20 ± 6
P3HT:**1f**	1.63 ± 0.04	3.8 ± 1.5	3.5 ± 0.7
P3HT:**1g**	1.27 ± 0.01	4.2 ± 0.8	37 ± 3
P3HT:**1h**	1.41 ± 0.02	3.2 ± 0.1	7.5 ± 0.4
P3HT:**1i**	1.28 ± 0.03	3.3 ± 0.1	43 ± 17
P3HT:**1j**	1.44 ± 0.04	6.0 ± 0.9	16 ± 4
P3HT:**1k**	1.51 ± 0.02	3.8 ± 0.6	42 ± 12
PTB7:PCBM	1.37 ± 0.01	1.5 ± 0.1	0.1 ± 0.01
PTB7:**1e**	1.37 ± 0.01	3.7 ± 0.4	0.7 ± 0.2

After establishing that alkyl group substitution on the benzyl ring was inferior to methoxy group substitution for solar cell performance, we next turned to study the effects of the number and position of the methoxy substituents. To this end, we synthesized fullerene derivatives **1d**–**1i** (Table 1), and fabricated photovoltaic devices from those derivatives. The performance parameters are

again summarized in Table 2.2. Examples of the *J*–*V* curves for these devices under AM1.5G illumination are plotted in Fig. 2.03b.

The most striking result of Fig. 2.03b and Table 2 is that 1,4-bisadduct fullerenes with bismethoxy-substituted benzyl rings lead to improved solar cell efficiency; in fact, most of the PCEs reach or surpass those of P3HT:PCBM. Both P3HT:**1e** and P3HT:**1i** show a ~20% enhancement in PCE compared to P3HT:PCBM (black squares in Fig. 3), and P3HT:**1d**, P3HT:**1g** and P3HT:**1h** all have comparable PCEs to P3HT:PCBM devices. P3HT:**1f** is clearly an exception, having the lowest PCE of the group, and we are currently investigating the morphology of this active layer to understand why.

Compared to the monomethoxy MeO-BBFs **1a**–**1c**, devices fabricated using **1d**–**1i** (except for **1f**) show both higher J_{sc} and V_{oc}. We measured n_{ideal} values for these devices (Table 3), and found the general trend that devices based on **1d**–**1i** have more ideal charge carrier recombination than those based on **1a**–**1c**. This indicates that the nanoscale BHJ morphology is improved by the addition of the second methoxy group on the benzyl rings of the MeO-BBFs. This morphology improvement also likely contributes to the increase in both J_{sc} and V_{oc}.

Figure 3b and Table 2.2 also reinforce the observation that the position of the methoxy group(s) has a significant effect on device performance. The dependence of V_{oc} on methoxy position can be summarized as follows: placing methoxy groups at the 2- or 2,6-positions increases V_{oc}, whereas placing methoxy groups at the 3- or 5- positions lowers the V_{oc}. In fact, fullerenes with two methoxy groups at the 3- (or 5-) position, such as **1d** and **1e**, show lower

V_{oc} than those with fewer, such as **1g**, **1h** and **1i**. When both methoxy groups are at the 3- and 5- positions, as with fullerene **1f**, the resultant device shows the lowest V_{oc}. With this trend in mind, we then synthesized the MeO-BBF derivative with methoxy groups at the 2,6-positions of each benzyl ring, which in principle should be the best-performing derivative. Unfortunately, this compound was not soluble enough in the solvents needed for device fabrication, so we could not test it in an organic photovoltaic device.

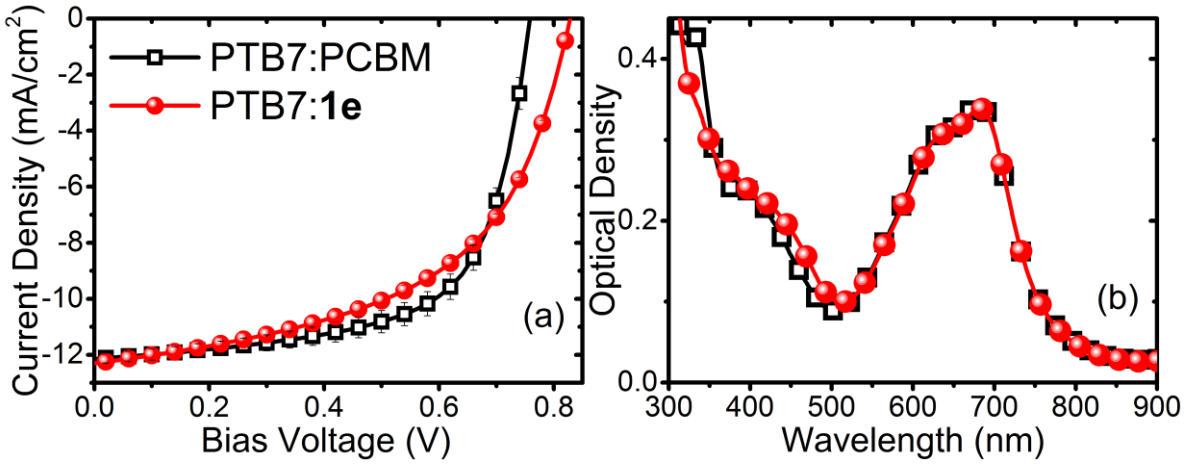

Fig. 2.04 a) Current density versus applied bias for photovoltaic devices based on PTB7:PCBM (open black square) and PTB7:**1e** (red circle). The error bars show 1 standard deviation for measurements over at least 6 independent devices. b) UV-visible absorption spectra for the same active layers used in (a).

As mentioned in the introduction, the most successful high-LUMO fullerenes studied to date (e.g., ICBA and its C_{70} analog) show poor compatibility with modern low bandgap push-pull polymers. To see if we could break this trend with our MeO-BBF derivatives, we investigated the compatibility of one of our best derivatives (**1e**) with the high-performance low-bandgap polymer PTB7 (Fig. 4). We employed the same device structure, with the active layer consisting of PTB7 and **1e** at a polymer:fullerene weight ratio of 1:1.5 with a thickness of

~90 nm. These active layers were used as-cast, without thermal annealing prior to cathode deposition. For comparison, we also fabricated PTB7:PCBM control devices, taking care to keep the two sets of devices thickness- and composition-matched, as shown by UV-Vis absorption (Fig. 2.04b).

Figure 4a and the bottom portion of Table 2.2 summarize the device performance results. Clearly, fullerene **1e**, which showed the best performance when blended with P3HT, also demonstrates excellent compatibility with PTB7. PTB7:**1e** devices show a higher V_{oc} and a similarly high J_{sc} as PTB7:PCBM devices. The overall device efficiency of PTB7:**1e** is slightly lower than PTB7:PCBM, however, due to a slightly lower *FF* that may be due to less efficient crystallization of derivative **1e** compared to PCBM, changing the resultant BHJ morphology.

Conclusions

In summary, we have synthesized a series of methoxylated 1,4-[60]fullerene bisadducts, **1a–k**, which have higher LUMO levels than PCBM. We evaluated their performance in BHJ solar cells and compared the resulting BHJ morphologies to those of the workhorse fullerene PCBM. Our best fullerene derivatives show more than 20% enhancement in device efficiency when combined with P3HT, largely due to the improved V_{oc} resulting from the higher LUMO of the 1,4-bis-substituted fullerenes. We found that adding methoxy groups to the benzyl rings increases the device performance and that the number and position of these groups has a dramatic effect on the solar cell efficiency due to morphological changes. Unlike previously-studied fullerene

bisadducts, which are outperformed by PCBM when combined into BHJs with low bandgap polymers, our 1,4-bisadduct **1e** demonstrated good compatibility with one of the best performing red polymers, PTB7. We are currently working on a deeper understanding of both the device physics and active-layer morphologies for these fullerene derivatives in polymer solar cells to help guide further synthesis and increase device performance. We believe that 1,4-bisbenzyl fullerene bisadducts in general and future C_{70} analogs of these molecules are promising candidates for replacing PCBM to improve the performance of conjugated polymer-based solar cells.

Supporting Information

Synthesis of the Fullerene Derivatives

Unless otherwise noted, all materials including dry solvents were obtained from commercial suppliers and used without further purification. All reactions were performed with dry solvents under an argon atmosphere in flame-dried glassware with standard vacuum-line techniques, unless specified otherwise. All work-up and purification procedures were carried out with reagent-grade solvents in air.

General procedure for the preparation of symmetric 1,4-bisbenzyl fullerene adducts 1a-f:

Trimethylhydroquinone (246 mg, 1.6 mmol, 5.4 eq) in 25 mL of benzonitrile and a suspension of C_{60} (216 mg, 0.3 mmol, 1.0 eq) in 25 mL of benzonitrile were both degassed under reduced pressure over 30 minutes. Tetrabutylammonium hydroxide (1 M in methanol, 3.3 mL, 11.0 equiv.) was added to the solution of trimethylhydroquinone at room temperature. The color of the solution immediately

changed from colorless to red. After stirring for 30 minutes at this temperature, the resulting red solution was transferred to the purple suspension of C_{60} in benzonitrile *via* a cannula over a 30-minute time period and stirred for an additional 30 minutes, giving a dark solution. To this solution, benzyl bromide was added (6.0 mmol, 20 eq) and the resulting solution stirred overnight at room temperature. The reaction mixture was treated with 1 mL of aqueous HCl (*ca*. 1 M), dried over anhydrous $MgSO_4$, and filtered through a pad of silica gel (eluted with toluene). The filtrate was concentrated under reduced pressure. Chromatography of the residue gave the desired 1,4-bisadduct.

1,4-Bis(2-methoxybenzyl)-1,4-dihydro[60]fullerene (1a): The synthesis of **1a** follows the general procedure (35%). ^{1}H NMR (500 MHz, $CDCl_3$) δ 7.54 (dd, *J* = 7.4, 1.7 Hz, 2H), 7.34 (td, *J* = 7.4, 1.7 Hz, 2H), 7.08 (td, *J* = 7.4, 1.0 Hz, 2H), 7.01 (d, *J* = 7.4 Hz, 2H), 4.07 (AB-q, *J* = 12.7 Hz, 2H), 3.88 (AB-q, *J* = 12.7 Hz, 2H), 3.82 (s, 6H). ^{13}C NMR (125 MHz, $CDCl_3$) δ 158.57, 158.11, 152.01, 148.76, 148.57, 147.14, 146.97, 146.86, 146.29, 145.45, 144.88, 144.86, 144.84, 144.79, 144.46, 144.28, 144.22, 144.20, 143.78, 143.75, 143.17, 143.12, 142.93, 142.70, 142.57, 142.09, 141.93, 140.46, 138.90, 137.41, 132.56, 129.05, 124.99, 120.76, 111.27, 60.11, 55.09, 42.34. FAB-HRMS m/z calculated for $C_{76}H_{19}O_2$ $[M+H]^+$: 963.1380, found 963.1390.

1,4-Bis(3-methoxybenzyl)-1,4-dihydro[60]fullerene (1b): The synthesis of **1b** follows the general procedure (40%). ^{1}H NMR (500 MHz, $CDCl_3$): *δ* (ppm) 7.39 (t, *J* = 7.9 Hz, 2H), 7.17 (d, *J* = 7.5 Hz, 2H), 7.13 (s, 2H), 6.90 (dd, *J* = 8.2, 1.7 Hz, 2H), 3.86 (s, 6H), 3.77 (AB-q, *J* = 12.8 Hz, 2H), 3.72 (AB-q, *J* = 12.8 Hz, 2H). ^{13}C NMR (125 MHz, $CDCl_3$) δ 159.58, 157.99, 151.84, 148.67, 148.64, 147.21, 147.00, 146.93,

146.20, 145.51, 145.02, 144.79, 144.75, 144.71, 144.39, 144.31, 144.26, 144.15, 143.94, 143.76, 143.20, 143.11, 142.99, 142.66, 142.51, 142.02, 140.54, 138.80, 137.86, 137.80, 130.56, 129.47, 127.73, 123.60, 117.57, 112.32, 60.44, 55.35, 48.61. FAB-HRMS m/z calculated for $C_{76}H_{19}O_2$ $[M+H]^+$: 963.1380, found 963.1403.

1,4-Bis(4-methoxybenzyl)-1,4-dihydro[60]fullerene (1c): The synthesis of **1c** follows the general procedure (30%). ^{1}H NMR (500 MHz, $CDCl_3$): *δ* (ppm) 7.50 (d, *J* = 8.2 Hz, 4H), 7.00 (d, *J* = 8.2 Hz, 4H), 3.80 – 3.70 (m, 10H). ^{13}C NMR (125 MHz, $CDCl_3$) δ 159.00, 158.07, 151.91, 148.76, 148.66, 147.20, 147.09, 146.99, 146.93, 146.28, 145.50, 145.34, 145.01, 144.85, 144.78, 144.72, 144.40, 144.31, 144.27, 144.17, 143.94, 143.75, 143.19, 143.11, 142.97, 142.67, 142.56, 142.51, 142.01, 140.51, 138.87, 137.92, 133.27, 132.10, 128.32, 113.89, 113.53, 60.89, 55.36, 47.85. FAB-HRMS m/z calculated for $C_{76}H_{19}O_2$ $[M+H]^+$: 963.1380, found 963.1390.

1,4-Bis(2,3-dimethoxybenzyl)-1,4-dihydro[60]fullerene (1d): The synthesis of **1d** follows the general procedure (35%). ^{1}H NMR (500 MHz, $CDCl_3$): *δ* (ppm) 7.23 (dd, *J* = 7.7, 1.5 Hz, 2H), 7.14 (t, *J* = 7.9 Hz, 2H), 6.91 (dd, *J* = 8.2, 1.5 Hz, 2H), 4.10 (AB-q, *J* = 12.7 Hz, 2H), 3.94 (s, 6H), 3.90 (AB-q, *J* = 15.4 Hz, 2H), 3.88 (s, 6H). ^{13}C NMR (125 MHz, $CDCl_3$) δ 158.17, 152.92, 152.07, 148.76, 148.59, 148.11, 147.25, 147.11, 146.97, 146.86, 146.40, 145.41, 145.03, 144.95, 144.91, 144.75, 144.42, 144.24, 144.23, 144.18, 143.79, 143.77, 143.12, 143.09, 142.88, 142.60, 142.53, 142.04, 141.96, 140.42, 138.80, 137.85, 129.86, 124.48, 123.46, 111.86, 60.89, 60.08, 55.75, 42.08. FAB-HRMS m/z calculated for $C_{78}H_{23}O_4$ $[M+H]^+$: 1023.1591, found 1023.1587.

1,4-Bis(2,5-dimethoxybenzyl)-1,4-dihydro[60]fullerene (1e): The synthesis of **1e** follows the general procedure (32%). ^{1}H NMR (500 MHz, $CDCl_3$): δ (ppm) 7.14 (d, *J* = 3.1 Hz, 2H), 6.93 (d, *J* = 8.9 Hz, 2H), 6.85 (dd, *J* = 8.9, 3.1 Hz, 2H), 4.00 (AB-q, *J* = 12.7 Hz, 2H), 3.83 (s, 6H), 3.82 (AB-q, *J* = 12.7 Hz, 2H), 3.77 (s, 6H). ^{13}C NMR (125 MHz, $CDCl_3$) δ 158.65, 153.45, 152.44, 151.99, 148.74, 148.56, 147.10, 147.08, 146.97, 146.83, 146.27, 145.40, 144.90, 144.81, 144.79, 144.77, 144.41, 144.25, 144.19, 144.17, 143.74, 143.69, 143.12, 143.07, 142.87, 142.63, 142.53, 142.49, 142.08, 141.84, 140.36, 138.84, 137.29, 126.13, 119.20, 112.69, 112.06, 60.02, 55.84, 55.71, 42.44. FAB-HRMS m/z calculated for $C_{76}H_{19}O_2$ $[M+H]^+$: 1023.1591, found 1023.1576.

1,4-Bis(3,5-dimethoxybenzyl)-1,4-dihydro[60]fullerene (1f): The synthesis of **1f** follows the general procedure (40%). ^{1}H NMR (500 MHz, $CDCl_3$): δ (ppm) 6.73 (s, 4H), 6.45 (s, 2H), 3.84 (s, 12H), 3.78 (AB-q, *J* = 14.4 Hz, 2H), 3.74 (AB-q, *J* = 14.4 Hz, 2H). ^{13}C NMR (125 MHz, $CDCl_3$) δ 160.75, 160.72, 157.96, 151.86, 148.67, 148.67, 147.20, 147.00, 146.94, 146.22, 145.51, 145.02, 144.76, 144.71, 144.39, 144.30, 144.26, 144.16, 143.89, 143.76, 143.19, 143.11, 142.97, 142.66, 142.59, 142.51, 142.05, 142.01, 140.57, 138.81, 138.51, 137.81, 109.74, 98.85, 60.35, 55.46, 48.90. FAB-HRMS m/z calculated for $C_{78}H_{23}O_4$ $[M+H]^+$: 1023.1591, found 1023.1581.

Synthesis of the Asymmetric 1,4-Bisbenzyl Fullerene C_{60} Adducts 1g–k via Monobenzylated Adducts 2a,b,e.

1-(2-Methoxybenzyl)-1,2-dihydro[60]fullerene (2a): A suspension of C_{60} (144 mg, 0.2 mmol) and Cs_2CO_3 (196 mg, 0.6 mmol) in dry DMSO (25 mL) was prepared and 1-propanethiol (45 µL, 0.5 mmol) was added to the suspension. The resulting mixture was stirred for 2 hours under argon at room temperature. 2-

Methoxybenzyl chloride (250 mg, 1.6 mmol) was added to the resulting dark-red solution. Stirring continued for another 2 hours and the color of the solution turned green, indicative of an alkylated C_{60} monoanion. Following this, acetic acid (0.5 mL) was added, and after 5 minutes, the solution was poured into 100 mL of methanol. The solids were collected by centrifugation and then dissolved in a minimum volume of CS_2. Chromatography, using a mixture of cyclohexane and toluene (2:1 by volume), gave 1-(2-methoxybenzyl)-1,2-dihydro[60]fullerene **2a** (93 mg, 55%). ^{1}H NMR (500 MHz, $CDCl_3$) δ 7.72 (dd, *J* = 7.5, 1.6 Hz, 1H), 7.40 (ddd, *J* = 8.2, 7.6, 1.7 Hz, 1H), 7.11 (td, *J* = 7.5, 1.1 Hz, 1H), 7.06 (dd, *J* = 8.3, 0.6 Hz, 1H), 6.73 (s, 1H), 4.82 (s, 2H), 3.92 (s, 3H). ^{13}C NMR (125 MHz, $CDCl_3$) δ 158.21, 156.18, 154.25, 147.50, 147.36, 147.17, 146.47, 146.45, 146.39, 146.26, 146.22, 145.93, 145.50, 145.44, 145.39, 145.35, 144.76, 144.69, 143.32, 143.16, 142.62, 142.61, 142.30, 142.09, 142.03, 141.71, 141.60, 140.21, 139.90, 136.56, 135.48, 133.19, 129.36, 124.64, 121.00, 111.36, 66.01, 59.41, 55.22, 46.74. MALDI-TOF-MS m/z calculated for $C_{68}H_{11}O$ [M+H$^+$]: 843, found 843.

1-(3-Methoxybenzyl)-1,2-dihydro[60]fullerene (2b): To a suspension of C_{60} (144 mg, 0.2 mmol) and Cs_2CO_3 (196 mg, 0.6 mmol) in dry DMSO (25 mL) was added 1-propanethiol (45 µL, 0.5 mmol). The mixture was stirred for 2 hours under argon at room temperature. 3-methoxybenzyl bromide (42 µL, 0.3 mmol) was added to the resulting dark red solution and the stirring continued for 20 minutes. The color of the solution turned green, indicative of a substituted C_{60} monoanion. Acetic acid (0.5 mL) was added, and after 5 minutes the solution was poured into 100 mL of methanol. The solids were collected by centrifugation and then dissolved in a minimum volume of CS_2. Chromatography using a mixed solvent of cyclohexane and toluene (2:1 by

volume) gave 1-(3-methoxybenzyl)-1,2-dihydro[60]fullerene **2b** (64 mg, 38%). ^{1}H NMR (500 MHz, $CDCl_3$): δ (ppm) 7.49 – 7.38 (m, 2H), 7.34 (s, 1H), 6.96 (d, *J* = 7.1 Hz, 1H), 6.65 (s, 1H), 4.74 (s, 2H), 3.90 (s, 3H). ^{13}C NMR (125 MHz, $CDCl_3$) δ 159.82, 155.41, 153.91, 147.55, 147.39, 147.05, 146.51, 146.48, 146.35, 146.27, 145.88, 145.60, 145.53, 145.49, 145.48, 144.81, 144.67, 143.33, 142.67, 142.30, 142.14, 142.09, 141.99, 141.75, 141.70, 140.33, 140.09, 137.32, 136.43, 136.13, 129.94, 123.89, 117.59, 112.93, 65.82, 59.12, 55.19, 53.16. MALDI-TOF-MS m/z calculated for $C_{68}H_{11}O$ [M+H$^+$]: 843, found 843.

1-(2,5-dimethoxybenzyl)-1,2-dihydro[60]fullerene (2e): To a suspension of C_{60} (144 mg, 0.2 mmol) and Cs_2CO_3 (196 mg, 0.6 mmol) in dry DMSO (25 mL) 1-propanethiol (45 µL, 0.5 mmol) was added. The mixture was stirred for 2 hours under argon at room temperature. 2,5-dimethoxybenzyl chloride (298 mg, 1.6 mmol) was added to the resulting dark-red solution and stirring continued for another 1.5 hours. Following this, the color of the solution turned green, indicating the presence of a C_{60} monoanion. Acetic acid (0.5 mL) was added and five minutes later the solution was poured into 100 mL of methanol. The solids were collected by centrifugation and then dissolved into a minimum volume of CS_2. Chromatography, using a mixed solvent of cyclohexane and toluene (1:1 by volume), gave 1-(2,5-dimethoxybenzyl)-1,2-dihydro[60]fullerene **2e** (98 mg, 56%). ^{1}H NMR (500 MHz, $CDCl_3$): δ (ppm) 7.26 (d, *J* = 2.2 Hz, 1H), 6.97 (d, *J* = 8.9 Hz, 1H), 6.89 (dd, *J* = 8.9, 3.0 Hz, 1H), 6.72 (s, 1H), 4.77 (s, 2H), 3.89 (s, 3H), 3.82 (s, 3H). ^{13}C NMR (125 MHz, $CDCl_3$) δ 156.06, 154.25, 153.53, 152.37, 147.51, 147.36, 147.17, 146.48, 146.42, 146.39, 146.28, 146.23, 145.94, 145.52, 145.45, 145.41, 145.39, 144.77, 144.70, 143.33, 142.64, 142.63, 142.31, 142.11, 142.02, 141.72, 141.64, 140.25, 139.95, 136.55, 135.57, 129.12,

128.37, 125.64, 119.49, 113.31, 112.11, 65.90, 59.31, 55.69, 55.57, 46.75. MALDI-TOF-MS m/z calcd for $C_{69}H_{13}O_2$ [M+H$^+$]: 873, found 873.

1-(2,5-dimethoxybenzyl)-4-(2-methoxybenzyl)-1,4-dihydro[60]fullerene (1g): To a de-gased solution of 1-(2-methoxybenzyl)-1,2-dihydro[60]fullerene **2a** (0.05 mmol, 1 eq) in 10 mL dry benzonitrile, a 1 M THF solution of *t*-BuOK (75 μL, 0.075 mmol, 1.5 eq) was added via syringe with stirring. After 10 min, 2,5-dimethoxybenzyl chloride (77 mg, 0.5 mmol, 10 eq) (prepared from the reaction of 2,5-dimethoxybenzyl alcohol with $SOCl_2$) was added to the solution. The solution was then heated to 70 ˚C and stirred for 7 hours. An aqueous solution of NH_4Cl (0.1 mL) was added after the solution was cooled to room temperature. The solution was then poured into 100 mL methanol. The solids were collected by centrifuging and then redissolved in 1 mL CS_2. Chromatography gave 1-(2,5-dimethoxybenzyl)-4-(2-methoxybenzyl)-1,4-dihydro[60]fullerene (**1g**) (20 mg, 40%). ^{1}H NMR (500 MHz, $CDCl_3$): δ (ppm) 7.54 (dd, *J* = 7.4, 1.7 Hz, 1H), 7.35 (ddd, *J* = 8.1, 7.6, 1.6 Hz, 1H), 7.12 (d, *J* = 3.1 Hz, 1H), 7.09 (td, *J* = 7.4, 1.0 Hz, 1H), 7.02 (d, *J* = 7.7 Hz, 1H), 6.93 (d, *J* = 8.9 Hz, 1H), 6.85 (dd, *J* = 8.9, 3.1 Hz, 1H), 4.07 (AB-q, *J* = 12.7 Hz, 1H), 4.00 (AB-q, *J* = 12.7 Hz, 1H), 3.89 (AB-q, *J* = 12.7 Hz, 1H), 3.83 (s, 3H), 3.82 (s, 3H), 3.77 (s, 3H), 3.70 (AB-q, *J* = 12.7 Hz, 1H). ^{13}C NMR (125 MHz, $CDCl_3$): δ (ppm) 158.75, 158.63, 158.22, 153.37, 152.45, 152.07, 151.99, 148.75, 148.55, 147.10, 146.97, 146.82, 146.37, 146.22, 145.40, 144.90, 144.82, 144.78, 144.76, 144.41, 144.25, 144.19, 144.17, 143.76, 143.73, 143.69, 143.68, 143.11, 143.07, 142.86, 142.63, 142.53, 142.49, 142.07, 141.85, 141.83, 138.84, 138.83, 137.32, 137.27, 132.53, 129.00, 126.13, 125.06, 120.61, 119.30, 112.57, 112.01, 111.34, 60.14, 60.00, 55.87, 55.70, 55.20, 42.40, 42.35. MALDI-TOF-MS m/z calculated for $C_{77}H_{21}O_3$ [M+H$^+$]: 993, found 993.

1-(2,6-dimethoxybenzyl)-4-(2-methoxybenzyl)-1,4-dihydro[60]fullerene (1h): To a de-gased solution of 1-(2-methoxybenzyl)-2-H-dihydro[60]fullerene **2a** (0.05 mmol, 1 eq) in 10 mL dry benzonitrile, a 1.0 M THF solution of *t*-BuOK (75 μL, 0.075 mmol, 1.5 eq) was added through syringe with stirring. After 10 minutes, 2,6-dimethoxybenzyl chloride (77 mg, 0.5 mmol, 10eq) (prepared from the reaction of 2,6-dimethoxybenzyl alcohol with $SOCl_2$) was added. The solution was heated to 70 ℃ and stirred for 6 hours. An aqueous solution of NH_4Cl (0.1 mL) was added after the solution was cooled to room temperature. The solution was then poured into 100 mL methanol. The solids were collected by centrifuging and then redissolved in 1 mL CS_2. Chromatography gave 1-(2,6-dimethoxybenzyl)-4-(2-methoxybenzyl)-1,4-dihydro[60]fullerene (**1h**) (18 mg, 36%). ^{1}H NMR (500 MHz, $CDCl_3$): *δ* (ppm) 7.46 (d, *J* = 6.8 Hz, 1H), 7.35 – 7.28 (m, 2H), 7.01 (t, *J* = 7.3 Hz, 1H), 6.94 (d, *J* = 8.2 Hz, 1H), 6.75 (d, *J* = 8.3 Hz, 2H), 4.48 (AB-q, *J* = 12.7 Hz, 2H), 4.43 (AB-q, *J* = 12.7 Hz, 1H), 3.96 (AB-q, *J* = 12.5 Hz, 1H), 3.90 (s, 4H), 3.83 (AB-q, *J* = 12.5 Hz, 1H), 3.73 (s, 3H). ^{13}C NMR (125 MHz, $CDCl_3$) δ 159.53, 159.23, 158.33, 157.94, 152.54, 151.88, 148.99, 148.63, 148.99, 148.48, 147.31, 147.25, 147.07, 147.04, 147.02, 146.97, 146.93, 146.75, 145.75, 145.33, 145.30, 145.09, 145.00, 144.84, 144.79, 144.74, 144.70, 144.65, 144.45, 144.43, 144.23, 144.21, 144.17, 144.16, 144.10, 143.87, 143.65, 143.63, 143.34, 143.16, 143.11, 143.02, 142.92, 142.84, 142.66, 142.62, 142.58, 142.50, 142.46, 142.06, 141.83, 141.70, 140.27, 139.01, 138.70, 137.46, 137.03, 132.31, 129.05, 128.82, 128.70, 124.93, 120.30, 113.71, 111.18, 104.39, 59.90, 55.68, 55.07, 42.41, 35.39. MALDI-TOF-MS m/z calculated for $C_{77}H_{21}O_3$ [M+H$^+$]: 993, found 993.

1-(2,5-dimethoxybenzyl)-4-(2,6-dimethoxybenzyl)-1,4-dihydro[60]fullerene (1i): To a de-gased solution of 1-(2,5-dimethoxybenzyl)-2-H-dihydro[60]fullerene **2e** (0.05 mmol, 1 eq) in 10 mL dry benzonitrile, a 1 M THF solution of *t*-BuOK (75 μL, 0.075 mmol, 1.5 eq) was added via syringe with stirring. After 10 min, 2,6-dimethoxybenzyl chloride (77 mg, 0.5 mmol, 10 eq) (prepared from the reaction of 2,6-dimethoxybenzyl alcohol with $SOCl_2$) was added to the solution. The solution was then heated to 70 ℃ and stirred for 6 hours. An aqueous solution of NH_4Cl (0.1 mL) was added after the solution was cooled to room temperature. The solution was then poured into 100 mL methanol. The solids were collected by centrifuging and then redissolved in 1 mL CS_2. Flash chromatography gave 1-(2,5-dimethoxybenzyl)-4-(2,6-dimethoxybenzyl)-1,4-dihydro[60]fullerene (**1i**) (20 mg, 40%). ^{1}H NMR (500 MHz, $CDCl_3$): δ (ppm) 7.32 (t, J = 8.3 Hz, 1H), 7.05 (d, J = 2.7 Hz, 1H), 6.89 – 6.79 (m, 2H), 6.76 (d, J = 8.4 Hz, 2H), 4.50 (AB-q, J = 12.6 Hz, 1H), 4.44 (AB-q, J = 12.6 Hz, 1H), 3.91 (s, 6H), 3.87 (AB-q, J = 12.6 Hz, 1H), 3.80 (s, 3H), 3.74 (AB-q, J = 12.6 Hz, 1H), 3.68 (s, 3H). ^{13}C NMR (125 MHz, $CDCl_3$) δ 159.54, 159.27, 158.24, 153.23, 152.57, 152.18, 151.81, 149.00, 148.59, 148.50, 147.32, 147.26, 147.08, 147.04, 147.03, 146.97, 146.93, 146.76, 145.66, 145.34, 145.31, 145.09, 145.02, 144.84, 144.80, 144.75, 144.72, 144.66, 144.45, 144.43, 144.24, 144.22, 144.17, 144.10, 143.88, 143.67, 143.62, 143.52, 143.34, 143.16, 143.10, 143.03, 142.93, 142.85, 142.67, 142.62, 142.59, 142.50, 142.46, 142.07, 141.85, 141.68, 140.28, 139.00, 138.71, 137.48, 137.04, 129.05, 128.84, 128.24, 126.03, 125.31, 121.26, 119.34, 115.50, 113.76, 112.30, 111.78, 104.44, 59.92, 59.74, 55.95, 55.72, 55.57, 42.54, 35.41. MALDI-TOF-MS m/z calculated for $C_{78}H_{23}O_4$ [M+H$^+$]: 1023, found 1023.

1-(3-methoxybenzyl)-4-(4-*t*-butylbenzyl)-1,4-dihydro[60]fullerene (1j): To a de-gased solution of 1-(3-methoxybenzyl)-2-H-dihydro[60]fullerene (**2b**, 0.05 mmol, 1 eq) in 10 mL of dry benzonitrile, a 1 M THF solution of *t*-BuOK (75 μL, 0.075 mmol, 1.5 eq) was added through a syringe. After 10 minutes, 4-*t*-butylbenzyl bromide (mg, 0.5 mmol, 10 eq) was added. The solution was stirred at room temperature for 4 hours. An aqueous solution of NH_4Cl (0.1 mL) was added and the solution was poured into 100 mL methanol. The solids were collected by centrifuge and then redissolved in 1 mL CS_2. Chromatography gave 1-(3-methoxybenzyl)-4-(p-*t*-butylbenzyl)-1,4-dihydro[60]fullerene (**1j**, 20 mg, 40%). ^{1}H NMR (500 MHz, $CDCl_3$): *δ* (ppm) 7.61 (AB-q, *J* = 7.9 Hz, 2H), 7.56 (AB-q, *J* = 7.9 Hz, 2H), 7.31 (t, *J* = 7.8 Hz, 1H), 7.04 (d, *J* = 7.4 Hz, 1H), 7.00 (s, 1H), 6.85 (d, *J* = 7.9 Hz, 1H), 4.06 (AB-q, *J* = 13.1 Hz, 1H), 3.96 (AB-q, *J* = 13.1 Hz, 1H), 3.84 (s, 3H), 3.30 (s, 2H), 1.28 (s, 9H). ^{13}C NMR (125 MHz, $CDCl_3$) δ 159.26, 158.64, 157.93, 152.34, 151.56, 150.71, 148.78, 148.67, 148.65, 148.63, 147.22, 147.20, 147.00, 146.99, 146.97, 146.93, 146.87, 145.66, 145.50, 145.05, 144.98, 144.84, 144.81, 144.75, 144.73, 144.71, 144.40, 144.33, 144.31, 144.26, 144.18, 144.13, 143.98, 143.86, 143.71, 143.20, 143.17, 143.13, 143.07, 143.04, 142.93, 142.68, 142.66, 142.57, 142.46, 142.15, 142.06, 141.91, 140.49, 138.83, 138.81, 137.87, 137.61, 133.56, 130.91, 129.15, 125.72, 123.61, 117.36, 112.22, 60.94, 60.34, 55.33, 48.27, 48.07, 34.62, 31.33. FAB-HRMS m/z calculated for $C_{79}H_{25}O$ $[M+H]^+$: 989.1900, found 989.1909.

1-(3-methoxybenzyl)-4-(2-methylbenzyl)-1,4-dihydro[60]fullerene (1k): To a de-gased solution of 1-(3-methoxybenzyl)-2-H-dihydro[60]fullerene (**2b**) (0.05 mmol, 1 eq) in 10 mL dry benzonitrile, a 1 M THF solution of *t*-BuOK (75 μL, 0.075 mmol, 1.5 eq) was added through a syringe. After 10 minutes, 2-methylbenzyl bromide (92 mg,

0.5 mmol, 10 eq) was added and the solution was stirred at room temperature for 4 hours. An aqueous solution of NH_4Cl (0.1 mL) was then added and the solution was poured into 100 mL methanol. The solids were collected by centrifuge and then redissolved in 1 mL CS_2. Chromatography gave 1-(3-methoxybenzyl)-4-(2-methylbenzyl)-1,4-dihydro[60]fullerene (**1k**, 19 mg, 40%). ^{1}H NMR (500 MHz, $CDCl_3$): *δ* (ppm) 7.62 (d, *J* = 7.3 Hz, 1H), 7.41 – 7.34 (m, 2H), 7.31 – 7.27 (m, 2H), 6.99 (d, *J* = 7.5 Hz, 1H), 6.94 (s, 1H), 6.80 (dd, *J* = 8.3, 1.7 Hz, 1H), 4.20 (AB-q, *J* = 13.3 Hz, 1H), 4.07 (AB-q, *J* = 13.3 Hz, 1H), 3.82 (s, 3H), 3.41 (s, 2H), 2.72 (s, 3H). ^{13}C NMR (125 MHz, $CDCl_3$) δ 159.36, 158.30, 157.58, 152.12, 151.54, 148.77, 148.71, 148.68, 148.43, 147.26, 147.24, 147.02, 147.00, 146.97, 146.82, 146.71, 145.65, 145.57, 145.14, 145.08, 144.84, 144.75, 144.64, 144.43, 144.35, 144.30, 144.19, 144.15, 144.11, 143.93, 143.84, 143.73, 143.27, 143.25, 143.19, 143.16, 143.10, 143.02, 142.75, 142.71, 142.65, 142.61, 142.47, 142.22, 142.08, 141.99, 140.67, 138.89, 138.86, 138.03, 137.55, 137.52, 137.46, 134.84, 132.43, 131.43, 129.31, 128.08, 126.41, 123.52, 117.32, 112.32, 60.68, 60.29, 55.07, 48.64, 45.37, 20.98. FAB-HRMS m/z calculated for $C_{76}H_{19}O$ $[M+H]^+$: 947.1430, found 947.1433

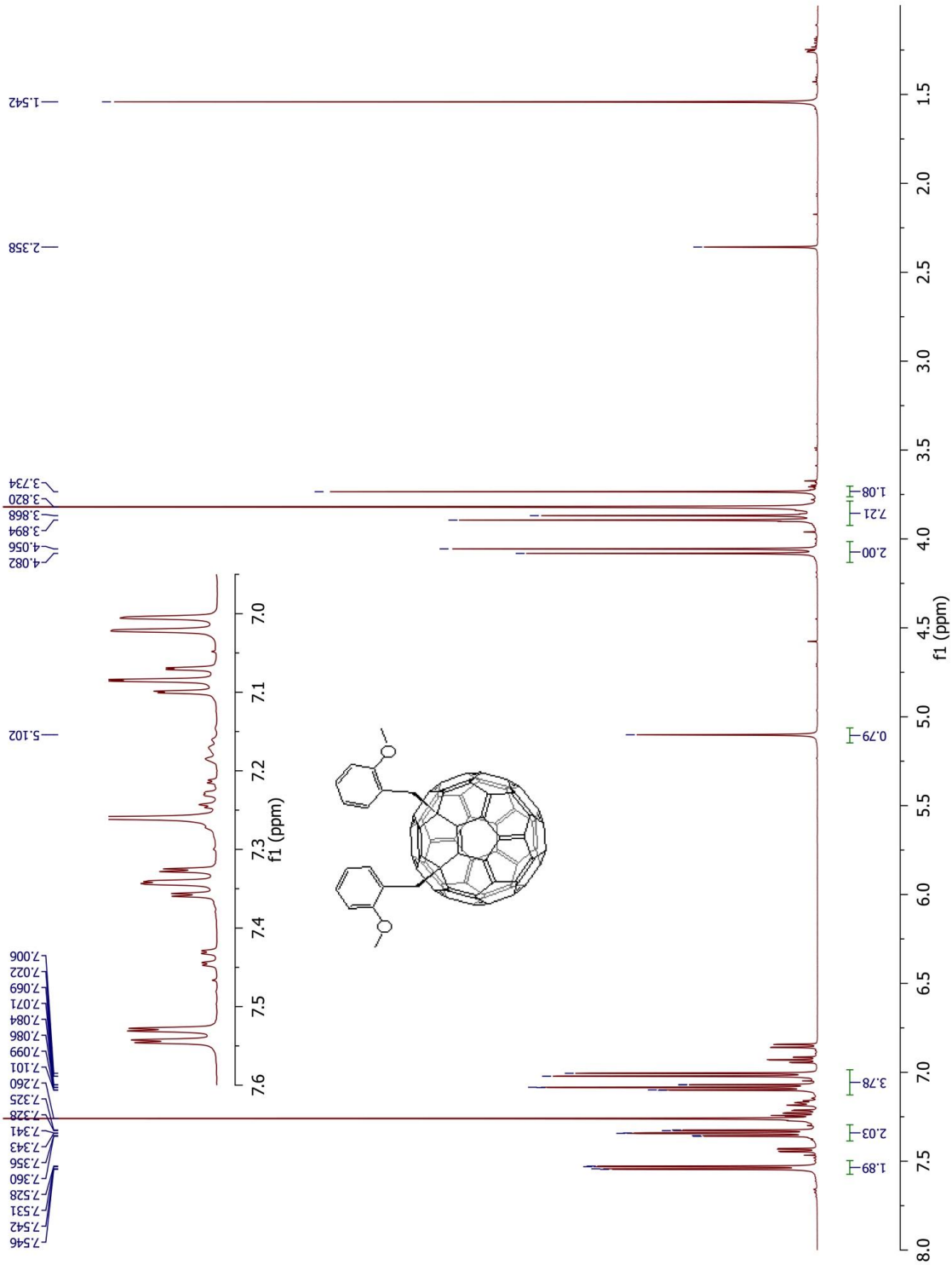

Figure S1. ^{1}H NMR spectrum of compound **1a** (500 MHz, $CDCl_3/CS_2$ (1:1)).

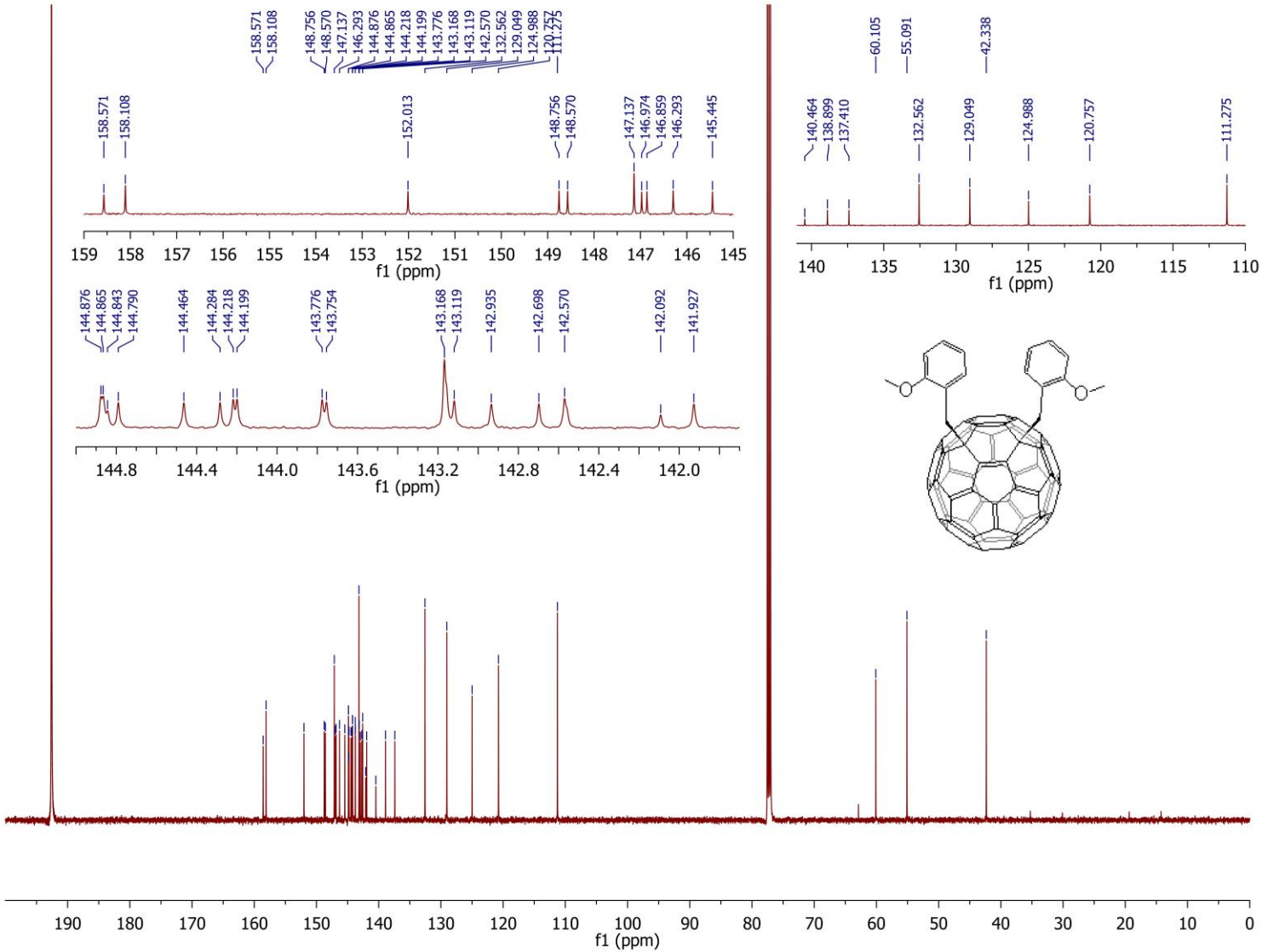

Figure S2. ^{13}C NMR spectrum of compound **1a** (125 MHz, $CDCl_3/CS_2$ (1:1)).

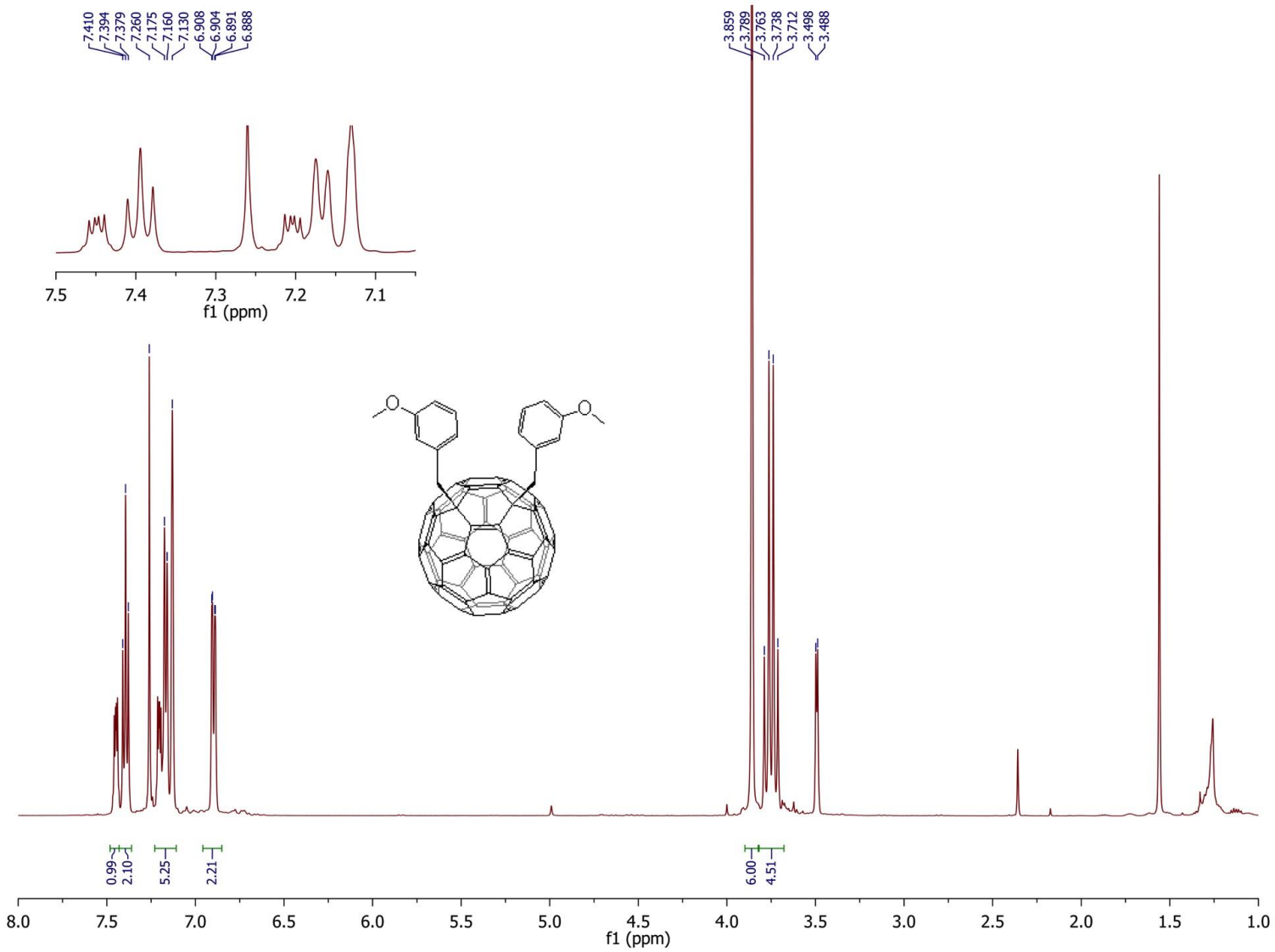

Figure S3. ^{1}H NMR spectrum of compound **1b** (500 MHz, $CDCl_3/CS_2$ (1:1)).

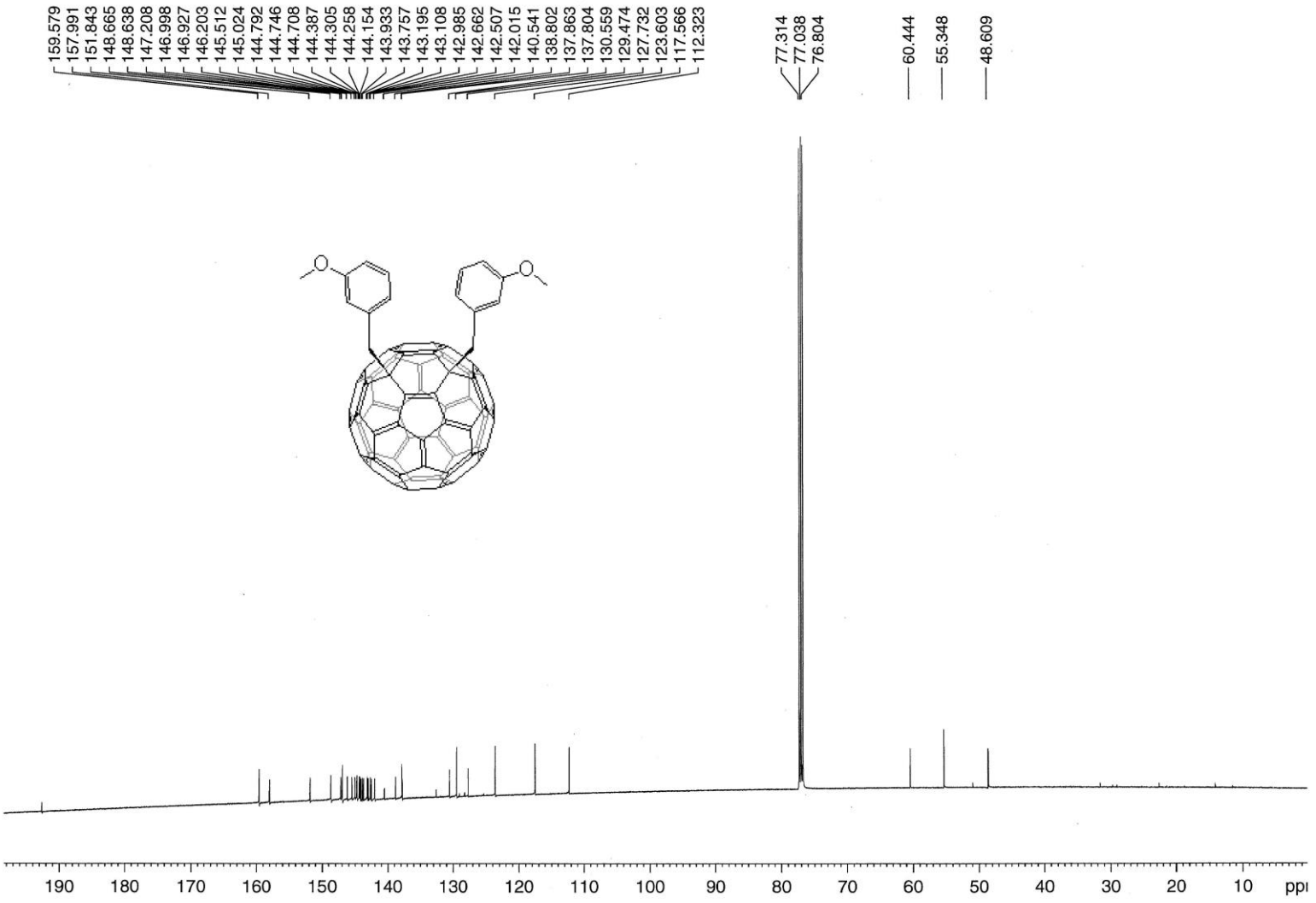

Figure S4. ^{13}C NMR spectrum of compound **1b** (125 MHz, $CDCl_3/CS_2$ (1:1)).

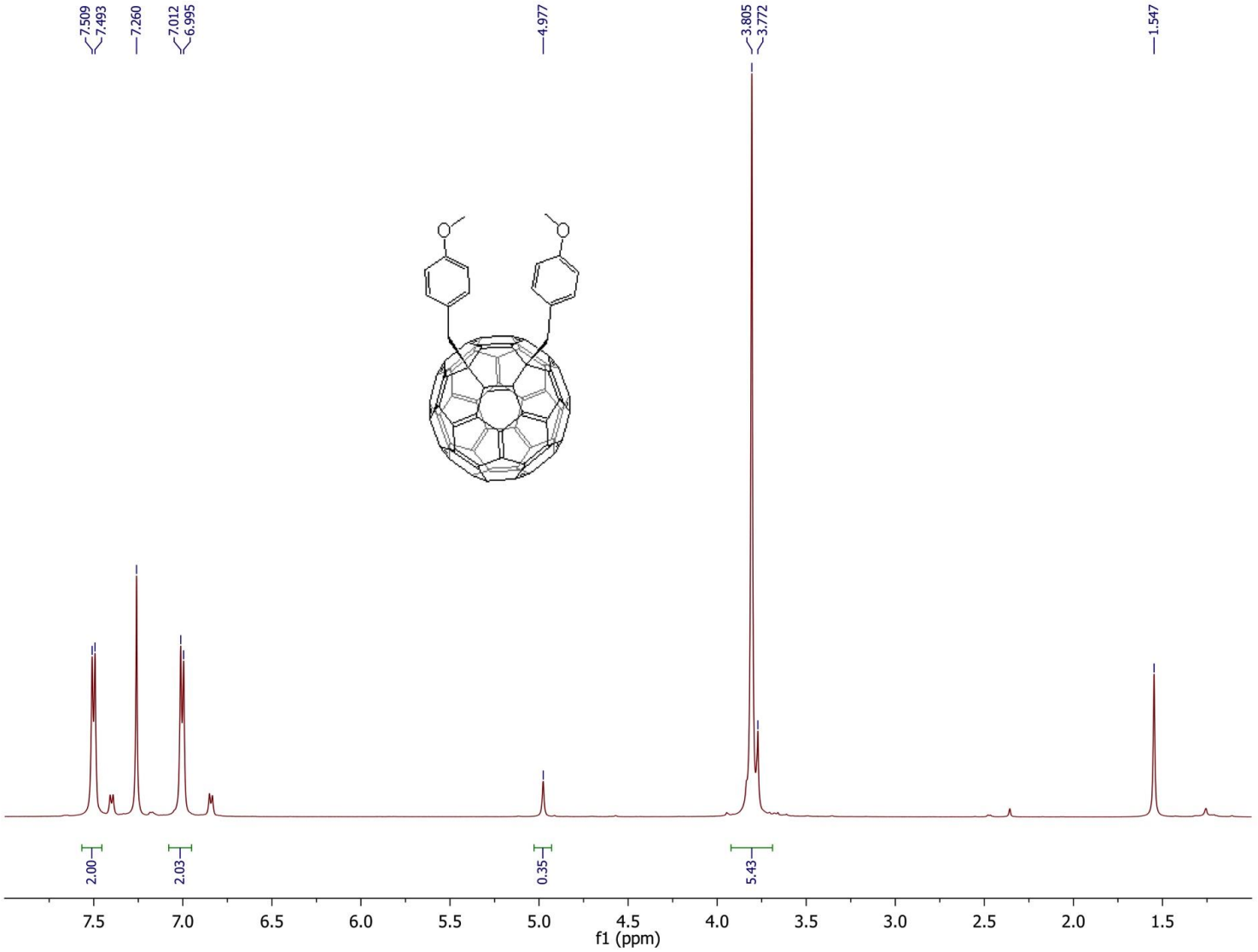

Figure S5. ^{1}H NMR spectrum of compound **1c** (500 MHz, $CDCl_3$).

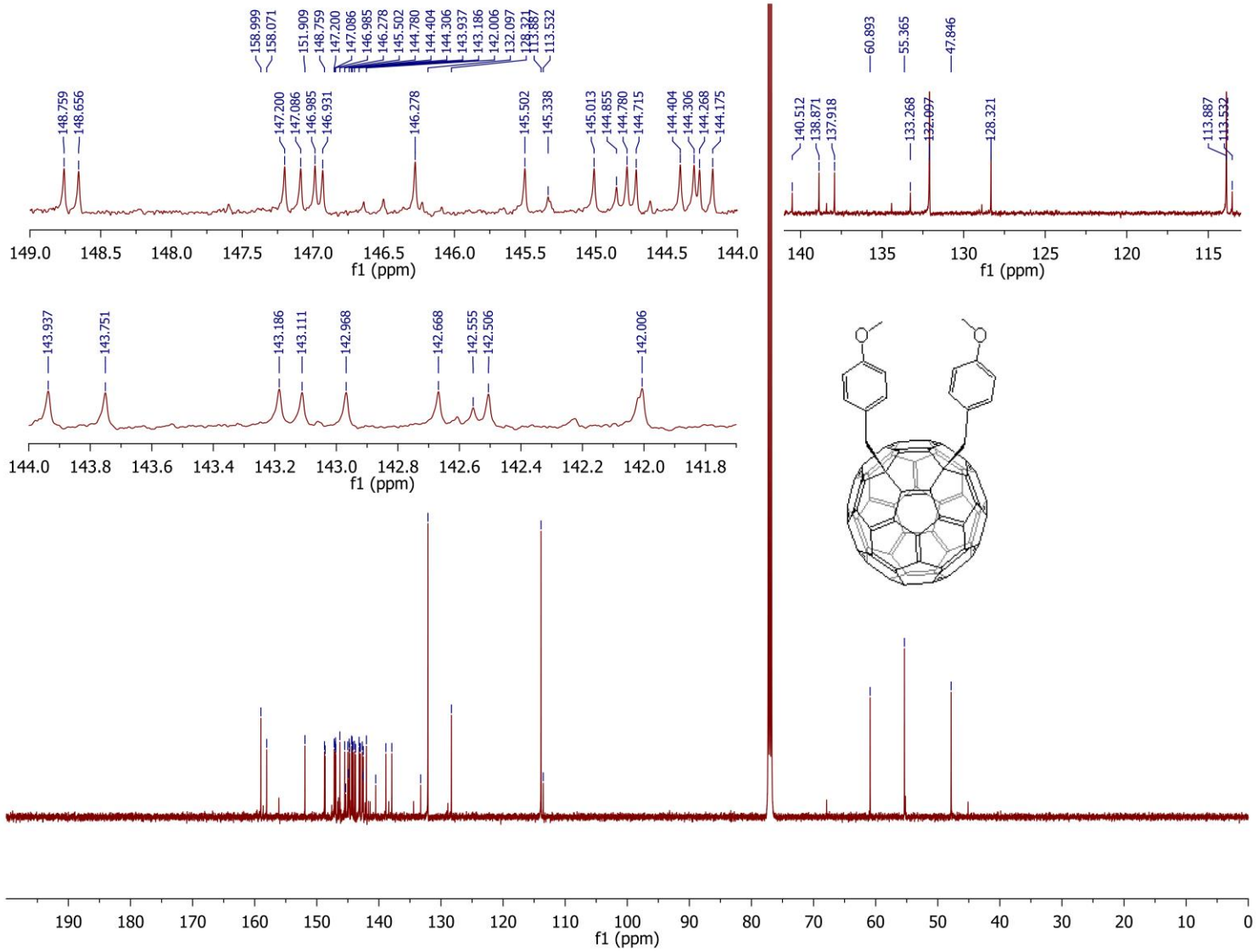

Figure S6. ^{13}C NMR spectrum of compound **1c** (125 MHz, $CDCl_3$).

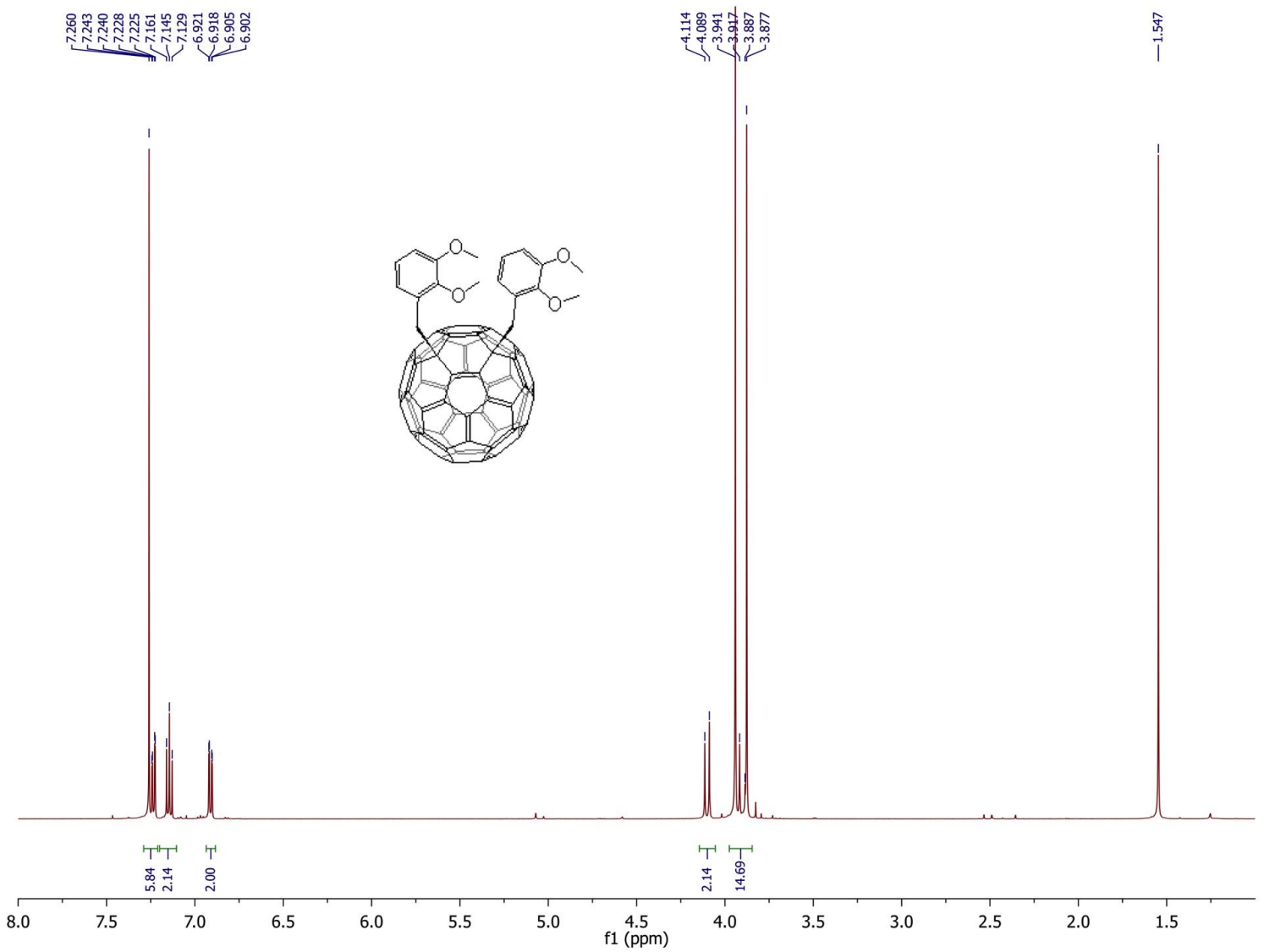

Figure S7. ^{1}H NMR spectrum of compound **1d** (500 MHz, $CDCl_3/CS_2$ (1:1)).

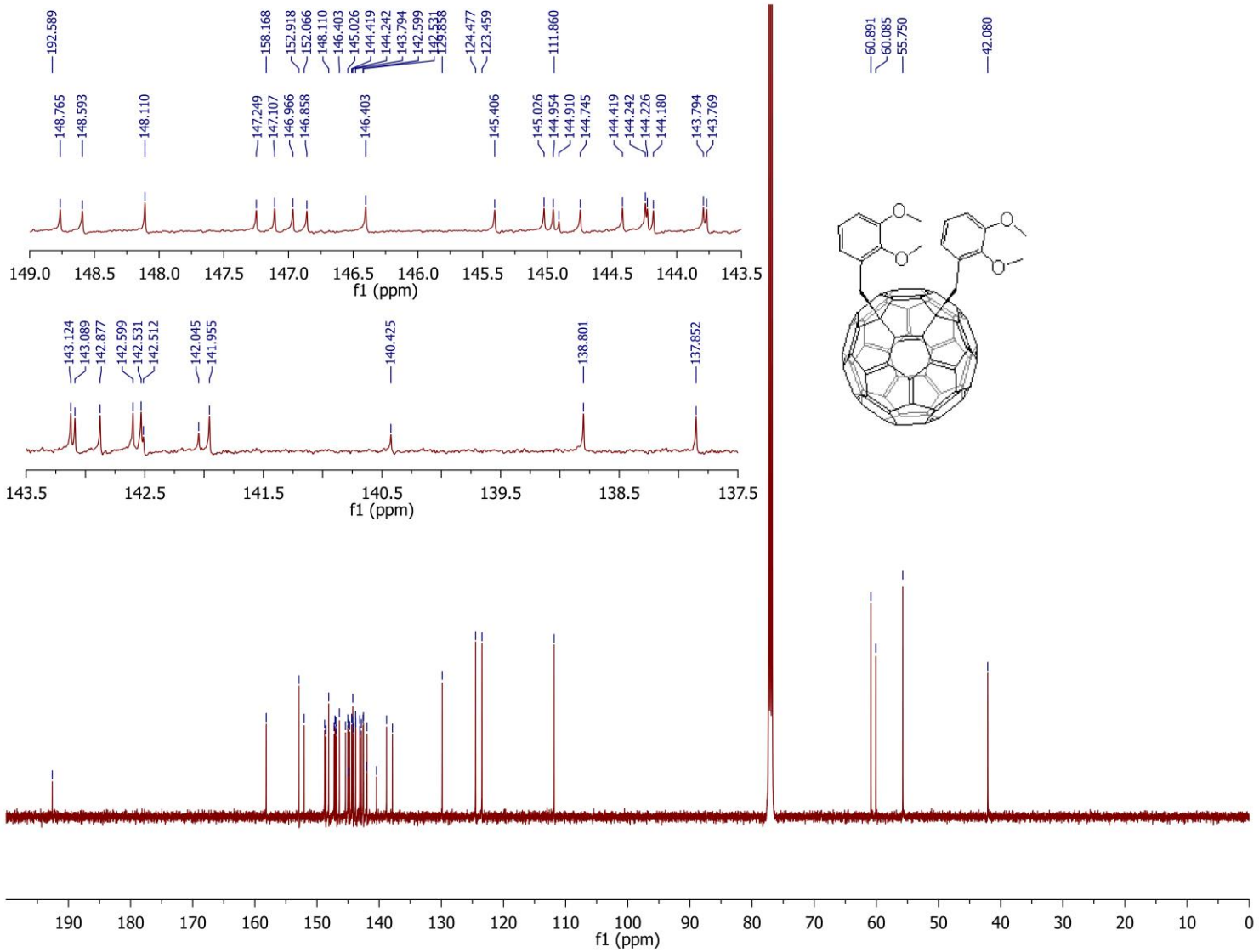

Figure S8. ^{13}C NMR spectrum of compound **1d** (125 MHz, $CDCl_3/CS_2$ (1:1)).

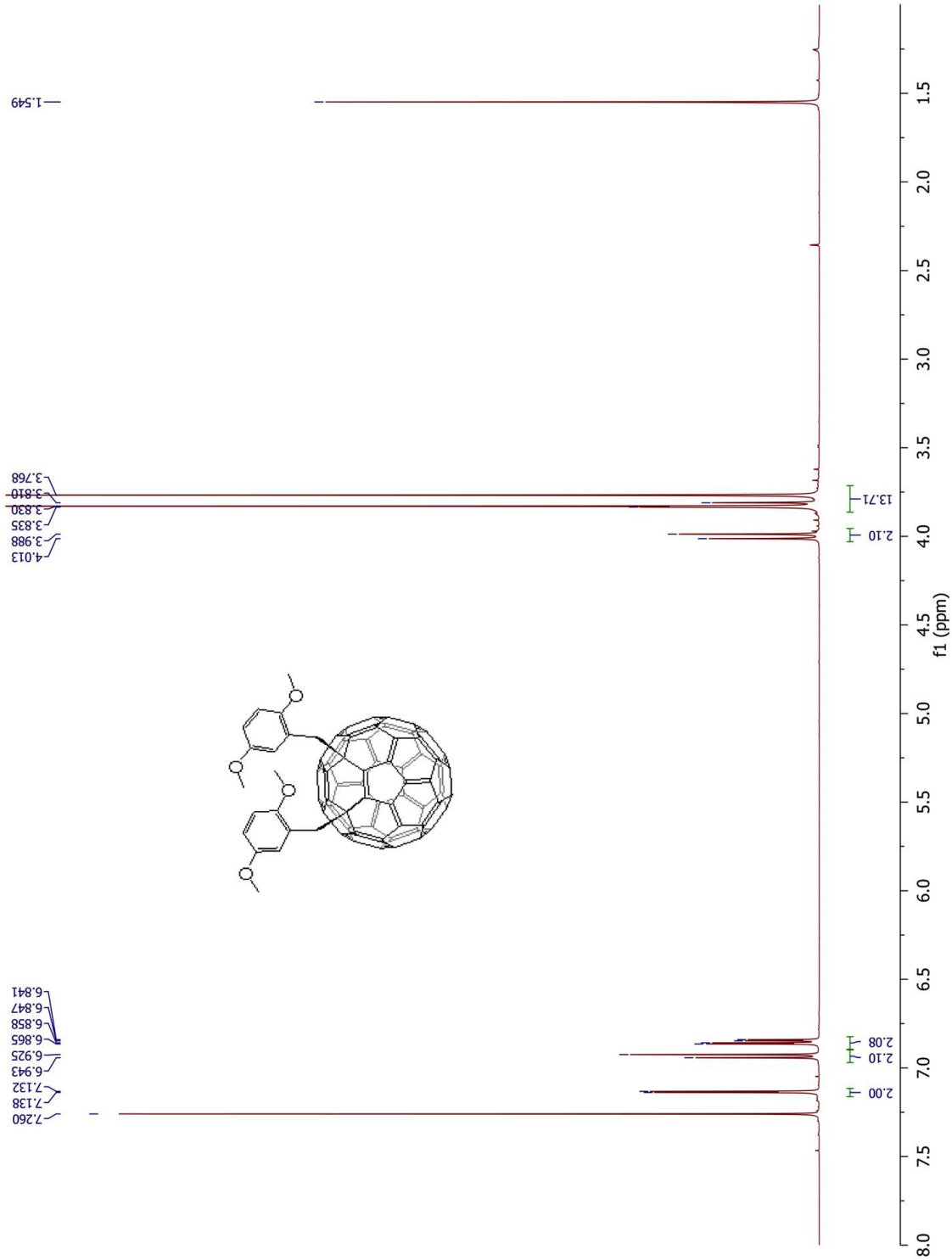

Figure S9. ^{1}H NMR spectrum of compound **1e** (500 MHz, $CDCl_3$).

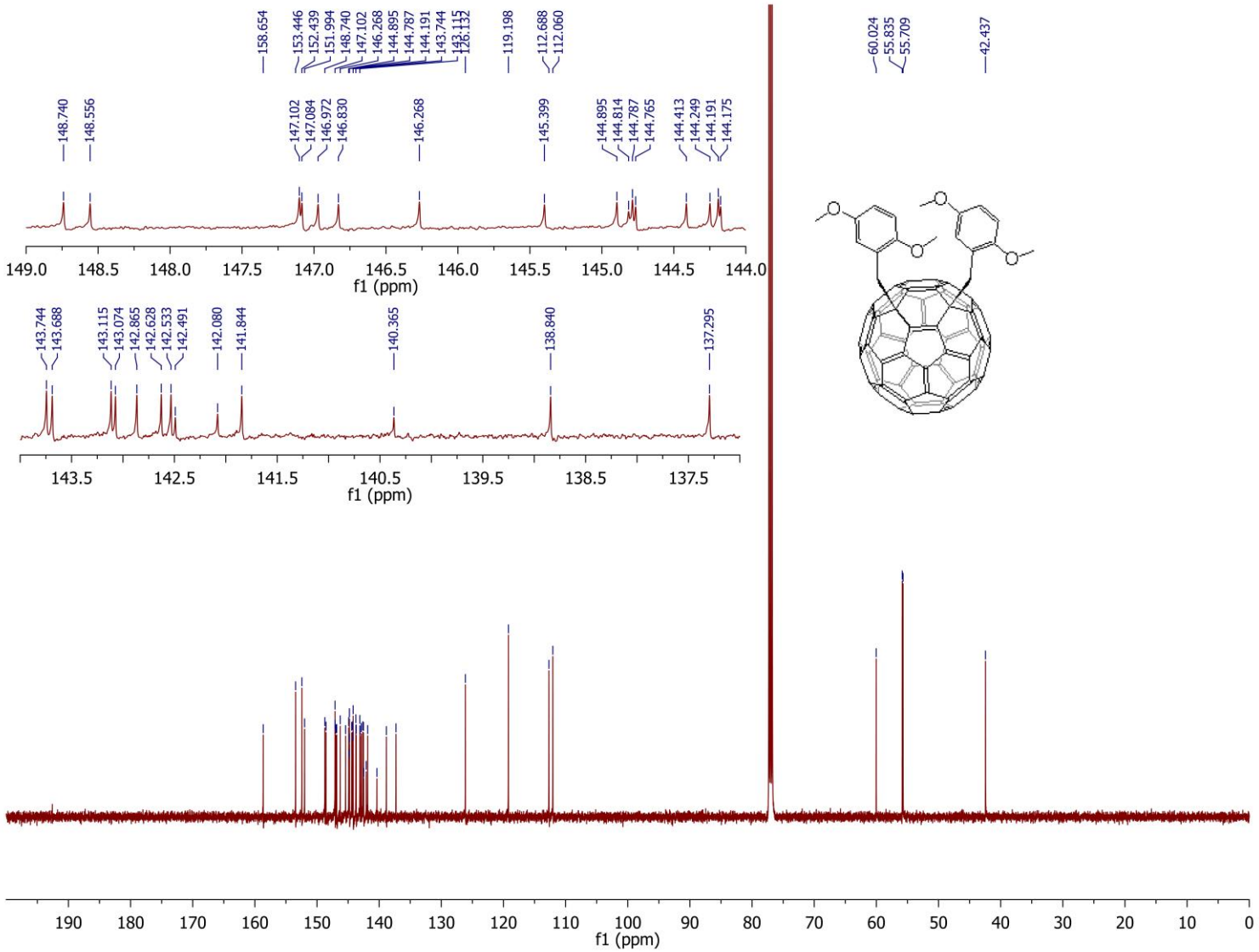

Figure S10. ^{13}C NMR spectrum of compound **1e** (125 MHz, $CDCl_3$).

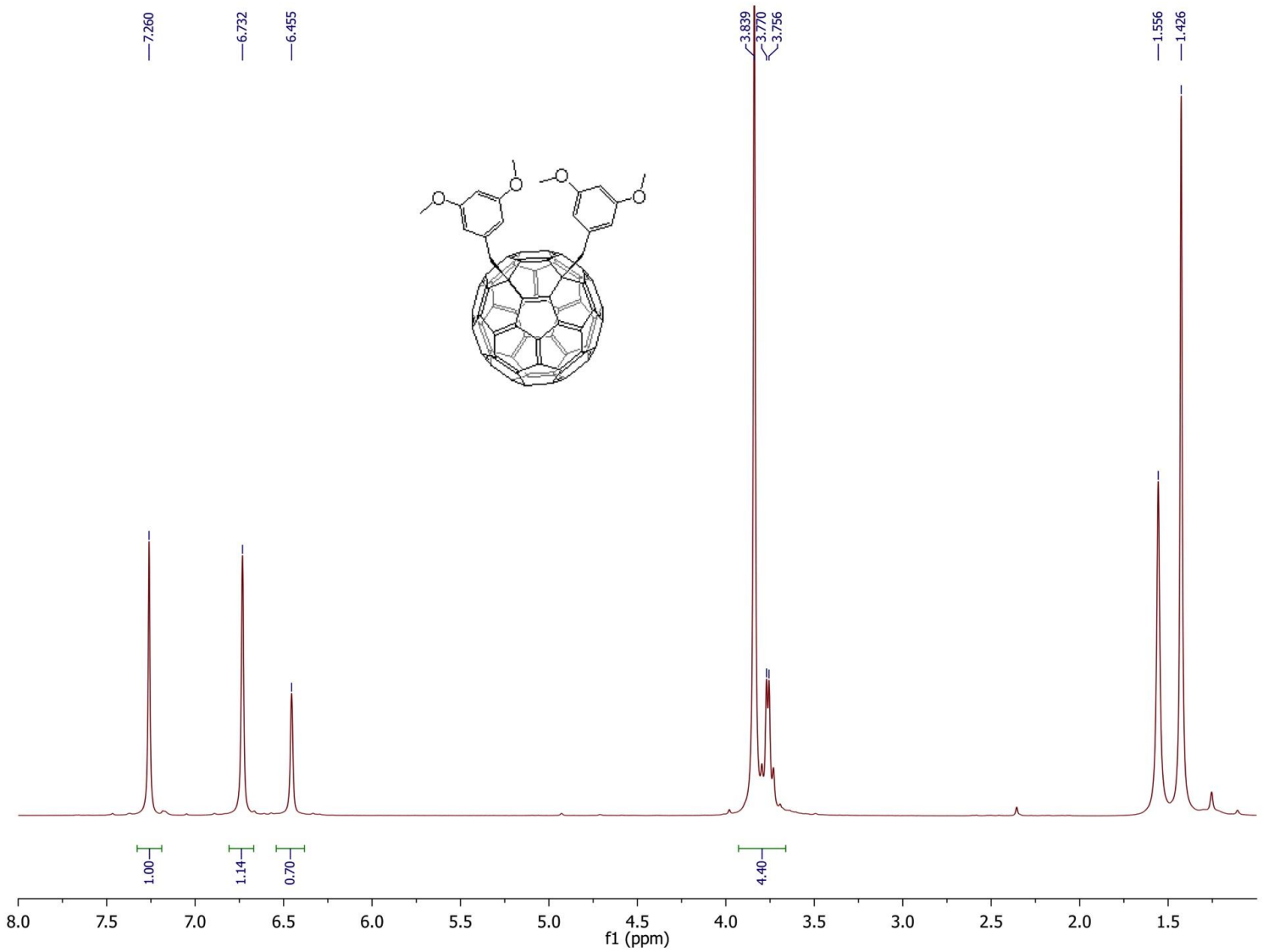

Figure S11. ^{1}H NMR spectrum of compound **1f** (500 MHz, $CDCl_3$).

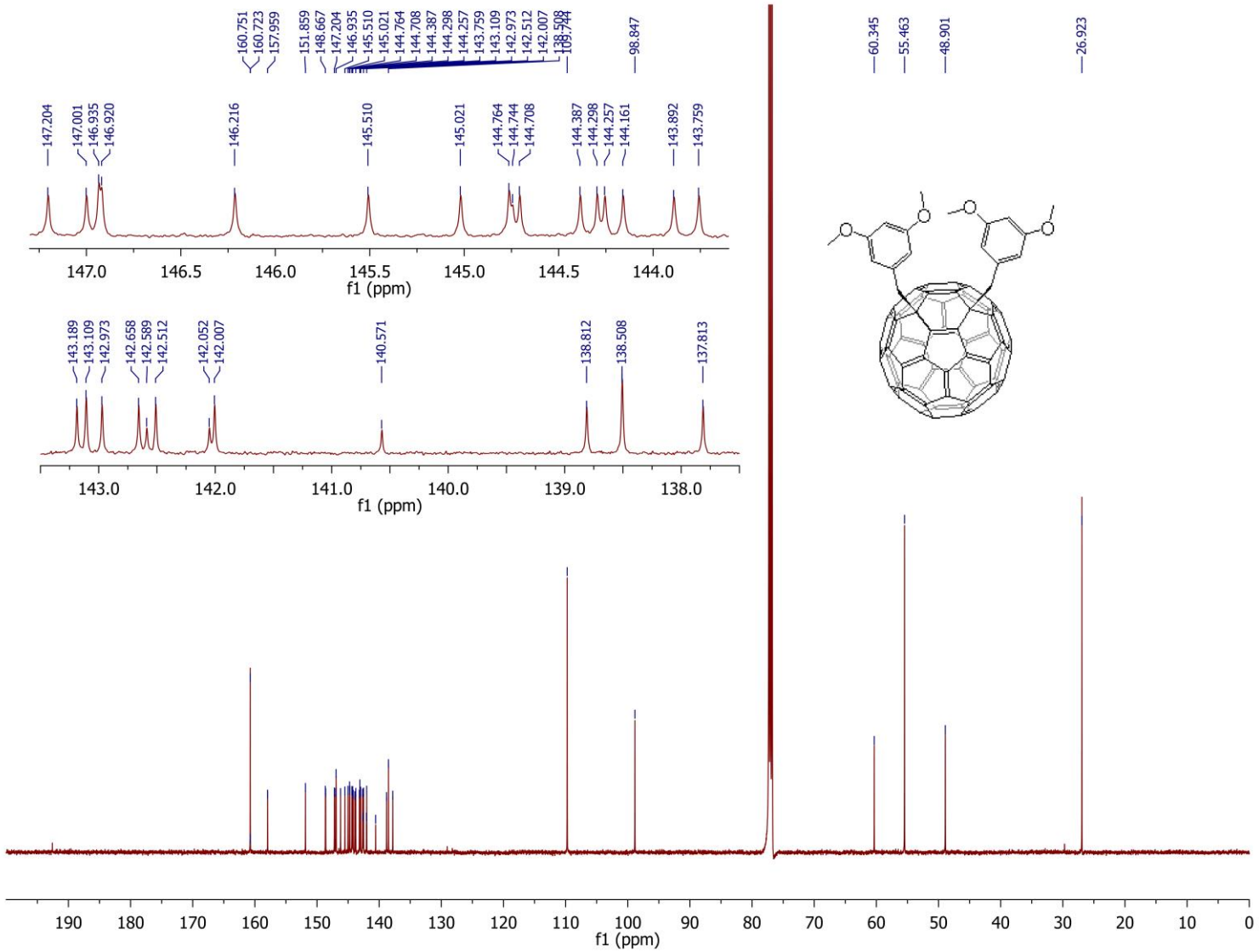

Figure S12. ^{13}C NMR spectrum of compound **1f** (125 MHz, $CDCl_3$).

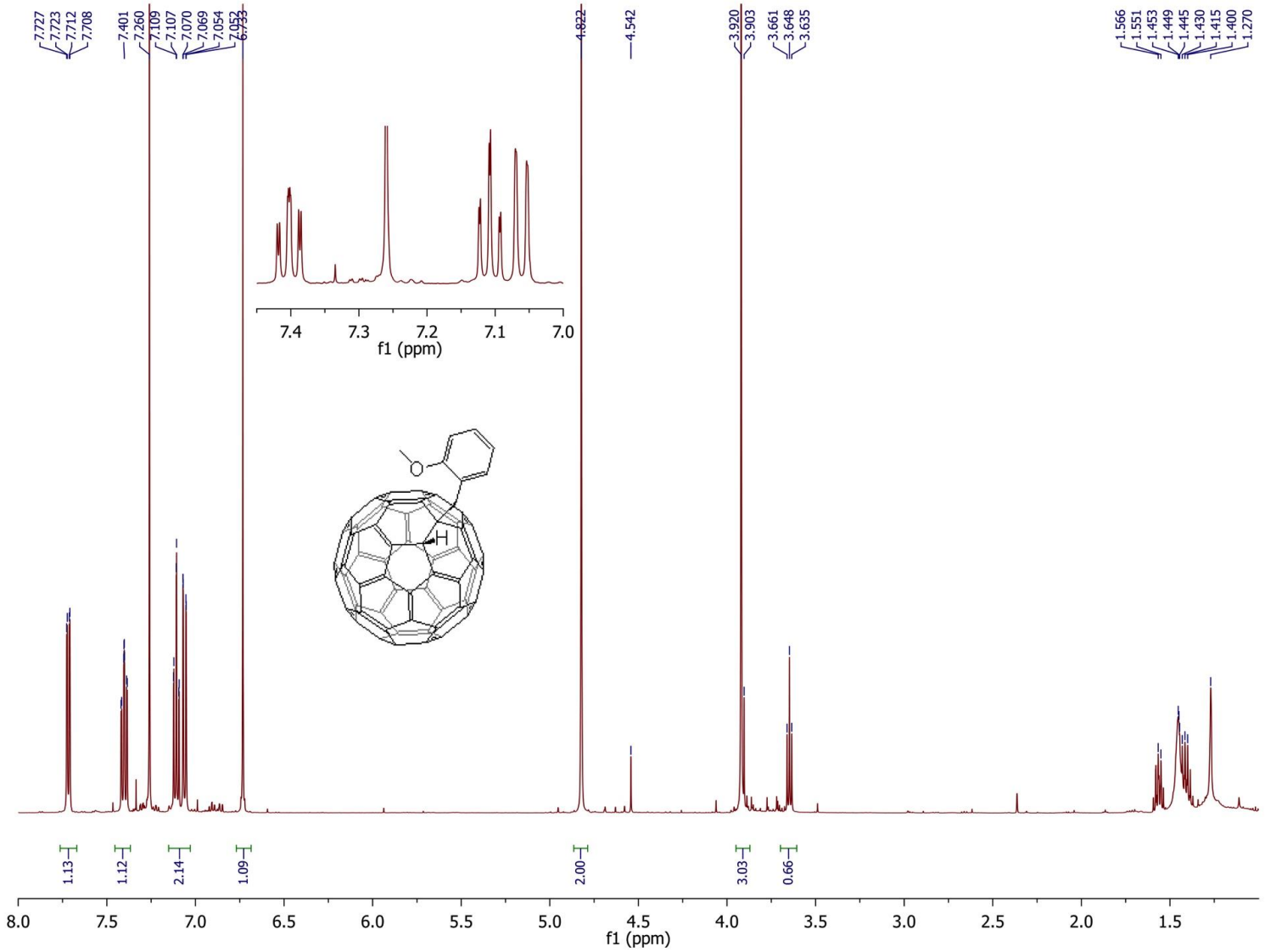

Figure S13. ^{1}H NMR spectrum of compound **2a** (500 MHz, $CDCl_3/CS_2$ (1:1)).

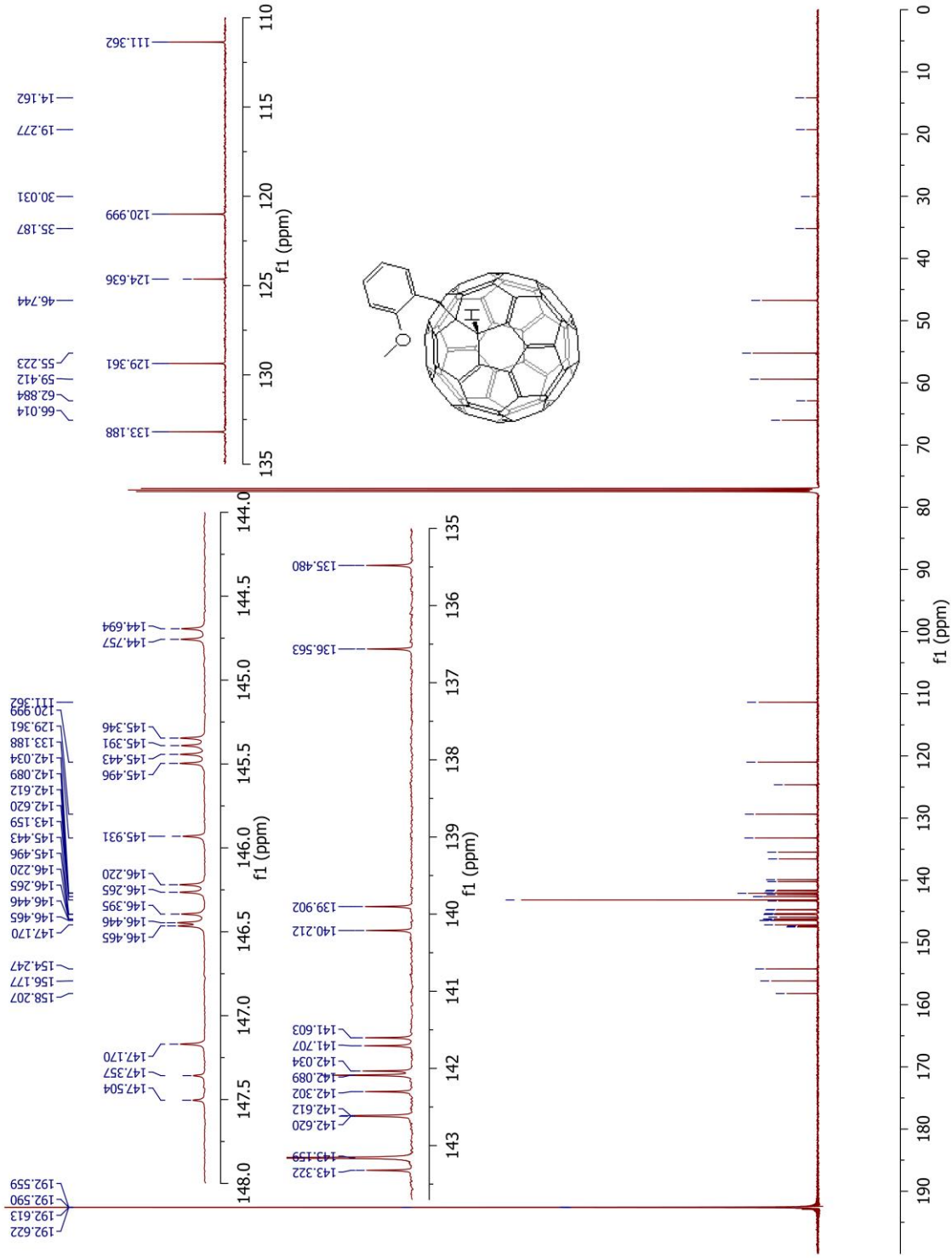

Figure S14. ^{13}C NMR spectrum of compound **2a** (125 MHz, $CDCl_3/CS_2$ (1:1)).

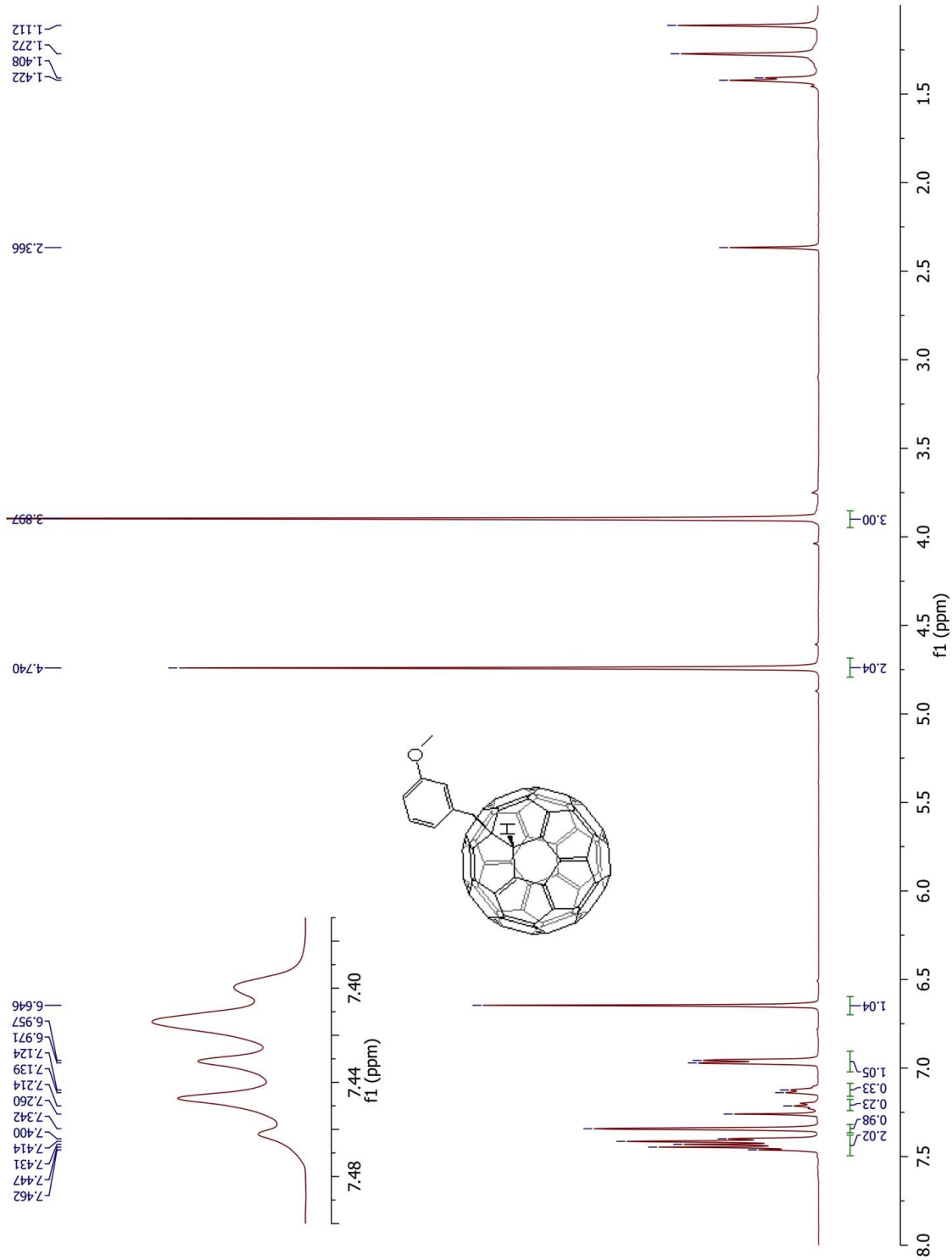

Figure S15. ^{1}H NMR spectrum of compound **2b** (500 MHz, $CDCl_3/CS_2$ (1:1)).

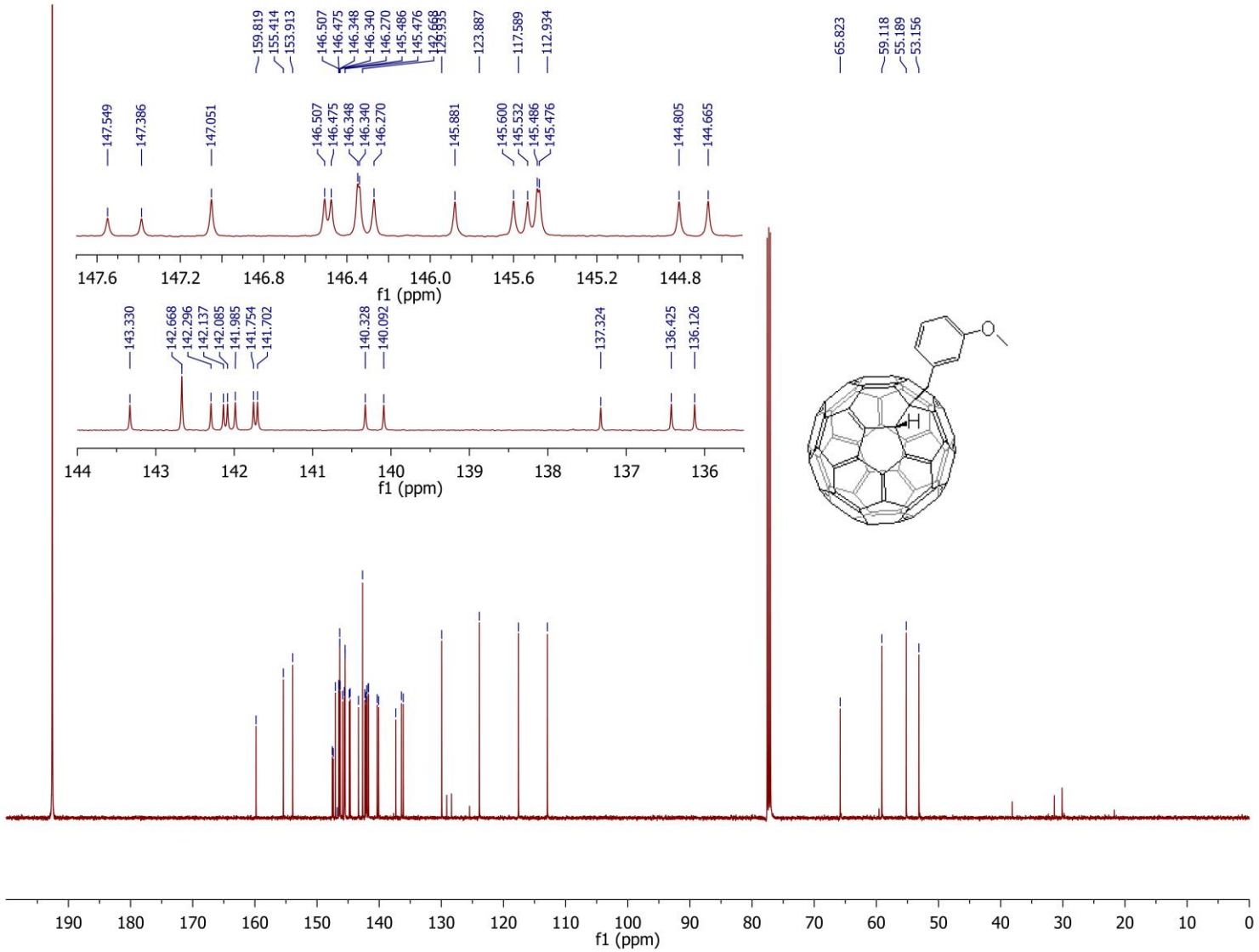

Figure S16. ^{13}C NMR spectrum of compound **2b** (125 MHz, $CDCl_3/CS_2$ (1:1)).

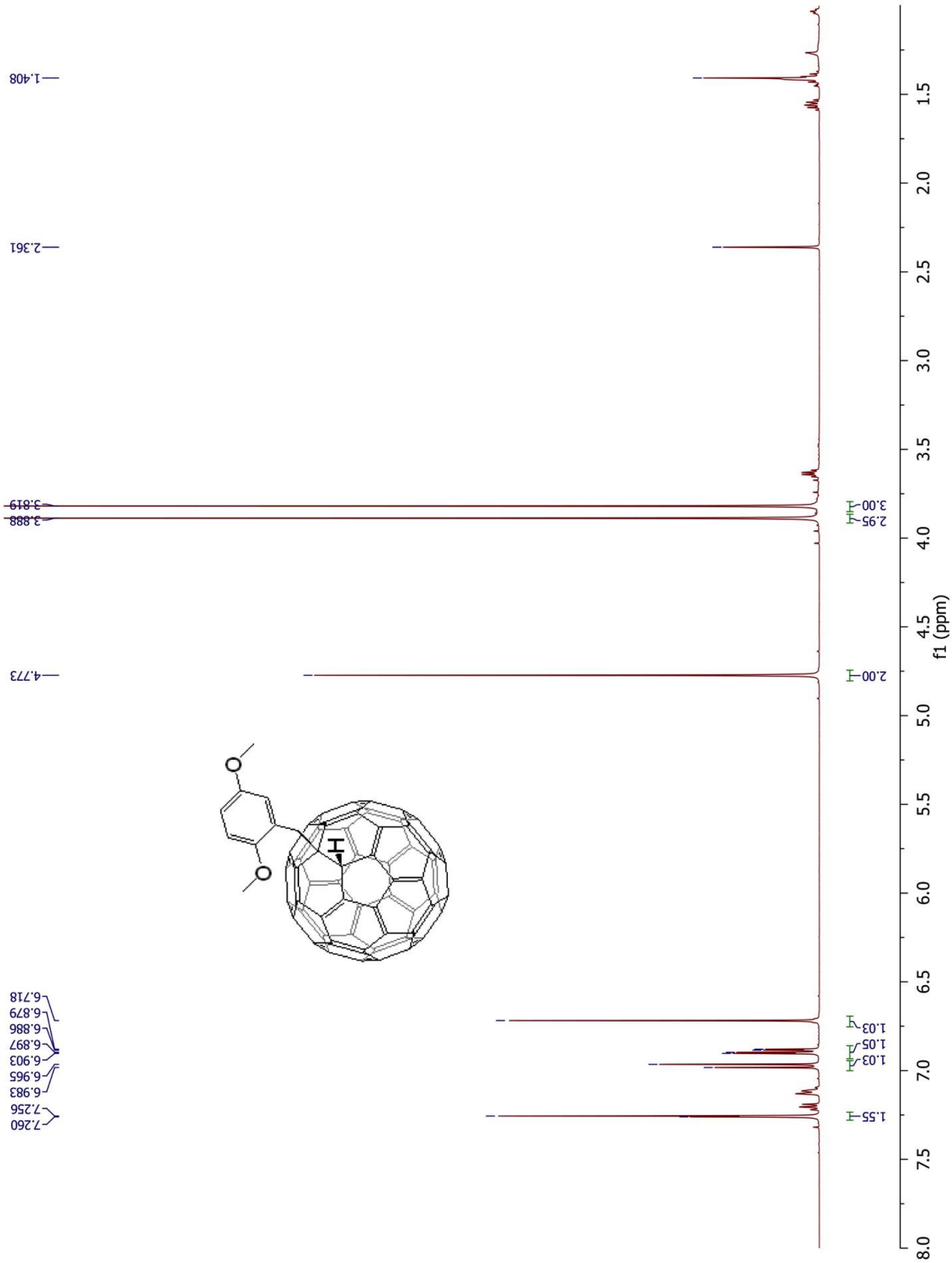

Figure S17. ^{1}H NMR spectrum of compound **2e** (500 MHz, $CDCl_3/CS_2$ (1:1)).

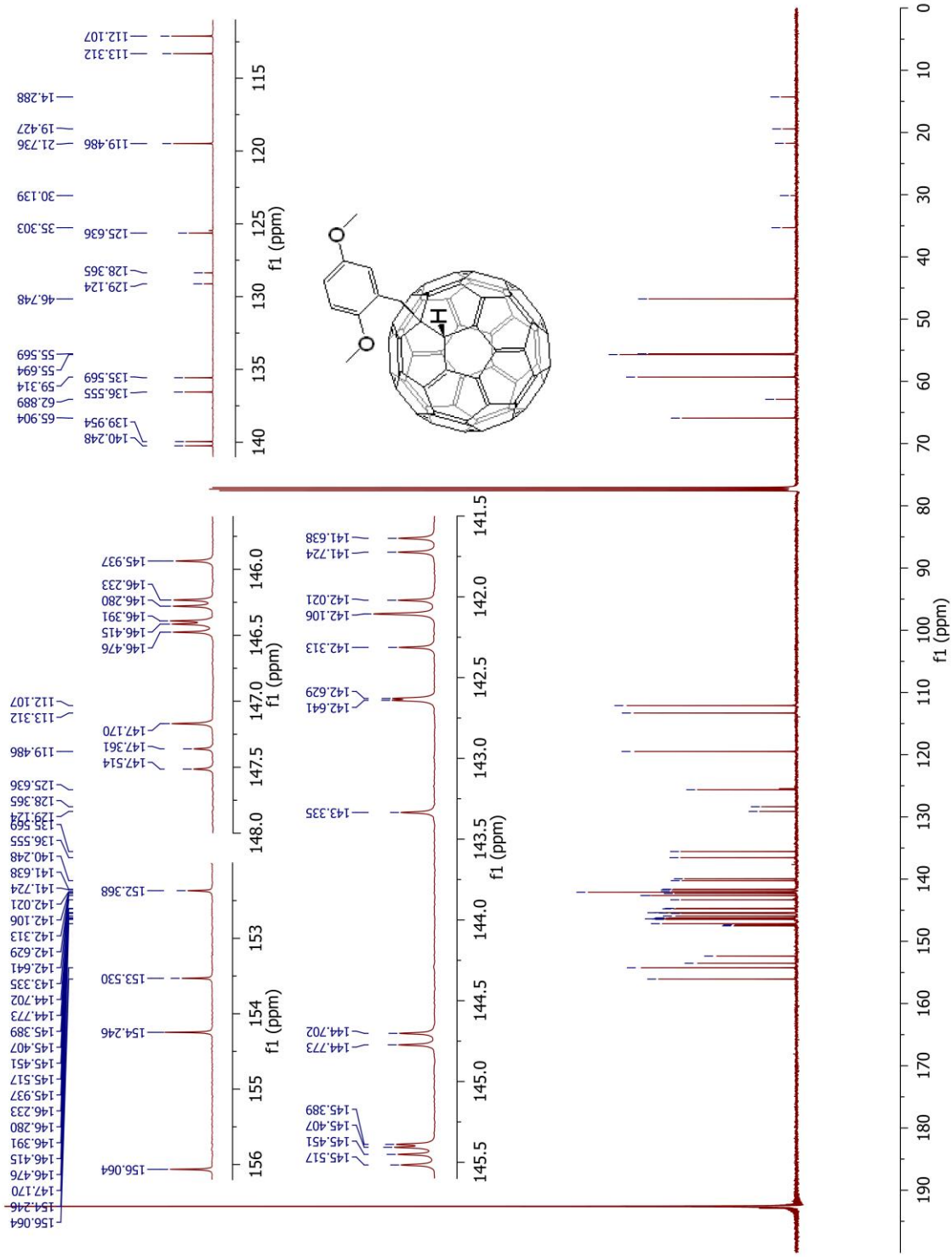

Figure S18. ^{13}C NMR spectrum of compound **2e** (125 MHz, $CDCl_3/CS_2$ (1:1)).

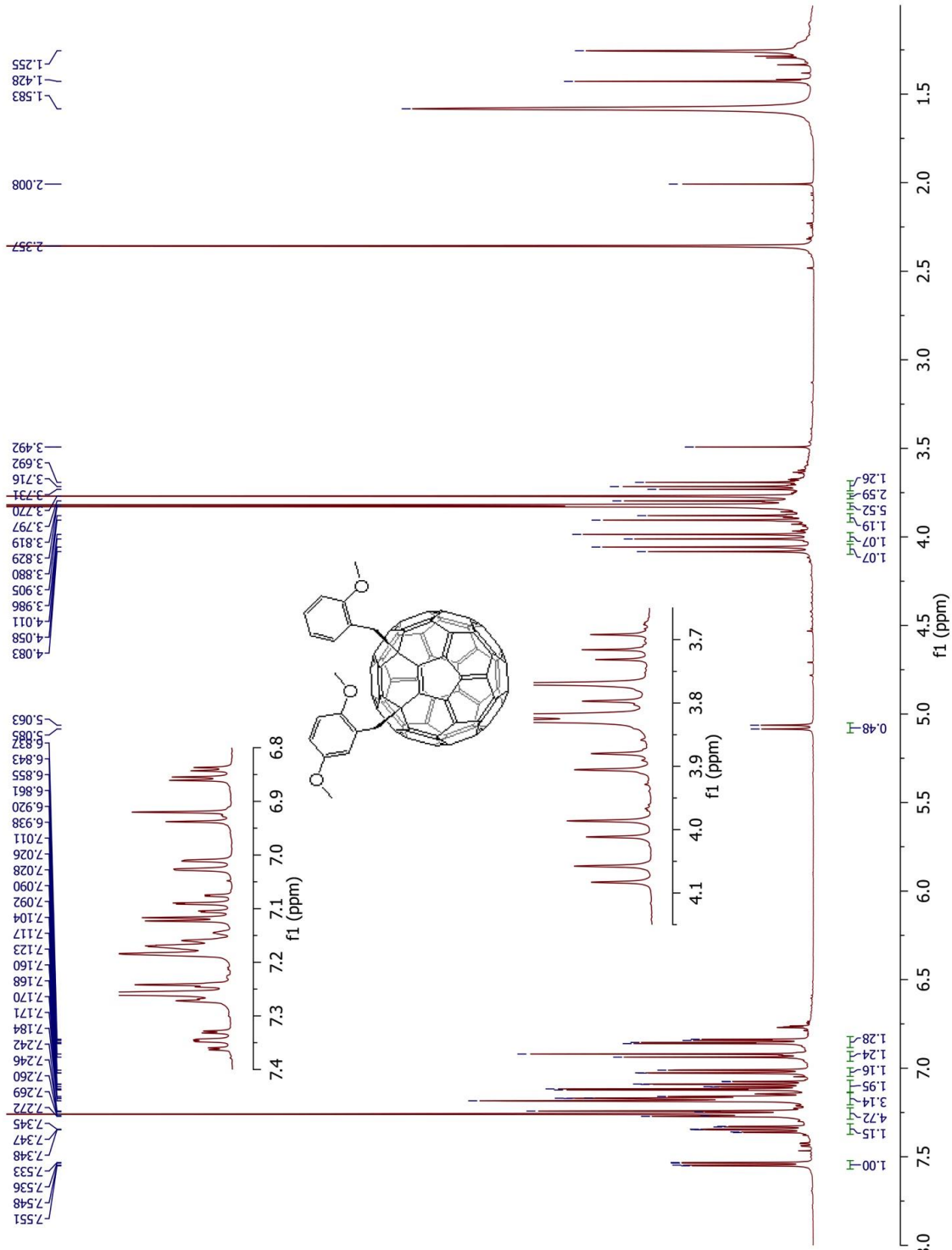

Figure S19. ^{1}H NMR spectrum of compound **1g** (500 MHz, $CDCl_3/CS_2$ (1:1)).

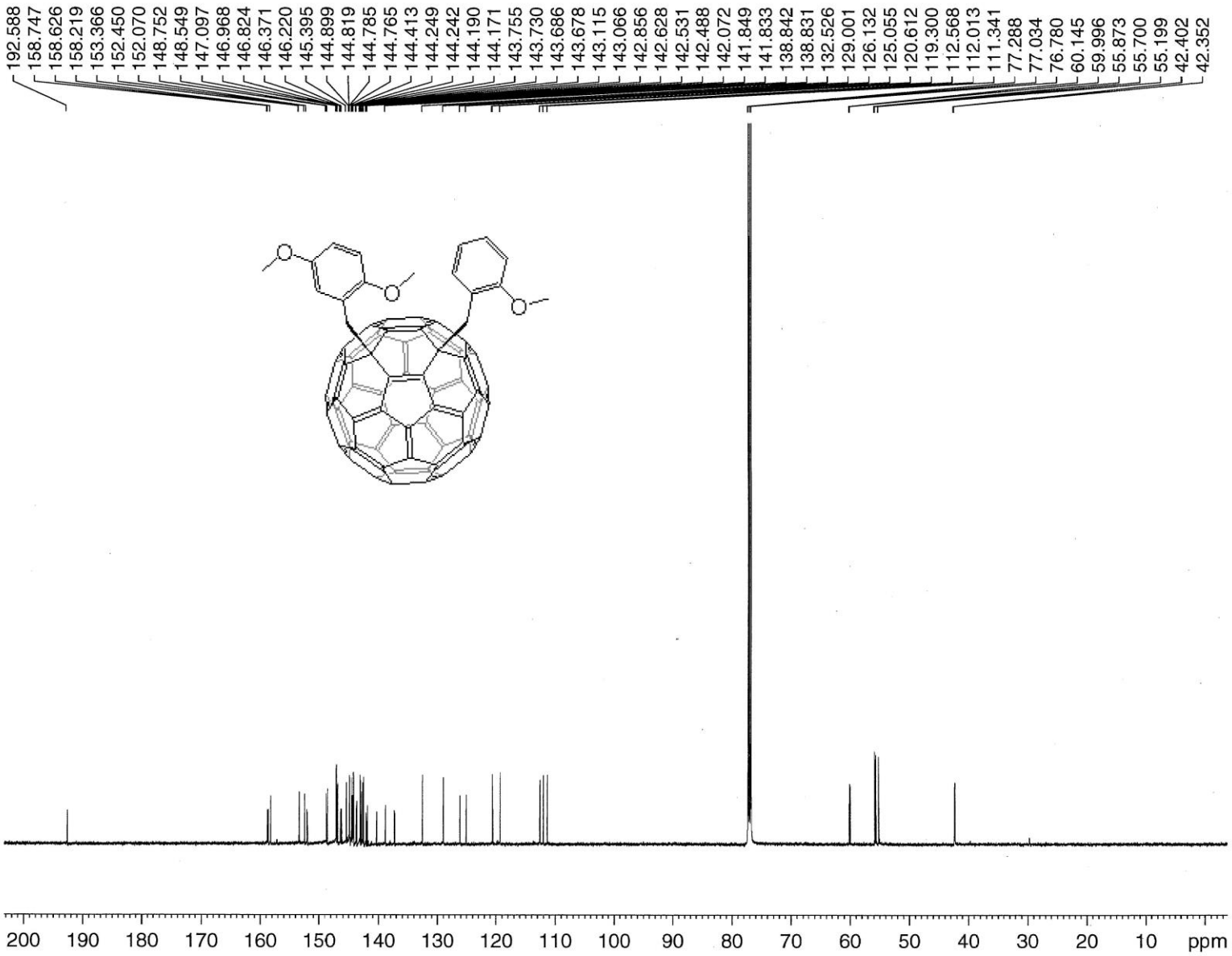

Figure S19.1. ^{13}C NMR Spectrum of compound **1g** (125 MHz, $CDCl_3/CS_2$ (1:1)).

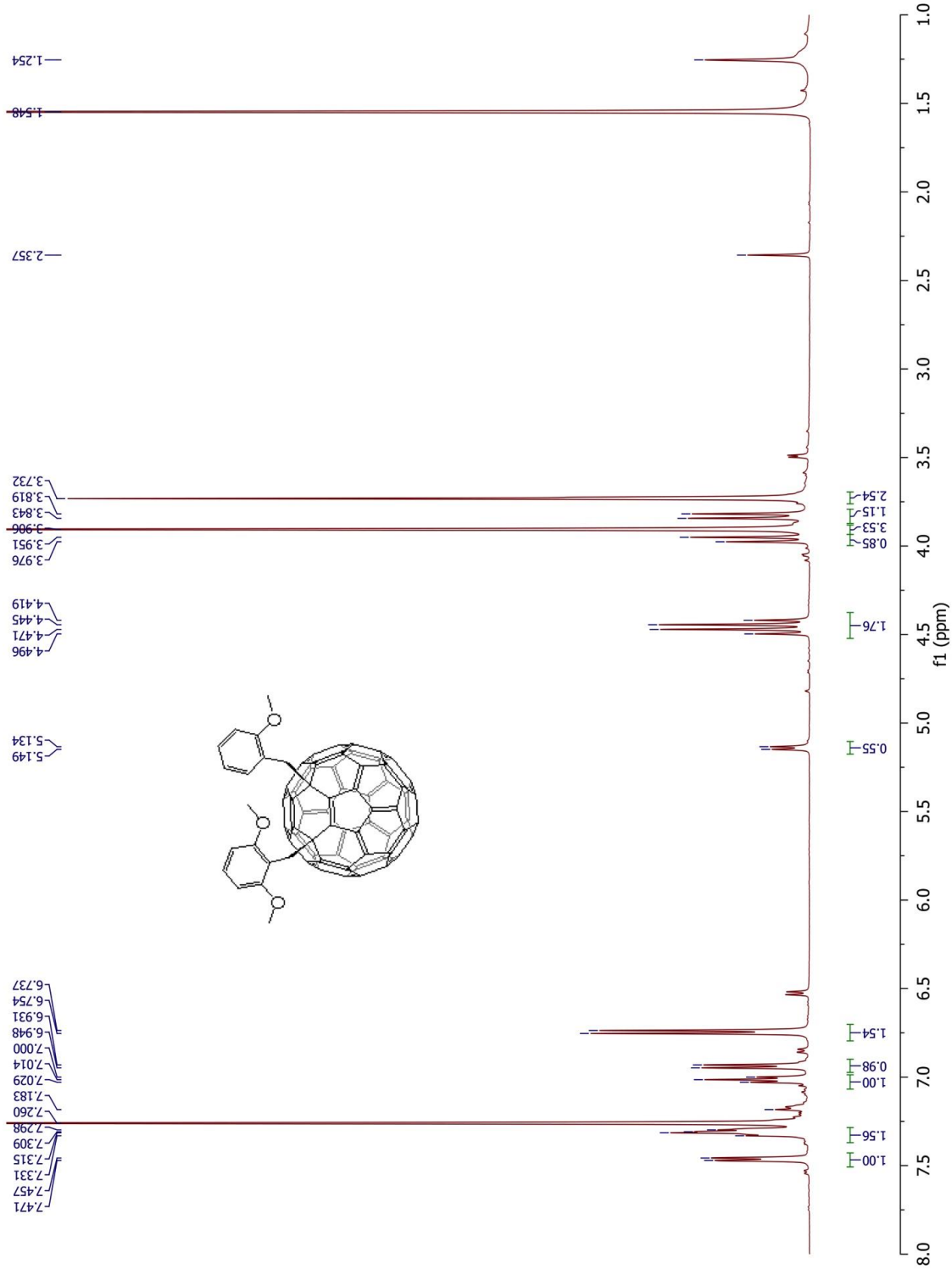

Figure S20. ^{1}H NMR spectrum of compound **1h** (500 MHz, $CDCl_3$).

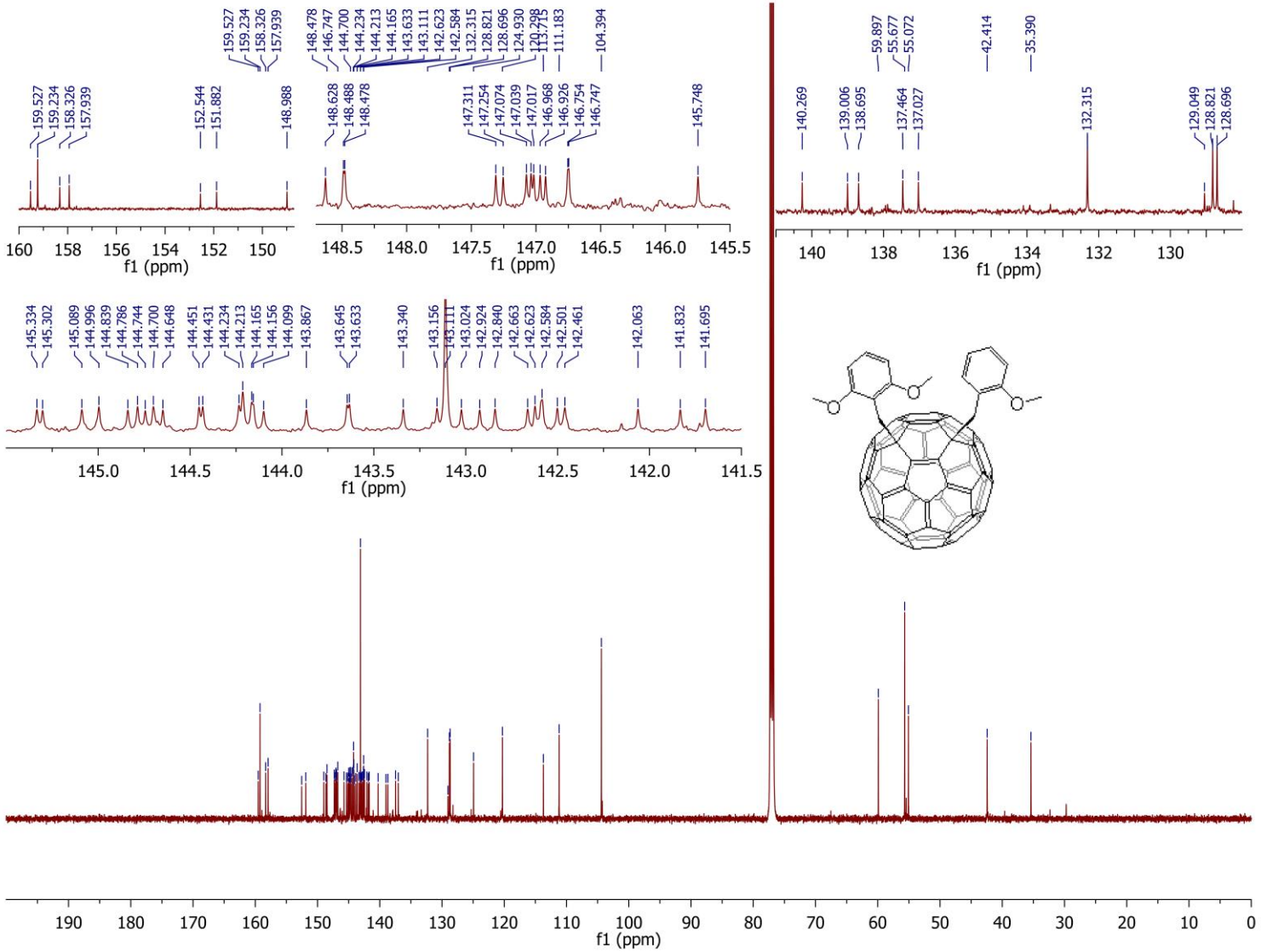

Figure S21. ^{13}C NMR spectrum of compound **1h** (125 MHz, $CDCl_3$).

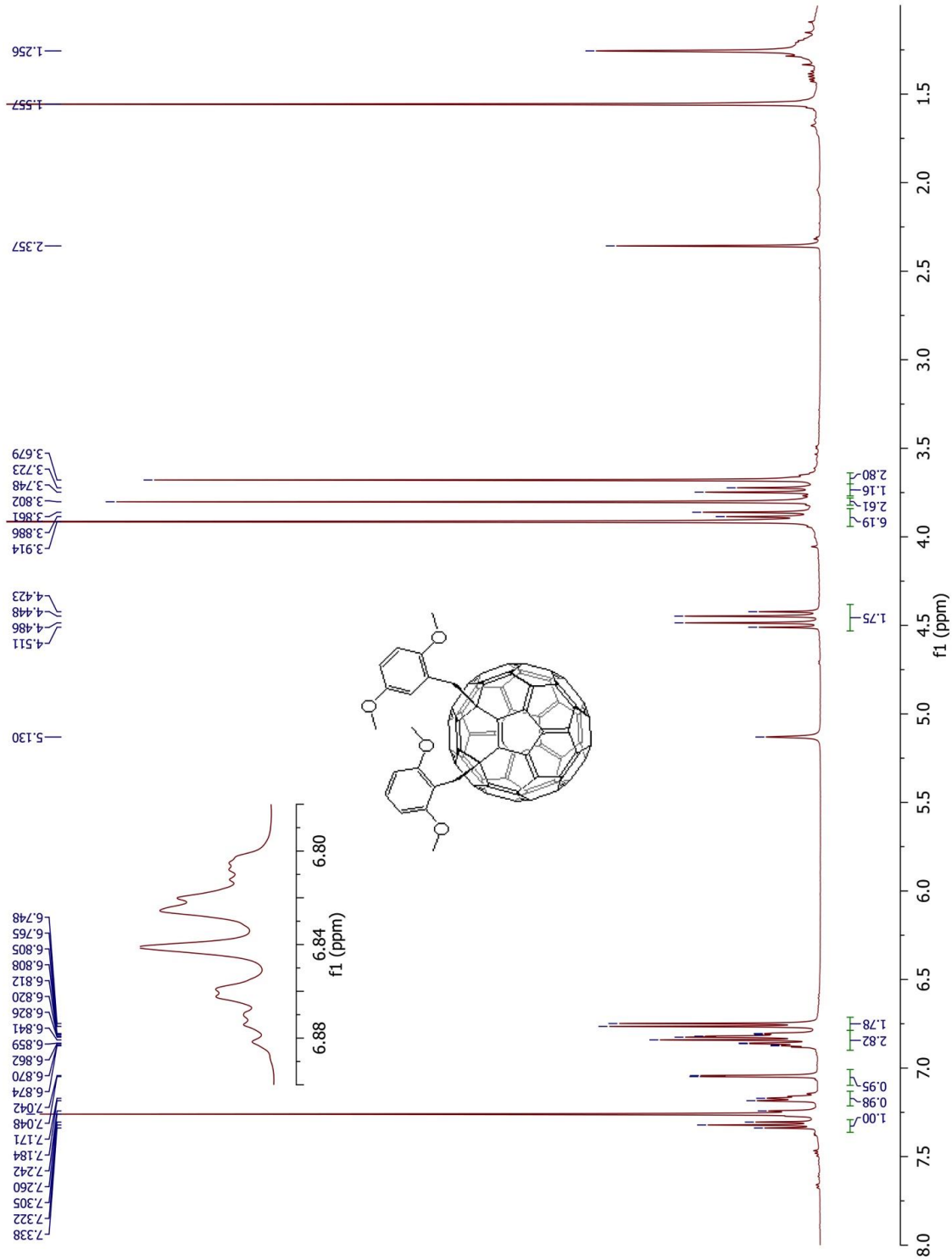

Figure S22. ^{1}H NMR spectrum of compound **1i** (500 MHz, $CDCl_3/CS_2$ (1:1)).

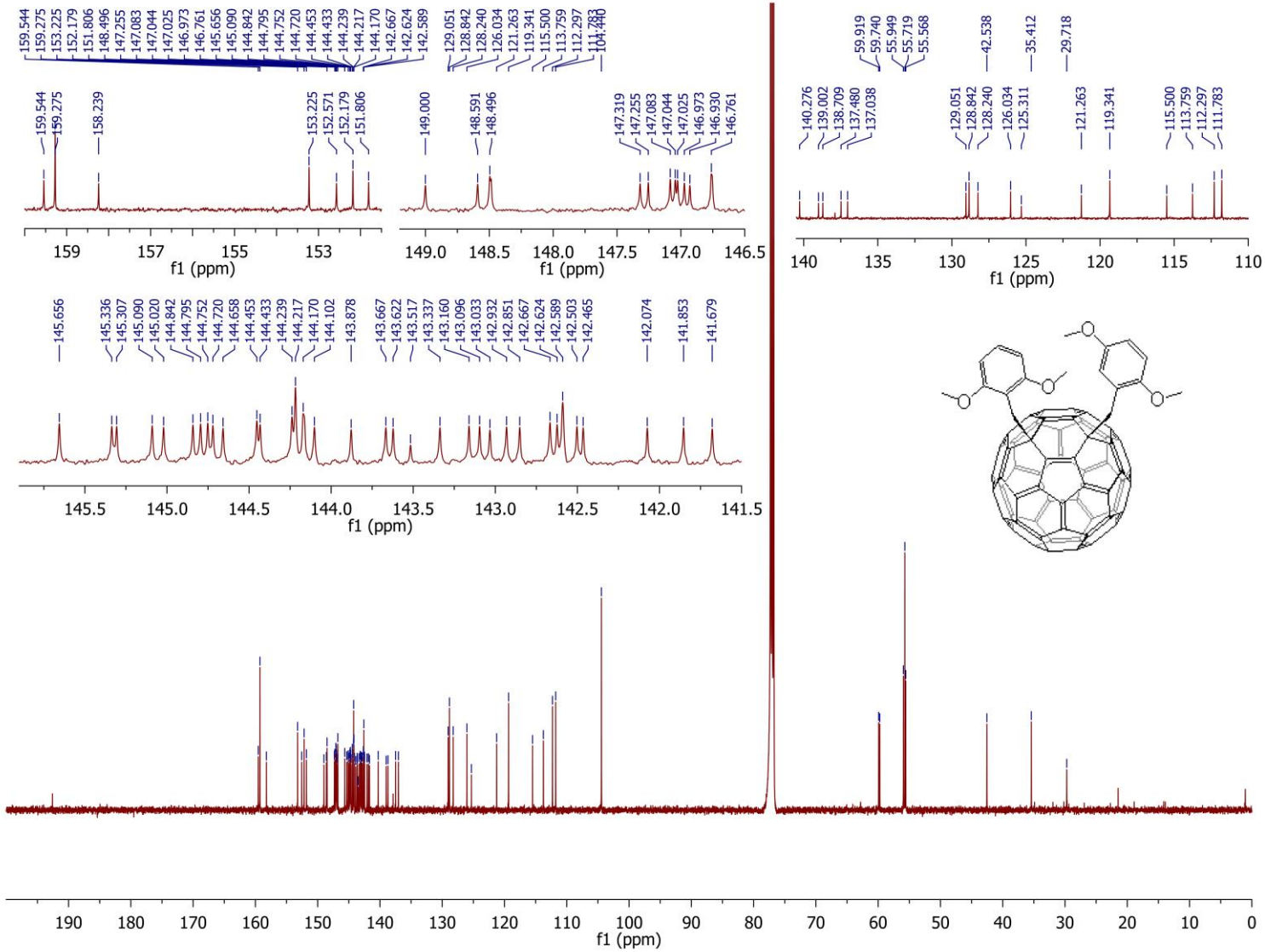

Figure S23. ^{13}C NMR spectrum of compound **1i** (125 MHz, $CDCl_3/CS_2$ (1:1)).

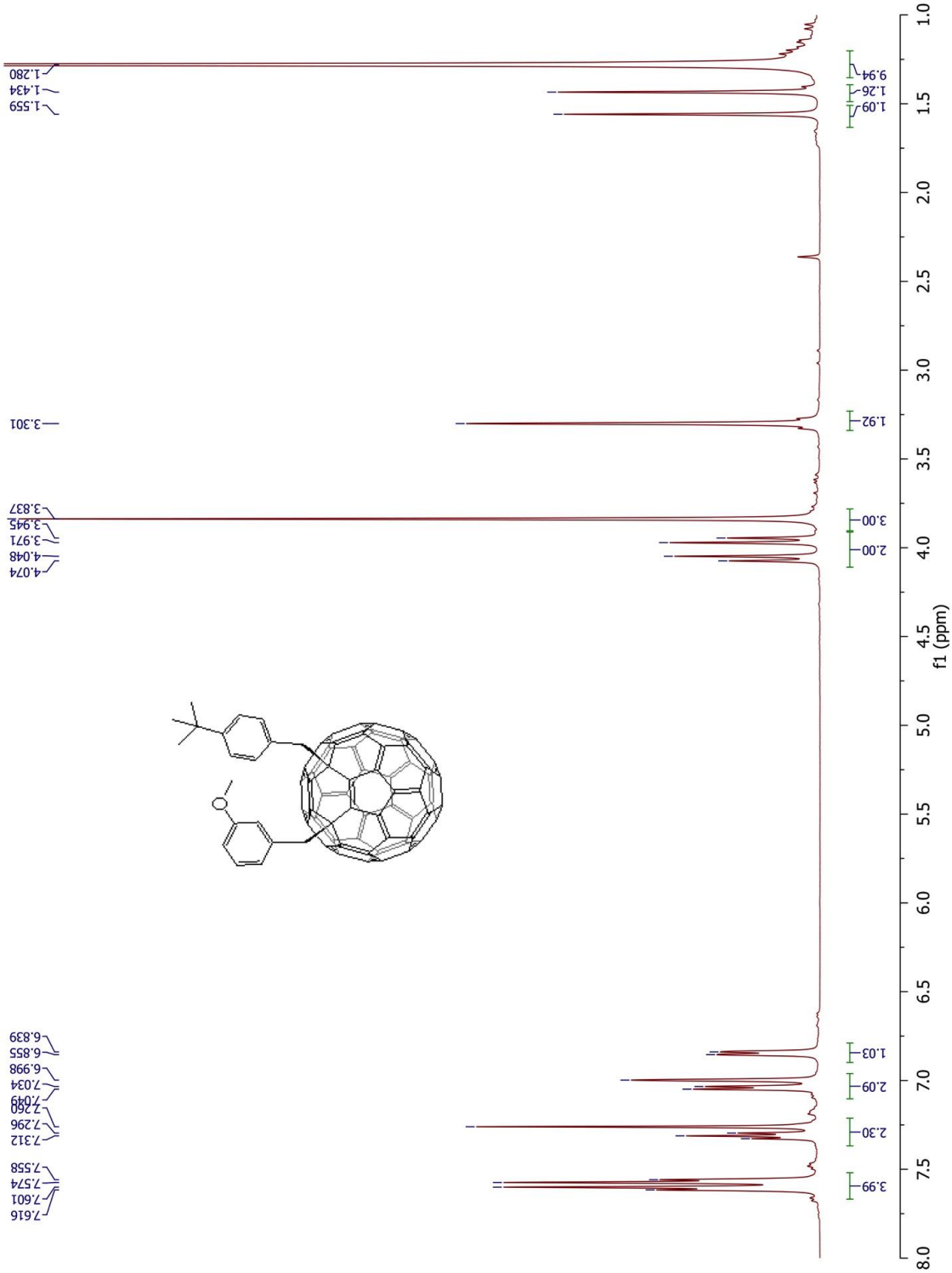

Figure S24. ^{1}H NMR spectrum of compound **1j** (500 MHz, $CDCl_3$).

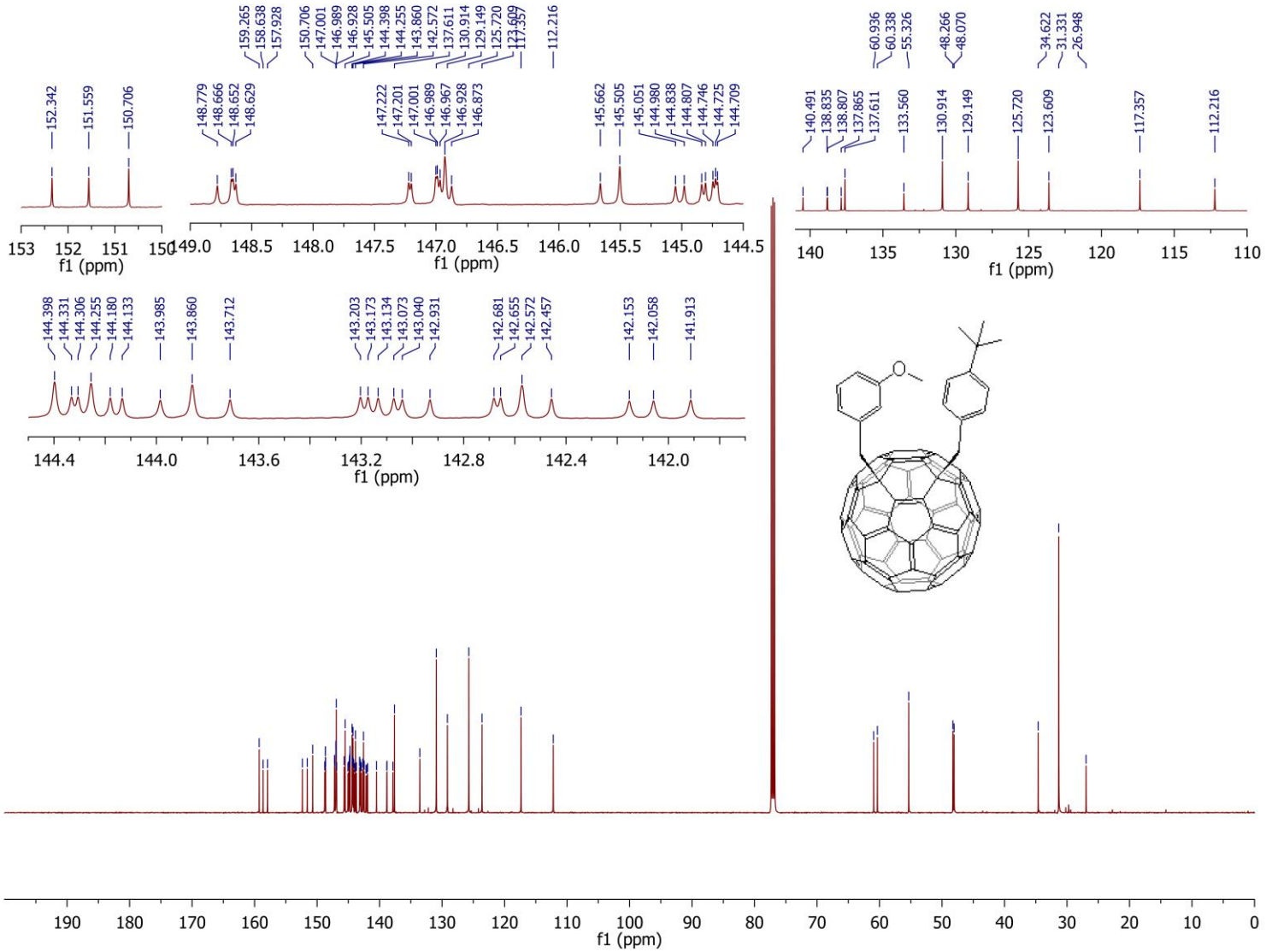

Figure S25. ^{13}C NMR spectrum of compound **1j** (125 MHz, $CDCl_3$).

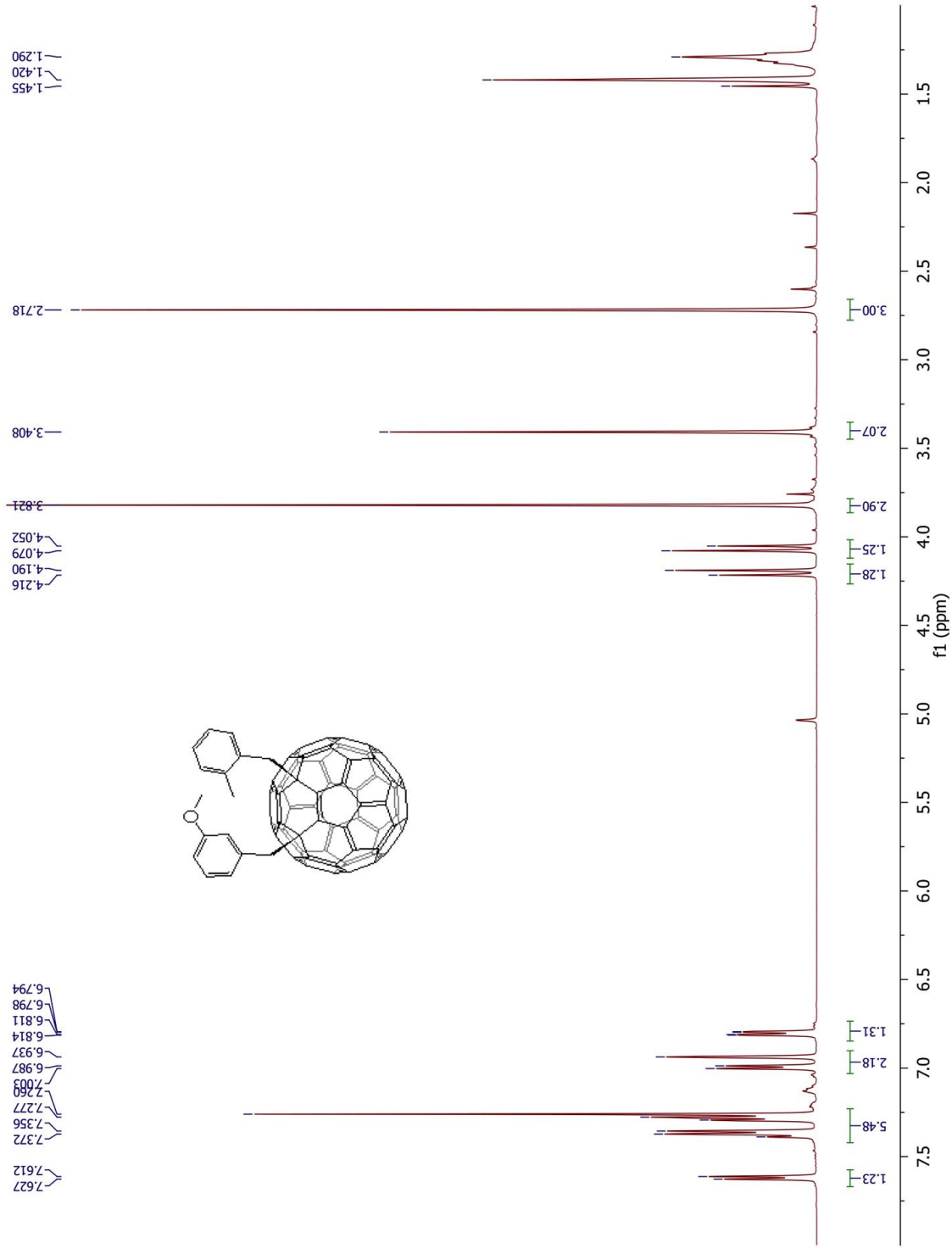

Figure S26. ^{1}H NMR spectrum of compound **1k** (500 MHz, $CDCl_3/CS_2$ (1:1)).

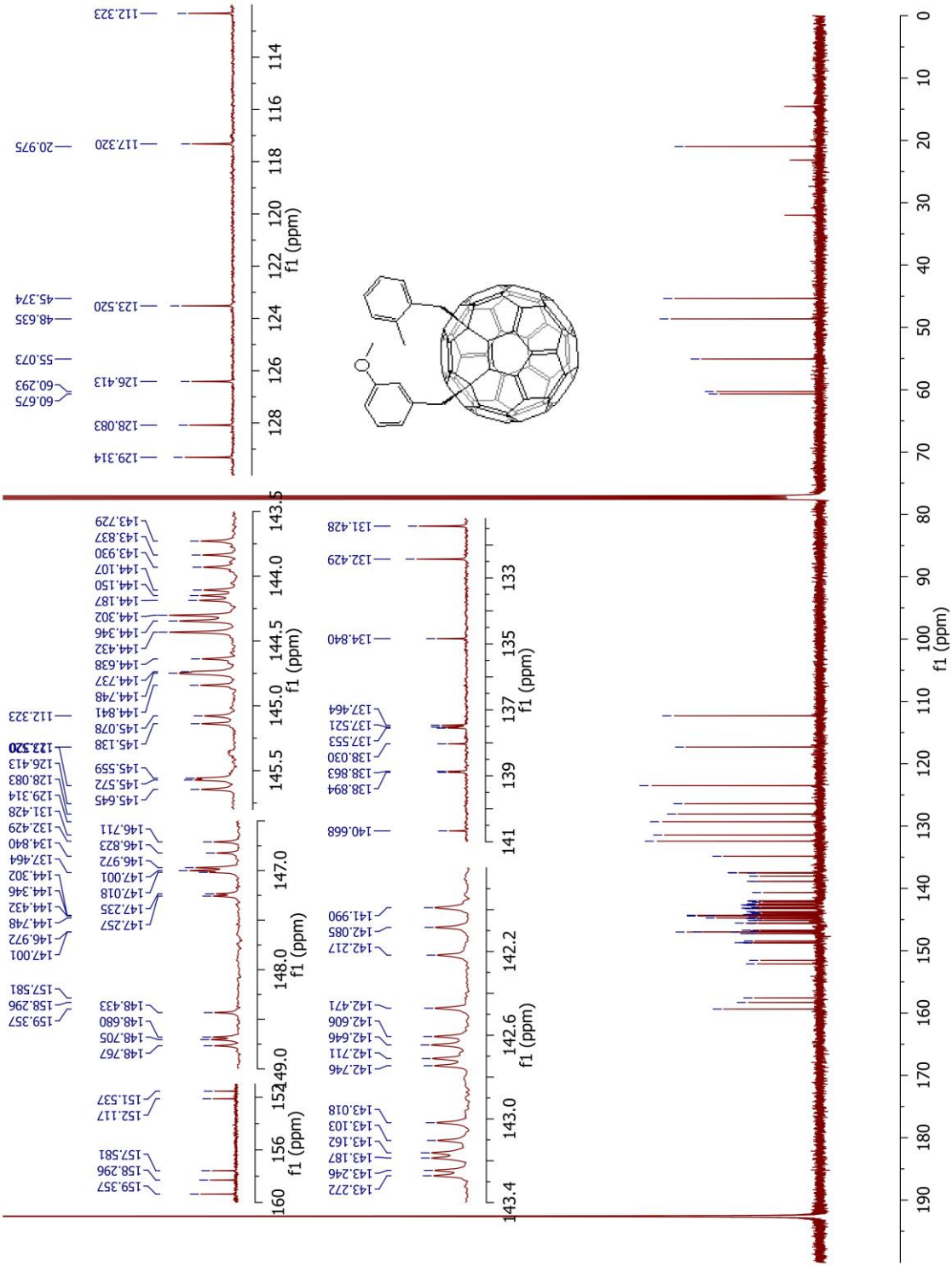

Figure S27. ^{13}C NMR spectrum of compound **1k** (125 MHz, $CDCl_3/CS_2$ (1:1)).

UV-Visible Absorption and External Quantum Efficiency (EQE)

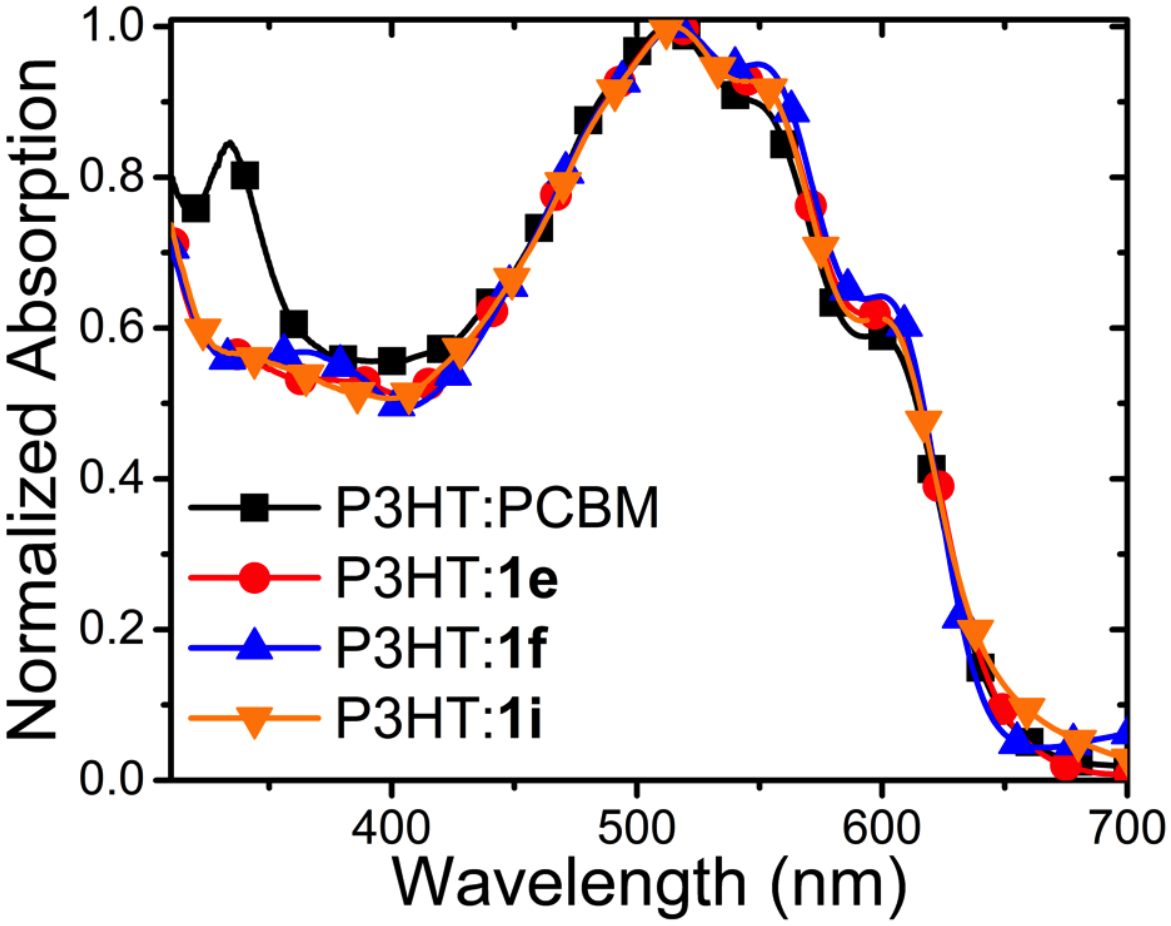

Figure 2.S28. Typical UV-visible absorption spectra for P3HT:fullerene bis-adduct films.

In Figure S28, together with P3HT:PCBM, we plot the UV-visible absorption spectra of films made with P3HT:**1e**, P3HT:**1f** and P3HT:**1i**. These examples show that the absorption profile of the MeO-BBF does not display a well-defined absorption peak near 340 nm, unlike PCBM. Instead, the bis-adduct peaks are slightly shifted to the red compared to PCBM. The same trend is observed in the EQE measurements over the same wavelength range, as shown below in Figure 2.S29 for P3HT:**1e** and P3HT:PCBM. The current densities obtained by integrating the EQE spectra for

P3HT:PCBM and P3HT:**1e** are 8.38 mA/cm^2 and 8.57 mA/cm^2, respectively, which confirm the J_{sc}'s we obtained directly from the *J-V* measurements.

Figure S30 is the EQE spectra for PTB7:PCBM and PTB7:**1e**, which yield integrated current densities of 11.9 mA/cm^2 and 11.8 mA/cm^2, respectively, confirming the J_{sc}'s we measured directly from the *J-V* curves.

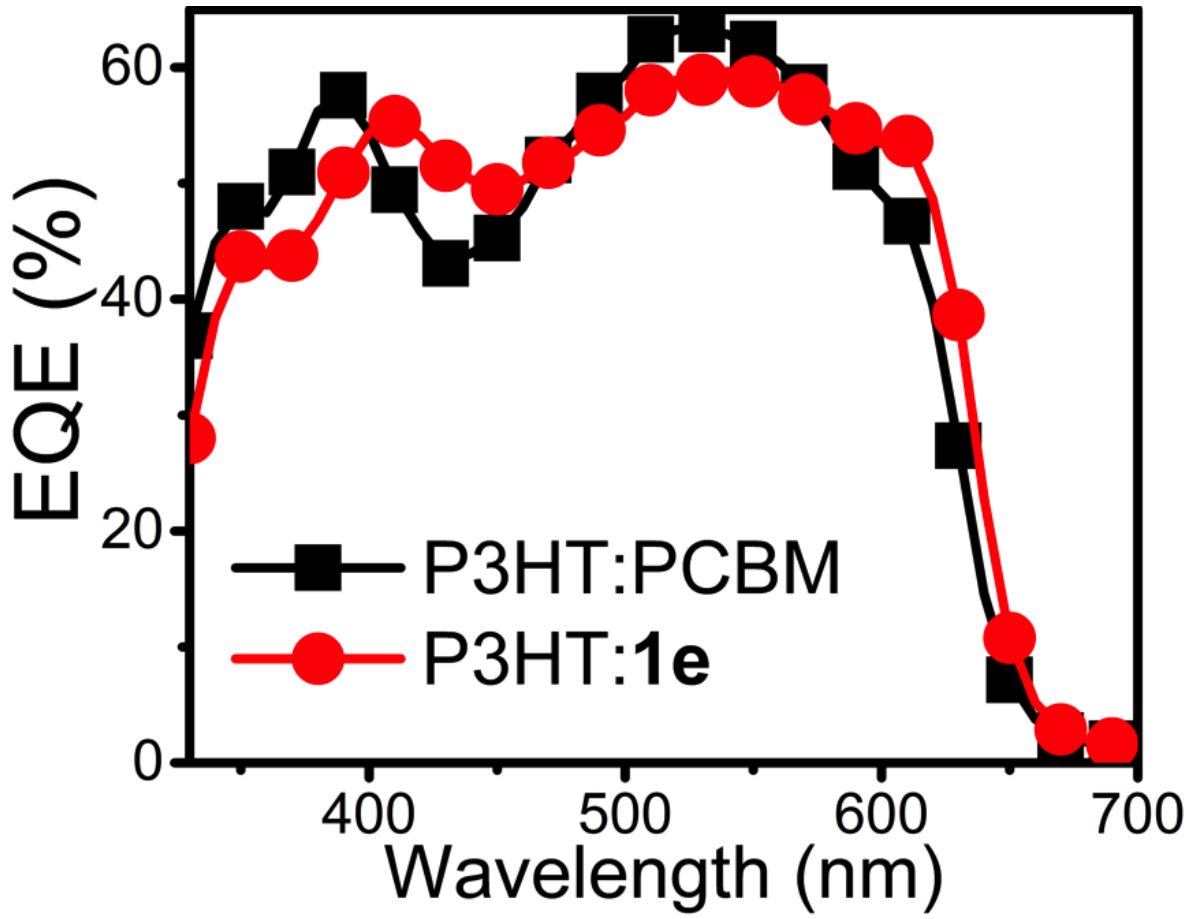

Figure 2.S29. EQE spectra taken on the same P3HT:fullerene devices used in Figure 2.03 of the main text.

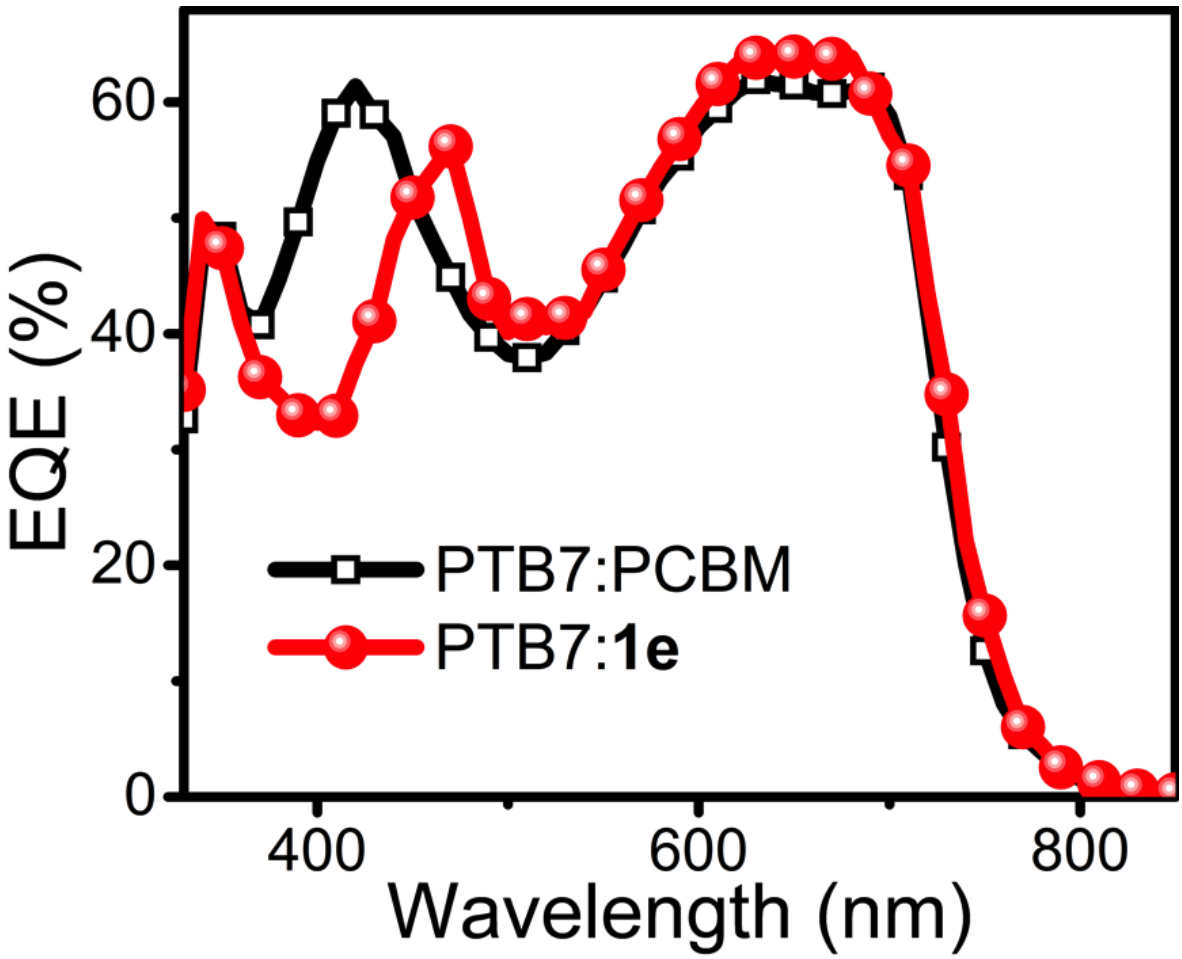

Figure 2.S30. EQE spectra taken on the same PTB7:fullerene devices used in Figure 2.03 of the main text.

Parameters Summarized from 2D-GIWAXS Measurements

Table 2.S1. Summary of GIWAXS Parameters

	(200) Peak Position ($Å^{-1}$)	(200) Peak Area (A.U.)	(200) Peak FWHM (A.U.)	Fullerene Peak Position ($Å^{-1}$)	Fullerene Peak Area (A.U.)	Fullerene FWHM (A.U.)
P3HT:PCBM	0.774	15.9	5.1	1.401	112	28.7
P3HT:**1b**	0.776	14.1	5.2	1.404	98	29.2
P3HT:**1k**	0.772	12.9	4.9	1.405	114	29.6
P3HT:**1j**	0.774	12.8	4.6	1.392	111	30.9

Electrochemical Properties

Two cyclic voltammograms are displayed in Figure 2.S31 to show the typical electrochemical properties of MeO-BBFs. The peaks located at more negative voltages are for the fullerenes and the peaks at more positive voltages come from the oxidation/reduction of ferrocene/ferrocenium (Fc/Fc^{+}). Table 2.S2 summarizes the results on more MeO-BBFs as well as PCBM.

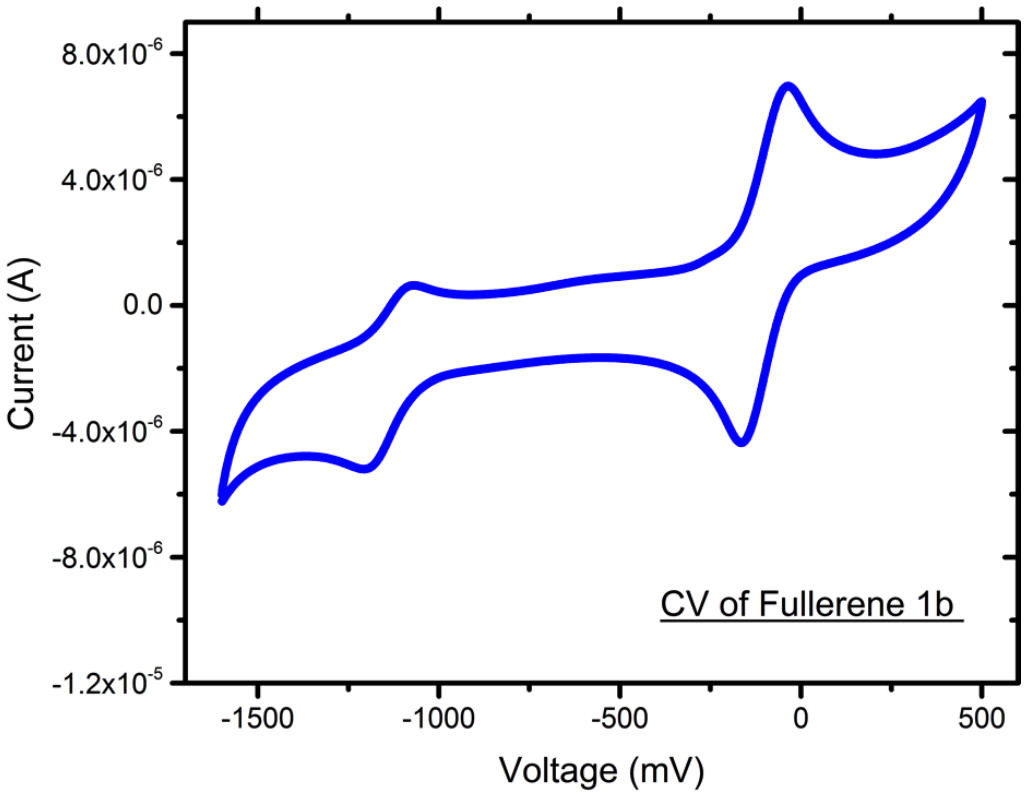

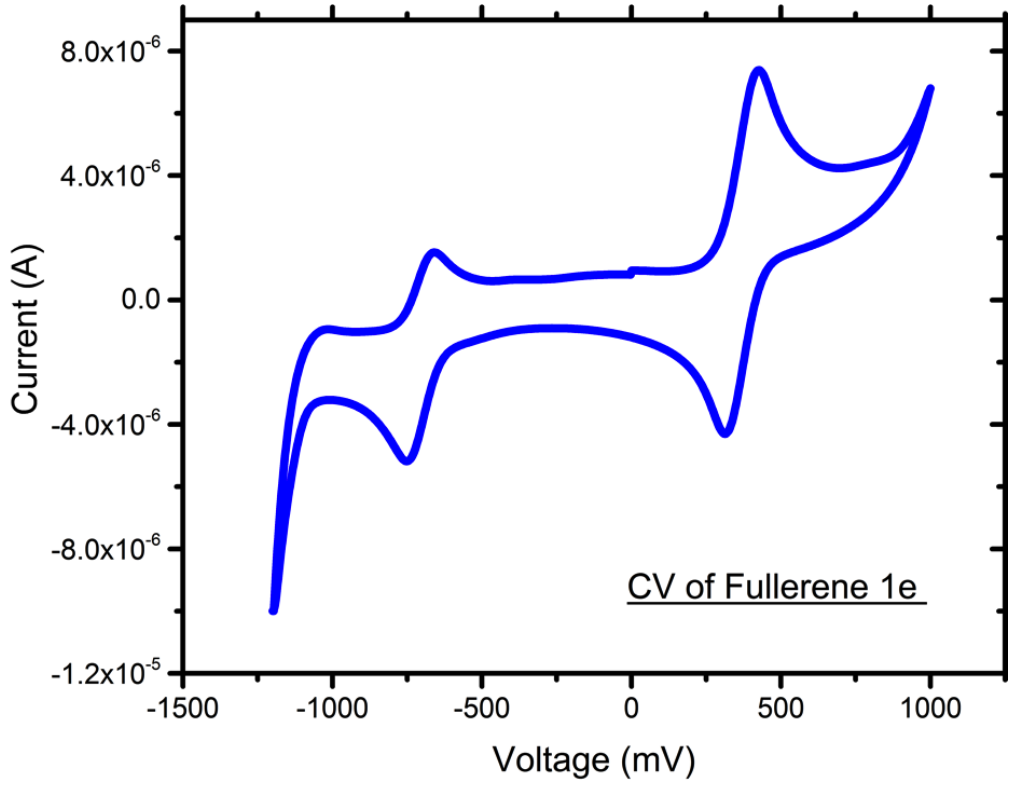

Figure 2.S31. Cyclic voltammogram of fullerene 1b and 1e.

Table 2.S2. Fullerene LUMO Levels Calculated Using Density Functional Theory and Determined by Cyclic Voltammetry

Method:	*Theory (DFT)*		*Experimental (CV)*	
Compound	*HOMO (eV)*	*LUMO (eV)*	*$E_{1/2}$ vs Fc/Fc$^+$ (V)*[b]	*LUMO (eV)*[c]
PCBM	–5.66	–3.09	–0.98	–3.81
1,4-bisbenzyl	–5.62	–3.06		
2-(OMe) (**1a**)[a]	–5.46	–2.93	–1.07	–3.73
3-(OMe) (**1b**)[a]	–5.55	–2.99	–1.04	–3.76
4-(OMe) (**1c**)[a]	–5.55	–3.01	–1.05	–3.75
2,3-$(OMe)_2$ (**1d**)[a]	–5.38	–2.84		
2,5-$(OMe)_2$ (**1e**)[a]	–5.36	–2.87	–1.07	–3.73
3,5-$(OMe)_2$ (**1f**)[a]	–5.47	–2.92		
2,6-$(OMe)_2$ [a]	–5.31	–2.79		
2,3,6-$(OMe)_3$ [a]	–5.23	–2.72		
1j			–1.03	–3.77
1k			–1.04	–3.76

[a] Substituent positions of the corresponding 1,4-bisbenzyl derivatives

[b] The first reduction potential ($E_{1/2}$) are listed relative to Fc/Fc$^+$.

[c] The energy level of Fc/Fc$^+$ was assumed to be –4.8 eV relative to vacuum.[63]

Acknowledgments

We thank Prof. Kendall N. Houk for his insightful suggestions on the DFT calculations. This work was supported by the Center for Molecularly Engineered Energy Materials (MEEM), an Energy Frontier Research Center (EFRC) funded by the U.S. Department of Energy (DOE), Office of Science, Office of Basic Energy Sciences (BES) under Contract Number DE-AC06-76RLO-1830 (device studies, X-ray diffraction, manuscript preparation). Additional support was provided by the National Science Foundation under Grants CHE-1112569 and CBET- 1510353 (optical, device studies, and fullerene synthesis). Portions of this research were carried out at the Stanford Synchrotron Radiation Lightsource, a Directorate of SLAC National Accelerator Laboratory and an Office of Science User Facility operated for the U.S. Department of Energy Office of Science by Stanford University.

References

1 C. Deibel and V. Dyakonov, *Rep. Prog. Phys*, 2010, **73**, 96401.

2 M. Jørgensen, J. E. Carlé, R. R. Søndergaard, M. Lauritzen, N. A. Dagnæs-Hansen, S. L. Byskov, T. R. Andersen, T. T. Larsen-Olsen, A. P. L. Böttiger, B. Andreasen, L. Fu, L. Zuo, Y. Liu, E. Bundgaard, X. Zhan, H. Chen and F. C. Krebs, *Sol. Energy Mater. Sol. Cells*, 2013, **119**, 84–93.

3 F. C. Krebs, N. Espinosa, M. Hösel, R. R. Søndergaard and M. Jørgensen, *Adv. Mater.*, 2014, **26**, 29–39.

4 R. R. Søndergaard, M. Hösel and F. C. Krebs, *J. Polym. Sci. Part B Polym. Phys.*, 2013, **51**, 16–34.

5 M. C. Scharber and N. S. Sariciftci, *Prog. Polym. Sci.*, 2013, **38**, 1929–1940.

6 G. Yu, J. Gao, J. C. Hummelen, F. Wudl and A. J. Heeger, *Science (80-.).*, 1995, **270**, 1789–1791.

7 A. J. Heeger, *Adv. Mater.*, 2014, **26**, 10–27.

8 C.-Z. Li, H.-L. Yip and A. K.-Y. Jen, *J. Mater. Chem.*, 2012, **22**, 4161.

9 Y. Liu, J. Zhao, Z. Li, C. Mu, W. Ma, H. Hu, K. Jiang, H. Lin, H. Ade and H. Yan, *Nat. Commun.*, 2014, **5**, 5293.

10 H. Zhou, L. Yang and W. You, *Macromolecules*, 2012.

11 I. Etxebarria, J. Ajuria and R. Pacios, *Org. Electron.*, 2015, **19**, 34–60.

12 Z. He, C. Zhong, S. Su, M. Xu, H. Wu and Y. Cao, *Nat. Photonics*, 2012, **6**, 591–595.

13 J. C. Hummelen, B. W. Knight, F. Lepeq, F. Wudl, J. Yao and C. L. Wilkins, *J. Org. Chem.*, 1995, **60**, 532–538.

14 M. M. Wienk, J. M. Kroon, W. J. H. Verhees, J. Knol, J. C. Hummelen, P. a van Hal and R. A. J. Janssen, *Angew. Chem. Int. Ed. Engl.*, 2003, **42**, 3371–5.

15 Y. He, H. Chen, J. Hou and Y. Li, *J. Am. Chem. Soc.*, 2010, **132**, 1377–1382.

16 Y. He and Y. Li, *Phys. Chem. Chem. Phys.*, 2011, **13**, 1970–83.

17 X. Meng, Q. Xu, W. Zhang, Z. Tan, Y. Li, Z. Zhang, L. Jiang, C. Shu and C. Wang, *ACS Appl. Mater. Interfaces*, 2012, **4**, 5966–5973.

18 C. Zhang, S. Chen, Z. Xiao, Q. Zuo and L. Ding, *Org. Lett.*, 2012, **14**, 1508–1511.

19 B. Kim, J. Lee, J. H. Seo, F. Wudl, S. H. Park and C. Yang, *J. Mater. Chem.*, 2012, **22**, 22958.

20 Y. He, M. Shao, K. Xiao, S. C. Smith and K. Hong, *Sol. Energy Mater. Sol.*

Cells, 2013, **118**, 171–178.

21 S. Chen, G. Ye, Z. Xiao and L. Ding, *J. Mater. Chem. A*, 2013, **1**, 5562–5566.

22 D. He, C. Zuo, S. Chen, Z. Xiao and L. Ding, *Phys. Chem. Chem. Phys.*, 2014, **16**, 7205–7208.

23 D. He, X. Du, Z. Xiao and L. Ding, *Org. Lett.*, 2014, **16**, 612–615.

24 G. Ye, S. Chen, Z. Xiao, Q. Zuo, Q. Wei and L. Ding, *J. Mater. Chem.*, 2012, **22**, 22374–22377.

25 J.-H. Huang, Y.-S. Hsiao, E. Richard, C.-C. Chen, P. Chen, G. Li, C.-W. Chu and Y. Yang, *Appl. Phys. Lett.*, 2013, **103**, 43304.

26 M. A. Faist, S. Shoaee, S. Tuladhar, G. F. A. Dibb, S. Foster, W. Gong, T. Kirchartz, D. D. C. Bradley, J. R. Durrant and J. Nelson, *Adv. Energy Mater.*, 2013, **3**, 744–752.

27 J. C. Aguirre, C. Arntsen, S. Hernandez, R. Huber, A. M. Nardes, M. Halim, D. Kilbride, N. Kopidakis, S. H. Tolbert, B. J. Schwartz and N. Daniel, *Adv. Funct. Mater.*, 2013, **24**, 784–792.

28 M. Lenes, G.-J. A. H. Wetzelaer, F. B. Kooistra, S. C. Veenstra, J. C. Hummelen and P. W. M. Blom, *Adv. Mater.*, 2008, **20**, 2116–2119.

29 Y. He, G. Zhao, B. Peng and Y. Li, *Adv. Funct. Mater.*, 2010, **20**, 3383–3389.

30 X. Meng, G. Zhao, Q. Xu, Z. Tan, Z. Zhang, L. Jiang, C. Shu, C. Wang and Y. Li, *Adv. Funct. Mater.*, 2014, **24**, 158–163.

31 Y.-J. Cheng, M.-H. Liao, C.-Y. Chang, W.-S. Kao, C.-E. Wu and C.-S. Hsu, *Chem. Mater.*, 2011, **23**, 4056–4062.

32 N. C. Miller, S. Sweetnam, E. T. Hoke, R. Gysel, C. E. Miller, J. A. Bartelt, X. Xie, M. F. Toney and M. D. McGehee, *Nano Lett.*, 2012, **12**, 1566–70.

33 D. Di Nuzzo, G.-J. A. H. Wetzelaer, R. K. M. Bouwer, V. S. Gevaerts, S. C. J. Meskers, J. C. Hummelen, P. W. M. Blom and R. A. J. Janssen, *Adv. Energy Mater.*, 2013, **3**, 85–94.

34 S. Shoaee, S. Subramaniyan, H. Xin, C. Keiderling, P. S. Tuladhar, F. Jamieson, S. A. Jenekhe and J. R. Durrant, *Adv. Funct. Mater.*, 2013, **23**, 3286–3298.

35 A. A. Bakulin, A. Rao, V. G. Pavelyev, P. H. M. van Loosdrecht, M. S. Pshenichnikov, D. Niedzialek, J. Cornil, D. Beljonne and R. H. Friend, *Science*, 2012, **335**, 1340–4.

36 C. J. Brabec, C. Winder, N. S. Sariciftci, J. C. Hummelen, A. Dhanabalan, P. A. van Hal and R. A. J. Janssen, *Adv. Funct. Mater.*, 2002, **12**, 709–712.

37 W. Li, W. S. C. Roelofs, M. M. Wienk and R. A. J. Janssen, *J. Am. Chem. Soc.*, 2012, **134**, 13787–95.

38 A. B. Sieval, N. D. Treat, D. Rozema, J. C. Hummelen and N. Stingelin, *Chem. Commun.*, 2015, **51**, 8126–8129.

39 Y. Matsuo, H. Oyama, I. Soga, T. Okamoto, H. Tanaka, A. Saeki, S. Seki and E. Nakamura, *Chem. Asian J.*, 2013, **8**, 121–128.

40 Y. Matsuo, A. Iwashita, Y. Abe, C.-Z. Li, K. Matsuo, M. Hashiguchi and E. Nakamura, *J. Am. Chem. Soc.*, 2008, **130**, 15429–15436.

41 Y. Matsuo, Y. Sato, T. Niinomi, I. Soga, H. Tanaka and E. Nakamura, *J. Am. Chem. Soc.*, 2009, **131**, 16048–16050.

42 H. Tanaka, Y. Abe, Y. Matsuo, J. Kawai, I. Soga, Y. Sato and E. Nakamura, *Adv. Mater.*, 2012, **24**, 3521–3525.

43 A. Varotto, N. D. Treat, J. Jo, C. G. Shuttle, N. A. Batara, F. G. Brunetti, J. H.

Seo, M. L. Chabinyc, C. J. Hawker, A. J. Heeger and F. Wudl, *Angew. Chem. Int. Ed.*, 2011, **50**, 5166–5169.

44 Y. Liang, Z. Xu, J. Xia, S.-T. Tsai, Y. Wu, G. Li, C. Ray and L. Yu, *Adv. Mater.*, 2010, **22**, 1–4.

45 R. Subramanian, K. M. Kadish, M. N. Vijayashree, X. Gao, M. T. Jones, M. D. Miller, K. L. Krause, T. Suenobu and S. Fukuzumi, *J. Phys. Chem.*, 1996, **100**, 16327–16335.

46 E. Allard, L. Rivitre, J. Delaunay, D. Dubois and J. Cousseau, *Tetrahedron Lett.*, 1999, **40**, 7223–7226.

47 F. Cheng, Y. Murata and K. Komatsu, *Org. Lett.*, 2002, **4**, 2541–2544.

48 E. Allard, J. Delaunay and J. Cousseau, *Org. Lett.*, 2003, **5**, 2239–2242.

49 E. Allard, F. Cheng, S. Chopin, J. Delaunay, D. Rondeau and J. Cousseau, *New J. Chem.*, 2003, **27**, 188–192.

50 J. Cousseau, E. Allard and S. Chopin, *Comptes Rendus Chim.*, 2006, **9**, 1051–1057.

51 M. Toganoh, K. Suzuki, R. Udagawa, A. Hirai, M. Sawamura and E. Nakamura, *Org. Biomol. Chemsitry*, 2003, **1**, 2604–2611.

52 R. Subramanian, P. Boulas, M. N. Vijayashree, F. D'Souza, M. T. Jones and K. M. Kadish, *J. Chem. Soc. Chem. Commun.*, 1994, 1847.

53 S. A. Hawks, J. C. Aguirre, L. T. Schelhas, R. J. Thompson, R. C. Huber, A. S. Ferreira, G. Zhang, A. A. Herzing, S. H. Tolbert and B. J. Schwartz, *J. Phys. Chem. C*, 2014, **118**, 17413–17425.

54 S. E. Wheeler and K. N. Houk, *J. Am. Chem. Soc.*, 2008, **130**, 10854–10855.

55 S. E. Wheeler, *J. Am. Chem. Soc.*, 2011, **133**, 10262–10274.

56 F. B. Kooistra, J. Knol, F. Kastenberg, L. M. Popescu, W. J. H. Verhees, J. M. Kroon and J. C. Hummelen, *Org. Lett.*, 2007, **9**, 551–554.

57 H. Sirringhaus, P. J. Brown, R. H. Friend, M. M. Nielsen, K. Bechgaard, B. M. W. Langeveld-Voss, A. J. H. Spiering, R. A. J. Janssen, E. W. Meijer, P. Herwig and D. M. de Leeuw, *Nature*, 1999, **401**, 685–688.

58 M. Sanyal, B. Schmidt-Hansberg, M. F. G. Klein, A. Colsmann, C. Munuera, A. Vorobiev, U. Lemmer, W. Schabel, H. Dosch and E. Barrena, *Adv. Energy Mater.*, 2011, **1**, 363–367.

59 Y. Kim, S. Cook, S. M. Tuladhar, S. A. Choulis, J. Nelson, J. R. Durrant, D. D. C. Bradley, M. Giles, I. McCulloch, C.-S. Ha and M. Ree, *Nat. Mater.*, 2006, **5**, 197–203.

60 G. Zhang, R. C. Huber, A. S. Ferreira, S. D. Boyd, C. K. Luscombe, S. H. Tolbert and B. J. Schwartz, *J. Phys. Chem. C*, 2014, **118**, 18424–18435.

61 G. A. H. Wetzelaer, M. Kuik, M. Lenes and P. W. M. Blom, *Appl. Phys. Lett.*, 2011, **99**, 153506.

62 R. A. Street, A. Krakaris and S. R. Cowan, *Adv. Funct. Mater.*, 2012, **22**, 4608–4619.

63 J. Pommerehne, H. Vestweber, W. Guss, R. F. Mahrt, H. Bässler, M. Porsch and J. Daub, *Adv. Mater.*, 1995, **7**, 551–554.

3. Long-Lived Photoinduced Polaron Formation in Conjugated Polyelectrolyte-Fullerene Assemblies

In biological photosynthetic systems, energy cascade structures promote the spatial separation of photogenerated charges created at the reaction center, preventing their recombination. These energy cascade structures require close proximity of the electron donors and acceptors, on the scale of ~1 nm, and the corresponding electron transfer (ET) processes take only a few picoseconds (*1*). Similarly, photoexcitation in artificial organic photovoltaic (OPV) cells generates dissociated charges at a donor-acceptor interface on sub-picosecond time scales. However, OPVs suffer a large degree of recombination because they rely on phase separation of the conjugated polymer donor and fullerene acceptor into domains on the length scale of 10 to 20 nm to facilitate efficient exciton diffusion and charge transfer (*2*,(*3*). The high charge densities present in OPVs, coupled with the low dielectric constant of organic materials, favor carrier recombination before the charges can be extracted through external electrodes. If OPVs could be designed to use ET cascade structures that are reminiscent of photosynthetic complexes, it should be possible to greatly improve charge separation and reduce recombination losses (*4*).

Here we describe how molecular self-assembly can enable dissolved OPV materials (conjugated polymers and fullerenes) in aqueous solution to mimic the ET cascade structures of biological complexes and allow us to 'spatially' control photogenerated charges. We demonstrate efficient long-time charge separation following photoexcitation: the ET cascade produces separated polarons that are exceptionally

stable for weeks, a lifetime that is unprecedented for OPV materials. Although long polaron lifetimes have been observed in covalently linked donor-acceptor dyads and triads (*5*) and micellar structures (*6*), it is the fact that we are using standard organic photovoltaic materials that sets this work apart. In addition, our use of self-assembly provides potential future advantages in reproducibility and scalability, both of which are major hurdles for conventional OPVs with kinetically-controlled structures (*7*–*9*). Finally, the photoinduced charge separation we achieve takes place in water, opening possibilities for the 'green' production of artificial photosynthetic devices.

The particular materials used in this study are a combination of a conjugated polyelectrolyte, poly(fluorene-alt-thiophene) (PFT) (*10*), and several regioisomers of the charged fullerene derivatives C_{60}-*N*,*N*-dimethylpyrrolidinium iodide ($C_{60}(PI)_n$), where *n* is the number of charged pyrrolidinium iodide groups (*11*) (Fig. 3.01, A to C). PFT is a water-soluble semiconducting polyelectrolyte whose bis-alkylated sp^3-hybridized fluorenyl carbon forms a wedge-shaped monomer that facilitates the assembly of the charged polymer into rod-like micelles (Fig. 1B); details of how this polymer assembles have been published previously (*10*). Because of the charged nature of the polymer, the electron acceptor(s) must also carry cationic charges to avoid heterocoagulation. The synthesis of $C_{60}(PI)_n$, depending on the reaction conditions, produced multiadducts with *n* ranging from 2 to 5, including multiple regioisomers for each *n*. To avoid confusion, we will refer to $C_{60}(PI)_n$ with n = 3-5 as 'higher' adducts, and fullerenes with n = 2 will be referred to as 'mixed-bis' adducts.

We achieved control over the solution-phase aggregation of these materials by exploiting the different solubility properties of the conjugated polyelectrolyte and charged

fullerene derivatives. Mixed-bis adducts show limited solubility (without PFT) in aqueous solution, while higher adducts are water soluble at high concentration. This difference suggests that the mixed-bis adducts should co-assemble in aqueous solution with PFT, a result we confirmed by cryogenic electron microscopy (cryoEM), small-angle X-ray scattering (SAXS), and luminescence quenching studies. CryoEM images of pure PFT, PFT:mixed-bis adducts and PFT:high adducts are shown in Fig. 1, D to F. Pure PFT samples self-assemble into branched micelles that are roughly 4 ± 0.5 nm in diameter and 30 to 50 nm in length. CryoEM images of PFT assembled with mixed-bis adducts are visually similar to the pure PFT, indicating association of the $C_{60}(PI)_2$ with the PFT micelles. In contrast, cryoEM images of PFT:high adducts appear blurry because these solutions contain separate PFT and fullerene agglomerates.

This interpretation of co-assembly of PFT with 'mixed-bis' adducts is also supported by SAXS measurements (Fig. 2, A and B). We radially averaged the SAXS data and fit it to a power law to extract the exponent α, which is related to the polymer fractal structure (*12*, *13*). Values of α = 1, 2 and 4 correlate to rigid rod, lamellar, and spherical structures, respectively, although interactions between molecules cause deviations from these ideal slopes. Analysis of SAXS data for pure PFT yielded α = 1.5 at low *q* (rod-like at large size), increasing to α = 3.7 at high *q* (sphere-like at small size). Deviation from α = 1 arose from the branched network seen by cryoEM (Fig. 1D) (*14*). SAXS power-law slopes for $C_{60}(PI)_n$ high-adducts correspond to a percolation network at low *q* and rod-like behavior at high *q*, indicating aggregation (*12*, *15*). SAXS data from the combined PFT:high adducts solution was well approximated as the mass-scaled sum of the pure PFT and pure fullerene scattering, suggesting a non-assembled mixture,

similar to that seen by cryoEM. By contrast, mass-scaled SAXS from solutions of PFT and mixed-bis adducts is nearly identical to the pure PFT. These results provide strong evidence that $C_{60}(PI)_2$ and PFT coassemble into a single micellar aggregate.

Finally, electronic interactions in the polymer-fullerene assemblies were confirmed with luminescence quenching, which provides an indirect measure of the photo-induced charge transfer from the polymer to the fullerenes (*16*). Solutions of PFT:high adducts showed relatively little PL quenching, presumably because the donors and acceptors were not in close physical proximity, but aqueous solutions of PFT with the mixed-bis adducts had significant PL quenching, indicating both physical and electronic contact (Fig. 3A). The data indicate that over 75% of the PFT excitations were quenched in the presence of the mixed-bis adducts.

We determined the dynamics of charge separation in these donor-acceptor assemblies using ultrafast broad-band transient absorption spectroscopy on dilute aqueous solutions of co-assembled PFT with mixed-bis adducts (*17*). Representative transient absorption spectra at different probe delays following excitation at 470 nm are shown in Fig. 3.03B. We assigned the negative transient absorption peak near 520 nm to stimulated emission, as the spectral features and the lifetime (Fig. 3.03C) matched the fluorescence emission. Interestingly, the 690-nm absorption of the PFT hole polaron (P^+) appeared on a sub-picosecond time scale after photoexcitation (*18*, *19*). This ultrafast appearance of P^+ confirmed that the $C_{60}(PI)_2$ adducts must be co-assembled with PFT, because other geometries would require diffusion or other structural rearrangements that could not occur so quickly. Once formed, Fig. 3.03C shows that about 75% of the PFT

polarons in these dilute samples decayed back to the ground state in ~200 ps. The remaining polarons survived past the nanosecond time scale.

To mimic biological charge-separation systems, co-assembly and rapid charge separation are required, but if they are followed by rapid recombination, the charges cannot be extracted. A fullerene acceptor that is optimized for charge separation thus needs to contain one class of compounds that can assemble intimately with the PFT for efficient charge transfer, and a second class of compounds that can assemble more loosely, allowing us to pull the electron away from the PFT and prevent recombination. Fortunately, both types of compounds were already available within our mixed-bis sample, and their properties could be examined simply by separating $C_{60}(PI)_2$ regioisomers. Our mixed-bis samples were primarily composed of four isomers (10% *trans*-1, 39% *trans*-2, 44% *trans*-3 and 7% *trans*-4). Structures of each of the isomers are shown in Fig. 4, A to D. We partially separated these isomers by silica gel column chromatography of the neutral pyrrolidine precursors (prior to quaternization), producing fractions that we refer to as *trans*-1,2 (29% *trans*-1 and 71% *trans*-2), and *trans*-3,4 (14% *trans*-2, 74% *trans*-3 and 12% *trans*-4). The full characterization of all of these materials is found in Figs. S1-S22 of the supporting on-line material (SOM) (*17*). The *trans*-1,2 fullerenes have charges on nearly opposite sides of the buckyball, and can be viewed as isotropically-charged molecules that should not easily insert into a PFT micelle. By contrast, the angle between charges in *trans*-3 is ~145º and *trans*-4 is 103°, suggesting more amphiphilic molecules that could insert into the PFT micelle.

The co-assembly of PFT with *trans*-1,2 and *trans*-3,4 was examined via SAXS. Raw scattering data for all of the samples looked similar to pure PFT (Fig. 3.02C), but

Fourier analysis using cylindrical boundary conditions showed subtle variations. In Fig. 3.02D, PFT and PFT:*trans*-3,4 showed similar probability distributions, supporting the model of insertion of fullerene into the PFT micelle. Interestingly, PFT:*trans*-1,2 shows two peaks, reminiscent of a polymer micelle with a partial "shell" of fullerenes surrounding the outside. The PFT:mixed-bis data were well fit by a simple linear combination of the PFT:*trans*-1,2 and PFT:*trans*-3,4 probability distributions, further supporting the idea that *trans*-3,4 assembles on the inside of the polymer micelle while *trans*-1,2 surrounds the outside. The relative locations of the two different sets of fullerenes were also confirmed via solvatochromic absorption measurements, which are shown in Fig. S25 (*17*). These measurements show that the UV absorption of *trans*-1,2 fullerenes assembled with PFT matches that of the fullerenes in pure water, indicating that *trans*-1,2 sits outside of the PFT micelle. In contrast, the absorption of the *trans*-3,4 fullerenes assembled with PFT matches that of the fullerenes in organic solvents, indicating that *trans*-3,4 sits in a lower dielectric environment like the micelle interior.

Figs. 3.04, F and G show luminescence quenching measurements that further support the idea that different isomers of $C_{60}(PI)_2$ assemble in different places in the PFT micelle. The luminescence decays shown in Fig. 4G were taken using a Kerr-gated time-resolved fluorescence set-up using CS_2 as the gate medium, providing a time resolution of ~1 ps (*20*). Clearly, the PFT fluorescence is quenched nearly to the instrument limit in concentrated solutions when assembled with *trans*-3,4 fullerenes, verifying that the photoinduced charge transfer to these fullerenes is ultrafast. In contrast, there is almost no fast quenching of the PFT emission with an equal amount of *trans*-1,2 fullerenes, reflecting their assembled position predominantly on the outside of the micelle, out of

range for fast ET. Fig. 4F shows steady-state luminescence measurements on these same samples. Consistent with the time-resolved data, assemblies of PFT with *trans*-1,2 fullerenes showed little luminescence quenching, whereas PFT assembled with *trans*-3,4 fullerenes had strong quenching. These quenching results suggested that not only can we selectively associate fullerenes with polymer micelles using the number of charges, we can also control the position of the fullerene within the micelle by the placement of the charges (Fig. 3.04E).

Given this degree of control, the next step was to examine long lived excitations in assemblies of PFT and mixed-bis adducts containing both intimately assembled *trans*-3,4 and more isotropically-charged *trans*-1,2 fullerenes. Ideally, this co-assembly should permit rapid photo-induced electron transfer from PFT to the *trans*-3,4 fullerenes, followed by a second electron transfer step to the *trans*-1,2 fullerenes. If this type of directed ET cascade occurs, electrons on the *trans*-1,2 fullerenes would then be stabilized in the high dielectric environment of the water surrounding the micelle, preventing recombination with the PFT. Indeed, we found that photoexcitation of aqueous PFT:mixed-bis adduct solutions caused a dramatic color change from yellow to dark green over time (Fig. 3D); once exposed to light, and the color change was essentially permanent, lasting days to weeks. Dilute solutions, like those used to collect the data in Figs. 3.03B,C, required extensive light exposure (Fig. 3.0S24 (*17*)), but when higher concentrations were used, the color change took place in just a few seconds under room lights, indicating that the quantum yield for long-lived charge separation is much higher than the ~25% in dilute solutions (*cf.* Fig. 3.03B).

PFT is a blue-absorbing polymer with an absorption maximum at 430 nm in water and little to no absorbance past 550 nm (*10*). The color change from yellow to green was confirmed to arise from the appearance of the PFT hole polaron (P^+) by comparing steady-state data (Fig. 3D) with both transient absorption data (Fig. 3B) and absorption from PFT oxidized with iodine, both of which shows absorbs in the sub-gap region at ~690 nm (Fig. S23 (*17*)) (*21*). The Fig. 3D inset shows that simultaneously, a substantially weaker negative (N^-) polaron absorption peak caused by the $C_{60}(PI)_2$ molecular anion was observed at 1180 nm. The low intensity of the N^- absorption has several origins: 1) the absorption cross-section of fullerene anions is much smaller than that of the polymer polarons (*22*); 2) the weak N^- absorption peak sits on top of a broad scattering background from the co-assembled micelles in solution; and 3) the N^- polaron might react with impurities in the water, despite our best efforts to deoxygenate the solutions by freeze-pump-thaw techniques (*23*).

To further confirm the formation of stable, separated N^- and P^+ polarons after exposure to light, we performed electron paramagnetic resonance (EPR) experiments. Figure 3E shows the EPR signal from the green PFT:mixed-bis adducts solution; the *g*-factors for the N^- and P^+ polarons are 2.0004 and 2.0040, respectively, in good agreement with reported values for many other polymer-fullerene systems (*24*). The N^- polaron line width we observed is broader than that in other polymer-fullerene systems, both because of the interaction of the water dipoles with the polarons and because of different spin-relaxation times for the electron and hole (*25*, *26*). The critical difference between our co-assembled system and previous systems, however, is that the previous EPR work required active photoexcitation (light-induced EPR) in order to observe the polaron

signals. In contrast, once exposed to light, the polarons created in our PFT:$C_{60}(PI)_2$ solutions remained stable essentially indefinitely.

Final confirmation that the long-lived separated charges resulted from a self-assembled ET cascade comes by examining the details of absorption and luminescence for a range of samples in different solvents. As discussed above, aqueous solutions of PFT and *trans*-1,2 fullerenes show little PL quenching (Fig. 3.04F,G), but they did briefly turn green during the course of the dissolution, indicating polaron formation (possibly from disordered polymer that transiently allowed the fullerene to partly insert into the micelle). By contrast, despite the efficient luminescence quenching in solutions of PFT co-assembled with the *trans*-3,4 fullerenes (Fig. 3.04F,G), the solutions did not turn green and ultrafast experiments (data not shown) indicate that polarons are formed on sub-ps time scales (as in Fig. 3.03B), but recombine with 100% yield over the next few hundred ps. These results indicate that controlling the spatial position of the fullerenes can dramatically affect carrier dynamics. Moreover, photoexcitation of green-colored PFT:mixed-bis fullerene solutions results in increased luminescence quenching because PFT excitons are further quenched by P^+-polarons (Fig. 3.03F). However, when tetrahydrofuran (THF), which is known to disassemble the polymer micelles (*27*), was added to the co-assembled green system, the luminescence signal regained its intensity, indicating a fully reversible system (Fig. 3.03F). These results further support the idea that intimate assemblies with well-controlled molecular positions are required to facilitate a charge transfer cascade and avoid recombination. When nanoscale architecture is optimized, the result is stable polarons that could potentially be applied to improve organic photovoltaic cells via suppression of charge recombination.

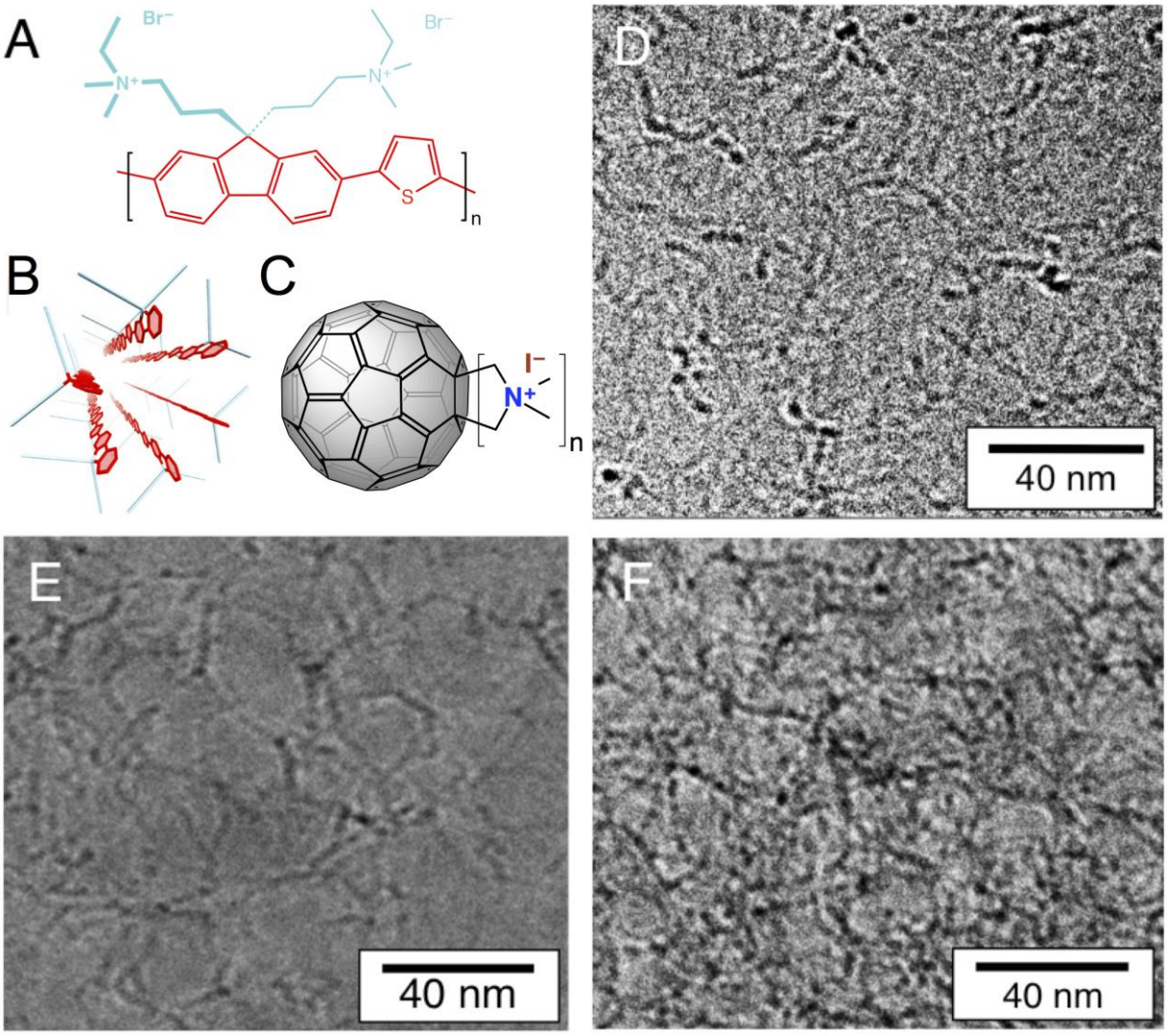

Fig. 3.01. PFT and charged fullerene structure and assembly. PFT structure (A); cartoon of a PFT micelle (B); charged fullerenes (C). CryoEM images of pure PFT (D), PFT:'mixed-bis' adducts (E) and PFT:high adducts (F).

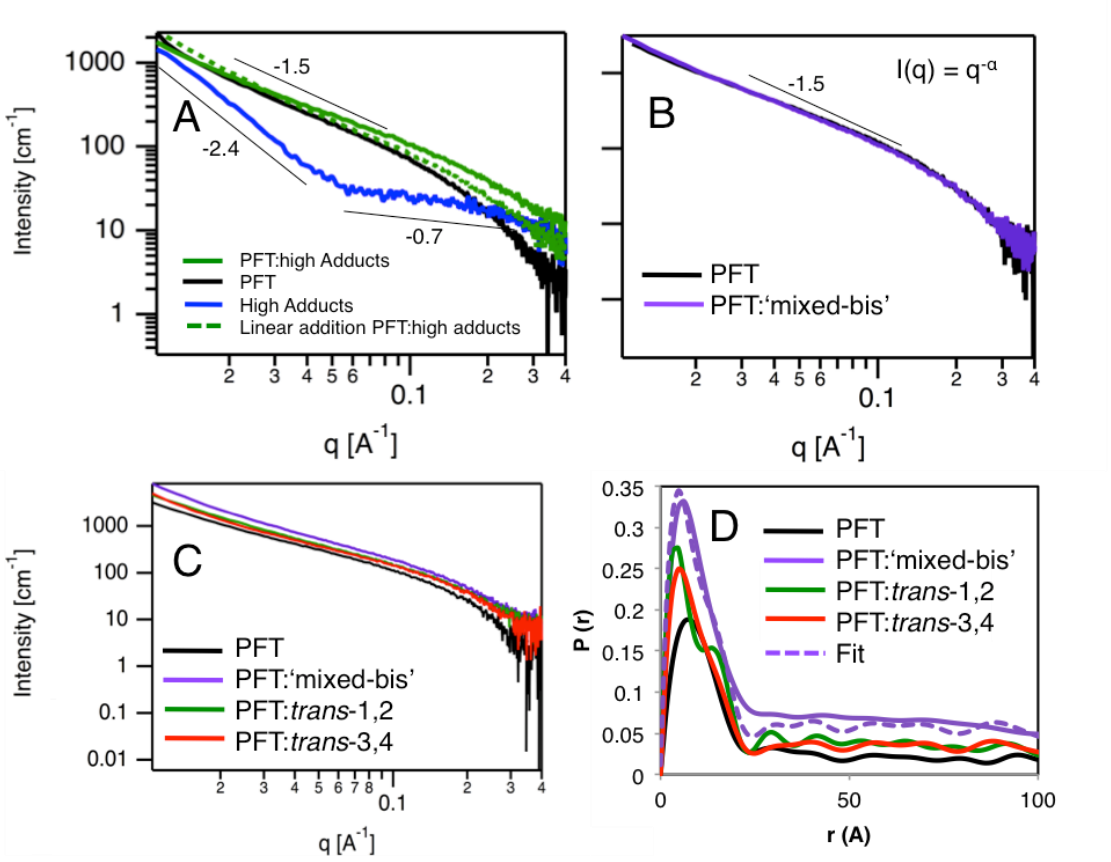

Fig. 3.02. SAXS data for PFT and PFT/fullerene mixtures. A) Data for PFT:high-adducts is reasonably approximated by a sum of PFT+high-adducts. B) The PFT:'mixed-bis' profile overlap mass-scaled PFT data. C) Raw data for all PFT and PFT:bis-fullerene samples are similar. D) Fourier transformed P(r) data for the samples in (C) shows different fullerene environments for *trans*-1,2 and *trans*-3,4, with PFT:mix-bis corresponding to the sum of the two.

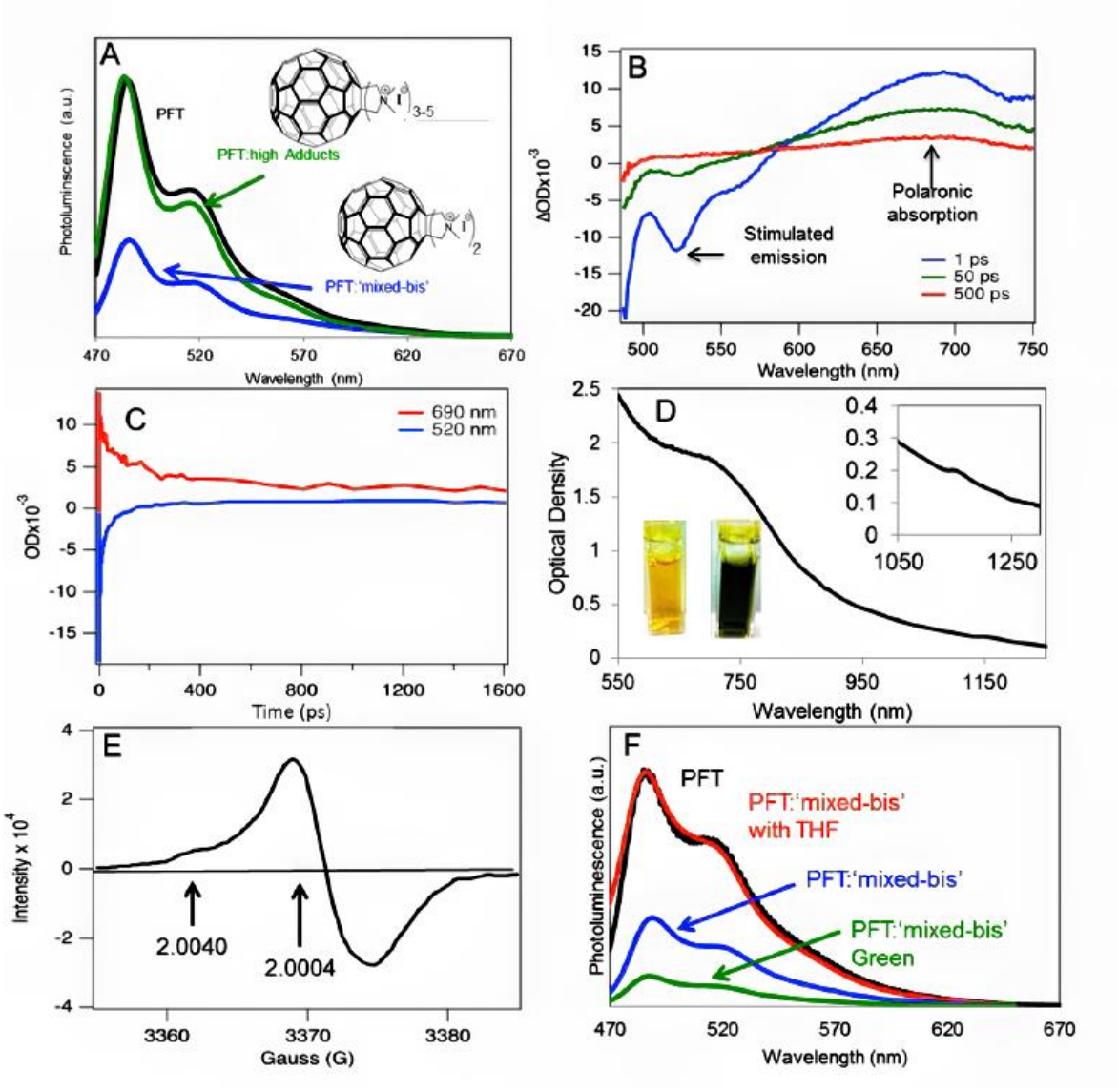

Fig. 3.03. Formation of P^+ and N^- polarons requires intimate assembly of the polymer and fullerene. (A) PL of PFT, PFT:high adducts, and PFT:'mixed bis'; (B) pump-probe spectroscopy for PFT:dilute 'mixed bis' solutions excited at 470 nm showing the rapid formation of both excitons and polarons; (C) time decays for the stimulated emission and the polaronic absorption from (B). Absorption from a green PFT/concentrated fullerene solution showing both P^+ and N^- polarons (D). EPR from a similar green solution, again showing both P^+ and N^- polarons (E). PL for various PFT:concentrated 'mixed bis' solutions showing that polarons quench luminescence, but the addition of THF, which, destroys the PFT/fullerene assembly, restores PL intensity (F).

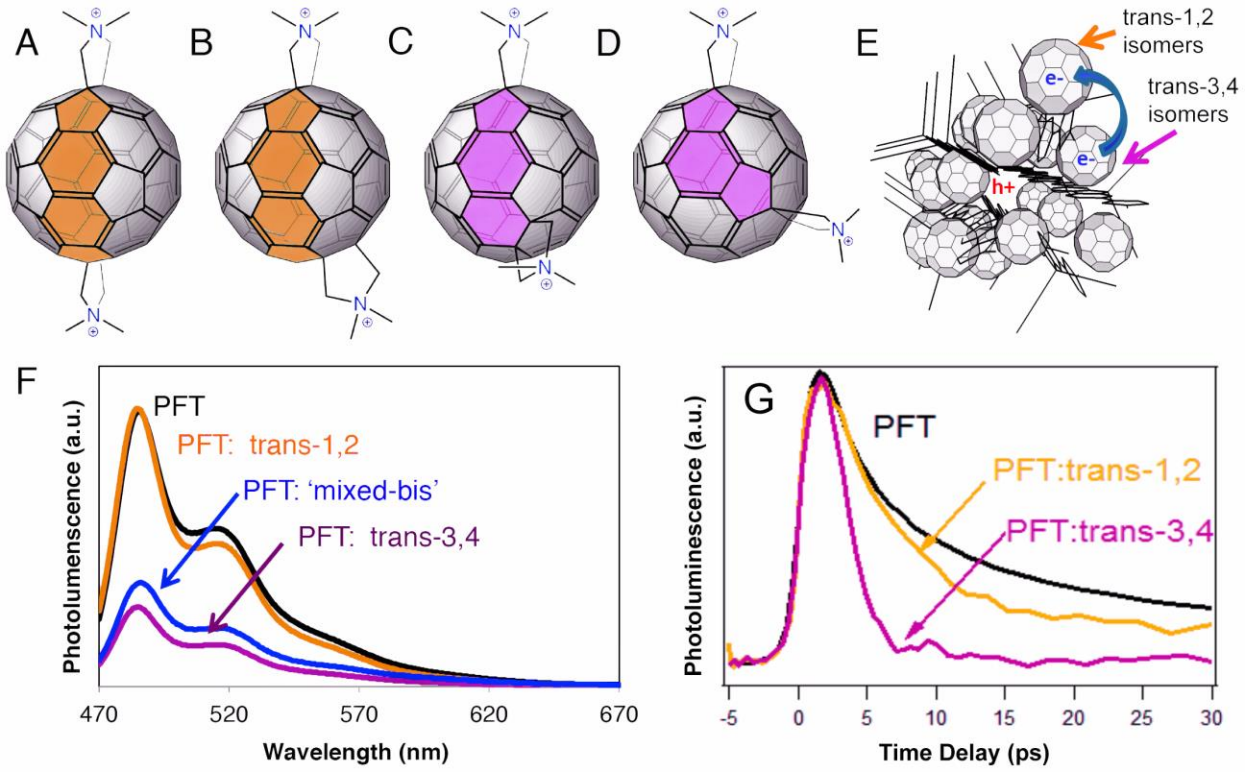

Fig. 3.04. Spectroscopic evidence for long-lived charged species in solution. Chemical structures of *trans*-1 bis (A), *trans*-2 bis (B), *trans*-3 bis (C) and *trans*-4 bis (D) with colored connectivities between the pyrrolidine locations provided for easier visualization. Cartoon depicting the assembly of *trans*-1,2 and *trans*-3,4 bis with PFT leading to long-lived polarons in solution (E). PL of PFT, PFT:'mixed-bis', PFT:*trans*-3,4 bis, and PFT:*trans*-1,2 bis (F). Time-resolved luminescence for assembled PFT:concentrated *trans*-3,4 bis, and PFT:*trans*-1,2 bis samples (G).

Supplementary Material:

PFT synthesis has been previously reported (*10*).

Synthesis of Bis-*N*-methylfulleropyrrolidine isomers:

Bis-N-methylpyrrolidine adducts were synthesized according to published methods (*28*, *29*) and were separated according to the following procedure: The crude product was dry loaded onto a silica column pre-treated with 2% triethylamine in toluene with an unusually large ratio of silica gel to product 1:~500 and the column was run with an extremely slow elution rate (~1-2 mL/min). The column was first eluted with toluene to yield a purple fraction of C_{60} followed by a second brown fraction containing the monoadduct (r_f = 0.70 2/10/88 TEA/Et_2O/PhMe). After elution of the monoadduct, the eluent was changed to 2/10/88 TEA/Et_2O/PhMe and two closely spaced fractions. The first fraction gives two spots by TLC corresponding to the *Trans-1* and *Trans-2* isomers (r_f = 0.50 and r_f = 0.43 2/10/88 TEA/Et_2O/PhMe) and the second fraction gives two spots by TLC corresponding to the *Trans-2* and *Trans-3* isomers (r_f = 0.43 2/10/88 TEA/Et_2O/PhMe r_f = 0.33 2/10/88 TEA/Et_2O/PhMe). Subsequent fractions contain many spots with r_f ranging from 0.2 to 0.33 (2/10/88 TEA/Et_2O/PhMe) corresponding to a complex mixture of *Trans-3*, *4*, *e*, and *cis-3* isomers which can be separated by HPLC using published methods.(*29*) ^{1}H NMR, ^{13}C NMR and MALDI-TOF spectra for the *Trans-1* and *Trans-2* and *Trans-2* and *Trans-3* mixtures match with previously reported spectra for the pure compounds.(*29*)[,4]

Synthesis of Bis-*N,N*-dimethylfulleropyrrolidinium Iodide isomeric mixtures:

Bis-N,N-dimethylpyrrollidinium adducts were synthesized from the corresponding bis-N-methylpyrrolidine adducts according to published methods.[5]

Bis-*N*-methylfulleropyrrolidine (*trans-1/trans-2* mixture)

Trans-1 isomer: ^{1}H NMR 500 MHz $CS_2/CDCl_3$ δ (ppm): 4.64 (s, 8H), 3.12 (s, 6H). ^{13}C NMR 125 MHz $CS_2/CDCl_3$ δ (ppm): 153.48 (8C), 147.72 (4C), 146.18 (8C), 145.58 (8C), 144.30 (8C), 142.39 (4C), 140.88 (8C), 136.64 (8C), 70.28 (4C), 68.99 (4C), 41.66 (2C).

Trans-2 isomer: ^{1}H NMR 500 MHz $CS_2/CDCl_3$ δ (ppm): 4.62 (d, *J* = 9.2 Hz, 2H), 4.43 (d, *J* = 9.2 Hz, 2H), 4.32 (d, *J* = 9.2 Hz, 2H), 4.28 (d, *J* = 9.2 Hz, 2H), 3.05 (s, 6H). ^{13}C NMR 125 MHz $CS_2/CDCl_3$ δ (ppm): 158.85 (2C), 153.20 (2C), 153.06 (2C), 152.43 (2C), 148.45 (2C) 147.74 (2C), 147.16 (2C), 147.11 (2C), 146.50 (2C), 146.37 (2C), 146.22 (2C), 145.78 (2C), 145.70 (2C), 145.40 (2C), 145.31 (2C), 144.30 (2C), 143.92 (2C) 143.76 (2C), 142.71 (2C), 142.68 (2C), 142.63 (2C), 142.51 (2C), 141.65 (2C), 141.61 (2C), 140.88 (2C), 139.75 (2C), 134.70 (2C), 133.94 (2C), 70.18 (2C), 70.03 (2C), 69.86 (2C), 69.69 (2C), 41.60 (2C)

MALDI-TOF MS: found m/z 833.9539 calc. m/z 834.1157

Bis-*N*-methylfulleropyrrolidine (*trans-2/trans-3* mixture)

Trans-2 isomer: ^{1}H NMR 500 MHz $CS_2/CDCl_3$ δ (ppm): 4.63 (d, *J* = 9.2 Hz, 2H), 4.45 (d, *J* = 9.2 Hz, 2H), 4.33 (d, *J* = 9.2 Hz, 2H), 4.23 (d, *J* = 9.2 Hz, 2H), 3.03 (s 6H). ^{13}C NMR 125 MHz $CS_2/CDCl_3$ δ (ppm): 158.87 (2C), 153.22 (2C) 153.08 (2C), 152.45

(2C), 148.46 (2C), 147.75 (2C), 147.18 (2C), 147.11 (2C), 146.50 (2C) 146.38 (2C), 146.22 (2C), 145.78 (2C), 145.72 (2C), 145.40 (2C), 145.27 (2C), 144.30 (2C), 143.93 (2C), 143.77 (2C), 142.73 (2C), 142.69 (2C), 142.63 (2C), 142.51 (2C), 141.66 (2C), 141.63 (2C), 141.03 (2C), 139.74 (2C), 134.72 (2C), 133.96 (2C), 70.21 (2C), 70.05 (2C), 69.87 (2C), 69.70 (2C), 41.63 (2C)

Trans-3 isomer: ^{1}H NMR 500 MHz $CS_2/CDCl_3$ δ (ppm): 4.39 (d, *J* = 9.0 Hz, 2H), 4.30 (d, *J* = 9.0 Hz, 2H), 4.14 (d, *J* = 9.0 Hz, 2H), 4.04 (d, *J* = 9.0 Hz, 2H), 2.92 (s, 6H) ^{13}C NMR 125 MHz $CS_2/CDCl_3$ δ (ppm): 158.18 (2C), 155.60 (2C), 155.52 (2C) 154.89 (2C), 149.19 (2C), 149.05 (2C), 149.00 (2C), 148.83 (2C), 148.31 (2C), 148.30 (2C), 146.71 (2C), 145.38 (2C), 145.25 (2C), 145.23 (2C), 144.99 (2C), 144.71 (2C), 144.02 (2C), 143.71 (2C), 142.65 (2C), 141.76 (2C), 141.57 (2C) 141.37 (2C), 141.18 (2C), 139.93 (2C), 136.59 (2C), 135.72 (2C), 129.15 (2C) 128.42 (2C), 79.47 (2C), 70.23 (2C), 70.14 (2C), 69.31 (2C), 41.54 (2C)

MALDI-TOF MS: found m/z 834.0555 calc. m/z 834.1157.

Bis-*N,N*-dimethylfulleropyrrolidinium Diiodide (*trans-1*/*trans-2* mixture)

Trans-1 isomer: ^{1}H NMR 500 MHz DSMO-D_6 δ (ppm): 6.00 (s, 8H) 4.22 (s, 12H). ^{13}C NMR 125 MHz DSMO-D_6 δ (ppm): 151.49 (8C), 147.36 (4C), 145.47 (8C), 145.21 (8C), 144.93 (4C), 141.56 (8C), 140.04 (8C), 136.19 (8C), 72.89 (4C), 67.20 (4C), 52.26 (4C).

Trans-2 isomer: ^{1}H NMR 500 MHz DSMO-D6 δ (ppm): 5.99 (d, *J* = 12,4 Hz, 2H), 5.81 (d, *J* = 12.4 Hz, 2H), 5.69 (d, *J* = 12.4 Hz, 2H), 5.65 (d, *J* = 12.4 Hz, 2H), 4.24 (s, 6H), 4.02 (s, 6H). ^{13}C NMR 125 MHz DSMO-D_6 δ (ppm): 155.97 (2C), 150.99 (2C), 150.91

(2C), 150.18 (2C), 147.66 (2C), 147.38 (2C), 146.87 (2C), 146.41 (2C), 146.12 (2C), 145.98 (2C), 145.45 (2C), 145.25 (2C), 145.07 (2C), 144.90 (2C), 143.83 (2C), 143.18 (2C), 143.02 (2C), 142.57 (2C), 142.23 (2C), 141.86 (2C), 141.48 (2C), 141.25 (2C), 140.54 (2C), 139.31 (2C), 138.97 (2C), 134.39 (2C), 133.68 (2C), 128.90 (2C), 72.69 (2C), 72.60 (2C), 67.93 (2C), 67.63 (2C), 52.58 (2C), 52.20 (2C).

Mixture is 17% *trans-1* and 83% *trans-2* by comparison of the N-CH_3 integral intensities in the ^{1}H NMR spectrum of the mixture.

ESI-MS: *m/z* 432.0731, 100% rel. intensity ($C_{68}H_2$-$N_2I_2^{2+}$) calculated 432.0813. 991.0811, 10% rel. intensity ($C_{68}H_2$-N_2I^{+}) calculated 991.0671.

Bis-*N,N*-dimethylfulleropyrrolidinium Diiodide (*trans-2*/*trans-3* mixture)

Trans-2 isomer: ^{1}H NMR 500 MHz DSMO-D6 δ (ppm): 5.99 (d, *J* = 12,4 Hz, 2H), 5.81 (d, *J* = 12.4 Hz, 2H), 5.69 (d, *J* = 12.4 Hz, 2H), 5.65 (d, *J* = 12.4 Hz, 2H), 4.25 (s, 6H), 4.03 (s, 6H). ^{13}C NMR 125 MHz DSMO-D_6 δ (ppm): 155.96 (2C), 150.99 (2C), 150.90 (2C), 150.17 (2C), 147.69 (2C), 147.40 (2C), 146.89 (2C), 146.43 (2C), 146.12 (2C), 146.02 (2C), 145.48 (2C), 145.28 (2C), 145.10 (2C), 144.92 (2C), 143.86 (2C), 143.26 (2C), 143.05 (2C), 142.60 (2C), 142.25 (2C), 141.90 (2C), 141.53 (2C), 141.31 (2C), 140.56 (2C), 139.38 (2C), 139.01 (2C), 134.47 (2C), 133.75 (2C), 128.94 (2C), 72.68 (2C), 72.60 (2C), 67.95 (2C), 67.66 (2C), 52.60 (2C), 52.22 (2C).

Trans-3 isomer: ^{1}H NMR 500 MHz DSMO-D6 δ (ppm): 5.76 (d, *J* = 12,4 Hz, 2H), 5.62 (d, J = 12.4 Hz, 2H), 5.52 (d, J = 12.4 Hz, 2H), 5.39 (d, J = 12.4 Hz, 2H), 4.07 (s, 6H) 3.92 (s, 6H). ^{13}C NMR 125 MHz DSMO-D_6 δ (ppm): 155.29 (2C), 153.03 (2C), 152.76 (2C), 152.10 (2C), 148.95 (2C), 148.44 (2C), 148.22 (2C), 148.06 (2C), 148.03 (2C),

147.91 (2C), 146.17 (2C), 145.04 (2C), 144.97 (2C), 144.67 (2C), 144.54 (2C), 143.97 (2C), 143.73 (2C), 143.59 (2C), 143.29 (2C), 143.26 (2C), 141.86 (2C), 141.61 (2C), 141.11 (2C), 140.66 (2C), 140.40 (2C), 138.36 (2C), 136.31 (2C), 135.68 (2C), 128.25 (2C), 72.57 (2C), 71.87 (2C), 68.35 (2C), 68.02 (2C), 52.53 (2C), 52.25 (2C)

Mixture is 28% *trans-2* and 72% *trans-3* by comparison of the N-CH_3 integral intensities in the ^{1}H NMR spectrum of the mixture.

ESI-MS: *m/z* 432.0731, 100% rel. intensity ($C_{68}H_{20}N_2I_2^{2+}$) calculated 432.0813. 849.1381 15% rel. intensity ($C_{67}H_{17}N_2^+$) calculated 849.1392. 991.1392, 10% rel. intensity ($C_{68}H_2$-N_2I^+) calculated 991.0671.

Bis-*N,N*-dimethylfulleropyrrolidinium Diiodide (*trans*-1/*trans-2*/*trans-3*/*trans-4* mixture)

Trans-1 isomer: ^{1}H NMR 500 MHz DSMO-D_6 δ (ppm): 6.00 (s, 8H), 4.22 (s, 12H).

Trans-2 isomer: ^{1}H NMR 500 MHz DSMO-D6 δ (ppm): 5.99 (d, *J* = 12,4 Hz, 2H), 5.81 (d, *J* = 12.4 Hz, 2H), 5.69 (d, *J* = 12.4 Hz, 2H), 5.65 (d, *J* = 12.4 Hz, 2H), 4.23 (s, 6H), 4.05 (s, 6H).

Trans-3 isomer: ^{1}H NMR 500 MHz DSMO-D6 δ (ppm): 5.76 (d, *J* = 12,4 Hz, 2H), 5.62 (d, *J* = 12.4 Hz, 2H), 5.52 (d, *J* = 12.4 Hz, 2H), 5.39 (d, *J* = 12.4 Hz, 2H), 4.01 (s, 6H), 3.91 (s, 6H).

Trans-4 isomer: ^{1}H NMR 500 MHz DSMO-D6 δ (ppm): 5.65 (d, *J* = 12,4 Hz, 2H), 5.51 (d, *J* = 12.4 Hz, 2H), 5.44 (d, *J* = 12.4 Hz, 2H), 5.41 (d, *J* = 12.4 Hz, 2H), 3.88 (s, 6H), 3.80 (s, 6H).

Mixture is 5% *trans-1*, 48% *trans-2*, 42% *trans-3*, and 5% *trans-4* by comparison of the N-CH_3 integral intensities in the ^{1}H NMR spectrum of the mixture.

ESI-MS: *m/z* 432.0768, 100% rel. intensity ($C_{68}H_{2}N_2I_2^{2+}$) calculated 432.0813. 991.0811, 10% rel. intensity ($C_{68}H_{2}N_2I^{+}$) calculated 991.0816.

CryoEM

For cryoEM, grids were prepared by placing a small drop (~4 µl) of sample solution onto glow discharged holy carbon mesh Quantifoil 200 mesh grids with 3.5 µm holes spaced 1 µm apart. The grids were then blotted and plunged immediately into liquid nitrogen cooled liquid ethane to rapidly freeze the samples in vitrified ice. The cryo grids were visualized with an FEI Tecnai F20 transmission electron microscope at an accelerating voltage of 200 kV. Images were collected on a 16 megapixel CCD camera at ~50,000x magnification with a defocus value of approximately 3 µm.

Small-angle X-ray scattering (SAXS)

Small-angle X-ray scattering (SAXS) experiments were conducted at the Stanford Synchrotron Radiation Laboratory (SSRL) Beamline 4-2. Using a syringe, 100 µL of each sample was loaded in a quartz capillary and held at 25°C. Scattered X-rays (at 12 keV) were collected with a Rayonix MX225-HE detector (sample to detector distance = 1.7 m). The two-dimensional data was radially averaged to obtain one-dimensional scattering curves.

Electron paramagnetic resonance

Electron paramagnetic resonance was performed at UCLA in the Molecular Instrumentation Center (MIC). Experiments were performed on the Bruker EMX EPR spectrometer in a nitrogen finger dewar to keep the sample frozen at 95 K. The microwave frequency was 9.437 GHz, amplitude of 4 G, microwave power of 0.02 mW and a scan time of 20.972 s for 32 accumulated scans.

Pump-probe transient absorption spectroscopy

A femtosecond Ti:Sapphire amplifier (Coherent, Legend Elite) seeded with a broadband Ti:Sapphire oscillator (Coherent, Mantis) was used for ultrafast pump-probe transient absorption experiments. Spectral and kinetic data acquisition was accomplished using a commercially built spectrometer (HELIOS, Ultrafast Systems LLC). The amplifier output consisting of 40 fs, 3 mJ pulses centered around 800 nm (at 1 kHz repetition rate) was split into two beams of roughly equal power. One of the beams was directed to an Optical Parametric Amplifier (Light Conversion, TOPAS-C) to create 470 nm pump pulses. A small portion of the amplifier output was focused onto a sapphire crystal to generate white light continuum (WLC) probe laser pulses. The probe beam was directed onto a computer-controller translation stage so that the time-delay between the pump and the probe could be varied. The pump and probe pulses were focused into the sample in a non-collinear geometry, making it possible to select only the WLC probe pulses for detection. The probe beam was focused onto the sample such that the spot-size of probe beam was smaller than the pump beam in order to ensure that the data collected came

from a uniformly excited region. Solution-phase samples of a concentration of 1mg/ml were filled in glass cuvettes with 1 mm path-length to ensure sufficient transmission of the probe light. The transmitted probe beam through the sample was collimated onto a fiber optic cable using a telescope and then dispersed onto a one dimensional CCD detector. We chopped the pump beam at a frequency of 500 Hz and recorded the pump on/pump off signals for each consecutive pair of pulses to calculate the normalized transient absorption spectrum for a particular probe delay. We used a modest pump pulse energy of 60 nJ (spot size ~ 5 mm) for excitation and ensured that we were safely in the linear regime.

Spectra

UV-vis absorption spectra were taken on a Perkin-ElmerLambda25spectrometer in a 0.1 cm glass cell in DMSO. ^{1}H and ^{13}C NMR spectra were taken on a 500 MHz Bruker Avance AV 500 spectrometer equipped with a 5mm dual cryoprobe.

Cyclic Voltammagram

Cyclic Voltammagrams were acquired on a BAS CV-50W cyclic voltammetric analyzer with a sweep rate of 50 mV/s under Ar atmosphere in PhCN with 0.1 M TBAH, 0.01 M $AgNO_3$, and 0.05 M Bisfulleropyrrolidinium Iodide salt using an Ag/Ag^{+} non-aqueous reference electrode with platinum working and counter electrodes. Ferrocene was added as a reference.

Mass Spectrometry

ESI-MS spectra were acquired on a waters LCT premier with Acquity UPLC. MALDI-TOF MS were acquired on an Applied Biosystems Voyager-DE-STR MALDI-TOF.

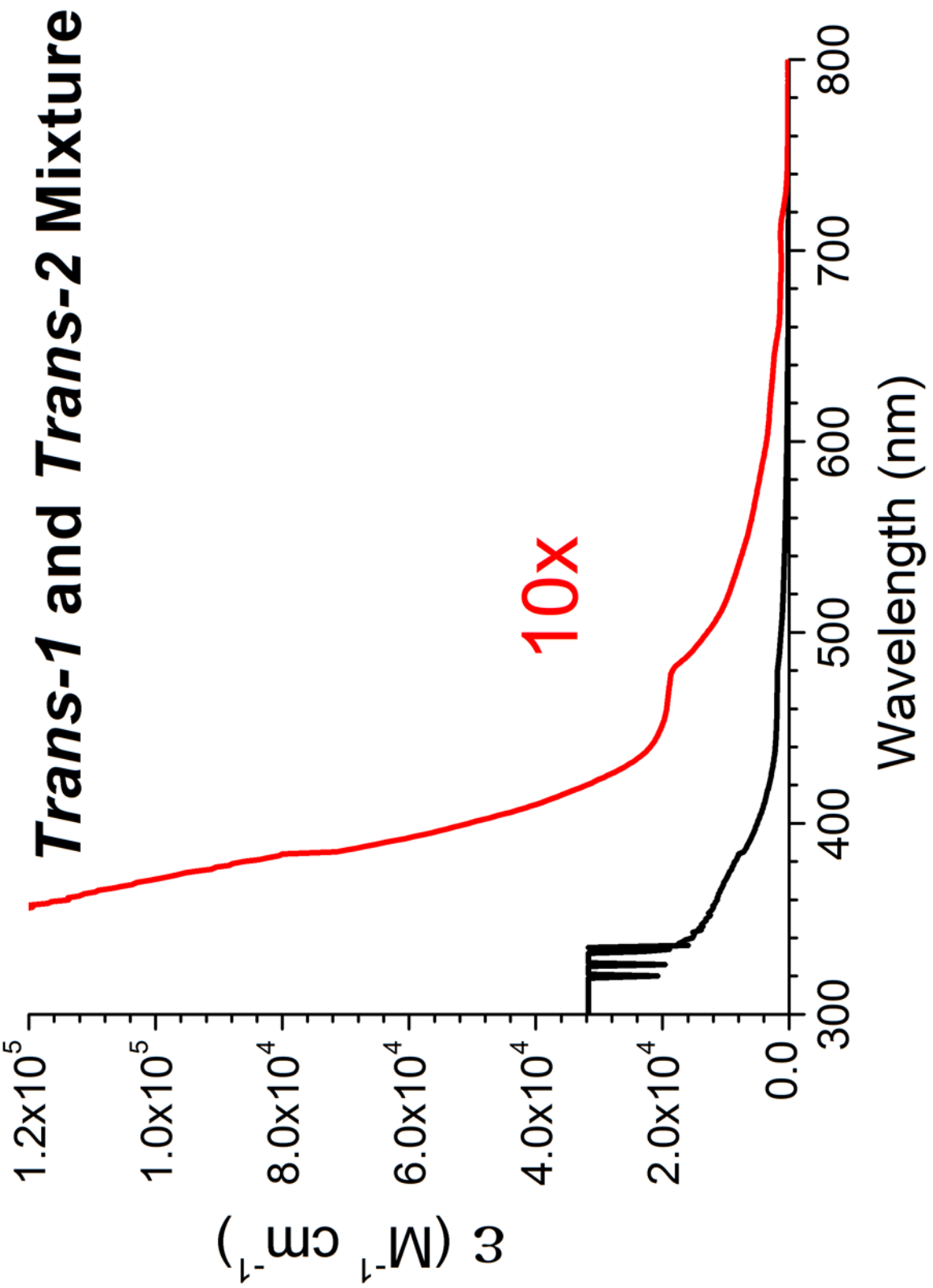

Fig 3.S1. UV-vis of *Trans-1* and *Trans-2* Bis-*N,N*-dimethylfulleropyrrolidinium Diiodide Mixture (0.89 mM in DMSO 0.1 cm cuvette)

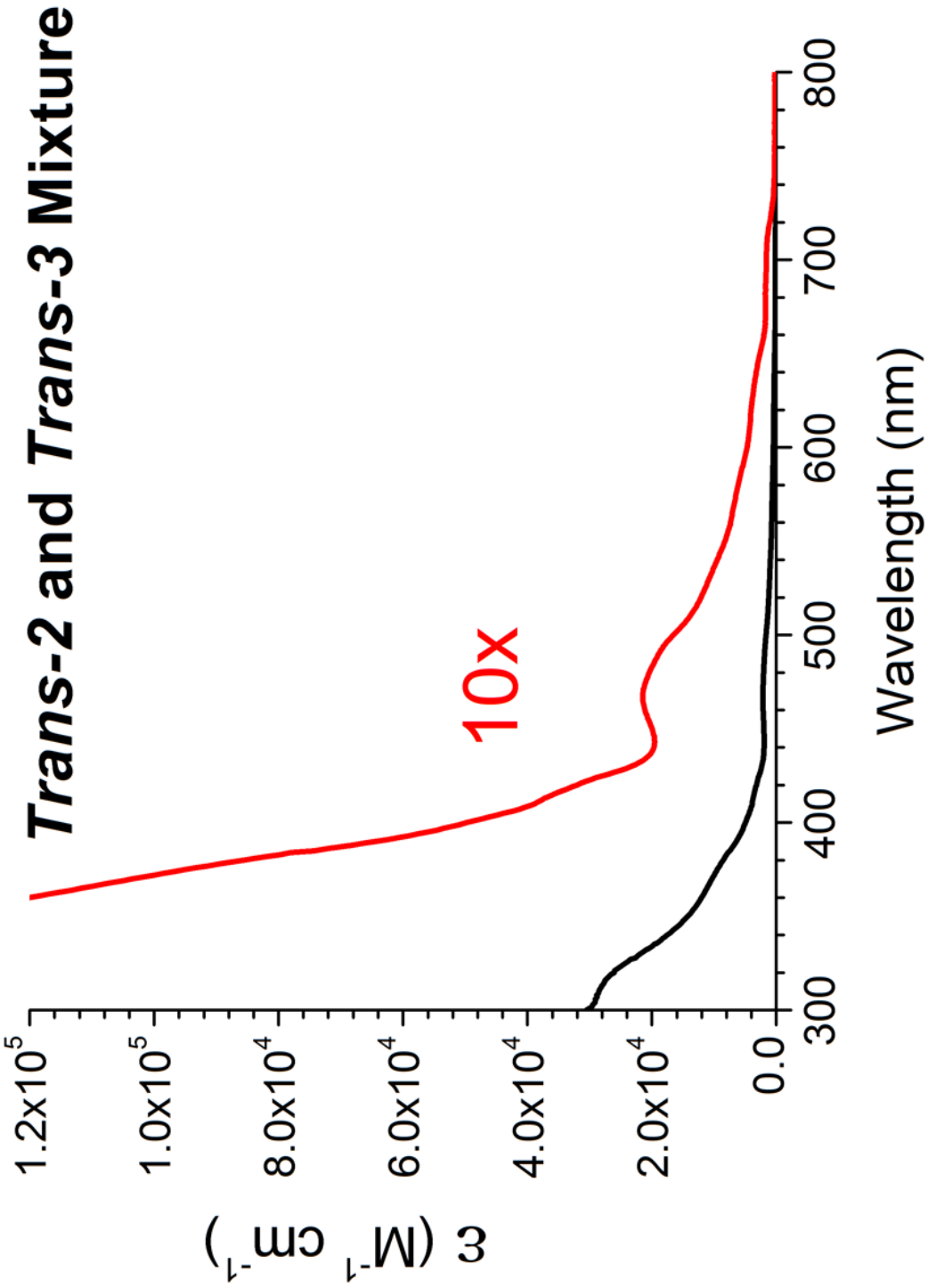

Fig 3.S2. UV-vis of *Trans-2* and *Trans-3* Bis-*N,N*-dimethylfulleropyrrolidinium Diiodide Mixture (0.72 mM in DMSO 0.1 cm cuvette)

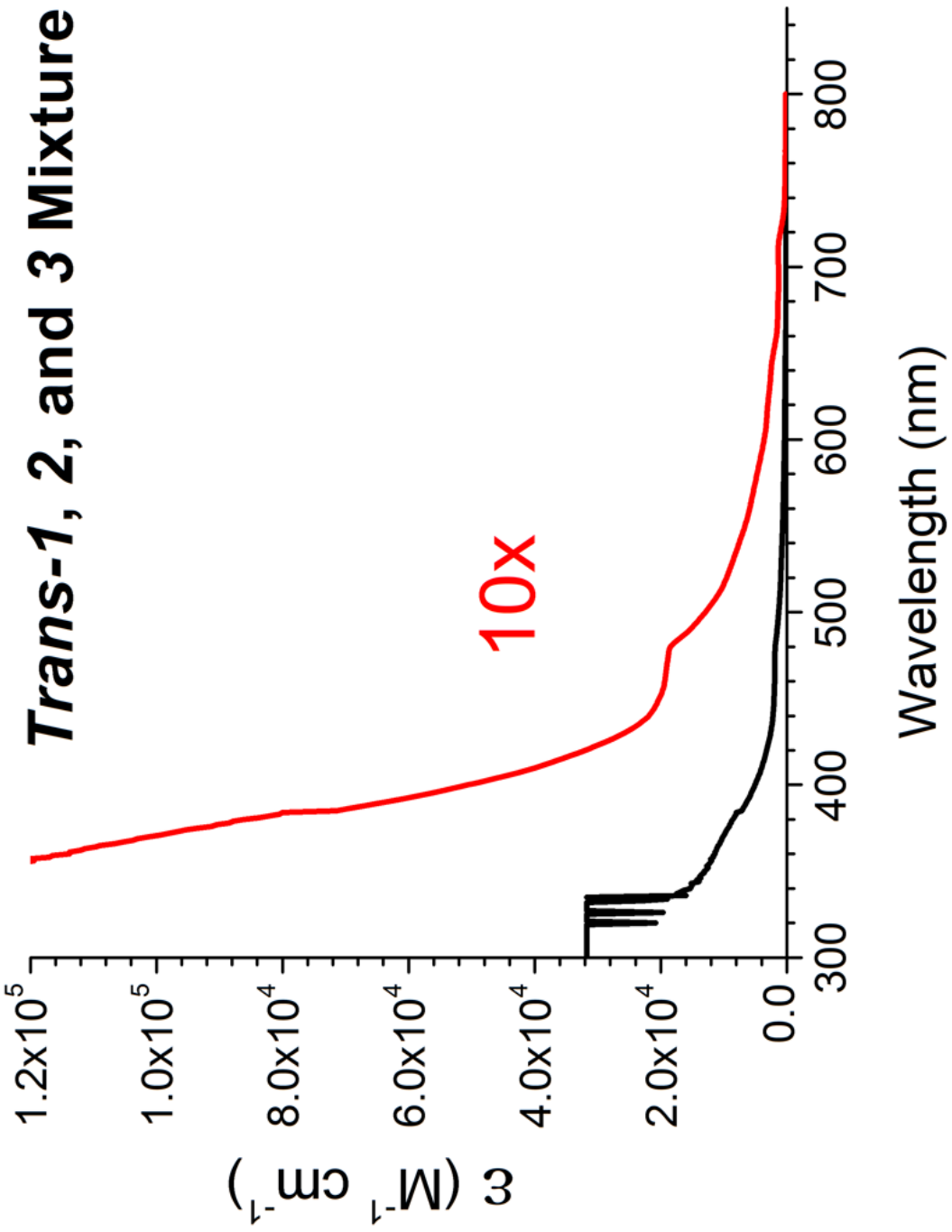

Fig 2.S3. UV-vis of *Trans-1 Trans-2* and *Trans-3* Bis-*N,N*-dimethylfulleropyrrolidinium Diiodide Mixture (1.9 mM in DMSO 0.1 cm cuvette)

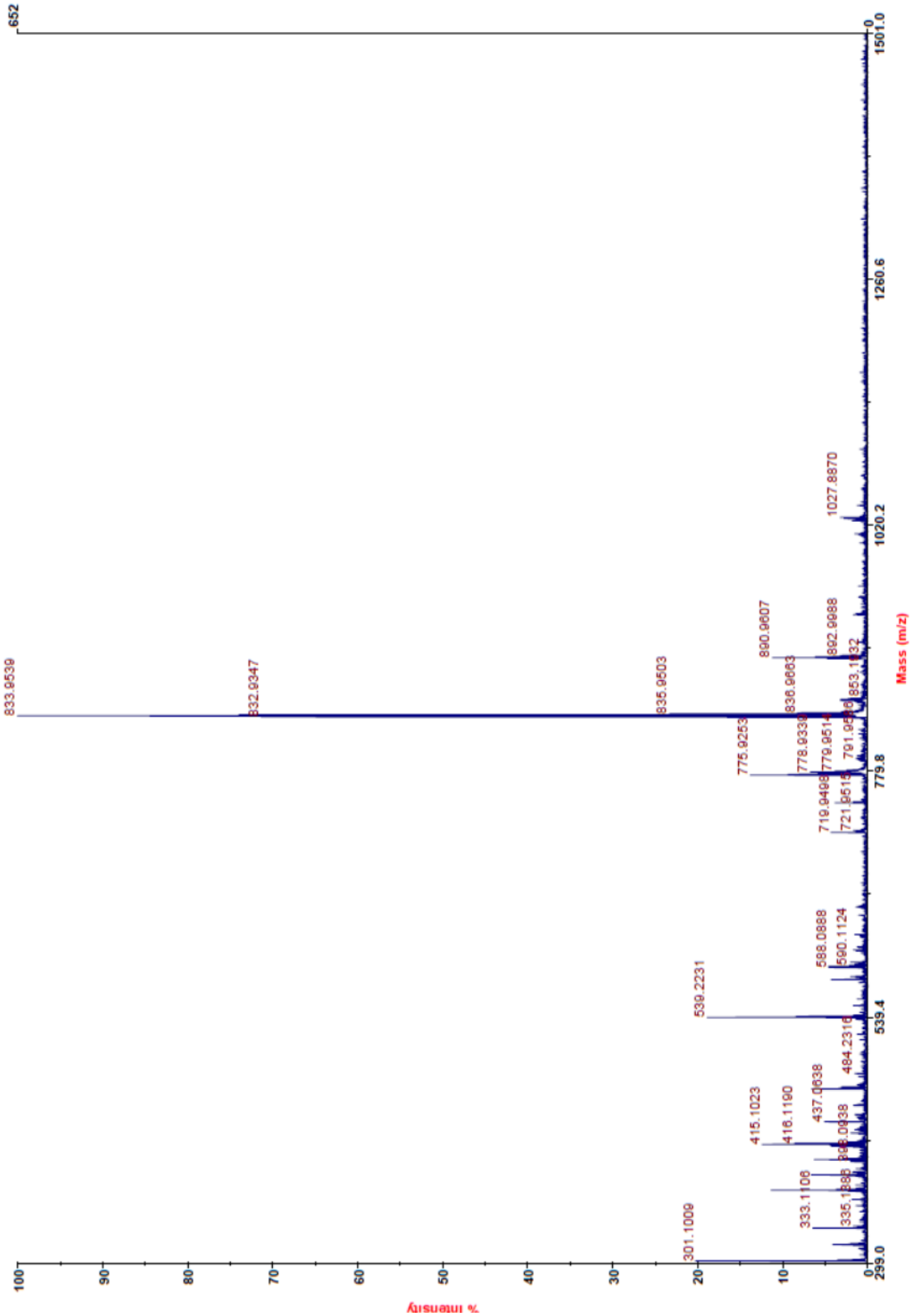

Fig S4. MALDI-TOF MS spectrum of Bis-*N*-methylfulleropyrrolidine *trans-1/trans-2* mixture.

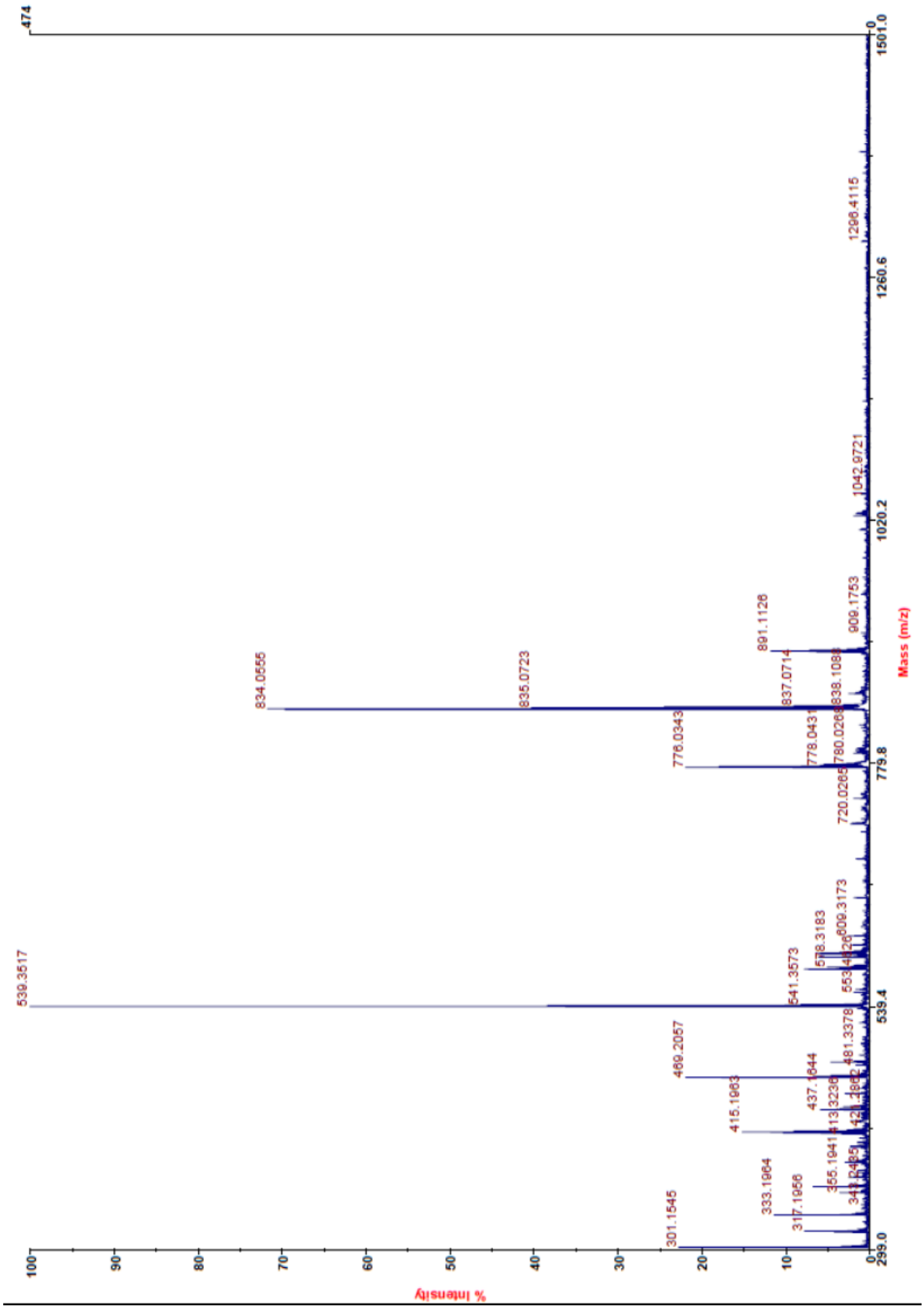

Fig 3.S5. MALDI-TOF MS spectrum of Bis-*N*-methylfulleropyrrolidine *trans-2/trans-3* mixture.

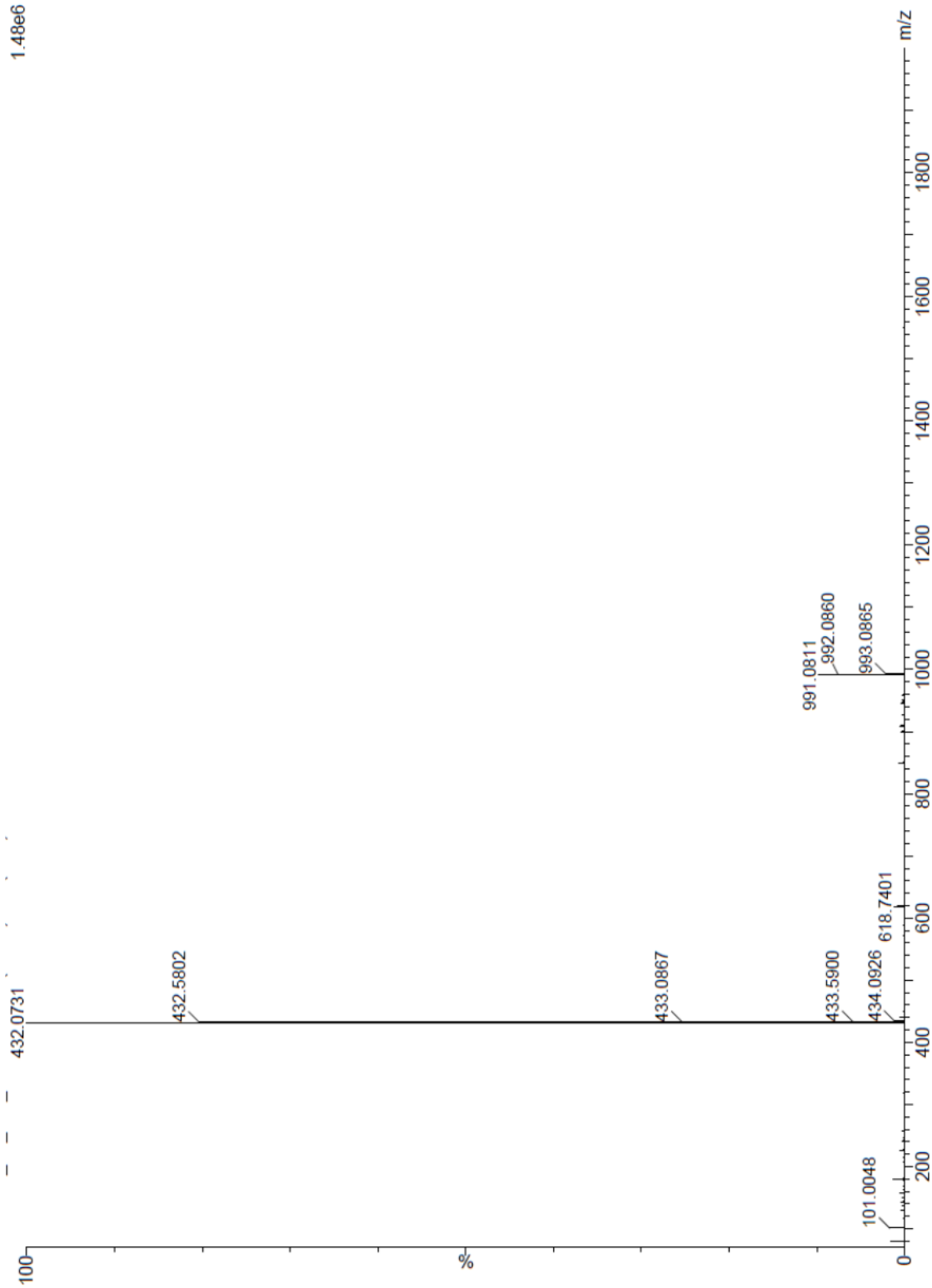

Fig 3.S6. ESI-MS of *Trans-1* and *Trans-2* Bis-*N,N*-dimethylfulleropyrrolidinium Diiodide Mixture 1:1 DMSO/MeOH

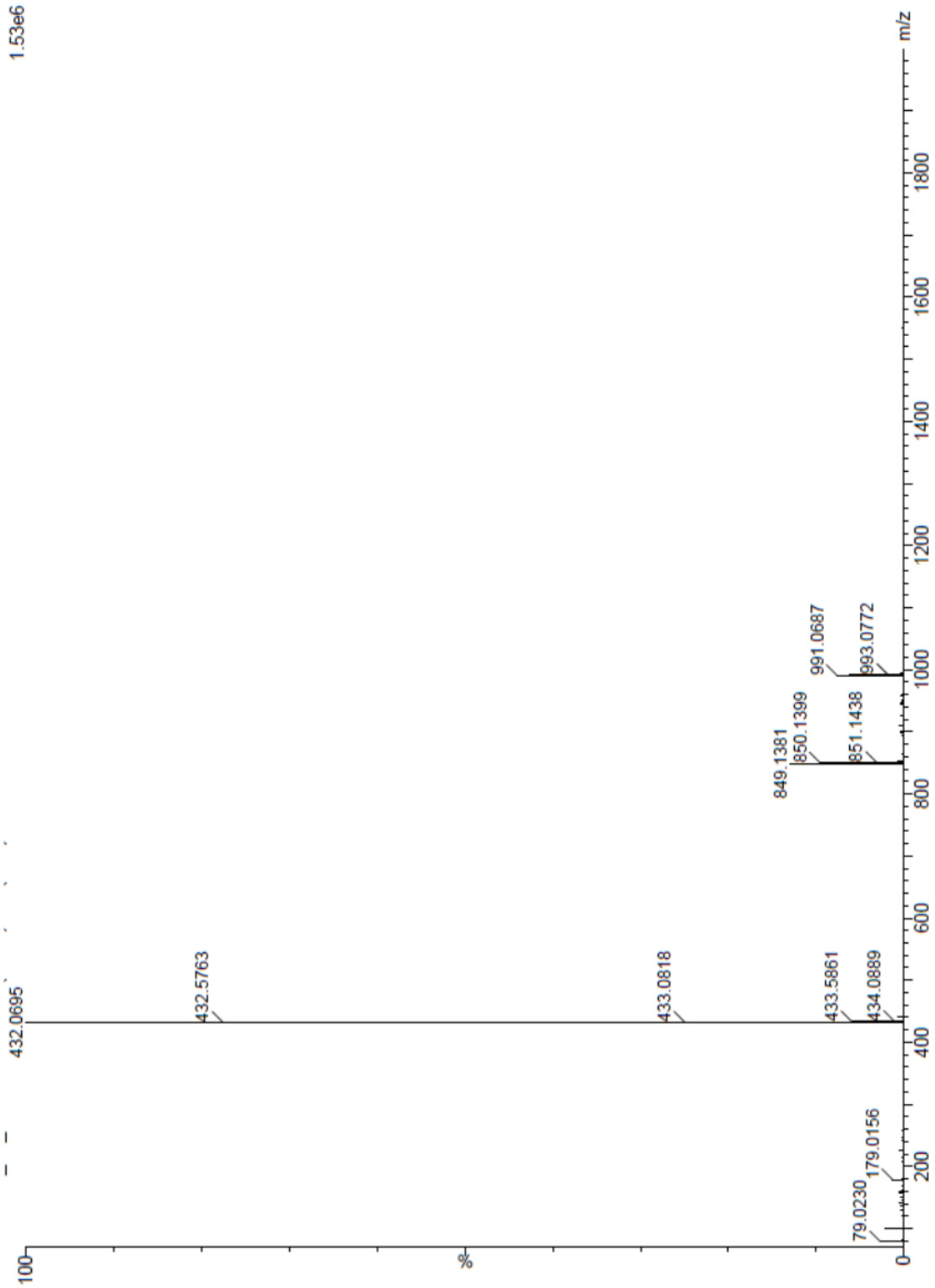

Fig 3.S7. ESI-MS spectrum of *Trans-2* and *Trans-3* Bis-*N,N*-dimethylfulleropyrrolidinium Diiodide Mixture 1:1 DMSO/MeOH

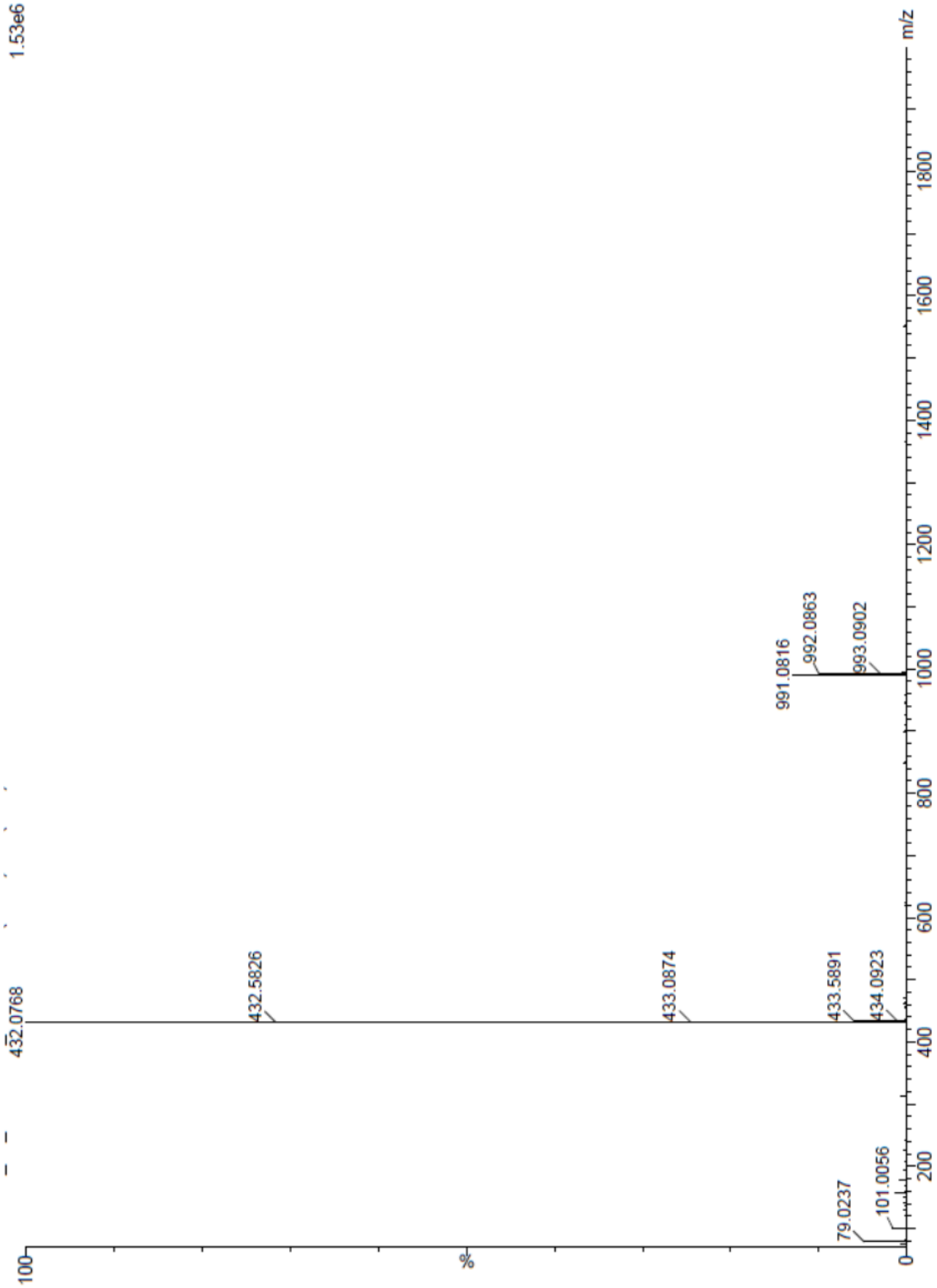

Fig 3.S8. ESI-MS spectrum of *Trans-1, Trans-2* and *Trans-3* Bis-*N,N*-dimethylfulleropyrrolidinium Diiodide Mixture 1:1 DMSO/Me

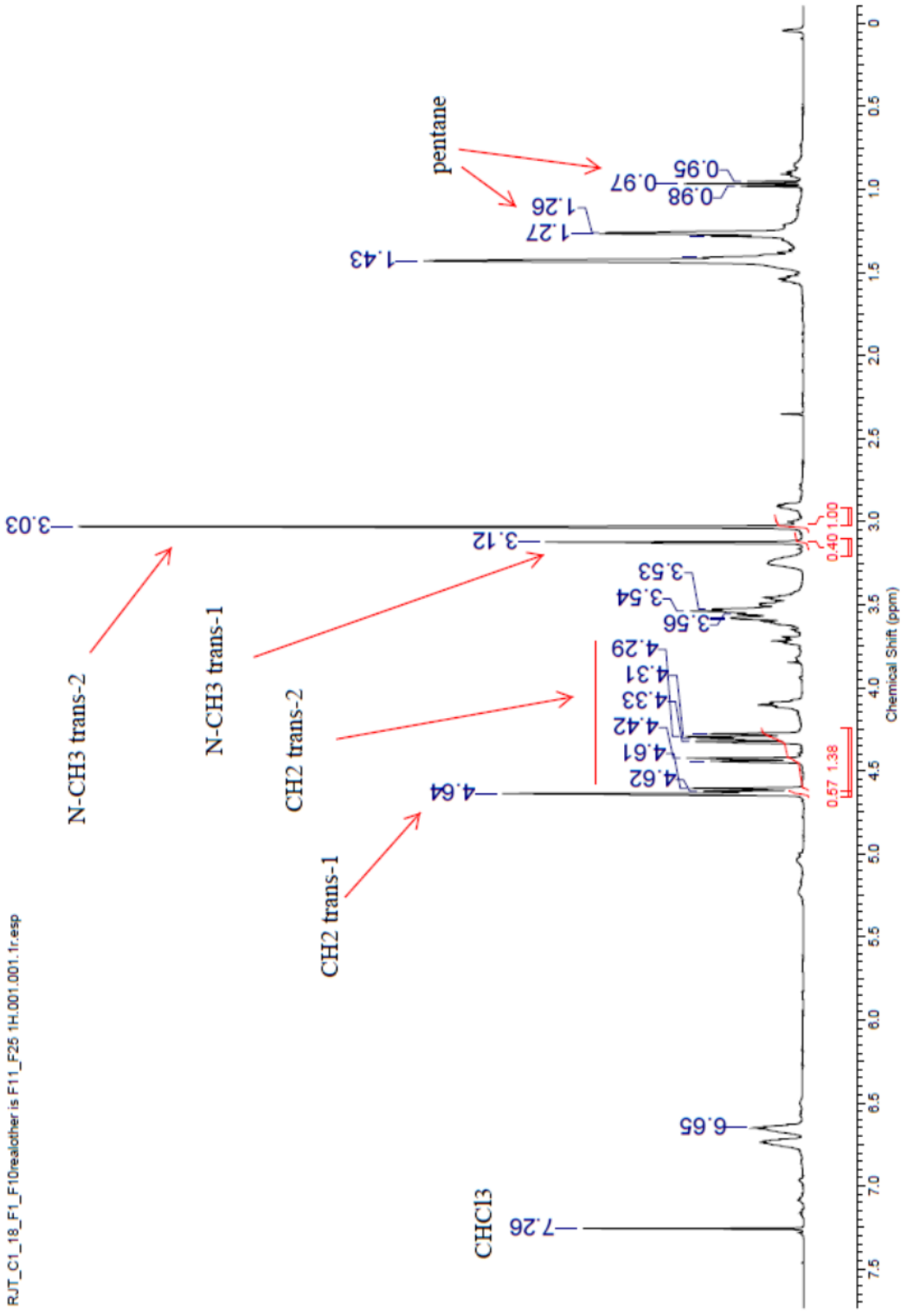

Fig 3.S9. ^{1}H NMR $CDCl_3/CS_2$ δ (ppm) *Trans-1* and *Trans-2* Bis-*N*-methylfulleropyrrolidine mixture

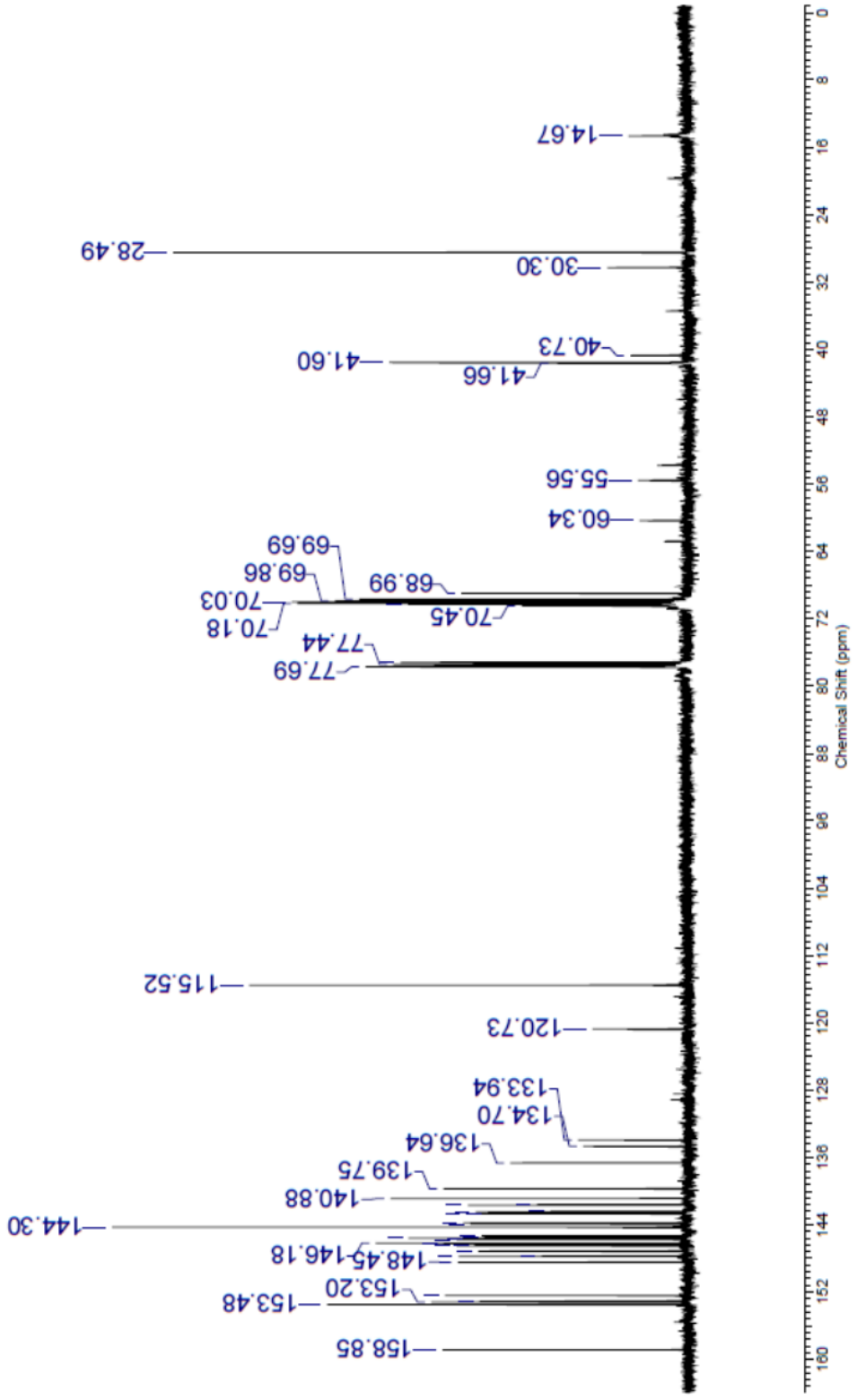

Fig 3.S10. ^{13}C NMR $CDCl_3/CS_2$ δ (ppm) *Trans-1* and *Trans-2* Bis-*N*-methylfulleropyrrolidine mixture

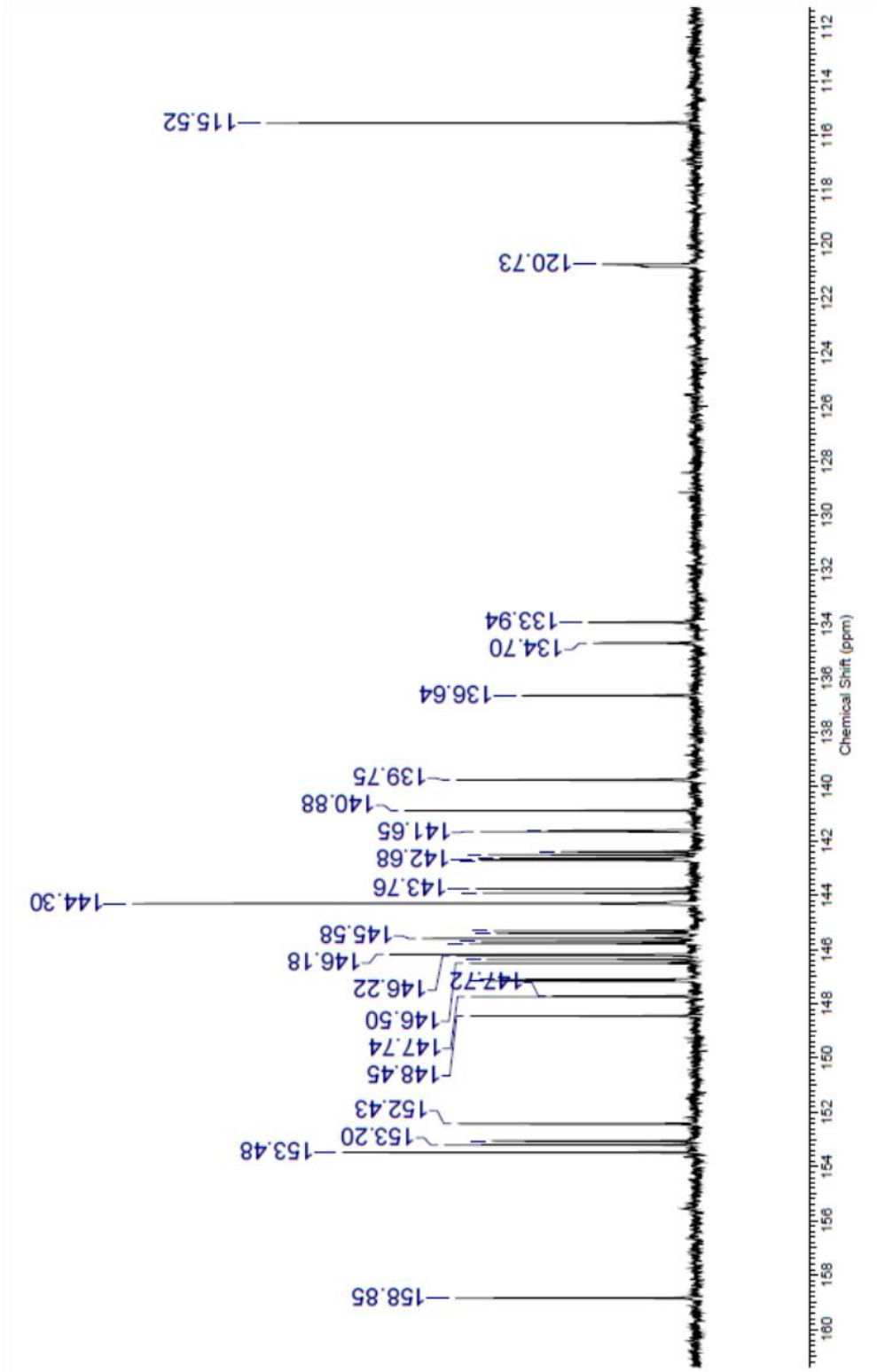

Fig 3.S11. ^{13}C NMR $CDCl_3/CS_2$ δ (ppm) *Trans-1* and *Trans-2* Bis-*N*-methylfulleropyrrolidine mixture (Aromatic Region)

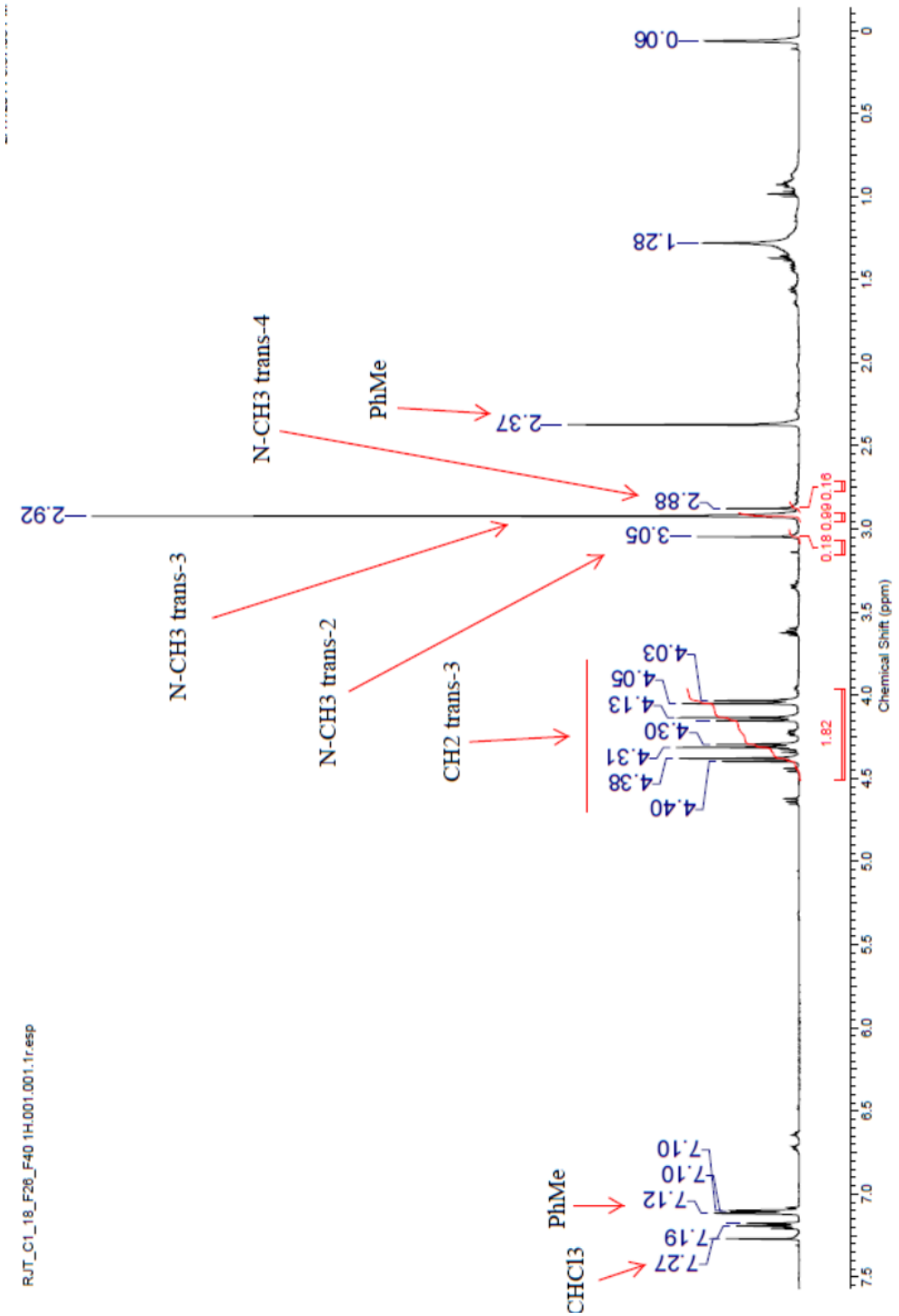

Fig 3.S12. ^{1}H NMR $CDCl_3/CS_2$ δ (ppm) *Trans-2* and *Trans-3* Bis-*N*-methylfulleropyrrolidine mixture

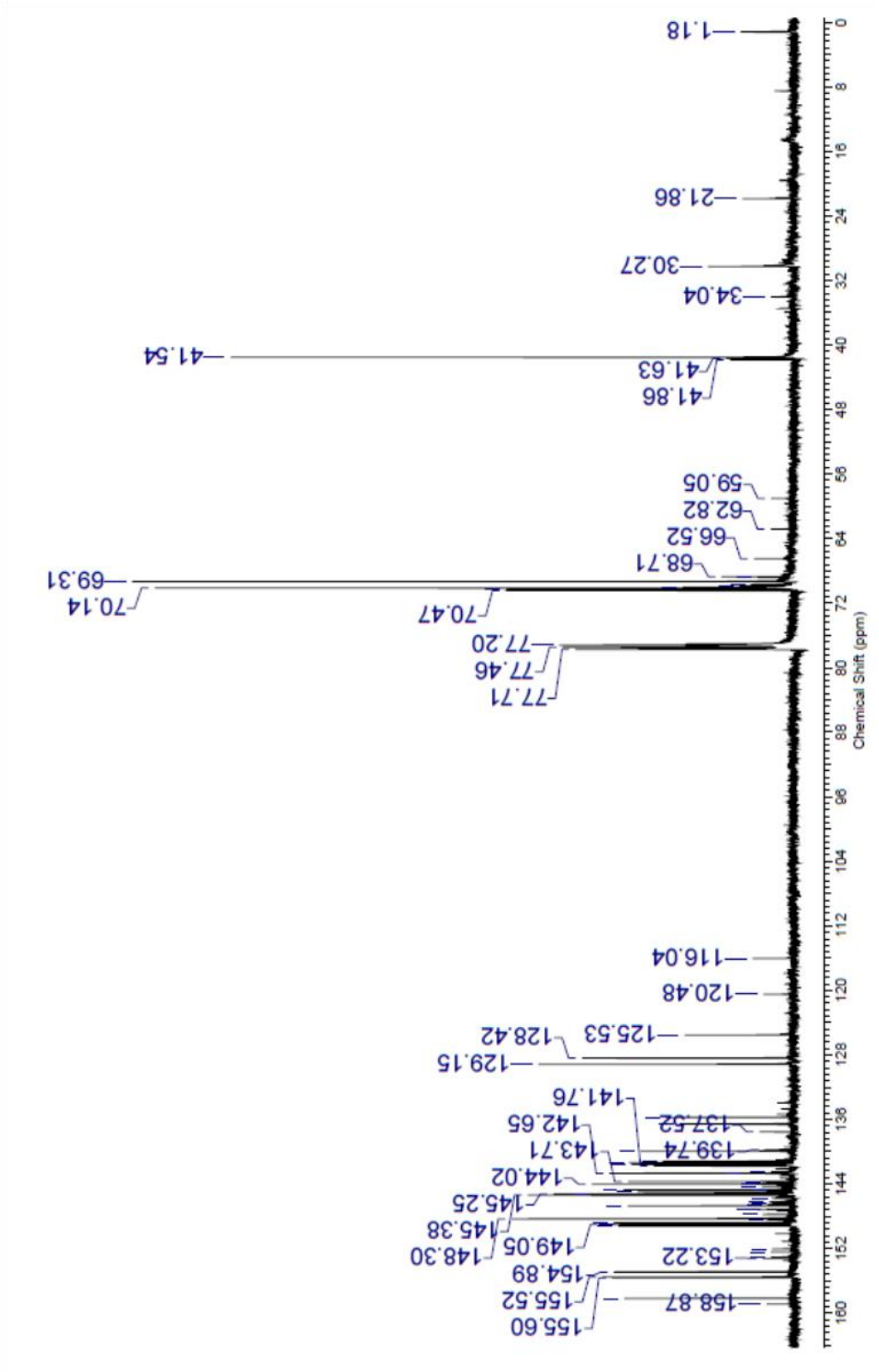

Fig S13. ^{13}C NMR $CDCl_3/CS_2$ δ (ppm) *Trans-2* and *Trans-3* Bis-*N*-methylfulleropyrrolidine mixture

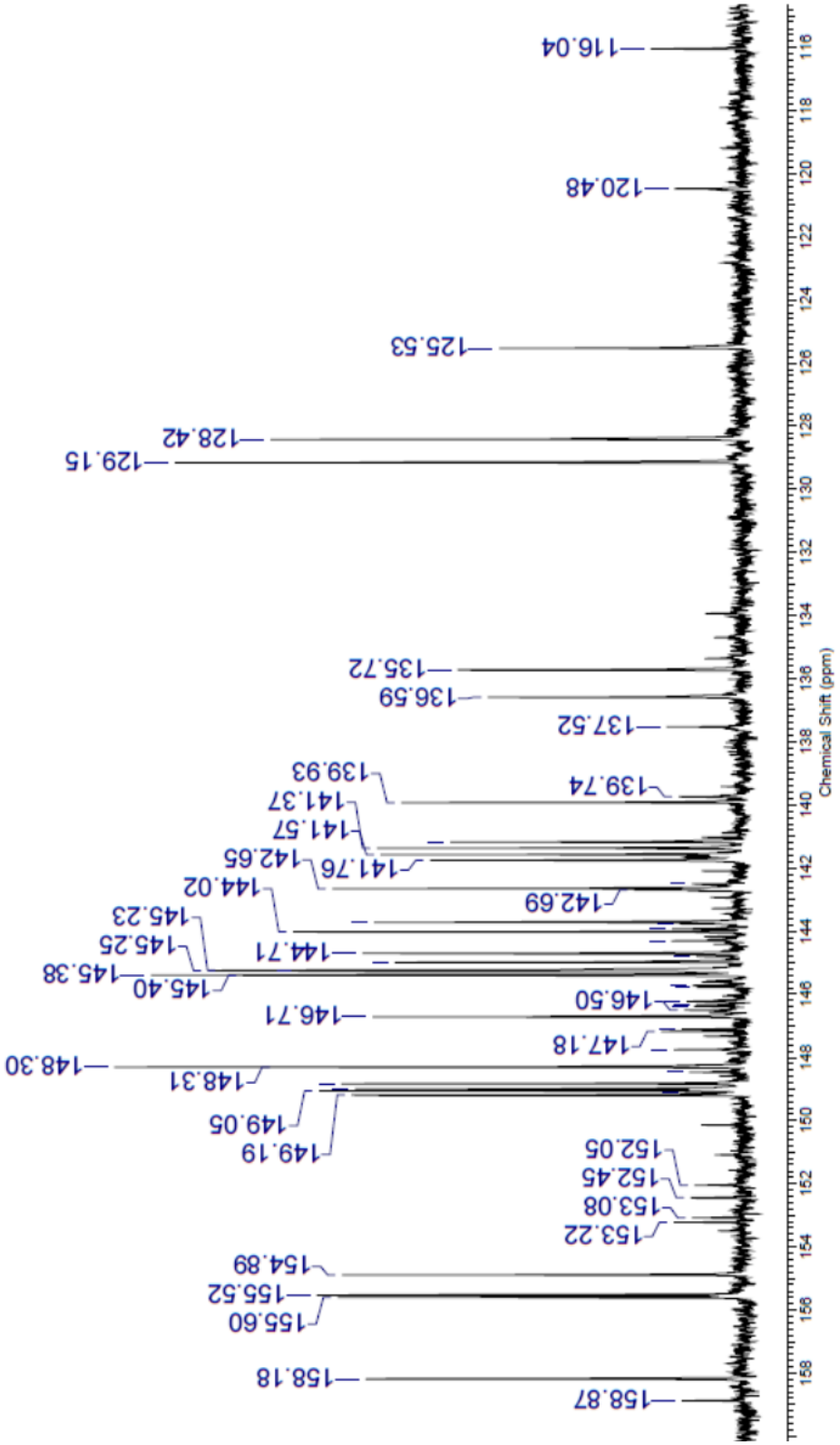

Fig 3.S14. ^{13}C NMR $CDCl_3/CS_2$ δ (ppm) *Trans-2* and *Trans-3* Bis-*N*-methylfulleropyrrolidine mixture (Aromatic)

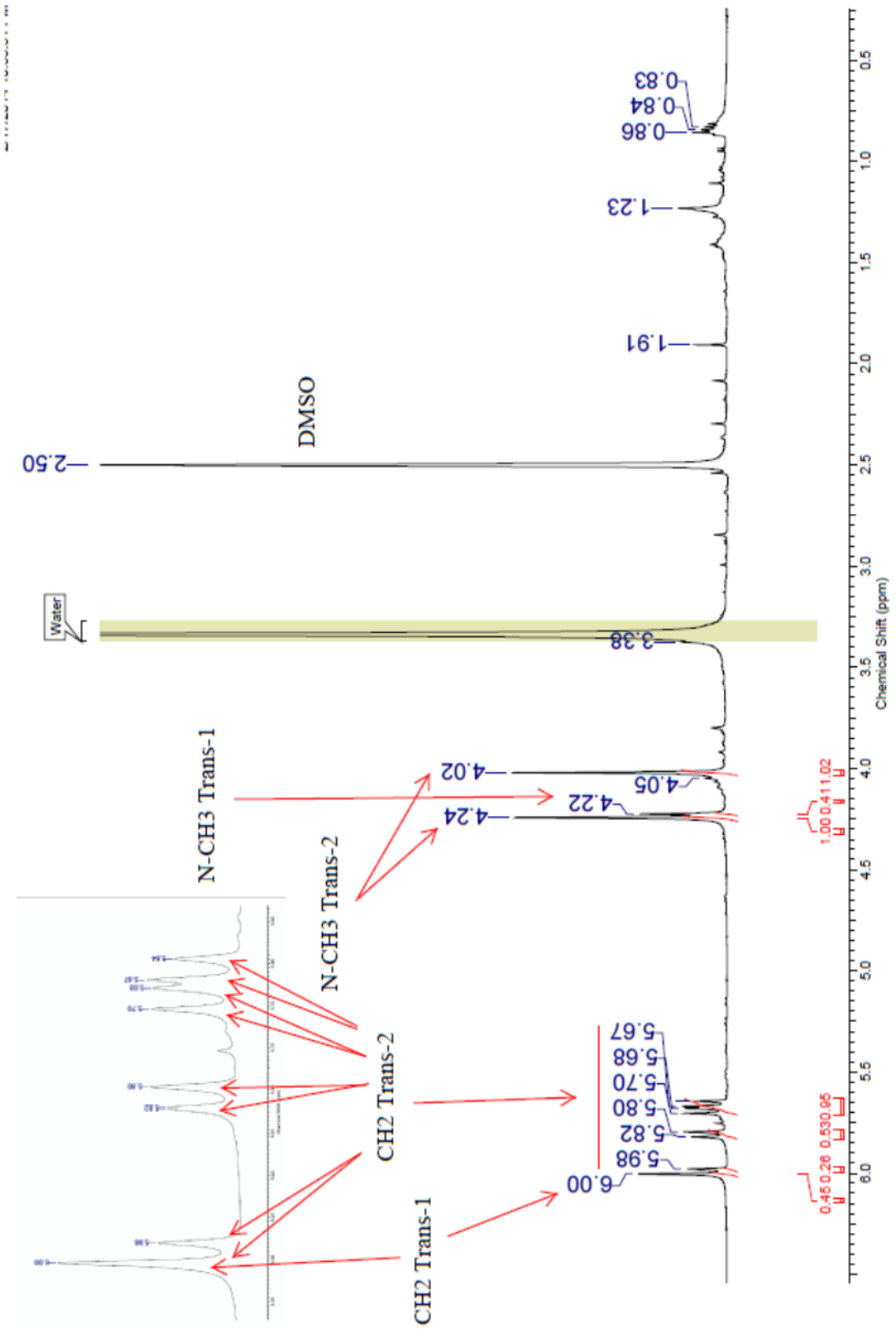

Fig 3.S15. ^{1}H NMR DSMO-D_6 δ (ppm) *Trans-1* and *Trans-2* Bis-*N,N*-dimethylfulleropyrrolidinium Diiodide Mixture

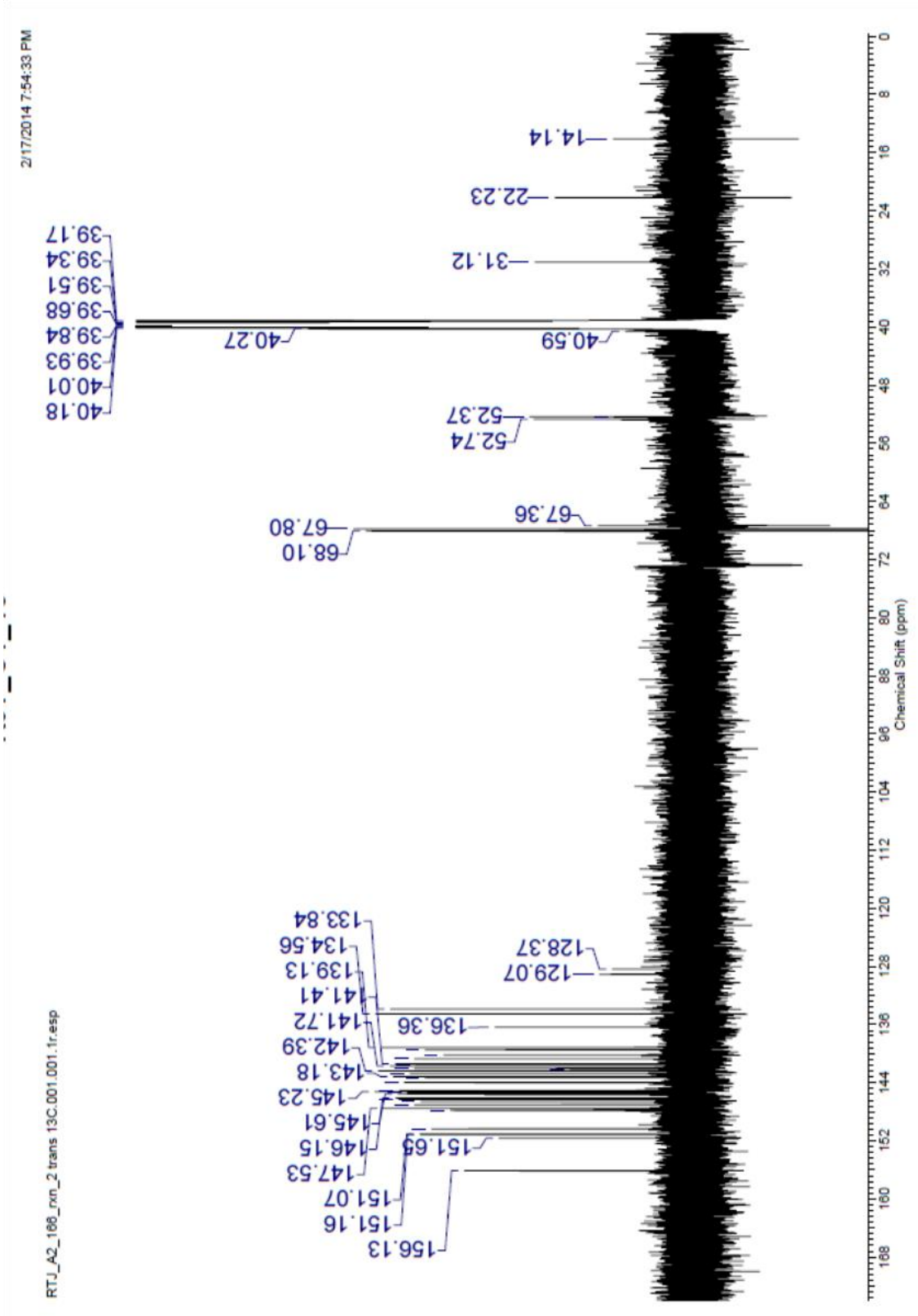

Fig 3.S16. ^{13}C NMR DSMO-D_6 δ (ppm) *Trans-1* and *Trans-2* Bis-*N,N*-dimethylfulleropyrrolidinium Diiodide Mixture

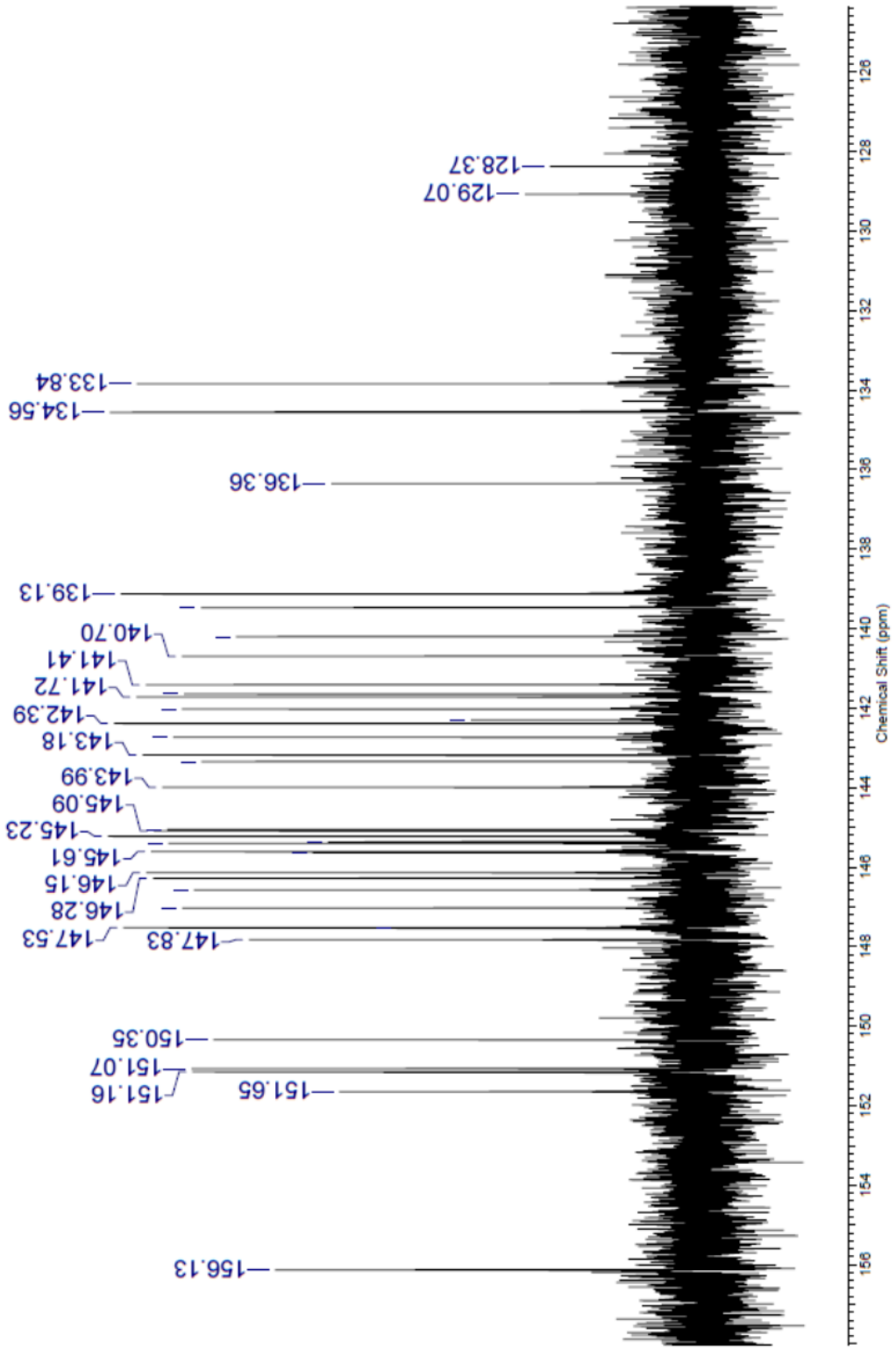

Fig 3.S17. ^{13}C NMR Aromatic Region DSMO-D_6 δ (ppm) *Trans-1* and *Trans-2* Bis-*N*,*N*-dimethylfulleropyrrolidinium Diiodide Mixture

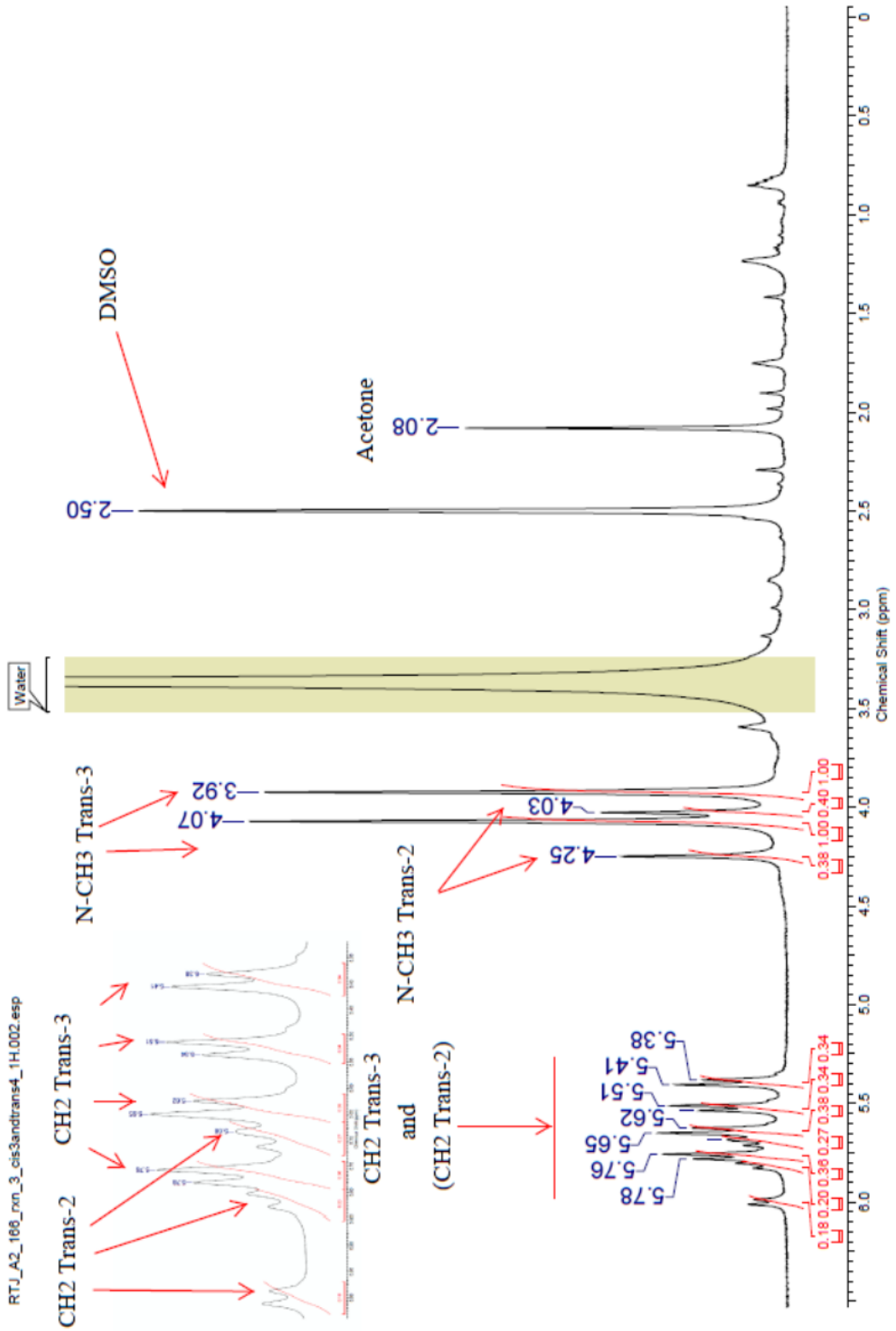

Fig 3.S18. ^{1}H NMR DSMO-D_6 δ (ppm) *Trans-2* and *Trans-3* Bis-*N,N*-dimethylfulleropyrrolidinium Diiodide Mixture

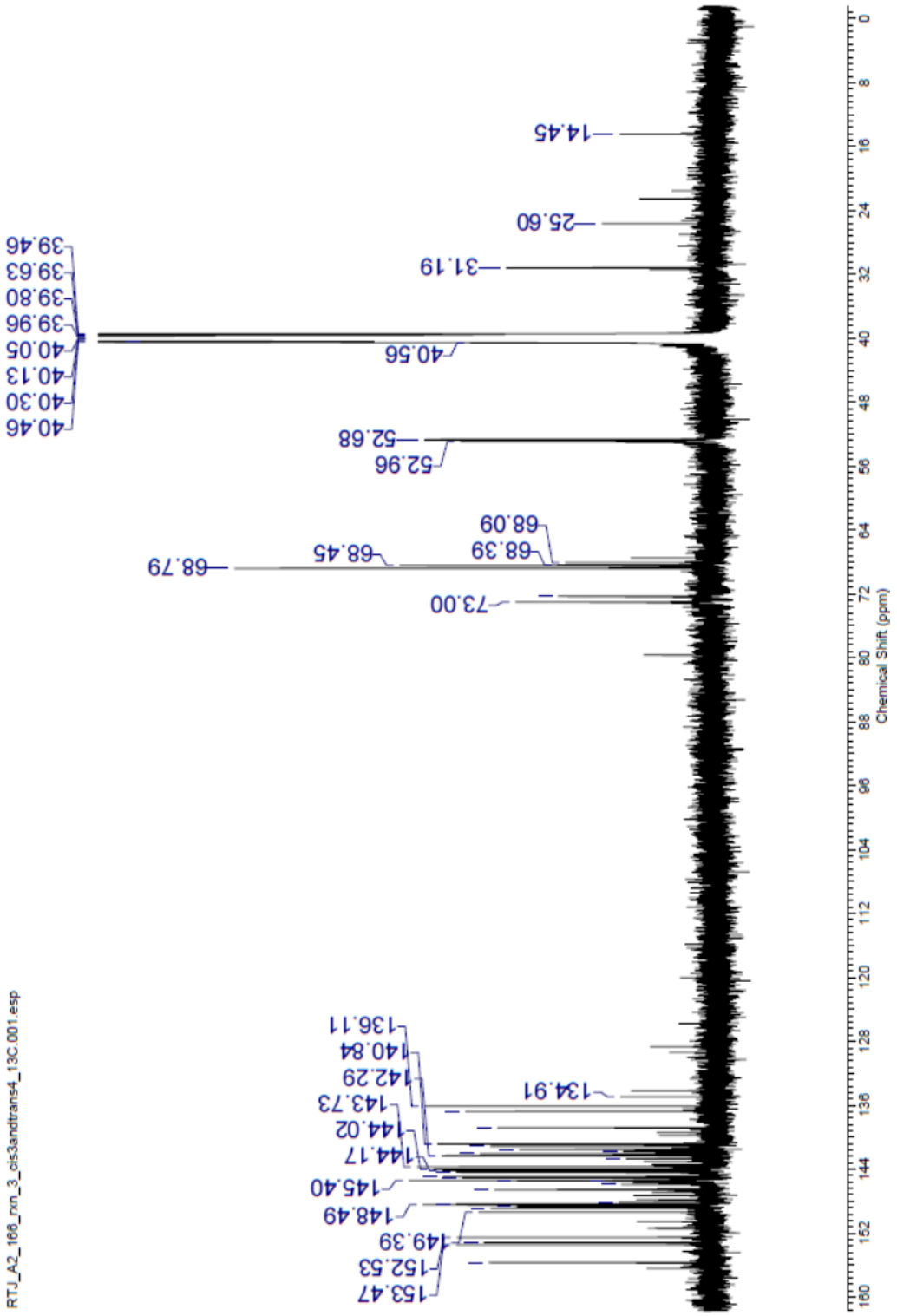

Fig S19. ^{13}C NMR DSMO-D_6 δ (ppm) *Trans-2* and *Trans-3* Bis-*N,N*-dimethylfulleropyrrolidinium Diiodide Mixture

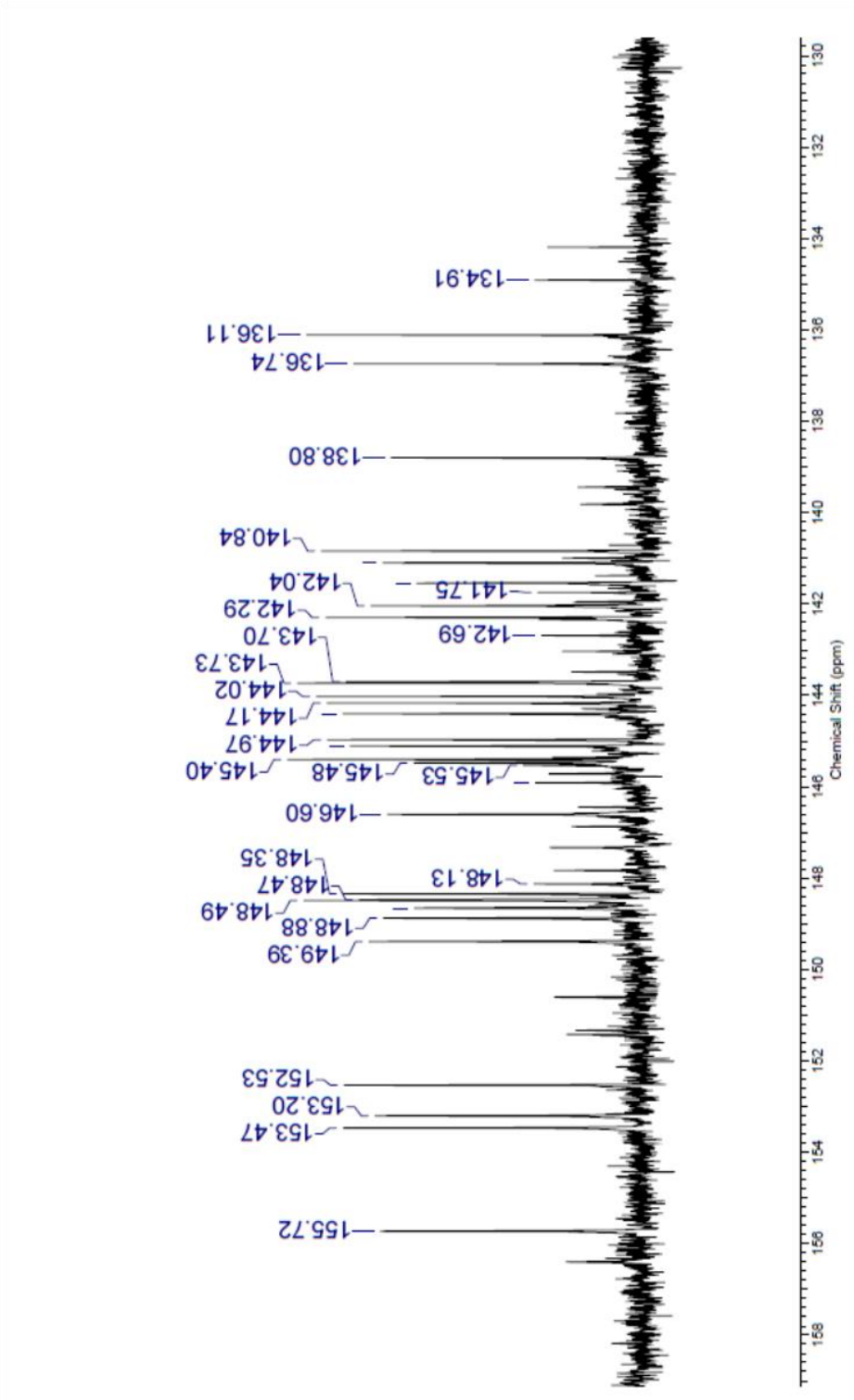

Fig 3.S20. ^{13}C NMR Aromatic Region DSMO-D_6 δ (ppm) *Trans-2* and *Trans-3* Bis-*N,N*-dimethylfulleropyrrolidinium Diiodide Mixture**.**

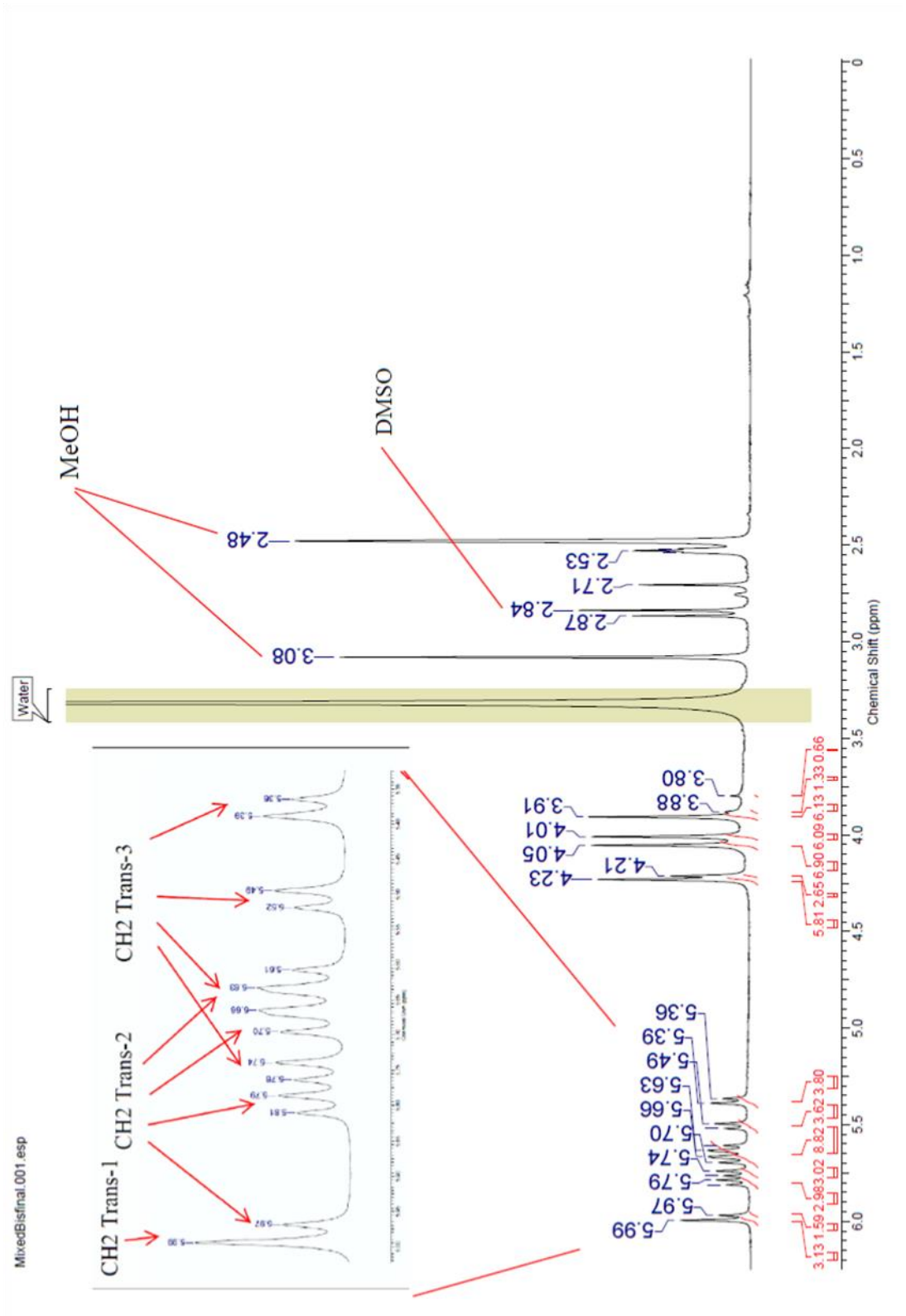

Fig 3.S21. ^{1}H NMR DSMO-D_6 δ (ppm) *Trans-1, Trans-2* and *Trans-3* Bis-*N,N*-dimethylfulleropyrrolidinium Diiodide Mixture

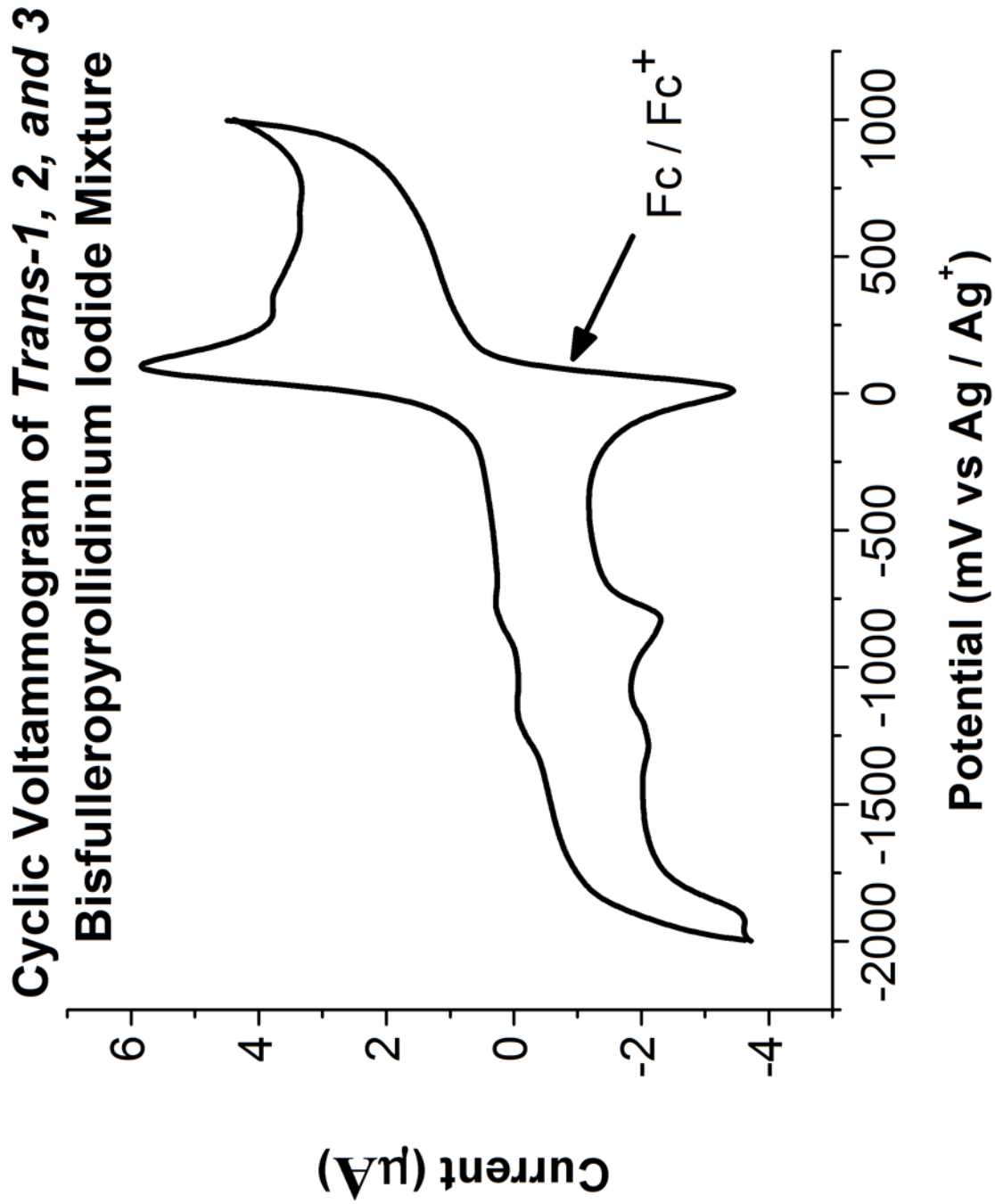

Fig 3.S22. Cyclic Voltammagram of *Trans-1, 2,* and *3* mixture of Bisfulleropyrrolidinium Iodide Mixture

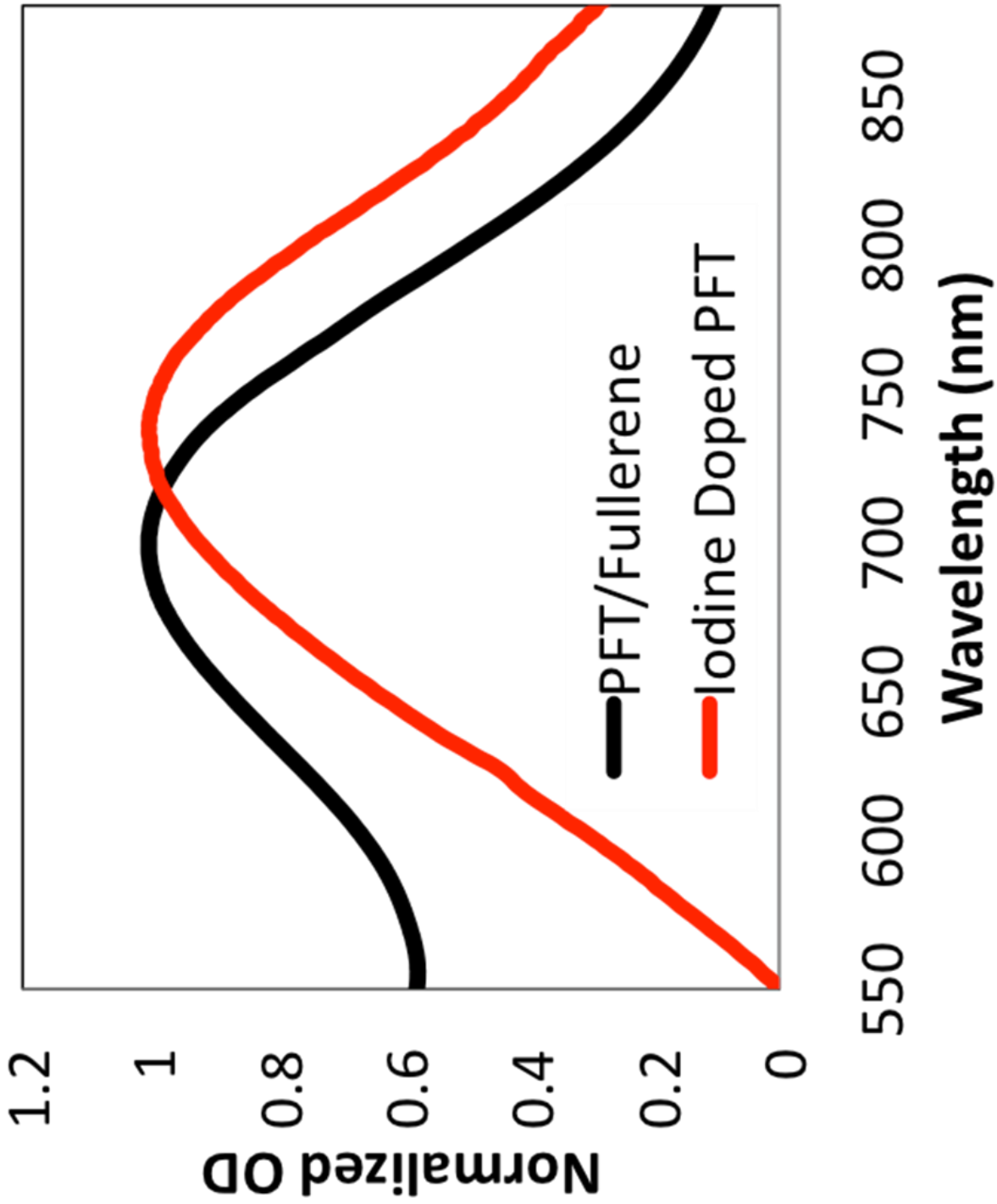

Fig. 3.S23. PFT:bis adducts vs. iodine doped PFT absorption. PFT:bis adducts absorption is at 690 nm, iodine doped PFT absorption at 730 nm.

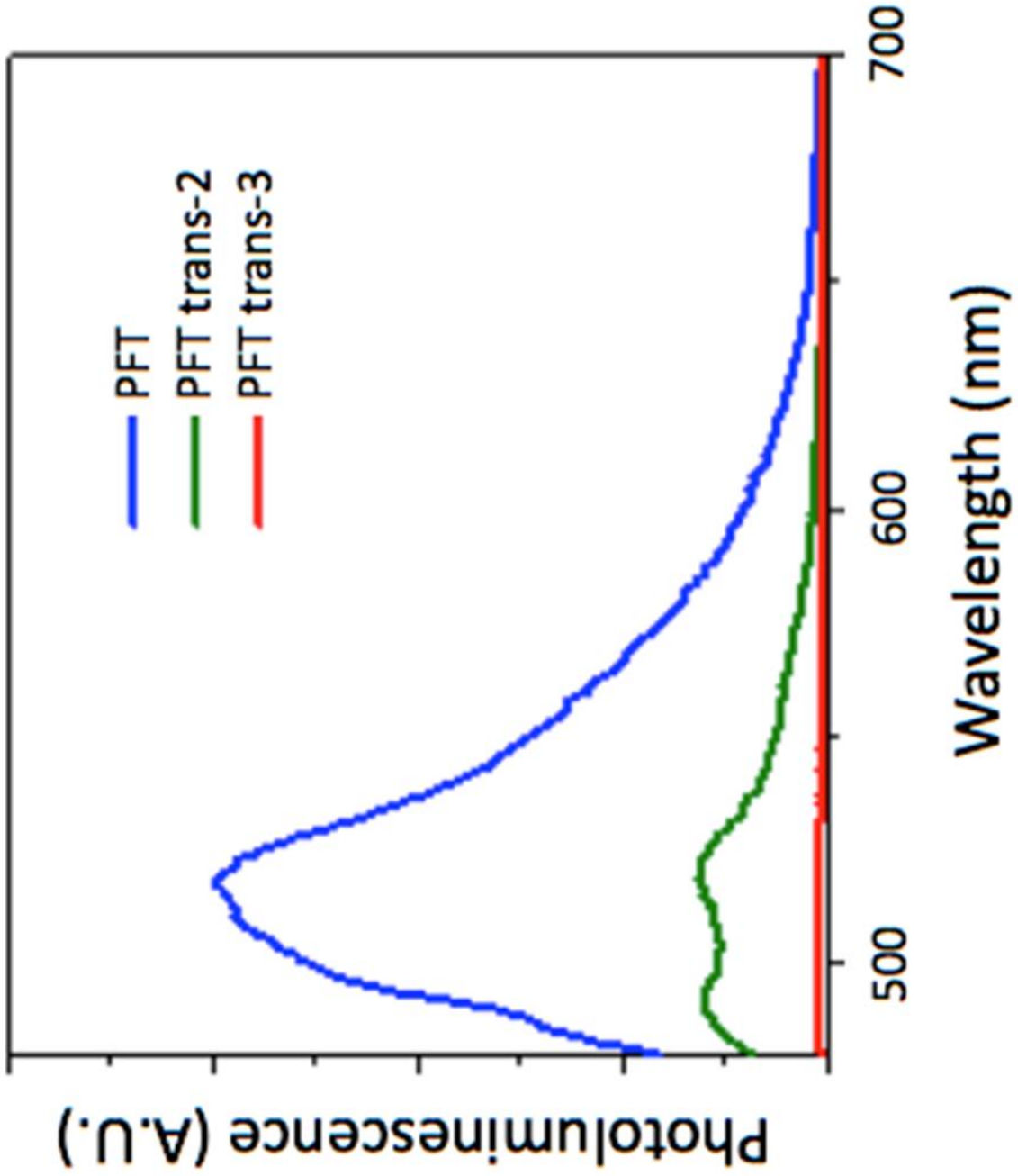

Fig. 3.S24. PL quenching of concentrated (1 mg/mL) PFT:fullerene samples used in broad-band transient absorption spectroscopy

Acknowledgments: This work was supported by the National Science Foundation (NSF) under grant CHE-1112569 and by the Center for Molecularly Engineered Energy Materials (MEEM), an Energy Frontier Research Center (EFRC) funded by the U.S. Department of Energy (DOE) under Contract DE-AC06-76RLO-1830. A.S.F acknowledges support from The Clean Green IGERT (NSF DGE-0903720). This work made use of facilities support by the NSF under equipment grant CHE-1048804. Portions of this work were conducted at the Stanford Synchrotron Radiation Lightsource (SSRL), which is supported under DOE Contract DE-AC02-76SF00515. The SSRL Structural Molecular Biology Program is supported by the DOE Office of Biological and Environmental Research, and by the National Institutes of Health, National Institute of General Medical Sciences (including P41GM103393). We acknowledge the use of instruments at the Electron Imaging Center for NanoMachines supported by the NIH (1S10RR23057 to ZHZ) and CNSI at UCLA.

References

1. A. W. Rutherford, Photosystem II, the water-splitting enzyme. *Trends Biochem. Sci.* **14**, 227–32 (1989).

2. J. Piris *et al.*, Photogeneration and Ultrafast Dynamics of Excitons and Charges in P3HT/PCBM Blends. *J. Phys. Chem. C*. **113**, 14500–14506 (2009).

3. P. E. Shaw, A. Ruseckas, I. D. W. Samuel, Exciton Diffusion Measurements in Poly(3-hexylthiophene). *Adv. Mater.* **20**, 3516–3520 (2008).

4. S. Gélinas *et al.*, The Binding Energy of Charge-Transfer Excitons Localized at Polymeric Semiconductor Heterojunctions. *J. Phys. Chem. C*, 7114–7119 (2011).

5. J. Verhoeven, On the Role of Spin Correlation in the Formation, Decay, and Detection of Long-Lived, Intramolecular Charge-Transfer States. *J. Photochem. Photobiol. C Photochem. Rev.* **7**, 40–60 (2006).

6. T. Miura, K. Maeda, H. Murai, T. Ikoma, Long-Distance Sequential Charge Separation at Micellar Interface Mediated by Dynamic Charge Transporter: A Magnetic Field Effect Study. *J. Phys. Chem. Lett.* **6**, 267–271 (2015).

7. C. Lungenschmied *et al.*, Flexible, long-lived, large-area, organic solar cells. *Sol. Energy Mater. Sol. Cells*. **91**, 379–384 (2007).

8. T. Yasuda, Y. Shinohara, T. Ishi-i, L. Han, Use of benzothiadiazole–triphenylamine amorphous polymer for reproducible performance of polymer–fullerene bulk-heterojunction solar cells. *Org. Electron.* **13**, 1802–1808 (2012).

9. T. Costa *et al.*, Self-Assembly of Poly{1,4-phenylene-[9,9-bis(4-phenoxy-butylsulfonate)]fluorene-2,7-diyl} with Oppositely Charged Phenylenevinylene Oligoelectrolytes. *J. Phys. Chem. B*, 613–623 (2014).

10. A. P.-Z. Clark *et al.*, Self-Assembling Semiconducting Polymers-Rods and Gels from Electronic Materials. *ACS Nano*. **7**, 962–977 (2013).

11. A. Cassell, C. Asplund, J. Tour, Self- Assembling Supramolecular Nanostructures from a C60 Derivative: Nanorods and Vesicles. *Angew. Chemie …*. **38**, 2403–2405 (1999).

12. G. Beaucage, Small-angle scattering from polymeric mass fractals of arbitrary mass-fractal dimension. *J. Appl. Crystallogr.* **29**, 134–146 (1996).

13. S. Choudhary, S. R. Bhatia, Rheology and nanostructure of hydrophobically modified alginate (HMA) gels and solutions. *Carbohydr. Polym.* **87**, 524–530 (2012).

14. Y.-C. Li *et al.*, Fractal aggregates of conjugated polymer in solution state.

Langmuir. **22**, 11009–15 (2006).

15. U. Jeng *et al.*, Complex structure of fullerene star ionomers and sodium dodecyl sulfate resolved by contrast variation with SANS and SAXS. *Nucl. Instruments Methods Phys. Res. Sect. A Accel. Spectrometers, Detect. Assoc. Equip.* **600**, 294–296 (2009).

16. Y. Park, Y. Park, J. Gao, J. Grey, C. Wang, PPV and C 60 Nanocomposite with Enhanced Miscibility and Enhanced Photo-Induced Charge Transfer through Ground State Electrostatic Interactions. *Polymer (Guildf).* **55**, 855–859 (2014).

17. See supplementary online material (SOM) for details.

18. R. Österbacka, C. P. An, X. M. Jiang, Z. V. Vardeny, Two-Dimensional Electronic Excitations in Self-Assembled Conjugated Polymer Nanocrystals. *Science (80-.).* **287**, 839–842 (2000).

19. F. Paquin *et al.*, Charge Separation in Semicrystalline Polymeric Semiconductors by Photoexcitation: Is the Mechanism Intrinsic or Extrinsic? *Phys. Rev. Lett.* **106**, 197401 (2011).

20. S. Arzhantsev, M. Maroncelli, Design and characterization of a femtosecond fluorescence spectrometer based on optical Kerr gating. *Appl. Spectrosc.* **59**, 206–20 (2005).

21. C. Chiang *et al.*, Electrical Conductivity in Doped Polyacetylene. *Phys. Rev. Lett.* **39**, 1098–1101 (1977).

22. T. Kato, T. Kodama, M. Oyama, S. Okazaki, T. Shida, ESR and optical studies of the radical anion of C60. *Chem. Phys. Lett.* **186**, 35–39 (1991).

23. D. M. Guldi, M. Prato, Excited-state properties of C(60) fullerene derivatives. *Acc. Chem. Res.* **33**, 695–703 (2000).

24. V. I. Krinichnyi, Dynamics of charge carriers photoinduced in poly(3-dodecylthiophene)/fullerene bulk heterojunction. *Sol. Energy Mater. Sol. Cells*. **92**, 942–948 (2008).

25. T. J. Savenije *et al.*, Observation of bi-polarons in blends of conjugated copolymers and fullerene derivatives. *Phys. Chem. Chem. Phys.* **13**, 16579–84 (2011).

26. J. Ceuster, E. Goovaerts, a. Bouwen, J. Hummelen, V. Dyakonov, High-frequency (95 GHz) electron paramagnetic resonance study of the photoinduced charge transfer in conjugated polymer-fullerene composites. *Phys. Rev. B*. **64**, 195206 (2001).

27. E. Kelley, T. Smart, A. Jackson, Structural changes in block copolymer micelles

induced by cosolvent mixtures. *Soft Matter*. **7**, 7094–7102 (2011).

28. M. Maggini, G. Scorrano, M. Prato, Addition of azomethine ylides to C60: synthesis, characterization, and functionalization of fullerene pyrrolidines. *J. Am. Chem. Soc.* **115**, 9798–9799 (1993).

29. Q. Lu, D. I. Schuster, S. R. Wilson, Preparation and Characterization of Six Bis(N-methylpyrrolidine)−C60 Isomers: Magnetic Deshielding in Isomeric Bisadducts of C60. *J. Org. Chem.* **61**, 4764–4768 (1996).

30. et al K. Kordatos, Isolation and Characterization of All Eight Bisadducts of Fulleropyrrolidine Derivatives. *J. Org. Chem.* **66**, 2802–2808 (2001).

31. D. M. Guldi, Probing the Electron-Accepting Reactivity of Isomeric Bis(pyrrolidinium) Fullerene Salts in Aqueous Solutions. *J. Phys. Chem. B*. **104**, 1483–1489 (2000).